

Pharmacometrics as a tool to individualize treatment with anti-infective drugs

Dissertation

zur

Erlangung des Doktorgrades (Dr. rer. nat.)

der

Mathematisch-Naturwissenschaftlichen Fakultät

der

Rheinischen Friedrich-Wilhelms-Universität Bonn

vorgelegt von

Muhammad Bilal

aus

Peshawar, Pakistan

Bonn, 2024

Angefertigt mit Genehmigung der Mathematisch Naturwissenschaftlichen Fakultät der
Rheinischen Friedrich-Wilhelms-Universität Bonn

Gutachter \ Betreuer: Prof. Dr. Uwe Fuhr

Gutachter: Prof. Dr. Ulrich Jaehde

Tag der Promotion: 06.03.2025

Erscheinungsjahr: 2025

Acknowledgements

I would like to take this opportunity to express my profound gratitude to all those people who, in different ways, contributed to the success of this work.

First and foremost, sincere thanks to my research supervisor Prof. Dr. med. Uwe Fuhr for the unwavering trust he placed in me and for the highly interesting projects he has given me. His enthusiasm for research has been a constant source of inspiration. I am grateful for his continuous support and all the scientific and non-scientific discussions and exchanges we have had. This experience has been invaluable in my personal and professional growth. I am grateful for his support, particularly in sad times which I greatly appreciate.

I would like to thank my co-supervisor Prof. Dr. Ulrich Jaehde for his support and feedback on my PhD projects and thesis and for facilitating my admission to the University of Bonn.

I would like to thank my academic mentor Dr. med. Max Taubert for the inspiring scientific and non-scientific discussions we had at the institute and later via Zoom/Teams calls, for having an open ear and for being the reviewer for my scientific publications.

I would like to thank Dr. Sami Ullah for introducing me to the field of pharmacometrics and for his valuable support and advice throughout my PhD projects.

I would like to thank my collaboration partners Dr. Michael Zoller, Dr. Johannes Zander and Dr. Uwe Liebchen from the Department of Anaesthesiology and the Institute of Laboratory Medicine, University Hospital, LMU Munich, for sharing clinical data, and for providing constructive feedback.

I would like to thank Prof. Dr. Charlotte Kloft (Freie University Berlin) and Prof. Dr. Wilhelm Huisinga (University of Potsdam) for providing me with the opportunity to become a member of the Graduate Research Training Program PharMetrX batch 2021.

I thank Prof. Dr. Mats O. Karlsson for allowing me to participate in Uppsala Summer School, Uppsala, Sweden.

I extend my sincere thanks to colleagues, both current and former, at the Center for Pharmacology, Department I of Pharmacology, Cologne including Qian Dong, Zhendong Chen, Chih-Hsuan Hsinng, Xia Li, Usman Arshad, Soeren Büsker, Nidha Shapoo, Lobna El Tabei, Christian Krauss,

Chunli Chen, and Yali Wu for their cooperation, mutual support, and for the wonderful time we spent together. I will always cherish the memories of this experience. I would also like to extend my thanks to my PharMetrX year 2021 colleagues including Mattia Berton, Olga Teplytska, Franziska Thoma, Elena Pascual García, Sara Iannuzi, Franz Weber and Davide Bindellinei for the great time we spent together during the PharMetrX modules in Berlin and Potsdam.

I am grateful to the Deutscher Akademischer Austauschdienst (DAAD) and the Higher Education Commission of Pakistan for providing stipend during my PhD studies.

I wish to acknowledge my parents and family for their support, prayers, and encouragement particularly my father who was diagnosed with cancer after I left Pakistan for Germany to pursue my PhD. I was fortunate to spend the last few days with him. And last but not least I would like to express my heartfelt appreciation to my wife for her support, understanding, unconditional love, and always being there for me.

"Read, in the Name of your Lord Who created."

Al-Quran

Dedicated to the memory of my late father, Fazal Muhammad Malakzai, who always encouraged and supported me to read

List of Publications

This commutative thesis is based on the following four publications:

1. Bilal M, El Tabei L, Büsker S, Krauss C, Fuhr U, Taubert M. Clinical Pharmacokinetics and Pharmacodynamics of Cefiderocol. Clin Pharmacokinet. 2021; 60(12):1495-1508. The DOI: [10.1007/s40262-021-01063-5](https://doi.org/10.1007/s40262-021-01063-5).
2. Bilal M, Zoller M, Fuhr U, Jaehde U, Ullah S, Liebchen U, Büsker S, Zander J, Flury BB, Taubert M. Cefepime Population Pharmacokinetics, Antibacterial Target Attainment, and Estimated Probability of Neurotoxicity in Critically Ill Patients. Antimicrob Agents Chemother. 2023;67(7):1–13. DOI: [10.1128/aac.00309-23](https://doi.org/10.1128/aac.00309-23).
3. Bilal M, Ullah S, Jaehde U, Trueck C, Zaremba D, Wachall B, Wargenau M, Scheidel B, Wiesen MHJ, Gazzaz M, Chen C, Büsker S, Fuhr U, Taubert M, Dokos C. Assessment of body mass-related covariates for rifampicin pharmacokinetics in healthy Caucasian volunteers. Eur J Clin Pharmacol. 2024. DOI: [10.1007/s00228-024-03697-3](https://doi.org/10.1007/s00228-024-03697-3).
4. Abouellil A, Bilal M, Taubert M, Fuhr U. A population pharmacokinetic model of remdesivir and its major metabolites based on published mean values from healthy subjects. Naunyn Schmiedebergs Arch Pharmacol. 2023;396(1):73–82. DOI: [10.1007/s00210-022-02292-6](https://doi.org/10.1007/s00210-022-02292-6).

Table of Contents

1	Introduction	1
1.1	Pharmacometrics	1
1.2	Population Pharmacokinetics.....	2
1.3	PopPK Approaches.....	3
1.3.1	Traditional PopPK Methods	3
1.3.2	Direct PopPK Methods	4
1.3.3	NONMEM.....	6
1.3.4	Monolix	8
1.4	Pharmacokinetic/Pharmacodynamic Indices	10
1.4.1	Minimum Inhibitory Concentration and Clinical Breakpoints	10
1.4.2	Probability of Target Attainment.....	11
1.4.3	Antibacterials PK/PD Indices	12
1.4.4	Antiviral PK/PD Indices	14
1.5	Investigated Agents	15
1.5.1	Cefiderocol	15
1.5.2	Cefepime.....	16
1.5.3	Rifampicin	18
1.5.4	Remdesivir.....	20
2	Aims and Objectives.....	24
3	Clinical Pharmacokinetics and Pharmacodynamics of Cefiderocol	27
4	Cefepime Population Pharmacokinetics, Antibacterial Target Attainment, and Estimated Probability of Neurotoxicity in Critically Ill Patients	31
5	Rifampicin Assessment of body mass-related covariates for rifampicin pharmacokinetics in healthy Caucasian volunteers	36
6	A population pharmacokinetic model of remdesivir and its major metabolites based on published mean values from healthy subjects	40
7	Summary.....	44
8	References	49
	Information on the assistance received and resources used.....	66

List of abbreviations

ATP	Adenosine triphosphate
AUC	Area under the curve
AIC	Akaike information criterion
BBB	Blood-brain barrier
BH	Body height
BICc	Corrected Bayesian Information Criterion
BLAs	Biological licensing applications
BMI	Body mass index
BOV	Between occasion variability
BQL	Below quantitation limit
BSA	Body surface area
BSV	Between subject variability
BW	Body weight
BMI	Body mass index
BW	Body weight
CL _{CR}	Creatinine clearance calculated from the Cockcroft-Gault equation
CL _D	Elimination clearance in dialysis patients
CG	Cockcroft-Gault
CI	Confidence interval
CL	Clearance
C _{max}	Maximum concentration
CNS	Central nervous system
CL _{ND}	Elimination in Nondialysis Patients
COVID-19	Coronavirus disease outbreak in 2019
CSF	Cerebrospinal fluid
CV	Coefficient of variation
CVVHD	Continuous venovenous hemodialysis

CWRES	Conditional weighted residuals
DDIs	Drug-drug interactions
eCL _{CR}	Creatinine clearance estimated by the Cockcroft-Gault equation
EC ₅₀	50% effective concentration
EC ₉₀	90% effective concentration
ECOFF	Epidemiological cut-off value
EMA	European Medicines Agency
ESRD	End-stage renal disease
EUCAST	European Committee on Antimicrobial Susceptibility Testing
AUC	Area under the concentration-time curve
FFM	Fat-free mass
FDA	Food and Drug Administration
FD&C	Food, Drug, and Cosmetic
FO	First-order
FOCE	First-order conditional estimation
FOCE-I	First-order conditional estimation with interaction
f	Fraction unbound
$fT_{>MIC}$	Time that the free drug concentration exceeds the MIC over the dosing interval
GABA	γ -aminobutyric acid A
GFR	Glomerular filtration rate
GOF	Goodness of fit
ICU	Intensive care unit
IIV	Inter-individual variability
IOV	Inter-occasion variability
IPRED	Individual predictions
IM	Intramuscular
ITS	Iterative two-stage
IV	Intravenous

LCMS	Liquid chromatography-mass spectrometry
LC-MS/MS	Liquid chromatography-tandem mass spectrometry
mCL _{CR}	Measured creatinine clearance
MCS	Monte Carlo simulations
MIC	Minimum inhibitory concentration
MDRD	Modification of Diet in Renal Disease
MET	Mesenchymal-epithelial transition factor
ML	Maximum likelihood
NDA	New drug applications
NLME	Non-linear mixed-effects
NONMEM	Non-linear mixed-effects modelling
NPD	Naïve pooled data
OFV	Objective function value
PD	Pharmacodynamics
PK	Pharmacokinetics
PK/PD	Pharmacokinetic-pharmacodynamic
Pop	Population
PopPK	Population pharmacokinetics
PRED	Population predictions
PsN	Perl speaks NONMEM
PTA	Probability of Target Attainment
Q	Intercompartmental clearance
RSE	Relative standard error
Rslmx	R Speaks Monolix
SD	Standard deviation.
SAEM	Stochastic Approximation Expectation-Maximization
Shr	Shrinkage
STS	Starndart two-stage

TB	Tuberculosis
$T_{>MIC}$	Time over MIC
TDM	Therapeutic drug monitoring
V_1	Central volume of distribution
V_2	Peripheral volume of distribution
V_d	Volume of distribution
WHO	World Health Organization

1 Introduction

Anti-infective drugs are of paramount importance for the treatment of infectious diseases (1). An array of new drugs entered clinical use in the second half of the 20th century, providing physicians with the best options for treating infectious diseases. The mortality of acute meningococcal meningitis was reduced to 10% from 70–90% with subcutaneous sulphanilamide. However, its use also revealed the drug's safety issues. In the United States, the Food, Drug and Cosmetic (FD&C) Act was passed in 1938 due to the deaths linked to using the Elixir of Sulfanilamide. The FD&C Act was modified in 1962 due to the adverse effects of using thalidomide. This change resulted from the realization that the efficacy of the drug used should outweigh its adverse effects (2). A dose range should be investigated to characterize the response and identify the efficacious doses. (3). Individualizing doses with consideration to drug and patient-specific factors improves treatment outcomes i.e. maximizes the therapeutic effect and or minimizes the risk of toxicity in diverse patient populations (4). To find an appropriate dose for a drug it is important to know the underlying pharmacokinetics and pharmacodynamics of the drug (5). Computer-aided modelling and simulation of pharmacokinetic and pharmacodynamic data form the basis of pharmacometrics analysis (6).

1.1 Pharmacometrics

Pharmacometrics is an interdisciplinary field defined by the United States Food and Drug Administration (FDA) as “*the science that quantifies disease, drug and trial information to assist efficient drug development and or regulatory decisions*”(7). It started before 1960 with the study of the time courses of the drugs in biological fluids (pharmacokinetics, PK) (8). PK refers to the relationship between the influx of a drug (a broader concept than dose) and the time course of concentrations of the drug at various body sites, particularly the biophase(s) or sites where the drug exerts its effects. This correlation is determined by various subprocesses (submodels) involving drug absorption, distribution, metabolism, and elimination (9). The amalgamation of PK and clinical pharmacology principles were fundamental in developing advanced modelling approaches and tools to assess data from clinical trials (10). Pharmacometrics scientists in 1979 started using econometric and biometric methods, notably mixed effect modelling, to analyze and quantify patterns in data (11). The term “pharmacometrics” was coined by Benet and Rowland in 1982 and defined as “*the design, modeling and analysis of experiments involving complex dynamic systems in the field of pharmacokinetics and biopharmaceutics*”(12). In 1989, the FDA showed concern

about the PK of new drugs intended to be used in the geriatric population (13). A decade later in 1999, FDA issued its first guidance for the industry on population pharmacokinetics followed by a series of guidances over the next 10 years to individualize drug dosing based on exposure-response relationships in patients subgroups with renal/hepatic impairment, pediatrics and in patients receiving concomitant drug therapy and are at risk for drug-drug interactions (14,15).

1.2 Population Pharmacokinetics

Population pharmacokinetics (PopPK) enables the analysis of the data obtained from various unbalanced studies including in populations normally not included in PK analysis such as in pediatrics and or geriatrics. The PopPK studies typically are based on concentration vs. time data obtained in populations of healthy volunteers and of patients acquiring PK information about the drug under investigation. It identifies fixed effects defined as the typical PK parameters, denoting central tendency in the data, called population predictions, along with various variabilities. This includes Inter-individual variability or between-subject variability (IIV) and inter-occasional variability or between-occasion variability (IOV). IOV is defined as the variability between administrations of a drug on two or more occasions in a subject separated by sufficient time intervals where underlying PK varies between the two occasions. PopPK analysis also quantifies by estimating the extent of unexplained variability within the population. The magnitude of residual (unexplained) variability holds significance as an increase in residual variability decreases the safety and efficacy of the drug. The errors in concentrations due to measuring (assay variability), errors in sample time collection, or errors occur due to model misspecification are termed residual variability (16). The IIV quantified in the PopPK model could be explained by including covariates, clinical or demographic, in the model. It helps in identifying the need for dose adjustments in specific populations such as pregnant women, pediatric patients, obese patients and critically ill patients with hepatic or renal impairment. The PopPK analysis is a widely accepted approach to optimize dosing regimens not only during drug development but also to improve dosing regimens of existing drugs and to individualize treatment in clinical settings (17). A total of 317 new drug applications (NDAs) and biological licensing applications (BLAs) submitted to the FDA over the period from 2012 to 2022 contained PopPK approaches (18).

1.3 PopPK Approaches

Several PopPK approaches exist, used for estimating PK parameters in a population. Namely, classical or traditional methods and direct PopPK methods.

1.3.1 Traditional PopPK Methods

Traditional methods require rich datasets with many samples per individual to describe a PK parameter. The PK parameter is estimated for each subject while the PopPK parameter is obtained from the central tendency such as the mean or median and a covariance matrix. The residual error, the difference between the model and data, for each subject originates from model misspecification, assay errors, measurement errors, dosing time, sampling time and dosage preparations. Among those discussed here are two classical or traditional approaches: the Standard two-stage (STS) and the iterative two-stage (ITS) method.

1.3.1.1 Standard Two-Stage (STS) Method

The STS is the traditional approach to estimating the average pharmacokinetic parameter of the population and producing reliable estimates only with a rich dataset, which is not feasible across populations. First, the PK parameters of each individual are estimated followed by a measurement of the central tendency and the variability of these parameters in a group of individuals (a population). Sometimes, a covariate is included in the PK model as the third step (19). In the case of rich datasets, where it is considered to be the gold standard, the STS method can estimate parameters similar to the direct PopPK methods (20,21) However, the occurrence of some level of overestimation in inter-individual variability is expected in this method (22). For sparse datasets, the direct PopPK method outperforms the STS method. The STS method would produce poor individual estimates even with as many as five samples per subject, and when combined with other individual parameter estimates to derive population estimates, they can potentially produce suboptimal and or biased results (19).

1.3.1.2 Iterative Two-Stage (ITS) Method

The ITS method can be used in rich, sparse or in a combination of rich and sparse datasets. *A priori* population model is required for the initiation of this method. The values can be obtained from the literature, naïve pooled data (performed with the same data) method or from the STS method providing substantial informative data is available (23). This initial PopPK model serves as the set

of prior distributions for the Bayesian estimation of individual parameters for all individuals (Stage 1) both for sparse and rich datasets. Following this, the PopPK parameters are reestimated based on these new individual parameters, creating a new set of prior distributions. (Stage 2). The Bayesian estimation step is repeated using the new model until more precise estimates of the individual parameters are obtained and the difference between new and old prior distributions becomes zero. Similar to STS, ITS methods also yield individual and population parameters and can be performed in software supporting least squares regression and Bayesian estimates.

1.3.2 Direct PopPK Methods

Direct PopPK methods can analyze data with fewer samples per individual by pooling it into one dataset. Generally, the direct method performs better than the traditional methods by generating population parameter estimates without prior knowledge (19). The direct PopPK approaches are naïve pooled data, nonlinear mixed-effect models and nonparametric approaches.

1.3.2.1 Naïve Pooled Data (NPD) Method

The NPD method is the direct PopPK method analyzing the data simultaneously. It is less sophisticated in estimating variability and residual error. The sparse data from various subjects is aggregated into a single dataset and treated as if the data originated from a single individual. The NPD method can be used when only one sample per individual is available.

The simplicity of this method is both its advantage and its disadvantage. It is simple to use and computationally efficient and is expected to describe the observations well. However, it has been shown to produce bias in the PK parameter estimate. The random effects between subjects, IIV, cannot be differentiated from the residual error due to the assumption in this method that the data originated from a single individual and consequently variance in the PK parameters is not estimated. Simulations have shown that the NPD method produces incorrect PK estimates and is considered inferior (19). For the successful application of this method, it is recommended that the goal of the study is an estimation of typical individual value and not the distribution i.e. the variance of individual parameters about typical population value.

1.3.2.2 Nonlinear Mixed-Effects (NLME) Modelling Approach

The longitudinal data or data with repeated measurement, such as PK and dose-response data are inherently nonlinear to a given response regression function (24). In the nonlinear mixed effect modelling approach, the “effects” refers to the elements that contribute to the variability of the measured observations and are categorized into fixed effects and random effects. Fixed effects refer to the parameters that define the structure of the PK model (25,26). These are the components used to estimate the typical values as shown in the following expressions.

$$p_i = \theta \quad \text{Eq (1)}$$

Where p_i is the individual parameter and θ is the typical population value. The random effects account for any unexplained variability and are categorized into interindividual variability and residual variability. Based on data visualization, experience and trial & error various random effects (interindividual variability) can be modelled using additive (Eq.1), constant (Eq.2) or exponential function (Eq.3) as shown below.

$$p_i = \theta + \eta_i \quad \text{Eq (2)}$$

$$p_i = \theta + (1 + \eta_i) \quad \text{Eq (3)}$$

$$p_i = \theta * e^{\eta_i} \quad \text{Eq (4)}$$

Interindividual variability (η) is assumed to follow a normal distribution with mean zero and variance (ω^2) as shown in Eq. 4

$$\eta_i \sim N(0, \omega^2) \quad \text{Eq (5)}$$

As previously stated, the residual error (ε) refers to the difference between the model-predicted and observed concentration and is distributed normally with mean zero and variance (σ^2), and represents sources of all unexplained errors (variability) that occurred during data collection, bioanalytical processes and model development (misspecification). The residual variability is determined using the following equations (Eq 5). The residual variability (Eq 5) can be estimated by proportional (Eq 6), additive (Eq 7) and or combined error models (Eq 8).

$$y - F = \text{Error} \quad \text{Eq (6)}$$

$$Y = F * (1 + \varepsilon(1)) \quad \text{Eq (7)}$$

$$y = F + \varepsilon(2) \quad \text{Eq (8)}$$

$$y = F * (1 + \varepsilon(1)) + \varepsilon(2) \quad \text{Eq (9)}$$

Where y ; is observed data, F ; is model predicted data, ε ; is Epsilon.

A general nonlinear mixed-effects (NLME) with constant variance is as follows:

$$y_{ij} = f(p_i, x_{ij}) + \varepsilon_{ij} \quad Eq (10)$$

$$p_i = A_i\theta + B_i\eta_i \quad Eq (10.1)$$

$$\varepsilon_{ij} \sim N(0, \sigma^2) \quad Eq (10.2)$$

Where y_{ij} ; is the j th response of the i th subject,
 f ; is the real-valued function of p_i and predictor parameter x_{ij} ,
 x_{ij} ; data matrix of individual specific predictor values,
 p_i ; vector of individual-specific model parameters,
 θ ; vector of fixed effect (modelling population parameter)
 η_i ; vector of multivariate normally distributed random effects of the i th subject,
 A_i ; design matrix for combining fixed effects,
 B_i ; design matrix for combining random effects,
 ε_{ij} ; represents error model assumed to be independent of η_i , identical and normally distributed,
 σ^2 ; Error variance is assumed to be constant across observations,

The model parameter of NLME (Eq10) is estimated by the maximum likelihood (27) based on the marginal density of y as shown in equation 11.

$$p(y|\theta, \sigma^2, \Psi) = \int p(y|\theta, \eta, \sigma^2)p(\eta|\Psi)d\eta \quad Eq (11)$$

Where y ; represents response data,
 θ ; vector of fixed effect,
 σ^2 ; error variance,
 Ψ ; covariance matrix of random effects,
 η ; vector of unobserved random effects,
 $p(y|\theta, \sigma^2, \Psi)$; marginal density of y ,
 $p(y|\theta, \eta, \sigma^2)$ and $p(\eta|\Psi)$; represent the conditional density of y given the random effects of η , and the prior distribution of η , respectively.

The most widely used software for applying the NLME modelling is NONMEM followed by Monlix and Phoenix NLME (28).

1.3.3 NONMEM

NONMEM analyses all data simultaneously and proves particularly useful for randomly collected sparse data. Despite pooling data into one dataset, the individual subjects are still recognizable allowing the collection of multiple observations per individual. The output of a NONMEM model

consists of parameter estimates of means, variances and covariances with an underlying assumption of the normal or log-normal distribution of parameters before estimation. As the name indicates, variability is defined as mixed effects, with a difference between fixed effects i.e. the typical or average value in the population and random effects i.e. variability around the typical or average value (29). Estimation of covariates balances the data by reducing the potential risk of biasedness while allocating patients to treatment groups. Apart from the estimation of typical parameters, NONMEM has Bayesian estimation capability for computing post hoc individual parameter estimates. These post hoc estimates can be calculated conventionally after the estimation of typical population estimates or can be iteratively estimated alongside typical population estimates. Various estimation methods used in NONMEM are described below.

1.3.3.1 First Order

The First Order (FO) was the first method employed in PopPK studies which could differentiate variability in parameters between subjects and variability during sample measurement (residual variability). The FO method was also able to relate PK/PD parameters with patient characteristics even when the data was sparse. The FO method could analyze the data without requiring high computational power and optimize the objective function without going through complex integrals for every subject and hence quickly analyze the data (30). The FO approximation does not directly calculate the marginal likelihood, instead, it transforms the NLME model to a linear mixed-effect model via Taylor series approximation around the mean of random (η) effects, typically assumed to be zero (31). The marginal likelihood is then computed, assuming the Gaussian distribution of the data (32). The FO approximation can serve as a tool to obtain initial parameter estimates that can be used as starting values for more precise estimation algorithms like First Order Conditional Estimation or Laplace approximation (31).

1.3.3.2 First Order Conditional Estimation

The FO method was fast but very approximate and gave inaccurate results when the residual error and IIV were large. The First Order Conditional Estimation (FOCE) method, also an approximation method, gives more accurate results for a larger range of problems. FOCE is described as a first-order Taylor series approximation of the NLME model around the posterior mode of random effects. Both FOCE and Laplace depend on conditional estimates of random effects (31). It is more complex than the FO approximation because it involves estimating the empirical Bayes estimate

during each iteration (28). The FOCE method takes into consideration the integral of all the individual parameter values (ETAs or random effects) for each subject's joint density of observed data and random effects in determining the best overall effects (THETAS, OMEGAs and SIGMAs). Due to integration, the FOCE method is more computationally expensive than the FO method. To reduce the computational expense, the FOCE method estimates the mode of the joint density and variances of ETAs. Unlike the FO method which linearizes both inter- and intra-subject variability, the FOCE method treats both the variabilities differently. With Gaussian function approximation, the FOCE method evaluates the inter-subject variability while linearizing the intra-subject variability (30). FOCE approximation can only be used for an additive error model (28).

1.3.3.3 Laplace Method

The Laplace method is named after Pierre-Simon Laplace. Unlike FO approximation where direct linearization is used to approximate likelihood, the Laplace method uses first order Laplace integral method (32). The Laplace method is similar to the FOCE method, both are referred to as conditional estimation algorithms, except the Laplace method uses a second-order derivative to approximate the likelihood function making it more accurate but computationally more expensive than the FOCE method. The Laplace method is used when dealing with the non-normal distribution of the observed data or when the prediction model imparts high nonlinearity to the joint density of the individual parameters (30).

1.3.3.4 First-Order Conditional Estimation with Interaction

The First-Order Conditional Estimation with Interaction (FOCEI) method is commonly used for estimation in NONMEM and is a method of choice for PopPK modelling. It is considered more robust, especially for the complex NLME models. FOCEI employs first-order approximation around individual estimates of the random effects with estimation of interaction between random effects and residual variability during the optimization process (33). Bea et al have reported that for an additive error model, both FOCE and FOCEI can be used. However, for other error models, the FOCEI method should be preferred (28).

1.3.4 Monolix

Monolix, MOdèles NOn LInéaires à effets miXtes, literally means nonlinear models with mixed effects in French was developed to model longitudinal data employing the stochastic approximation

expectation-maximization algorithm (34). The incorporation of numerous diagnostic tools (35) with its extension to left-censored data in NLME models (36) and automatic model-building procedures made Monolix faster to learn for the users.

Monolix is part of the MonolixSuite which comprises several interconnected software applications for modelling and simulation of which only Monolix carries NLME modelling. Monolix has an R Application Programming Interface and thus enables users to interact with R programming language scripts. Moreover, the R Speaks Monolix (Rslmx) package offers additional methods for model development and evaluation tools such as Bootstrap (37).

1.3.4.1 Stochastic Approximation Expectation-Maximization

The Stochastic Approximation Expectation-Maximization (SAEM) is an iterative and stochastic algorithm for computing maximum likelihood (ML) implemented in Monolix. The SAEM algorithm became part of the NONMEM estimation algorithms with Version 7. This algorithm is extremely efficient for the estimation of population parameters (35) for a wide variety of models including categorical data, censored data, count data, time-to-event data, stochastic differential equation-based models (38), discrete mixed hidden Markov models (39) and mixed-effects diffusion models (40). SAEM is a stochastic implementation of the Expectation-Maximization (EM) algorithm. The EM algorithm was developed to find ML in situations involving missing data (in the case of NLME modelling, the missing data are random effects). The E-step (expectation) involves determining the expected value of the likelihood given the observed data and the current estimate of the missing data. In the the M-step (maximization) the algorithm estimates the parameters that maximize this expected likelihood based on the E-step. The two steps iterate until convergence is achieved (31). Delyon et al (41) proposed a stochastic version of EM by replacing the expectation step of the EM algorithm with one iteration of the stochastic approximation procedure (42). Kuhn and Lavielle (34) integrated this stochastic EM algorithm with a Monte Carlo Markov Chain procedure for illustrating ML. Lavielle and Mentre (43) later demonstrated the method's effectiveness in estimating the PopPK of saquinavir in HIV patients. The SAEM may be particularly useful when the conditional algorithms i.e. FOCEI and Laplace fail to converge, as it always converges to a solution, is fast, and is relatively less sensitive to initial parameter choices (31).

SAEM can provide an estimator close to the ML estimation in a few iterations. Though iterative, it is still preferable to provide an initial guess to minimize the required number of iterations and increase the probability of converging to the global maximum of ML. However, it is not guaranteed that SAEM will consistently converge in all situations (38). SAEM convergence depends strongly on initial estimates when Likelihood has several local maxima. To find the global maxima of objective functions with multiple local maxima, Kirkpatrick (44) proposed simulated annealing, a probabilistic optimization method to find the global maxima, improving the convergence of the SAEM algorithm.

SAEM is an effective tool in population modelling and has been shown to estimate population parameters accurately (39,40,45–47). SAEM has subsequently been implemented in NONMEM, R (saemix package), and MATLAB (as the function `nlmefitsa`) (38).

1.4 Pharmacokinetic/Pharmacodynamic Indices

The integration of Pharmacokinetic/Pharmacodynamic (PK/PD), the dose-concentration relationship of the drug usually in plasma vs time and the concentration-effect relationship over time, can be obtained by developing hybrid PK/PD indices. PK/PD indices ensure the optimal drug concentrations in the body and susceptibility of respective pathogen-causing infections to clinically relevant breakpoints (48) which can be used for dose optimization. Before discussing PK/PD indices of antibacterial and antivirals in detail, the minimum inhibitory concentration and clinical breakpoints, and probability of target attainment will be introduced.

1.4.1 Minimum Inhibitory Concentration and Clinical Breakpoints

Minimum inhibitory concentration (MIC) has been the key parameter to quantify bacterial susceptibility to antibiotics by *in vitro* testing methods (49,50). MIC is the lowest concentration that inhibits the visible growth of bacteria after incubation of 18-24 hours at 35 °C with a standard inoculum of about 5×10^5 colony-forming units per milliliter (51). The less susceptible the pathogen to the antibiotic, the higher the MIC value.

MIC breakpoint was initially defined as a value that separates the susceptible and resistant strain of the bacteria after the use of an antibiotic, an approach now called epidemiologic cut-off value. In contrast, the clinical breakpoints take the shape of the PK profile of the antibiotic into account and not only the MIC distribution. The clinical breakpoint is obtained through observation from

clinical and experimental studies to establish a PD target that predicts the treatment response to patients. Based on clinical breakpoints, pathogens are classified as susceptible or resistant to antibiotics (49) serving as a guide for clinicians to identify dosing regimens against bacterial infection by differentiating between patients who are likely or unlikely to respond to the antibiotic dosing regimen (52).

The European Committee on Antimicrobial Susceptibility Testing (EUCAST) reports the MIC distributions of pathogens (53) and categorizes them as susceptible (S), susceptible at an increased dose (I) and resistant (R) [4]. Species-specific MIC breakpoints are provided based on the above three categories for an antibiotic against a microorganism and defined as ‘S breakpoint’, (isolates of the S and I category), and ‘R breakpoint’, (isolates of the I and R category) (54). In case of the absence of species-specific MIC breakpoints for a pathogen, non-species related PK/PD breakpoints (likewise: S and R breakpoints) of the antibiotic are provided (55). Though MIC provides a simple way of assessing potential therapeutic success, it does not consider the individual pharmacokinetics of patients which might be important, particularly for critically ill patients which may cause high pharmacokinetic (PK) variability resulting in over - or - underexposure.

1.4.2 Probability of Target Attainment

The probability of target attainment (PTA) is the probability of achieving a certain value of a PD index ($T > MIC$) at a certain MIC in Monte Carlo simulations (MCS) (60). The PTA analysis is a powerful tool for dose regimen selection of anti-infective drugs based on simulations. In PTA analysis, the drug concentration-time profile of individuals (e.g. 1000) is generated via MCS based on the NLME model and assessed for the attainment of a predefined PD target (e.g. %65 $T > MIC$) as shown in Fig 2.

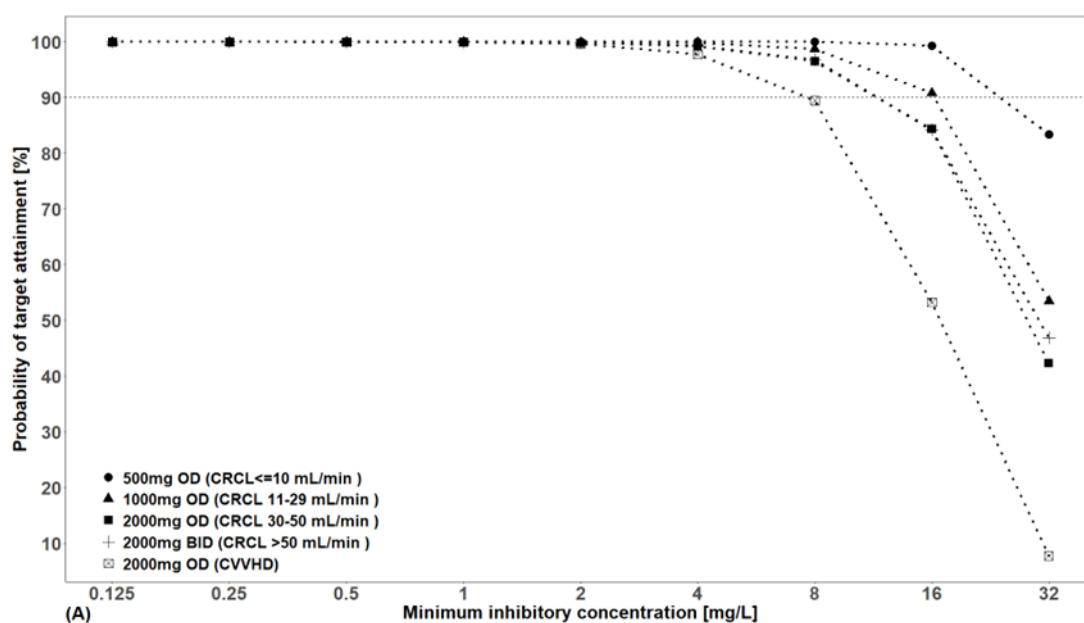


Fig 2. Probability of target attainment of cefepime (PD target % 65 $T_{>MIC}$) for MICs up to 32 mg/L for a range of dosing regimens based on creatinine clearance. OD, once a day, BID, twice a day, CVVHD; continuous venovenous hemodialysis

The PTA (%) is computed from the simulated subjects achieving the PD target and plotting or tabulating the PD index as a function of MIC for a range of dosing regimens of interest (66). A PTA of >90% is generally required, however, <90% is sometimes acceptable for poor tolerability of higher doses of the drug leading to adverse effects, low severity of the infection and or very few organisms with MIC at the upper end of the range (67). The PTA analysis is useful for identifying ineffective exposure or over-exposure of a standard dosing regimen and could be used to find alternative dosing regimens. Fig 2 shows the PTA versus MIC profile of different cefepime dosing regimens in renal impairment patients according to the Summary of Product Characteristics (68).

1.4.3 Antibacterials PK/PD indices

In terms of antibacterials, a PK/PD index may be defined as a quantitative relationship between a PK parameter such as the peak or highest concentration (C_{max}) or area under the concentration-time curve (AUC) and a microbiological parameter such as MIC (56). Based on the concentration or time-dependent antibacterial activity of antibiotics, PK/PD indices extensively used for various classes of antibiotics are AUC/MIC , C_{max}/MIC or fC_{max}/MIC and $T_{>MIC}$ or $fT_{>MIC}$ (57) (Fig 1.). The prefix f with PK/PD indices indicates the fraction of free or unbound drugs.

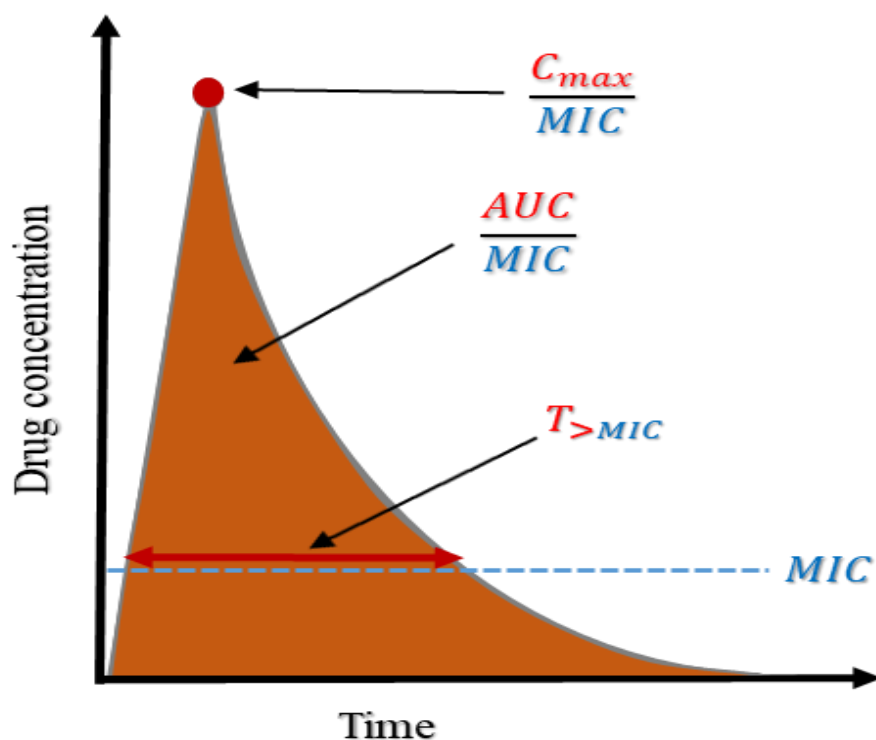


Fig 1. Graphical illustration of PK/PD indices. AUC, Area under the curve; C_{max}: Maximum concentration; MIC, Minimum inhibitory concentration; T>MIC, time that drug concentration exceeds the MIC

1.4.3.1 AUC/MIC

AUC/MIC is the ratio of area under the concentration-time curve to MIC for over 24 hours. It is easily calculated and appears to be the best index for both concentration-dependent antibiotics (58) such as fluoroquinolone and polymyxin (B, E[colistin]) and concentration and time-dependent antibiotics such as glycopeptide (vancomycin) (59).

1.4.3.2 C_{max}/MIC

C_{max}/MIC or *f*C_{max}/MIC is the ratio of free drug (*f*) peak concentration reached or estimated in the compartment of reference (e.g. plasma) typically over 24 hours divided by MIC (60,61). When the effect of antibiotic concentration dominates over time, the antibiotic displays concentration-dependent activity associated with free drug maximum concentration. The class of antibiotics which shows concentration-dependent killing characteristics is aminoglycosides (59). Generally, a C_{max}/MIC ratio of 8-10 is considered optimal for achieving antibacterial activity against Gram-negative bacteria. (62).

1.4.3.3 $T_{>MIC}$

$T_{>MIC}$ or $fT_{>MIC}$ is the cumulative percentage of 24 hours during which the unbound (f) drug concentration exceeds or remains above the MIC at steady-state PK conditions (61). An antibiotic shows a time-dependent effect when the effect of time is greater for a defined portion of the dosing interval above MIC. β -lactams antibiotics including penicillins, cephalosporins and carbapenems display a time-dependent antibacterial effect. For bacteriostatic effect, the free concentration must exceed the MIC for 35%–40%, 30% and 20% of the dosing interval for cephalosporins, penicillins and carbapenems, respectively. For bactericidal effect, the free concentration must exceed 60%–70%, 50% and 40%, respectively, for the same above-mentioned β -lactam classes (56)

1.4.4 Antiviral PK/PD Indices

The FDA recommends half-maximal inhibitory concentration/ concentration at half-maximum effect should be determined *in vitro* or animal model as an appropriate PD target to establish the efficacy of antiviral drugs (63). These models vary greatly depending on the virus type, antiviral agent, and the desired outcome (64). Antiviral PD is still variable and evolving. It has also been suggested to use EC_{95} as a PD parameter since the ultimate goal is complete eradication of the virus (65). For example, 80% $fT_{>EC95}$ has been linked to the efficacy of amprenavir (66).

Antiviral drug potency is commonly expressed using EC_{50} (50% effective concentration) or EC_{90} (90% effective concentration) and can be equivalent to MIC_{50} or MIC_{90} of antibacterial drugs, respectively (67). While EC_{90} is typically preferred, it may not be routinely reported and can only be inferred from EC_{50} under the conditions when the Hill coefficient is 1 (68). By linking the drug exposure parameters such as C_{max} , AUC and time above the measured potency to EC_{50} of the virus, the clinical effectiveness of the antiviral drugs can be predicted as the desired PK/PD indices (C_{max}/EC_{50} , AUC/EC_{50} and $T_{>EC50}$) (67). The time during which the free drug concentration remains above the measure of the potency of the drug, $T_{>EC50}$, of the drug to the virus may be most closely linked to the antiviral drug effect (e.g. amprenavir and zanamivir) (66,69). In this case, continuous infusion or drug administration with short dosing intervals may lead to maximal drug effects. Alternatively, the ratio of C_{max}/EC_{50} (e.g. for nelfinavir and remdesivir (70)) may be linked to the antiviral effect in this case least frequent administration with peak concentration results in the antiviral drug effect. When the continuous and fractioned doses have similar effects, then the PD

index of the ratio of AUC_{0-24}/EC_{50} (e.g. Oseltamivir and abacavir) is linked to the antiviral effect (71).

1.5 Investigated Agents

1.5.1 Cefiderocol

1.5.1.1 Chemical Structure and Mechanism of Action

Cefiderocol is the first antibiotic obtained by conjugation of a siderophore and a β -lactam ring. At the C-3 position, the pyrrolidinium group is linked with a catechol moiety, 2-chloro-3, 4-dihydroxybenzoic acid (Fig 3). Cefiderocol acts by binding to penicillin-binding proteins (PBPs) and inhibits bacterial cell wall synthesis (72). It employs the “Trojan horse mechanism”. The catechol group present in cefiderocol chelates with iron transporters of the bacteria which actively transport the antibiotic into bacterial cells (73).

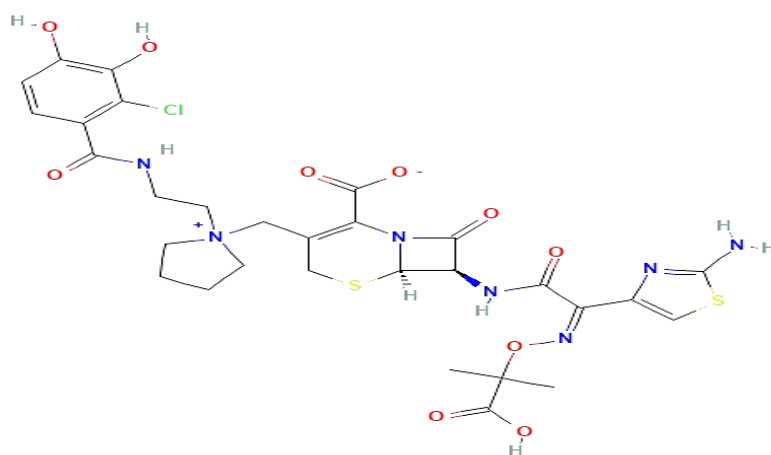


Fig 3. Chemical structure of cefiderocol (74)

1.5.1.2 Antibacterial Spectrum Therapeutic Indications

Cefiderocol has strong in vitro and in vivo activity against Gram-negative bacteria including carbapenem-resistant Enterobacteriaceae (75), and multidrug-resistant *Acinetobacter baumannii* and *Pseudomonas aeruginosa* (76). The pyrrolidinium at the C-3 position improves antibacterial activity and gives cefiderocol stability against β -lactamases while the carboxypropanoxyimino group at the C-7 position improves the transport of cefiderocol across the outer cell membrane [19]. The presence of catechol at C-3 is the key difference between cefiderocol and other cephalosporins.

It confers the siderophore activity by chelating with iron transporters. Bacterial strains with a deficiency in membrane iron transporters due to mutation show an increase in MIC i.e. ≥ 16 -fold (73). FDA and EMA approved cefiderocol in 2019 and 2020, respectively (77). Cefiderocol is effective in treating patients with pneumonia and bloodstream infections (BSI/sepsis) and complicated urinary tract infections (78). APEKS-cUTI and APEPKS-NP studies showed that cefiderocol is not inferior to imipenem-cilastatin and meropenem, respectively. In the CREDIBLE-CR study, a phase III clinical trial, cefiderocol showed similar clinical efficacy versus the best available therapy against infections caused by Gram-negative bacteria resistant to carbapenem (79).

1.5.1.3 Pharmacokinetics and Pharmacodynamics

Cefiderocol follows linear pharmacokinetics. The plasma protein binding is between 40% to 60% (80). The terminal elimination half-life ($t_{1/2}$) is 2 to 3 h (76). Cefiderocol is primarily excreted in urine with 60% to 70% unchanged. (72) and less than 10% excreted is metabolised (76). Dose adjustment is recommended for patients with poor kidney function. The recommended daily dose of cefiderocol is 2 g q8h with 3 h infusion for patients with CL_{CR} of >60 mL/min while the recommended dose for patients with CL_{CR} of 30-59 mL/min and 15-29 mL/min is 1.5 g q8h and 1 g q8h, respectively. In patients with ESRD, the recommended dose is 750 mg q12h. Cefiderocol shows time-dependent bacteriocidal activity similar to other β -lactam antibiotics. The % $T_{>MIC}$ best describe the efficacy of cefiderocol. (81). In the simulations for a dosing regimen of 2 g q8h with 3 h infusion with a PD target of 100% $T_{>MIC}$, the PTA was $>90\%$ for MIC of up to 4 μ g/mL for all infections except for BSI/sepsis patients (85%) (78).

1.5.2 Cefepime

1.5.2.1 Chemical Structure and Mechanism of Action

Cefepime belongs to the cephalosporin class of antibiotics which contains a six-member dihydro thiazine ring fused with a β -lactam ring forming a cephem skeleton (82). At position 7 of the cephem skeleton, cefepime has a methoxyimino group just like other third-generation cephalosporins (e.g. ceftriaxone, cefuroxime etc) (83). This modification gives cefepime stability against β -lactamases. It is different from third-generation cephalosporins by having positively charged N-methyl pyrrolidine substitution at position 3 of the cephem skeleton (Fig.4). This substitution gives cefepime the ability to penetrate the outer cell membrane of Gram-negative

bacteria rapidly. The intrinsic negatively charged carboxyl group and positively charged quaternary nitrogen group give cefepime its zwitterion property. Like other beta-lactam antibiotics, cefepime inhibits transpeptidases or PBPs, by binding to it and inhibits bacterial cell wall synthesis resulting in bacterial cell lysis and death (84). The molecular mass of cefepime is 480.6 and its formula is $C_{19}H_{24}N_6O_5S_2$ (85).

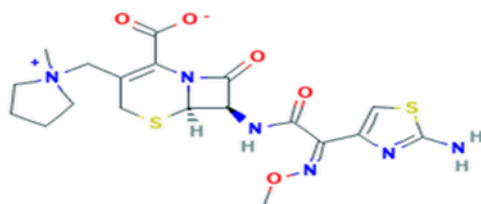


Fig 4. Chemical structure of cefepime (86)

1.5.2.2 Antibacterial Spectrum Therapeutic Indications

Cefepime, a fourth-generation broad-spectrum cephalosporin antibiotic, offers good activity both against Gram-positive and Gram-negative bacteria including *pseudomonas aeruginosa* (84). It is less prone to hydrolysis of AmpC-lactamases and shows strong activity against Enterobacteriaceae. Cefepime also exhibits strong activity against *haemophilus influenza* despite the production of β -lactamases. (87) However, cefepime is not as stable as carbapenems against extended-spectrum β -lactamases produced by *escherichia coli* and *klebsiella pneumonia* (88). The FDA and EMA have approved cefepime for the treatment of uncomplicated skin structure infections, uncomplicated and complicated urinary tract infections (UTIs), intra-abdominal infections, moderate to severe pneumonia and febrile neutropenia.(89).

1.5.2.3 Pharmacokinetics and Pharmacodynamics

Cefepime is administered parenterally primarily as an intravenous (IV) infusion over 30 to 60 minutes (90) or as a prolonged infusion from 3 to 24 hours (89). Studies have also reported over 3, 5, 10 or 15-minute IV push administration (91). C_{max} after IV administration is 2 to 3 times higher compared to intramuscular (IM) administration (92). When administered 2 g IV and IM dose, C_{max} is 137 ± 30.7 mg/L after 30 minutes compared with a C_{max} of 57.0 ± 9.50 mg/L after 90 (93,94). Moreover, cefepime has also been reported to be administered with subcutaneous infusion and appears to result in a PK profile similar to that of IM infusion (93,95). Cefepime is reasonably distributed in tissues and biological fluids (96) and has plasma protein binding ranging from

16-19% (90). The volume of distribution at a steady state varies between 18 to 22 litres and is not dependent on the dose (97). Cefepime clearance exhibits first-order kinetics and the drug is primarily excreted by the kidneys via glomerular filtration with at least 85% unchanged drug in urine (89). The $t_{1/2}$ of cefepime is approximately 2 hours in healthy subjects with normal renal function after IV administration (94). With the decrease in kidney function, the clearance decreases and $t_{1/2}$ increases proportionally. Creatinine clearance (CL_{CR}) is a good predictor of cefepime clearance and patients with low CL_{CR} may experience neurotoxicity with standard cefepime doses (98). On the other hand, patients with augmented renal clearance e.g. in cystic fibrosis have a shorter $t_{1/2}$ and high clearance leading to subtherapeutic plasma concentrations (89). The dose recommended by the manufacturer for adults with severe infection and renal impairment estimated by the Cockcroft-Gault equation is 2g q24h (30 to 60 mL/min), 1g q24h (11 to 29 mL/min) and 0.5g q24h (<10 mL/min) (99). The Cefepime dose approved by the FDA for infants between 2 to 12 months is 50 mg/kg every 8 to 12 hours (100). Hemodialysis removes cefepime and its clearance is proportional to the filter efficiency flow (101,102). Cefepime is not compatible with drugs such as vancomycin, gentamycin, tobramycin and theophylline (103).

Similar to other β -lactams, cefepime exhibits time-dependent antibacterial activity. $fT_{>MIC}$ of 40-70% is optimal for the pharmacodynamics (PD) activity of cefepime in murine models (89). In a clinical study of 36 patients, Tam et al. found microbiologic success associated with 100% $fT_{>MIC}$ (104). In patients with sepsis and the elderly, an $fT_{>MIC}$ threshold of 75–100% is found as a favorable predictor of treatment outcomes (105–107).

1.5.3 Rifampicin

1.5.3.1 Chemical Structure and Mechanism of Action

Rifampicin (Fig. 5) is a member of the rifamycin class of antibiotics derived from *Ammycolatopsis rifmaycinica* previously known as *ammycolatopsis mediterranei* and *streptomyces mediterranei*. It exhibits antibacterial activity by binding to the β -subunit of DNA-dependent RNA polymerase and suppressing its synthesis (108–111).

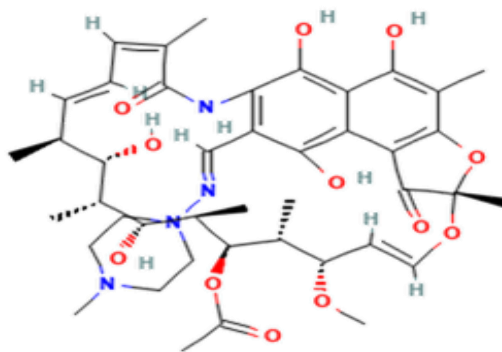


Fig 5. Chemical structure of Rifampicin (112)

1.5.3.2 Antibacterial Spectrum Therapeutic Indications

Rifampicin has bactericidal activity against *Mycobacterium* spp including *mycobacterium tuberculosis*, *mycobacterium avium-intracellulare complex* and *mycobacterium leprae*. Rifampicin is used as an alternative to doxycycline for the treatment of tick-borne pathogens such as *borrelia burgdorferi* and *anaplasma phagocytophilum*. It is used to treat brucellosis, legionnaires' disease and serious Gram-positive staphylococcal infections caused by *Staphylococcus aureus* and *Streptococcus pyogenes* in combination with other antibacterials. It is used against *Legionella pneumophila*, *Neisseria gonorrhoeae* and however, a susceptibility test is advised before treatment. It is used prophylactically for meningitis for individuals at risk of infections caused by Gram-negative bacteria *Neisseria meningitidis* and *Hemophilus influenza*. (113,114). Rifampicin is the first-line drug for the treatment of TB along with isoniazid, ethambutol and pyrazinamide and reduced treatment duration to six months by coadministering with pyrazinamide in the first two months (115). Rifampicin is also used in the treatment of leprosy along with dapsone, and clofazimine (116), pneumococcal meningitis in a combination of vancomycin (117), as well as Legionnaires disease caused by *Legionella* (113).

1.5.3.3 Pharmacokinetics and Pharmacodynamics

Rifampicin achieves a C_{max} of 10 mg/L after a single oral dose of 600 mg two hours of administration and has a half-life of 2.5 hours with the same dose. Peloquin et al have reported a serum rifampicin concentration between 8-24 mg/L 2 hours post-dose administration (118). Food when taken along with rifampicin lowered C_{max} by 22% (119). Rifampicin is primarily excreted by the liver and increases in the dose range from 300 to 450 mg, the liver's capacity to excrete the

the drug becomes saturated and any further increase in the dose leads to a more than proportional increase of the drug concentration in serum. Rifampicin exhibits autoinduction reducing the bioavailability of a single oral dose from 93% to 68% after multiple oral administration (120). Rifampicin is approximately 80% bound to blood plasma protein primarily to albumin. Rifampicin is well distributed to various tissues of the body with approximately 5% of the plasma concentrations crossing the blood-brain barrier and reaching cerebrospinal fluid (121). Rifampicin has a pronounced effect on the induction of CYP3A4 and could lead to subtherapeutic concentrations of drugs metabolized by CYP3A4 when administered concomitantly (122). It undergoes deacetylation in the liver forming the derivative desacetyl rifampicin which is more polar than rifampicin and also pharmacologically active (123).

Rifampicin exhibits concentration-dependent antibacterial activity. The work of Jayaram et al. (124) on the murine aerosol infection TB model found AUC/MIC to be the best PK/PD index for the rifampicin bactericidal activity. More recently Gumbo et al (125) using the *in vitro* TB model also found the PK/PD index of the AUC/MIC ratio to best correlate with the antibacterial activity of rifampicin while the fC_{max}/MIC ratio of ≥ 175 was associated with the prevention of resistance.

1.5.4 Remdesivir

Remdesivir was approved by the FDA on October 22, 2020, on conditional marketing authorization for adults and children aged ≥ 12 years weighing ≥ 40 kilograms for the treatment of the coronavirus disease outbreak in 2019 (COVID-19) which required hospitalization. The recommended dose is a loading dose of 200 mg IV infusion followed by a once-daily dose of 100 mg IV infusion for four days in patients not on mechanical ventilation or for 9 days in hospitalized patients on mechanical ventilation (126). Later on, on April 25, 2022, it was also approved for children ≥ 28 days old and weighing ≥ 3 kilograms, either hospitalized or non-hospitalized, exhibiting elevated risk for progression to severe COVID-19 i.e. prone to hospitalization or death. The recommended dose for pediatric patients (≥ 28 days and weighing < 40 -3 kilogram) was a single dose of 5 mg/kg IV infusion on day 1 with an additional dose of 2.5 mg/kg via IV infusion over 30 to 120 minutes (127).

1.5.4.1 Chemical Structure and Mechanism of Action

Remdesivir, chemically coded as GS-5734, is an adenosine (nucleoside) analog first reported for the treatment of the Ebola virus in 2016 (128). (Fig 6) (129). Inside the cell remdesivir, the single

diastereomer monophosphoramidate prodrug is metabolised first into GS-704277 (alanine metabolite), an intermediate metabolite, and later into monophosphate nucleoside analogue GS-441524. GS-441524 monophosphate is then phosphorylated to pharmacologically active triphosphate GS-443092. The GS-443092 competes with natural adenosine triphosphate (ATP) substrate selectively to inhibit the virus's RNA-dependent RNA polymerase resulting in delayed RNA chain termination during viral replication of Filoviridae virus (Ebola) and Coronaviridae including severe acute respiratory syndrome coronavirus (SARS-CoV, SARS-CoV-2) and Middle East respiratory syndrome coronavirus (MERS). Remdesivir and its metabolites GS-704277 and GS-441524 can be detected in plasma, but in blood, the active triphosphate GS-443092 can only be detected intracellularly in peripheral blood mononuclear cells (PBMCs) (130–132).

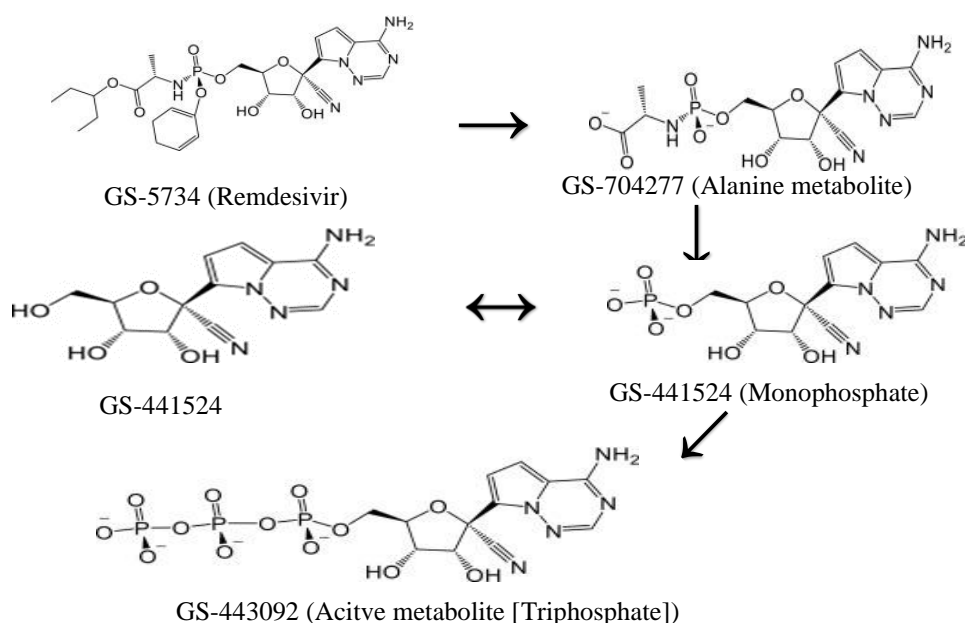


Fig 6. Schematic diagram and structures of remdesivir and metabolites ¹³⁸

1.5.4.2 Antiviral Spectrum

Remdesivir is a broad-spectrum antiviral drug and has shown activity against coronaviruses (MERS-CoV, SARS-CoV and SARS-CoV-2), filoviruses (Ebola virus and Marburg virus) and paramyxoviruses (Nipah virus and Hendra virus) (133). Remdesivir has shown effective treatment against ebola and nipha viruses in nonhuman primates.(134,135).

1.5.4.3 Pharmacokinetics and Pharmacodynamics

Oral administration of remdesivir is not suitable because of the extensive first-pass metabolism in the liver. In addition, the evaluation of intramuscular (IM) application in male rhesus monkeys was also suboptimal due to the variable and slow muscle release and the delayed appearance of the GS-443902 in PBMCs. The PK of the subcutaneous administration has yet to be assessed. Intravenous (IV) administration has delivered quickly and consistently GS-443902 into target cells and is therefore the preferred route of administration over IM. Remdesivir has a half-life ($t_{1/2}$) of approximately 1 hour following IV administration and quickly metabolised into intermediate, GS-704277, followed by the GS-441524 metabolite which has a $t_{1/2}$ of approximately 24.5 hours. The GS-441524 metabolite transforms into GS-443902, with an extended plasma $t_{1/2}$ of over 35 hours. This prolonged $t_{1/2}$ of the active triphosphate metabolite, GS-443902, supports the idea of once-daily administration and a loading dose of the remdesivir to achieve a steady state quickly (133). Remdesivir exhibits a moderate degree of protein binding in plasma with an unbound fraction of 12.1% in humans. On the contrary, GS-704277 and GS-441524 metabolites exhibit very low protein binding from all species with a mean unbound fraction ranging from 85% to 125. Remdesivir and its metabolite demonstrated dose proportional increase in exposure (AUC, C_{max}). In a single ascending dose study of 10 - 225 mg, C_{max} of remdesivir, GS-441524 and GS-704277 ranged from 57.5 - 4420 ng/mL, 3.20 - 257 ng/mL and 3.40 - 315.1 ng/mL, respectively. The AUC infinity also varied ranging from 230 - 5270 h.ng/mL, 55.2 - 7350 h.ng/mL and 11.1 - 807 h.ng/mL for remdesivir, GS-441524 and GS-704277, respectively. Remdesivir is widely distributed in most tissues including the liver and kidney. For the same ascending dose study mentioned above, the volume of distribution of remdesivir ranged from 45.1 to 73.4 L. The C_{max} of a single 75 mg 30 infusion in PBMCs was 3.3 μ M. This concentration was ~333 fold above the *in vitro* EC_{50} of 0.0099 μ M against SARS-CoV-2 in primary human airway epithelial cells after 48 hours of treatment (136). After a single 75 mg IV administration with 2 hours infusion and 30 minutes infusion in a healthy volunteer, the mean AUC of the triphosphate metabolite (GS-443902) in PBMC was 176 h. μ M and 394 h. μ M, respectively. Thus a shorter infusion time of remdesivir provided a higher concentration of the drug in PBMC (137). Remdesivir and its metabolites are primarily eliminated via the kidney (74%) and to a smaller extent in faeces (18%). After IV administration, 49% of the dose found in urine was the monophosphate GS-441524 metabolite followed by remdesivir with 10% (132). Remdesivir is dissolved in sulfobutylether- β -cyclodextrin to enhance its solubility

which is mainly excreted in urine (138,139). Remdesivir is not recommended for patients with severe kidney dysfunction i.e eGFR <30 mL/min (140,141) however, in a study conducted in ESRD patients infected with COVID-19, Sörgel et al reported that intermittent hemodialysis can prevent accumulation of GS-441524 (142). Choy et al have reported an EC₅₀ of 23.15 µM against SARS-CoV-2 fitting viral load in logarithm scale i.e. log₁₀ Tissue Culture Infective Dose 50/mL in Vero E6 cell line 48h post-infection (143) while in a recent study in the same cell line Wang et al have reported an EC₅₀ of 0.77 µM fitting viral load in linear scale i.e. the percentage of inhibition 48h post-infection (144).

The exposure-response relationship and time course of PD response of remdesivir and its metabolites is unknown (127).

2 Aims and Objectives

Overall, this research aimed to utilize pharmacometrics as a tool to improve the understanding of PK/PD of anti-infective drugs. The PopPk modelling and simulations approach was employed for dose optimization in critically ill patients and to find predictors of variability for dose individualization. The objectives of each project are described below.

Clinical Pharmacokinetics and Pharmacodynamics of Cefiderocol

The project (chapter 3) aimed to better understand the PK/PD of cefiderocol. The review discusses the PopPK models based on the data of recent clinical trials for dose optimization in patients with renal dysfunction. The review article aimed to provide a comprehensive summary of cefiderocol's safety, and efficacy compared with currently available antibiotics against infections caused by Gram-negative bacteria.

Cefepime Population Pharmacokinetics, Antibacterial Target Attainment, and Estimated Probability of Neurotoxicity in Critically Ill Patients

Pathophysiological changes in critically ill patients on co-medication for multiple diseases and renal impairment cause high variability in the pharmacokinetics of the drug resulting in over and or under exposure. The primary objective of this project (chapter 4) was to develop the PopPK model of cefepime to explore variability both inter-individual as well as inter-occasion variability and predictors of cefepime clearance. Moreover, the project aimed to do Monte Carlo simulations based on the PopPK model to optimize dosing regimens for cefepime efficacy and lower the risk of cefepime-induced neurotoxicity in patients with renal dysfunction.

Rifampicin Assessment of body mass-related covariates for rifampicin pharmacokinetics in healthy Caucasian volunteers

The project (chapter 5) aimed to assess the influence of body mass-related covariates on rifampicin's PK parameters utilizing the PopPK approach. The secondary objective was to explore the exposure to rifampicin for males and females using the best covariate model for dose individualization in patients treated with rifampicin.

A population pharmacokinetic model of remdesivir and its major metabolites based on published mean values from healthy subjects

Since limited information is available on pharmacokinetics of remdesivir and metabolites. This project (chapter 6) aimed to develop a PopPK model of remdesivir and its metabolites i.e. GS-704277 and GS-441524 to better understand its pharmacokinetic properties. The secondary objective was to conduct simulations based on the PopPK model to assess the recommended clinical doses of remdesivir for optimized dosing in patients with COVID-19 to avoid extreme exposure in patients with end-stage renal disease.

3 Clinical Pharmacokinetics and Pharmacodynamics of Cefiderocol

Muhammad Bilal^{1,2} Lobna El Tabei¹, Sören Büsker¹, Christian Krauss¹, Uwe Fuhr¹, Max Taubert¹

¹Department I of Pharmacology, Faculty of Medicine and University Hospital Cologne, Center for Pharmacology, University of Cologne, Gleueler Straße 24, 50931, Cologne, Germany.

²Department of Clinical Pharmacy, Institute of Pharmacy, University of Bonn, Bonn, Germany.

³Department I of Pharmacology, Faculty of Medicine and University Hospital Cologne, Center for Pharmacology, University of Cologne, Gleueler Straße 24, 50931, Cologne, Germany.
max.taubert@uk-koeln.de.

This is an open-access article under the terms of the Creative Commons Attribution 4.0 International License: <http://creativecommons.org/licenses/by-nc/4.0/>

Contribution: I designed the outline, performed the literature review, and finally wrote the manuscript with contributions from coauthors Lobna El Tabei, Sören Büsker, Christian Krauss, Uwe Fuhr and Max Taubert.

Introduction: Cefiderocol, previously known as S-649266, is a siderophore cephalosporin antibiotic developed by Shionogi & Co., Ltd, Japan (145). It was approved in the US (80) and Europe (146) in 2019 and 2020, respectively. Cefiderocol has a pyrrolidinium group at C-3 similar to cefepime and a carboxy propyl imino group at C-7 similar to ceftazidime (145). In addition, at the end of the C-3 side chain, the presence of the chlorocatechol group facilitates the transportation of the drug into bacterial cells (147). Cefiderocol has shown similar safety and efficacy to the best available therapy for the treatment of Gram-negative infections resistant to carbapenem (79).

Methods: The search was carried out in Google Scholar, PubChem, and PubMed between August 2020 and May 2021. The search included terms such as “cefiderocol”, “chemical structure”, “antimicrobial activity”, “pharmacokinetics”, “pharmacodynamics”, and “clinical trials”. The briefings of the FDA and EMA for cefiderocol were also included while writing this review article.

Results and Discussion: Cefiderocol has shown superior in-vitro activity against multi-drug resistant bacteria including *P. aeruginosa*, *A. baumannii* and Enterobacteriaceae compared to fluoroquinolones, carbapenems and other cephalosporins (145,148). It has shown more stability against *Klebsiella pneumoniae* carbapenemases compared to cefepime and meropenem (75). Cefiderocol uses the “Trojan horse” mechanism by chelating with iron transporters to enter bacterial cells and exert antibacterial activity (145).

Cefiderocol achieved a C_{max} of 153 mg/L and an AUC over the dosing interval was 366.5 mg h/L on day 10 following an IV administration of a 2000 mg q8h with 1h infusion in multiple ascending dose phase I study in healthy subjects. The time to reach C_{max} was 1 h (149). Cefiderocol is primarily eliminated in urine following linear kinetics with around 90% of the dose recovered unchanged. The plasma protein binding of cefiderocol is 57.8% (150). The $t_{1/2}$ of cefiderocol increased from 2.8 h in individuals with normal kidney function to 9.6 h in ESRD patients without dialysis, emphasizing that dosing should be based on renal function to achieve adequate therapeutic exposure (151,152). No clinically relevant drug-drug interactions of cefiderocol have been reported predominantly because of its no involvement with CYP enzymes and P-glycoprotein pathways

(153). A PopPK model with three compartments and linear elimination best describes the PK of cefiderocol with renal function as an important predictor of clearance (78,150,154). Cefiderocol shows time-dependent antibacterial activity and $fT_{>MIC}$ is the main predictor of the efficacy of cefiderocol (155,156). For patients with normal kidney function a dose of 2000 mg q8h with 3 h infusion for a PD target of 75% $fT_{>MIC}$ provided >90% PTA for MIC up to 4 mg/L. An increased dose frequency (q6h) is recommended for patients with augmented kidney function. The recommended cefiderocol dose for patients with moderate and severe renal function is 1500 mg q8h and 1000 mg q8h, respectively. For patients with ESRD, the recommended dose is 750 mg q12h. Hemodialysis removes approximately 60% of cefiderocol in 3 to 4 h (154). Cefiderocol was not inferior to imipenem/cilastatin (APEKS/cUTI study) and showed superiority based on post-hoc analysis for treating patients with cUTIs caused by bacteria susceptible to carbapenem (157). In a phase III clinical trial [APEKS-NP study] cefiderocol showed non-inferiority to meropenem in patients with nosocomial pneumonia infection (158). It had similar clinical and microbiological efficacy in treating bloodstream infections/sepsis, nosocomial pneumonia, and cUTI caused by Gram-negative bacteria resistant to carbapenems compared to the best available therapy (CREDIBLE-CR study) however, the mortality rate in the cefiderocol group was higher (34%) compared to best available therapy group (18%) (79). Due to a lack of data, the FDA and EMA provide no recommendation for cefiderocol in paediatric patients. However, a successful case has been reported in treating a 10-year-old patient with cystic fibrosis where cefiderocol was combined with meropenem/vaborbactam and bacteriophages for the treatment of drug-resistant *Achromobacter xylosoxidans* (159). Currently, human data on the use of cefiderocol in pregnancy and excretion into milk is not available however FDA and EMA labels recommend to use cefiderocol only if the benefits outweigh the potential risks (80,146).

Overall, cefiderocol provides an acceptable safety profile and favourable PK/PD properties, making it a promising choice to treat infections otherwise resistant to other antibiotics.

4 Cefepime Population Pharmacokinetics, Antibacterial Target Attainment, and Estimated Probability of Neurotoxicity in Critically Ill Patients

Muhammad Bilal ^{a,b}, Michael Zoller ^c, Uwe Fuhr ^a, Ulrich Jaehde ^b, Sami Ullah ^a, Uwe Liebchen ^c, Sören Büsker ^a, Johannes Zander ^d, Baharak Babouee Flury ^e, Max Taubert ^a

^a University of Cologne, Faculty of Medicine and University Hospital Cologne, Center for Pharmacology, Department I of Pharmacology, Cologne, Germany

^b Department of Clinical Pharmacy, Institute of Pharmacy, University of Bonn, Bonn, Germany

^c Department of Anaesthesiology, Hospital of the Ludwig Maximilians University of Munich, Munich, Germany

^d Laboratory of Dr. Brunner, Constance, Germany

^e Division of Infectious Diseases and Hospital Epidemiology, Kantonsspital St. Gallen, St. Gallen, Switzerland

Acknowledgement

Reproduced with permission from American Society of Microbiology

Contribution: I prepared and explored the dataset, developed a population pharmacokinetic model followed by covariate modelling and later performed Monte Carlo Simulations to assess the probability of target attainment and neurotoxicity and finally penned the manuscript.

Introduction: Cefepime is a fourth-generation cephalosporin antibiotic with a broad antibacterial spectrum both against Gram-positive and or Gram-negative bacteria (160) making it a drug of choice for patients in intensive care units (ICUs) (161). The pathophysiology of critically ill patients in ICU causes high variability in the PK of the drug resulting in over or under-exposure to the drug (162). In patients with normal kidney function, more than 80% of the drug is eliminated unchanged in urine (90). Dose adjustment is recommended for patients with creatinine clearance (CL_{CR}) below 60 mL/min (162). The efficacy of the cefepime is best described by the time-dependent, PK/PD index (163). In literature PD targets, ranging from $>50\% fT_{>MIC}$ to $100\% fT_{>4 \times MIC}$ have been reported (164–168). Patients with renal dysfunction are prone to cefepime-induced neurotoxicity (169). Various thresholds have been reported for cefepime-induced neurotoxicity based on plasma trough concentrations (170–172). The study aimed to identify a dosing regimen to minimize the neurotoxicity risk of cefepime while achieving a sufficient PTA.

Methods: The clinical study (ClinicalTrials.gov; NCT01793012) was conducted at University Hospital, Ludwig-Maximilians-Universität München, Germany. A total of 14 ICU patients with four patients on continuous venovenous hemodialysis (CVVHD) received a cefepime median dose of 2000 mg as a 30-minute IV infusion following local guidelines. Blood samples were collected for four consecutive days. A PopPK model was developed using NLME modelling software NONMEM with the FOCEI estimation method. A separate clearance was estimated for patients with CVVHD. For covariate modelling, covariates such as sex, age, and body weight along with serum creatinine, measured creatinine clearance (mCL_{CR}) and eCL_{CR} were tested on clearance and the volume of distribution. The goodness of fit (GOF) plots, bootstrap and prediction corrected visual predictive check (pcVPC) were used for model analysis. Monte Carlo simulations were performed using the mrgsovl package in R excluding CVVHD subjects. Cefepime doses up to 6,000 mg with continuous infusion and with dosing intervals of q8h, q12h, and q24h for CL_{CR} ranging from 0 to 150 mL/min were simulated. Two different PD targets of $65\% T_{>MIC}$ and $100\% T_{>2 \times MIC}$ with a PTA of 90% were selected. The MIC ranged from 2 to 16 mg/L. For the assessment

of neurotoxicity, the model developed by Boschung-Pasquier et al. based on plasma trough concentrations was used.

Results: A two-compartment model with linear elimination best described the 344 plasma cefepime concentrations. IIV was significant on clearance (CL) and volume of distribution. IOV when estimated on clearance of non-dialysis patients (CL_{ND}) was significant and improved the model. During the covariate analysis, eCL_{CR} was significant on the CL_{ND} . Based on plasma trough concentrations, prolonged dosing intervals i.e. q24h and q12h lowered the risk of neurotoxicity but also decreased efficacy i.e. higher daily doses were required to cover the same MIC target. The overall improvement in efficacy-versus-neurotoxicity risk was marginal. However, based on average plasma concentrations, an increase in the dosing intervals to q12h and q24h would deteriorate the balance of efficacy-versus-neurotoxicity risk. In comparison to q24h, q12h and q8h administration, simulations for continuous infusion (CI) predicted higher efficacy with a lower daily dose. It is important to consider kidney function while dosing cefepime and daily dosing with q8h should be preferred over prolonged dosing intervals to achieve a higher PD target and reduce neurotoxicity risk.

Discussion: Our PopPK model proposed a dosing regimen to balance the cefepime-induced neurotoxicity and its efficacy based on renal function. CI provided the best results followed by a shorter dosing interval of q8h for intermittent infusion (30 min). A two-compartment model with linear elimination from the central compartment with eCL_{CR} as a covariate on CL_{ND} best described the data. Despite its limitations, eCL_{CR} is a widely accepted marker for assessing renal function (173). In the literature, plasma trough concentrations have been used mainly to assess cefepime-induced neurotoxicity. Using the same logistic regression model (171) we performed simulations based on both plasma trough and average concentrations considering the exposure between the dosing intervals is not meaningless. We found out that irrespective of the concentrations used shorter dosing intervals of q8h provide better results in balancing the efficacy versus the risk of neurotoxicity relationship compared to prolonged dosing intervals. In our study, for eCL_{CR} of 120 mL/min and a PD target of 100% $T_{>2 \times MIC}$ with PTA of 90%, a dose of 1300 mg q8h covered MICs up to 2 mg/L and predicted a $\leq 20\%$ neurotoxicity risk. For the same eCL_{CR} group, Cheng et al suggested a dose of 1000 mg q8h to achieve a 40 to 44% probability of efficacy (taking 100% $T_{>MIC}$ with a MIC of 8mg/L as an efficacy target) and 1 to 6% of probability of

toxicity (taking a trough concentration of ≥ 20 mg/L as the toxicity target). The model was able to predict the dosing regimen to balance the efficacy versus neurotoxicity relationship. Further evaluations in larger groups with experimental PD assessment are needed to further explore the optimal dosing of cefepime in critically ill patients.

5 Rifampicin Assessment of body mass-related covariates for rifampicin pharmacokinetics in healthy Caucasian volunteers

Muhammad Bilal^{1, 2*}, Sami Ullah¹, Ulrich Jaehde², Christina Trueck¹, Dario Zaremba¹, Bertil Wachall³, Manfred Wargenau⁴, Bernhard Scheidel⁵, Martin H. J. Wiesen⁶, Malaz Gazzaz⁷, Chunli Chen^{1,8}, Sören Büsker¹, Uwe Fuhr¹, Max Taubert¹, Charalambos Dokos¹

¹ Department of Pharmacology, Faculty of Medicine and University Hospital Cologne, University of Cologne, Cologne, Germany

² Department of Clinical Pharmacy, Institute of Pharmacy, University of Bonn, Bonn, Germany

³ InfectoPharm Arzneimittel und Consilium GmbH, 64646 Heppenheim, Germany

⁴ M.A.R.C.O. GmbH & Co. KG, Düsseldorf, Germany

⁵ ACC GmbH Analytical Clinical Concepts, Leidersbach, Germany

⁶ Pharmacology at the Laboratory Diagnostics Centre, Therapeutic Drug Monitoring, Faculty of Medicine and University Hospital Cologne, University of Cologne, Cologne, Germany

⁷ Department of Clinical Pharmacy, College of Pharmacy, Umm Al-Qura University, Makkah, Saudi Arabia

⁸ Heilongjiang Key Laboratory for Animal Disease Control and Pharmaceutical Development, College of Veterinary Medicine, Northeast Agricultural University, 600 Changjiang Road, Xiangfang District, Harbin 150030, PR China

This is an open-access article under the terms of the Creative Commons Attribution 4.0 International License: <http://creativecommons.org/licenses/by-nc/4.0/>

Contribution: I prepared and explored the dataset, developed a population pharmacokinetic model followed by covariate modelling, and later performed simulations to assess the exposure of rifampicin in males and females and the effect of fat-free mass on the exposure of rifampicin, and I finally penned the manuscript.

Introduction: Rifampicin has been one of the key anti-tuberculosis (TB) drugs since its introduction in the late 1960s. It suppresses RNA synthesis in *Mycobacterium tuberculosis* by inhibiting DNA-dependent RNA polymerase (109). It has been adjusted to body weight (BW) dosing like some other anti-TB drugs by the World Health Organisation (174). However, research has reported that fat-free mass (FFM) is a better body size descriptor than BW, particularly with higher doses where high inter-individual variability (IIV) in rifampicin exposure is expected (175). It has also been reported that rifampicin clearance in females is lower than in males (176) The study aimed to apply the PopPK approach to assess the PK variability of rifampicin in healthy Caucasian individuals, identify the best body size predictor for exposure to rifampicin, and assess sex differences between males and females in the absence of auto-induction after single-dose administration.

Methods: BERIFA (EUDRACT-No: 2017–004418-24) was a phase I/IV open-label, cross-over, randomized bioequivalence study conducted at University Hospital Cologne, Germany. The study was conducted on 24 (11 males / 13 females) healthy Caucasian volunteers, each receiving a single oral 600 mg tablet of rifampicin either test or reference separated by a wash-out period of at least 9 days. A total of 20 samples per subject per day were obtained. For NLME modelling, the Monolix software 2023R1 (Lixoft®, Antony, France) was used. For decisions between non-nested models, the Corrected Bayesian Information Criterion (BICc) was used. IIV and IOV were tested on all PK parameters empirically. Covariate analysis was carried including the identity of rifampicin preparations along with age, sex, BW, FFM, body height (BH), body mass index (BMI), and body surface area (BSA). FFM was calculated using a semi-mechanistic model reported by Janmahasatian et al by incorporating sex, BW and BH (177). Diagnostic plots such as GOF plots, VPC, bootstrap, and statistical significance such as a decrease in objective function value (OFV) of 3.84 ($P < 0.05$) for forward inclusion and an increase in the OFV of 10.8 ($P < 0.001$) for backward elimination were the criteria for selecting final covariate model. MCS was performed for the base and final covariate model to explore the exposure of rifampicin using the mrgsove package in R.

Results: A total of 912 (median 8.19 mg/L) observed concentrations were best described by a zero-order absorption (Tk0) model with lag time (Tlag), one distribution compartment model and a nonlinear (Michaelis-Menten [MM]) elimination. IIV was significant on maximum elimination rate (V_{\max}/F) and volume of distribution (V/F). IOV was significant on V_{\max}/F , V/F , and Tlag Tk0 including a correlation between Tk0 and Tlag. An error model of combined additive and proportional error best explained the residual unexplained variability. FFM was the best covariate model followed by the BW+sex covariate model decreasing the OFV by 56.4 and 51.2 points, respectively. The decrease in IIV on V_{\max}/F in both covariate models was almost similar. MCS showed a reduced exposure to rifampicin in males compared to females with the same BW and BH and a decrease in overall exposure to higher FFM.

Discussion: We found that FFM followed by a combination of BW and sex explained the variability in PK of rifampicin better than the current well-established BW alone for dosing rifampicin. Rifampicin models reported in the literature vary in absorption (174,176,178,179), distribution (180–182) and elimination (183,184). In our model, a Tk0 with Tlag, and one-compartment model and MM elimination best described the data. Oral administration with liquid preparation of rifampicin achieved higher bioavailability compared to capsules and tablets (185). However, the identity (test or reference) rifampicin preparations in our study did not influence the PK parameters including absorption. The exposure of rifampicin increases more than linearly after dose administration (186) with saturable elimination being the reason (123) which is also confirmed by our results. Autoinduction was not observed in our model due to single-dose administration. FFM performed better than other covariates testing in our evaluation. It is based on a semi-mechanistic model (177) by incorporating sex, BW and BH and partially accounts for body composition however it does not distinguish between muscle and fat mass. Moreover, the experimental procedures used to find FFM are complex and/or costly and do not apply to populations including the elderly, children and some disease states (187). Using covariates such as sex, BW and BH which are available without further assumptions has the advantage of easy implementation. In conclusion, estimated FFM is the primary biological covariate to explain IIV in PK of rifampicin confirming previous findings in the African population (183) but needs to be further studied in Asian and Caucasian patients treated with rifampicin.

6 A population pharmacokinetic model of remdesivir and its major metabolites based on published mean values from healthy subjects

Ahmed Abouellil^{1,2}, Muhammad Bilal^{1,3}, Max Taubert¹, Uwe Fuhr¹

¹ Faculty of Medicine, Center for Pharmacology, Department I of Pharmacology, University Hospital Cologne, University of Cologne, Gleueler Straße 24, 50931 Cologne, Germany

² Immunosensation Cluster of Excellence, University Hospital Bonn, Bonn, Germany

³ Department of Clinical Pharmacy, Institute of Pharmacy, University of Bonn, Bonn, Germany

This is an open access article under the terms of the Creative Commons Attribution-4.0 International License: <http://creativecommons.org/licenses/by-nc/4.0/>

Contribution: I extracted and explored the data of remdesivir and its metabolites from the publication and developed an initial population pharmacokinetic model in NONMEM. The first author, Ahmad Abouellil, further developed the model in Monolix and wrote the initial draft of the manuscript. I finally reviewed the manuscript. All co-authors agree with the publication being used for the doctoral thesis.

Introduction: Remdesivir was the first medicine approved conditionally for the treatment of severe coronavirus disease (SARS-CoV-19) in 2020 by FDA and EMA (188,189). Later its use was expanded to non-hospitalized adults and pediatric patients for the treatment of mild to moderate SARS-CoV-19 infection (190). Remdesivir is a broad-spectrum antiviral drug originally tested against the Ebola virus disease (191) and showed strong activity against SARS-CoV-19 in both in vitro and animal models (188). Remdesivir is a prodrug and goes under extensive metabolism, producing GS-704277, an intermediate metabolite, followed by nucleoside analog GS-441524, both of which are quantifiable from plasma (192). The antiviral activity of remdesivir is attributed to its nucleoside analogue which inhibits viral RNA polymerase (137). The information on PK of remdesivir and its metabolites is scarce. This study aimed to develop a PopPK model to describe the PK parameters of remdesivir and its metabolites GS-704277 and GS-441524 and to determine suitable dosing regimens for patients.

Method: Arithmetic-concentration data was extracted using GetData Graph Digitizer software from published placebo-controlled randomized phase I single and multiple dose ascending remdesivir clinical trials conducted by the manufacturer Gilead Sciences, Inc., USA. In study 1, a single-dose study, 9 dose cohorts of remdesivir were administered at doses ranging from 3 mg to 225 mg over 120-min (cohort 1-8) and 30-min (cohort 9) IV infusion. In study 2, multiple dose study, subjects received 150 mg IV remdesivir over 60-min daily for 7 days in cohort 1 and 14 days in cohort 2. The published article lacked individual parameters for each dose cohort (193). A sharp increase in concentrations of remdesivir was observed following the end of the IV infusion. It was assumed that the IV line was washed with normal saline at the end of the infusion. To accommodate this sudden increase in the concentration, 4% of the administered dose was subtracted and was administered instantaneously at the end of infusion. A PopPK model was developed using Monolix (Lixoft, Antony, France). Since the data lacked inter-individual values, so inter dose cohorts variability was estimated. The final model was selected based on the physiological plausibility,

the goodness of fit plots and visual predictive check. Simulations were performed in Simulx (Lixoft, Antony, France) for 200 mg 30 min IV infusion on day 1 followed by 100 mg 30 min IV infusion for the next four days as recommended in Summary of Product Characteristics (194).

Results: A two-compartment model with first-order elimination from central compartments for remdesivir and its metabolites best described the data. The metabolism was assumed to occur in the central and peripheral compartments of remdesivir and the central compartment of GS-704277. The inter-cohort variability was estimated on the central and peripheral volume of distribution of GS-441524, on clearance of remdesivir and GS-704277 from the central compartment, and on metabolic formation clearance of GS-772477 and GS-442524 metabolites. Simulations following the 200 mg recommended loading dose showed that the C_{\max} for remdesivir, GS-704277 and GS-441525 were 13,700 μM , 807 μM and 726 μM , respectively. GS-704277 achieved t_{\max} at the end of infusion (30 min) while GS-221524 achieved t_{\max} 1 h after infusion.

Discussion: A PopPK model of metabolite GS-221524 only is reported by Sukeishi et al. in Japanese patients with renal dysfunction with an estimated glomerular filtration rate affecting the clearance of GS-221524 (195). We developed a PopPK model for remdesivir and its metabolites and estimated inter-dose variability using the NLME modelling approach. The model estimated a similar PK profile (C_{\max} , AUC and elimination half-life) of remdesivir, GS704277 and GS-441524 to previously published PK non-compartmental analysis of remdesivir (137,196). Our model was able to incorporate sequential metabolism from remdesivir to GS-704277 and then to GS441542 similar to the reported metabolic fate of remdesivir (193,197). The reported EC_{50} value of 180 nM in primary human airway epithelial cells infected with SARS-CoV-19 for GS-441524 (198) was achieved in 20 min following administration of 200 mg loading dose in our simulations suggesting to avoid high doses in patients with renal dysfunction. A possible reason could be that the inter-dose cohort variability estimated in mean concentrations estimated in our model might be magnitude lower than variability at the individual level in patients. Further investigations on individual levels for drug concentrations are needed to better understand the PK of remdesivir and its metabolites for which this model serves as a good starting point.

7 Summary

The main objective of this research work was to apply pharmacometrics as a tool to improve the dosing of anti-infective drugs in healthy volunteers and diseased populations. Population pharmacokinetic models were developed to describe unexplained variability of pharmacokinetic parameters followed by simulations for dose optimization. The results of each project are summarized below.

Clinical Pharmacokinetics and Pharmacodynamics of Cefiderocol

A comprehensive literature review on the pharmacokinetics and pharmacodynamics of cefiderocol was performed. Cefiderocol is a novel siderophore cephalosporin antibiotic approved in 2019 and 2020, respectively by the FDA and EMA for treating complicated urinary tract infections, pneumonia and blood-stream infections caused by Gram-negative bacteria (80,146).

Cefiderocol is obtained by conjugation of the β -lactam group with a siderophore. It is similar in structure to cefepime by having a pyrrolidinium group at C-3 and to ceftazidime by having a carboxy propyl imino group at C-7. Cefiderocol employs a “Trojan horse mechanism” to enter bacterial cell. The catechol moiety attached at the C-3 position chelates with iron which actively transports cefiderocol into bacterial cell where it inhibits bacterial cell wall synthesis by binding to PBPs. Cefiderocol has shown strong in vitro antibacterial activity against Gram-negative bacteria including the multi-drug resistant strains of *A.baumannii* and *P. Aeruginosa* (73).

Cefiderocol follows linear pharmacokinetics with 58% binding to plasma protein and primarily eliminated by the kidneys with around 90% of the drug recovered unchanged in the urine (199). The $t_{1/2}$ in patients with normal kidney function is around 2 to 3 h which increases to 9.6 h in patients with ESRD without hemodialysis (200). Cefiderocol do not interact with CYP enzymes and shows no clinically relevant drug-drug interactions (201). A three-compartment PopPK model best described the PK of cefiderocol with kidney function as a predictor of cefiderocol clearance (202). It shows time-dependent antibacterial activity. The recommended cefiderocol dose for patients with normal, moderate and severe renal function is 2000 mg, 1500 mg and 1000 mg q8h with 3 h infusion, respectively. While for ESRD patients the recommended dose is 750 mg q12h (203).

Cefiderocol was not inferior to imipenem/cilastatin in phase II clinical trials (APEKS-cUTI) and showed superiority based on post-hoc analysis for treating patients with urinary tract infections caused by bacteria susceptible to carbapenem (157). In the phase III clinical trial (APEPKS-NP), cefiderocol was non-inferior to meropenem in treating patients with nosocomial pneumonia (158). In another phase-III clinical trial, CREDIBLE-CR, cefiderocol showed similar clinical efficacy to the best available therapy for treating Gram-negative infections resistant to carbapenem (79). However, data on other populations including pregnant and breastfeeding women, and geriatric and pediatric patients is scarce. The evaluations suggested that cefiderocol dosing needs to be adjusted according to renal function to achieve adequate therapeutic exposure (150). Approximately 60% of the drug was removed in end-stage renal disease undergoing hemodialysis (204). The linear (predictable) pharmacokinetics, low potential for drug-drug interactions, acceptable safety profile and favorable pharmacokinetics and pharmacodynamics properties make cefiderocol a viable alternative to treat infections caused by multi-drug resistant Gram-negative bacteria.

Cefepime Population Pharmacokinetics, Antibacterial Target Attainment, and Estimated Probability of Neurotoxicity in Critically Ill Patients

Cefepime is a fourth-generation cephalosporin antibiotic approved by EMA and FDA in 1993 and 1996, respectively for the treatment of pneumonia, urinary tract infections, skin infections, intra-abdominal infections, and febrile neutropenia caused by both Gram-positive and Gram-negative bacteria (160,205,206).

Cefepime exhibits linear pharmacokinetics and has a low protein binding affinity of less than 20%. It is widely distributed in the body and is primarily eliminated via kidneys with more than 80% of the drug eliminated unchanged. The $t_{1/2}$ is approximately 2.5 h (90). The efficacy of cefepime is best described by $fT_{>MIC}$ (163). Pathophysiological changes may cause pharmacokinetic variability resulting in under and or over-exposure of the drug in critically ill patients. It has been reported that about 15% of patients in critical care units experience one or another symptom of cefepime-induced neurotoxicity (207). Although cefepime-induced neurotoxicity can be reversed once the drug is discontinued and or after hemodialysis however its recognition is difficult due to comorbidities and or due to adverse effects of other concomitant administered drugs.

The population pharmacokinetic model of cefepime quantified the pharmacokinetic variability and explored the predictor (estimated creatinine clearance) of clearance in critically ill patients. An outcome during model development of cefepime was that inter-individual variability estimated on clearance was 89% in the base model supporting the concept of individualized dosing in critically

ill patients. Taking each administration as a separate occasion, when tested on clearance of non-dialysis patients, was found to be highly significant indicating variability during treatment in intensive care unit patients with critical illness. Developing a population pharmacokinetics model with estimated creatinine clearance as a covariate explained the variability of clearance over time. Cefepime has been linked with neurotoxicity (207). This emphasizes the need to determine the optimal dosing of cefepime to balance efficacy and cefepime-induced neurotoxicity. Monte Carlo Simulations were performed by incorporating the logistic regression model of neurotoxicity to predict the neurotoxicity of cefepime based on both trough and average plasma concentrations. Monte Carlos Simulations suggested that a q8h dosing is a suitable choice offering a low risk of neurotoxicity and higher efficacy compared to q12h and q24h. A dose of 1333 mg q8h with an estimated creatinine clearance of 120 mL/min would achieve a probability of target attainment of 90% for a pharmacodynamic target of $100\% fT_{>2 \times MIC}$ with a probability of neurotoxicity less than 20% and cover minimum inhibitory concentrations up to 2 mg/L. Continuous infusion was found to be superior to other dosing regimens including q8h. It provided higher efficacy and lower risk of neurotoxicity with the same daily dose. In conclusion, it is important to take kidney function into account and a higher frequency (q8h) should be preferred while dosing cefepime. The study had a small sample size, heterogeneity in the patient population i.e. some patients were on dialysis, and lack of pharmacodynamic data to directly link cefepime concentrations and probability of neurotoxicity. Further evaluations are needed in large groups including pharmacodynamic data to explore the optimal dosing and the relationship between exposure and the probability of neurotoxicity of cefepime.

Rifampicin Assessment of body mass-related covariates for rifampicin pharmacokinetics in healthy Caucasian volunteers

Since its introduction in 1968 for the treatment of tuberculosis, rifampicin has been administered based on body weight (208,209). However, fat-free mass has been reported to be a better size descriptor (210).

A population pharmacokinetic model was developed based on data obtained from a bioequivalence study in healthy Caucasian volunteers. The two periods were assumed as two different occasions. Inter-individual variability was significant on maximum elimination rate and volume of distribution whereas inter-occasional variability was significant for zero-order absorption, lag time, maximum elimination rate and volume of distribution. Covariates such as body weight, fat-free mass, body

height, body mass index, body surface area, sex and identity of the preparation (test or reference) were tested on pharmacokinetic parameters to identify the best body size descriptor to explain variability in pharmacokinetic parameters of rifampicin. The test or reference formulations did not influence pharmacokinetic parameters including absorption. Fat-free mass was the best size descriptor followed by sex and body weight covariates. The decreased inter-individual variability in both models was almost similar. Body surface area, body weight only, body mass index, body height and sex were also significant covariates when tested but to a lesser extent than fat-free mass and body weight and sex.

Simulations based on the fat-free mass covariate model for both males and females with respective typical body weight and height showed that exposure to rifampicin decreased with an increase in fat-free mass and overall exposure in females was higher than in typical males for when using standard dosing. This indicates that sex could also be relevant for optimizing the dosing of rifampicin, either directly with body weight or indirectly via fat-free mass. The study was designed to assess the bioequivalence of two rifampicin preparations with a single oral 600 mg dose administration thus auto-induction of rifampicin was not considered during modelling. It was concluded that body mass composition should be considered for individualized dosing of rifampicin. Estimated fat-free mass is the best size descriptor for dosing rifampicin as reported previously in tuberculosis patients in African populations (183) but needs to be further evaluated in patients with other populations for the treatment of tuberculosis.

A population pharmacokinetic model of remdesivir and its major metabolites based on published mean values from healthy subjects

Remdesivir was one of the authorized antiviral medications during the COVID-19 pandemic approved in October 2020 with limited known pharmacokinetic information (192). The mean concentration-time profile of remdesivir and its metabolites i.e. GS-704277 and GS-441524 was obtained from published phase I clinical trials. Due to a lack of individual data, the inter-dose cohort variability was evaluated.

A PopPK model with two compartments for remdesivir and its metabolites with sequential metabolism best explained the data. The model assumed the metabolism of remdesivir to occur in both central and peripheral compartments to the intermediate metabolite GS-704277 and subsequent metabolism of GS-704277 to GS-441524 in the central compartment of GS-704277. The clearance of the parent drug (remdesivir) and both the metabolites occurred from the central

compartment. The simulations based on clinically recommended doses i.e. 200 mg loading dose followed by 100 mg dose revealed that the concentrations of the metabolite GS-441524 in plasma exceeded the reported EC_{50} values for primary human airway epithelial cells infected with SARS-CoV-19 indicating that the recommended doses of remdesivir effectively inhibit the SARS-CoV-19. Further studies should investigate the variability in concentrations at the individual patient level to better understand the pharmacokinetics of remdesivir and its metabolites. The model can be used to inform future studies on dosing remdesivir and to establish the relationship between the pharmacokinetics of remdesivir and its clinical efficacy in critically ill patients to avoid extreme exposure, especially in patients with end-stage renal disease.

In summary, this work demonstrates the potential of pharmacometrics in improving our understanding of the pharmacokinetics of cefiderocol, cefepime, rifampicin and remdesivir. The population pharmacokinetics models developed explained the variability in pharmacokinetic parameters and aided in identifying sources of these variabilities. Simulations based on population pharmacokinetic models supported the dose individualization of these anti-infective drugs.

8 References

1. Preijers T, Muller AE, Abdulla A, de Winter BCM, Koch BCP, Sassen SDT. Dose Individualisation of Antimicrobials from a Pharmacometric Standpoint: The Current Landscape. *Drugs* [Internet]. 2024;(0123456789). Available from: <https://doi.org/10.1007/s40265-024-02084-7>
2. Powers JH. Antimicrobial drug development - The past, the present, and the future. *Clin Microbiol Infect*. 2004;10(4):23–31.
3. Rayner CR, Smith PF, Andes D, Andrews K, Derendorf H, Friberg LE, et al. Model-Informed Drug Development for Anti-Infectives: State of the Art and Future. *Clin Pharmacol Ther*. 2021;109(4):867–91.
4. Tyson RJ, Park CC, Powell JR, Patterson JH, Weiner D, Watkins PB, et al. Precision Dosing Priority Criteria: Drug, Disease, and Patient Population Variables. *Front Pharmacol*. 2020;11(April):1–18.
5. Luterbach CL, Rao GG. Use of pharmacokinetic/pharmacodynamic approaches for dose optimization: a case study of plazomicin. *Curr Opin Microbiol* [Internet]. 2022;70:102204. Available from: <https://doi.org/10.1016/j.mib.2022.102204>
6. Trivedi A, Lee RE, Meibohm B. Applications of pharmacometrics in the clinical development and pharmacotherapy of anti-infectives. *Expert Rev Clin Pharmacol*. 2013;6(2):159–70.
7. McComb M, Bies R, Ramanathan M. Machine learning in pharmacometrics: Opportunities and challenges. *Br J Clin Pharmacol*. 2022;88(4):1482–99.
8. Wagner JG. History of pharmacokinetics. *Pharmacol Ther*. 1981;12(3):537–62.
9. Sheiner LB, Steimer JL. Pharmacokinetic/Pharmacodynamic Modeling in Drug Development. *Annu Rev Pharmacol Toxicol*. 2003 Nov 28;40:67–95.
10. Beare LZ, Jerry C, Furst DE, Izarter JG, Iadko T, Kodman JH, et al. Opportunities for integration of pharmacokinetics, pharmacodynamics, and toxicokinetics in rational drug development. In: *Clinical Pharmacology & Therapeutics*. 1991. p. 465–73.
11. Gobburu JVS. Pharmacometrics 2020. *J Clin Pharmacol*. 2010;50(9):151–7.
12. Benet LZ, Rowland M. Pharmacometrics: A New Journal Section. *J Pharmacokinetics Biopharm*. 1982;10(3).
13. Aarons L. Population pharmacokinetics: theory and practice. *Br J Clin Pharmacol*. 1991;32(6):669–70.
14. FDA. Guidance for Industry Population Pharmacokinetics. *FDA Guid*. 1999;(February):31.
15. Lesko LJ, Schmidt S. Individualization of drug therapy: History, present state, and opportunities for the future. *Clin Pharmacol Ther*. 2012;92(4):458–66.
16. Mould DR, Upton RN. Basic Concepts in Population Modeling, Simulation, and Model-

- Based Drug Development—Part 2: Introduction to Pharmacokinetic Modeling Methods. *CPT Pharmacometrics Syst Pharmacol* [Internet]. 2013 Apr [cited 2022 Oct 20];2(4):e38. Available from: /pmc/articles/PMC3636497/
17. de Velde F, Mouton JW, de Winter BCM, van Gelder T, Koch BCP. Clinical applications of population pharmacokinetic models of antibiotics: Challenges and perspectives. *Pharmacol Res* [Internet]. 2018;134(May):280–8. Available from: <https://doi.org/10.1016/j.phrs.2018.07.005>
 18. Hsu L-F, Tw LO. A Survey of Population Pharmacokinetic Reports Submitted to the USFDA: An Analysis of Common Issues in NDA and BLA from 2012 to 2021. *Clin Pharmacokinet*. 123AD;61:1697–703.
 19. Carter AA, Rosenbaum SE, Dudley MN. Review of methods in population pharmacokinetics. *Clin Res Regul Aff*. 1995;12(1):1–21.
 20. Talmage D. Egan, M.D.; Harry J. M. Lemmens, M.D.; Pierre Fiset, M.D.; David J. Hermann, Pharm.D.; Keith T. Muir, Ph.D.; Donald R. Stanski, M.D.; Steven L. Shafer MD. The Pharmacokinetics of the New Short-acting Opioid Remifentanyl (GI87084B) in Healthy Adult Male Volunteers. *Anesthesiology*. 1993;79:881–92.
 21. Gilman TM, Brunnemann SR, Segal JL. Comparison of population pharmacokinetic models for gentamicin in spinal cord-injured and able-bodied patients. *Antimicrob Agents Chemother*. 1993;37(1):93–9.
 22. Sheiner LB, Beal SL. Evaluation of methods for estimating population pharmacokinetic parameters II. Biexponential model and experimental pharmacokinetic data. *J Pharmacokinet Biopharm*. 1981;9(5):635–51.
 23. Steimer JL, Mallet A, Golmard JL, Boisvieux JF. Alternative approaches to estimation of population pharmacokinetic parameters: Comparison with the nonlinear mixed-effect model. *Drug Metab Rev*. 1984;15(1–2):265–92.
 24. Lee SY, Xu L. Influence analyses of nonlinear mixed-effects models. *Comput Stat Data Anal*. 2004;45(2):321–41.
 25. Whiting B, Kelman AW, Grevel J. Population Pharmacokinetics Theory and Clinical Application. *Clin Pharmacokinet*. 1986;11(5):387–401.
 26. Sheiner LB, Rosenberg B, Marathe V V. Estimation of population characteristics of pharmacokinetic parameters from routine clinical data. *J Pharmacokinet Biopharm*. 1977;5(5):445–79.
 27. Pinheiro JC, Bates DM, Journal S, Statistics G, Mar N, Pinheiro JC, et al. Interface Foundation of America Approximations to the Log-Likelihood Function in the Nonlinear Mixed-Effects Model Institute of Mathematical Statistics , and Interface Foundation of America Stable URL : <http://www.jstor.org/stable/1390625> Linked reference. 2016;4(1):12–35.
 28. Bae KS, Yim DS. R-based reproduction of the estimation process hidden behind NONMEM® part 2: First-order conditional estimation. *Transl Clin Pharmacol*.

- 2016;24(4):161–8.
29. Goutelle S, Woillard JB, Buclin T, Bourguignon L, Yamada W, Csajka C, et al. Parametric and Nonparametric Methods in Population Pharmacokinetics: Experts' Discussion on Use, Strengths, and Limitations. *J Clin Pharmacol*. 2022;62(2):158–70.
30. Bauer RJ. NONMEM Tutorial Part II: Estimation Methods and Advanced Examples. *CPT Pharmacometrics Syst Pharmacol*. 2019;8(8):538–56.
31. Bonate PL. *Pharmacokinetic-Pharmacodynamic Modeling and Simulation*. Second Edi. Basic Pharmacokinetics. Springer; 2011.
32. Nyberg J. Practical Optimal Experimental Design in Drug Development and Drug Treatment using Nonlinear Mixed Effects Models [Internet]. 2011. Available from: <http://repositorio.unan.edu.ni/2986/1/5624.pdf%0Ahttp://fiskal.kemenkeu.go.id/ejournal%0Ahttp://dx.doi.org/10.1016/j.cirp.2016.06.001%0Ahttp://dx.doi.org/10.1016/j.powtec.2016.12.055%0Ahttps://doi.org/10.1016/j.ijfatigue.2019.02.006%0Ahttps://doi.org/10.1>
33. Waroonrat Sukarnjanaset TW, Sutep Jarurattanasirikul. Evaluation of FOCEI and SAEM Estimation Methods in Population Pharmacokinetic Analysis Using NONMEM_ Across Rich, Medium, and Sparse Sampling Data. *Eur J Drug Metab Pharmacokinet*. 2018;43:729–36.
34. Kuhn E, Lavielle M. Maximum likelihood estimation in nonlinear mixed effects models. *Comput Stat Data Anal*. 2005;49(4):1020–38.
35. Lavielle M, Ribba B. Enhanced Method for Diagnosing Pharmacometric Models: Random Sampling from Conditional Distributions. *Pharm Res* [Internet]. 2016;33(12):2979–88. Available from: <http://dx.doi.org/10.1007/s11095-016-2020-3>
36. Samson A, Lavielle M, Mentré F. Extension of the SAEM algorithm to left-censored data in nonlinear mixed-effects model: Application to HIV dynamics model. *Comput Stat Data Anal*. 2006 Dec 1;51(3):1562–74.
37. Traynard P, Ayrat G, Twarogowska M, Chauvin J. Efficient Pharmacokinetic Modeling Workflow With the MonolixSuite: A Case Study of Remifentanyl. *CPT Pharmacometrics Syst Pharmacol*. 2020 Apr 1;9(4):198–210.
38. Lavielle M. *Mixed Effects Models for the Population Approach*. Mixed Effects Models for the Population Approach. 2014.
39. Delattre M, Lavielle M. Maximum likelihood estimation in discrete mixed hidden Markov models using the SAEM algorithm. *Comput Stat Data Anal* [Internet]. 2012;56(6):2073–85. Available from: <http://dx.doi.org/10.1016/j.csda.2011.12.017>
40. Delattre M, Lavielle M. Coupling the SAEM algorithm and the extended Kalman filter for maximum likelihood estimation in mixed-effects diffusion models. *Stat Interface*. 2013;6(4):519–32.
41. Delyon B, Lavielle M, Moulines E. Convergence of a stochastic approximation version of the EM algorithm. *Ann Stat*. 1999;27(1):94–128.

42. Allasonnière S, Chevallier J. A new class of stochastic EM algorithms. Escaping local maxima and handling intractable sampling. *Comput Stat Data Anal.* 2021;159.
43. Lavielle M, Mentré F. Estimation of population pharmacokinetic parameters of saquinavir in HIV patients with the MONOLIX software. *J Pharmacokinet Pharmacodyn.* 2007;34(2):229–49.
44. Kirkpatrick S. Optimization by Simulated Annealing: Quantitative Studies. *J Stat Phys.* 1984;34:975–86.
45. Delattre M, Savic RM, Miller R, Karlsson MO, Lavielle M. Analysis of exposure-response of CI-945 in patients with epilepsy: Application of novel mixed hidden Markov modeling methodology. *J Pharmacokinet Pharmacodyn.* 2012;39(3):263–71.
46. Makowski D, Lavielle M. Using SAEM to estimate parameters of models of response to applied fertilizer. *J Agric Biol Environ Stat.* 2006;11(1):45–60.
47. Chan PLS, Jacqmin P, Lavielle M, McFadyen L, Weatherley B. The use of the SAEM algorithm in MONOLIX software for estimation of population pharmacokinetic-pharmacodynamic-viral dynamics parameters of maraviroc in asymptomatic HIV subjects. *J Pharmacokinet Pharmacodyn.* 2011;38(1):41–61.
48. Dasgupta A. Usefulness of monitoring free (unbound) concentrations of therapeutic drugs in patient management. *Clin Chim Acta.* 2007;377(1–2):1–13.
49. Nielsen EI, Friberg LE. Pharmacokinetic-pharmacodynamic modeling of antibacterial drugs. *Pharmacol Rev.* 2013;65(3):1053–90.
50. Balouiri M, Sadiki M, Ibnsouda SK. Methods for in vitro evaluating antimicrobial activity: A review. *J Pharm Anal* [Internet]. 2016;6(2):71–9. Available from: <http://dx.doi.org/10.1016/j.jpha.2015.11.005>
51. Schmidt S, Barbour A, Sahre M, Rand KH, Derendorf H. PK/PD: new insights for antibacterial and antiviral applications. *Curr Opin Pharmacol.* 2008;8(5):549–56.
52. Macgowan AP, Wise R. Current procedures for establishing individual breakpoints. *J Antimicrob Chemother.* 2001;48(Suppl. S1):17–28.
53. EUCAST database: Antimicrobial wild type distributions of microorganisms [Internet]. Available from: <https://mic.eucast.org>
54. EUCAST. European Committee on Antimicrobial Susceptibility Testing Breakpoint tables for MICs Version 12.0. 2022;
55. Turnidge J, Paterson DL. Setting and revising antibacterial susceptibility breakpoints. *Clin Microbiol Rev.* 2007;20(3):391–408.
56. Hoo GSR, Liew YX, Kwa ALH. Optimisation of antimicrobial dosing based on pharmacokinetic and pharmacodynamic principles. *Indian J Med Microbiol* [Internet]. 2017;35(3):340–6. Available from: http://dx.doi.org/10.4103/ijmm.IJMM_17_278
57. Mouton JW, Dudley MN, Cars O, Derendorf H, Drusano GL. Standardization of

- pharmacokinetic/pharmacodynamic (PK/PD) terminology for anti-infective drugs: An update. *J Antimicrob Chemother.* 2005;55(5):601–7.
58. Corvaisier S, Maire PH, Bouvier D'Yvoire MY, Barbaut X, Bleyzac N, Jelliffe RW. Comparisons between antimicrobial pharmacodynamic indices and bacterial killing as described by using the Zhi model. *Antimicrob Agents Chemother.* 1998;42(7):1731–7.
59. Kuti JL. Optimizing Antimicrobial Pharmacodynamics: a Guide for Your Stewardship Program. *Rev Medica Clin Las Condes* [Internet]. 2016;27(5):615–24. Available from: <http://dx.doi.org/10.1016/j.rmcl.2016.08.001>
60. Rodríguez-Gascón A, Solinís MÁ, Isla A. The role of pk/pd analysis in the development and evaluation of antimicrobials. *Pharmaceutics.* 2021;13(6):1–27.
61. Mouton JW, Dudley MN, Cars O, Derendorf H, Drusano GL. Standardization of pharmacokinetic/pharmacodynamic (PK/PD) terminology for anti-infective drugs. *Int J Antimicrob Agents.* 2002;19(4):355–8.
62. Burgess DS. Use of pharmacokinetics and pharmacodynamics to optimize antimicrobial treatment of *Pseudomonas aeruginosa* infections. *Clin Infect Dis.* 2005;40(SUPPL.).
63. Bravo FJ, Cardin RD, Bernstein DI. A model of human cytomegalovirus infection in severe combined immunodeficient mice. *Antiviral Res.* 2007;76(2):104–10.
64. Pg M, Ls Y, Rowe M, Ho-yen D, J CPS. Techniques in Molecular Medicine. *Tech Mol Med.* 1999;162–4.
65. Drusano GL, Bilello JA, Preston SL, O'Mara E, Kaul S, Schnittman S, et al. Hollow-fiber unit evaluation of a new human immunodeficiency virus type 1 protease inhibitor, BMS-232632, for determination of the linked pharmacodynamic variable. *J Infect Dis.* 2001;183(7):1126–9.
66. Preston SL, Piliero PJ, Bilello JA, Stein DS, Symonds WT, Drusano GL. In Vitro-In Vivo Model for Evaluating the Antiviral Activity of Amprenavir in Combination with Ritonavir Administered at 600 and 100 Milligrams, Respectively, Every 12 Hours. *Antimicrob Agents Chemother.* 2003;47(11):3393–9.
67. Chaira T, Subramani C, Barman TK. ADME, Pharmacokinetic Scaling, Pharmacodynamic and Prediction of Human Dose and Regimen of Novel Antiviral Drugs. *Pharmaceutics.* 2023;15(4).
68. Zeitlinger M, Koch BCP, Bruggemann R, De Cock P, Felton T, Hites M, et al. Pharmacokinetics/Pharmacodynamics of Antiviral Agents Used to Treat SARS-CoV-2 and Their Potential Interaction with Drugs and Other Supportive Measures: A Comprehensive Review by the PK/PD of Anti-Infectives Study Group of the European Society of Antimicrob. *Clin Pharmacokinet* [Internet]. 2020;59(10):1195–216. Available from: <https://doi.org/10.1007/s40262-020-00924-9>
69. Brown AN, McSharry JJ, Weng Q, Adams JR, Kulawy R, Drusano GL. Zanamivir, at 600 milligrams twice daily, inhibits oseltamivir-resistant 2009 pandemic H1N1 influenza virus in an in vitro hollow-fiber infection model system. *Antimicrob Agents Chemother.*

2011;55(4):1740–6.

70. Arshad U, Pertinez H, Box H, Tatham L, Rajoli RKR, Curley P, et al. Prioritization of Anti-SARS-Cov-2 Drug Repurposing Opportunities Based on Plasma and Target Site Concentrations Derived from their Established Human Pharmacokinetics. *Clin Pharmacol Ther.* 2020;108(4):775–90.
71. McSharry JJ, Drusano GL. Antiviral pharmacodynamics in hollow fibre bioreactors. *Antivir Chem Chemother.* 2011;21(5):183–92.
72. Ito, A, Sato T, Ota M, Takemura M NT, Toba S, Kohira K, Miyagawa S, Ishibashi N, Matsumoto S, Nakamura R, Tsuji M YY. In Vitro Antibacterial Properties of Cefiderocol, a Novel Siderophore Cephalosporin, against Gram-Negative Bacteria. *Antimicrob Agents Chemother.* 2018;3(1):1–11.
73. Sato T, Yamawaki K. Cefiderocol: Discovery, Chemistry, and in Vivo Profiles of a Novel Siderophore Cephalosporin. *Clin Infect Dis.* 2019;69(Suppl 7):S538–43.
74. Summary of product characteristics of Fetroja. 2020.
75. Naoki Kohira, Joshua West, Akinobu Ito, Tsukasa Ito-Horiyama, Rio Nakamura, Takafumi Sato, Stephen Rittenhouse, Masakatsu Tsuji YY. In vitro antimicrobial activity of a siderophore cephalosporin, S-649266, against Enterobacteriaceae clinical isolates, including carbapenem-resistant strains. *Antimicrob Agents Chemother.* 2016;60(2):729–34.
76. Pharmacokinetics, Safety, and Tolerability of Cefiderocol, a Novel Siderophore Cephalosporin for Gram-Negative Bacteria, in Healthy Subjects - PubMed [Internet]. [cited 2020 Dec 1]. Available from: <https://pubmed.ncbi.nlm.nih.gov/29311072/>
77. Bilal M, El Tabei L, Büsker S, Krauss C, Fuhr U, Taubert M. Clinical Pharmacokinetics and Pharmacodynamics of Cefiderocol. *Clin Pharmacokinet* [Internet]. 2021;60(12):1495–508. Available from: <https://doi.org/10.1007/s40262-021-01063-5>
78. Kawaguchi N, Katsube T, Echols R, Wajima T. Population Pharmacokinetic and Pharmacokinetic/ Pharmacodynamic Analyses of Cefiderocol, a Parenteral Siderophore Cephalosporin, in Patients with Pneumonia, Bloodstream Infection/Sepsis, or Complicated Urinary Tract Infection Nao. *Antimicrob Agents Chemother.* 2021;65(3):1–13.
79. Bassetti M, Echols R, Matsunaga Y, Ariyasu M, Doi Y, Ferrer R, et al. Efficacy and safety of cefiderocol or best available therapy for the treatment of serious infections caused by carbapenem-resistant Gram-negative bacteria (CREDIBLE-CR): a randomised, open-label, multicentre, pathogen-focused, descriptive, phase 3 trial. *Lancet Infect Dis* [Internet]. 2021;21(2):226–40. Available from: [http://dx.doi.org/10.1016/S1473-3099\(20\)30796-9](http://dx.doi.org/10.1016/S1473-3099(20)30796-9)
80. Shionogi & Co. Ltd. Structured product label of Fetroja. 2020. https://www.accessdata.fda.gov/drugsatfda_docs/label/2020/209445s0021bl.pdf.
81. Mohammad Saydur Rahman Y-SK. A Novel Antibiotic Agent, Cefiderocol, for Multidrug-Resistant Gram-Negative Bacteria. *J Bacteriol Virol.* 2020;50(4):218–26.
82. Martín JF, Ullán R V., García-Estrada C. Regulation and compartmentalization of β -lactam

biosynthesis. *Microb Biotechnol*. 2010;3(3):285–99.

83. Chaudhry SB, Veve MP, Wagner JL. Cephalosporins: A Focus on Side Chains and β -Lactam Cross-Reactivity. *Pharmacy*. 2019;7(3):103.
84. Kessler RE. Cefepime microbiologic profile and update. *Pediatr Infect Dis J*. 2001;20(3):331–6.
85. Hardin TC, Pharm D, Jennings TS, Pharm D. Cefepime. 1994;
86. National Center for Biotechnology Information (2024). PubChem Compound Summary for CID 5479537, Cefepime. Retrieved April 25, 2024 from <https://pubchem.ncbi.nlm.nih.gov/compound/Maxipime>.
87. Tristram S, Jacobs MR, Appelbaum PC. Antimicrobial resistance in *Haemophilus influenzae*. *Clin Microbiol Rev*. 2007;20(2):368–89.
88. Paterson DL, Bonomo RA. Clinical Update Extended-Spectrum Beta-Lactamases : a Clinical Update. *Clin Microbiol Rev*. 2005;18(4):657–86.
89. Pais GM, Chang J, Barreto EF, Stitt G, Downes KJ, Alshaer MH, et al. Clinical Pharmacokinetics and Pharmacodynamics of Cefepime. *Clin Pharmacokinet* 2022 617 [Internet]. 2022 Jun 29 [cited 2023 May 15];61(7):929–53. Available from: <https://link.springer.com/article/10.1007/s40262-022-01137-y>
90. Okamoto MP, Nakahiro RK, Chin A, Bedikian A. Cefepime Clinical Pharmacokinetics. *Clin Pharmacokinet*. 1993 Nov;25(2):88–102.
91. Garrelts JC, Wagner DJ. The pharmacokinetics, safety, and tolerance of cefepime administered as an intravenous bolus or as a rapid infusion. *Ann Pharmacother*. 1999;33(12):1258–61.
92. Okamoto MP, Nakahiro RK, Chin A, Bedikian A, Gill MA. Cefepime: A new fourth-generation cephalosporin. *Am J Hosp Pharm*. 1994;51(4):463–77.
93. Barbhaiya RH, Knupp CA, Tenney J, Martin RR, Weidler DJ, Pittman KA. Safety, Tolerance, and Pharmacokinetics of Cefepime Administered Intramuscularly to Healthy Subjects. *J Clin Pharmacol*. 1990;30(10):900–10.
94. Barbhaiya RH, Forgue ST, Gleason CR, Knupp CA, Pittman KA, Weidler DJ, et al. Pharmacokinetics of cefepime after single and multiple intravenous administrations in healthy subjects. *Antimicrob Agents Chemother*. 1992;36(3):552–7.
95. Okamoto, Mark P.; Gill, Mark A.; Nakahiro, Randall K.*; Chin, Alfred; Yellin, Albert E.†; Berne, Thomas V.†; Sclar, David A.‡; Knupp, Catherine A.§; Heseltine, Peter N. R.†; Appleman MD. Tissue Concentrations of Cefepime in Acute Cholecystitis Patients. *J Pain Symptom Manage*. 2005;30(2):170–4.
96. Okamoto, Mark P.; Gill, Mark A.; Nakahiro, Randall K.*; Chin, Alfred; Yellin, Albert E.†; Berne, Thomas V.†; Sclar, David A.‡; Knupp, Catherine A.§; Heseltine, Peter N. R.†; Appleman MD. Tissue Concentrations of Cefepime in Acute Cholecystitis Patients. *Ther Drug Monit*. 1992;14:220–5.

97. Infectieus M, Jules I. Pharmacokinetics of cefepime: a review. 2000;(1993):103–15.
98. Chapuis TM, Giannoni E, Majcherczyk PA, Chiroléro R, Schaller MD, Berger MM, et al. Prospective monitoring of cefepime in intensive care unit adult patients. *Crit Care*. 2010;14(2):1–10.
99. Product Information: Maxipime®, cefepime hydrochloride for injection. (Revised December 2003). Princeton, NJ: Bristol-Myers Squibb Company.
100. Capparelli E, Hochwald C, Rasmussen M, Parham A, Bradley J, Moya F. Population pharmacokinetics of cefepime in the neonate. *Antimicrob Agents Chemother*. 2005;49(7):2760–6.
101. Rasluni H. Barbhaiya, PhD, Catherine A. Knupp, DVM M, S. Thomas Forgue, PhD, Gary R. Matzke, PharmD, David R. P. Guay P, and Kenneth A. Pittman P. Pharmacokinetics of cefepime in subjects with renal insufficiency. *Clin Pharmacol Ther*. 1990;48:268–78.
102. Maynor LM, Carl DE, Matzke GR, Gehr TWB, Farthing C, Farthing D, et al. An in vivo - in vitro study of cefepime and cefazolin dialytic clearance during high-flux hemodialysis. *Pharmacotherapy*. 2008;28(8):977–83.
103. Baririan N, Chanteux H, Viaene E, Servais H, Tulkens PM. Stability and compatibility study of cefepime in comparison with ceftazidime for potential administration by continuous infusion under conditions pertinent to ambulatory treatment of cystic fibrosis patients and to administration in intensive care units. *J Antimicrob Chemother* [Internet]. 2003 Mar 1 [cited 2023 Feb 2];51(3):651–8. Available from: <https://pubmed.ncbi.nlm.nih.gov/12615867/>
104. Tam VH, McKinnon PS, Akins RL, Rybak MJ, Drusano GL. Pharmacodynamics of cefepime in patients with Gram-negative infections. *J Antimicrob Chemother*. 2002;50(3):425–8.
105. McKinnon PS, Paladino JA, Schentag JJ. Evaluation of area under the inhibitory curve (AUC) and time above the minimum inhibitory concentration (T>MIC) as predictors of outcome for cefepime and ceftazidime in serious bacterial infections. *Int J Antimicrob Agents*. 2008;31(4):345–51.
106. Roberts JA, Paul SK, Akova M, Bassetti M, De Waele JJ, Dimopoulos G, et al. DALI: Defining antibiotic levels in intensive care unit patients: Are current β -lactam antibiotic doses sufficient for critically ill patients? *Clin Infect Dis*. 2014;58(8):1072–83.
107. Rhodes NJ, Kuti JL, Nicolau DP, Van Wart S, Nicasio AM, Liu J, et al. Defining Clinical Exposures of Cefepime for Gram-Negative Bloodstream Infections That Are Associated with Improved Survival. *Antimicrob Agents Chemother*. 2016;60(3):1401–10.
108. Floss HG, Yu TW. Rifamycin - Mode of action, resistance, and biosynthesis. *Chem Rev*. 2005;105(2):621–32.
109. Mosaei H, Zenkin N. Inhibition of RNA Polymerase by Rifampicin and Rifamycin-Like Molecules. *EcoSal Plus*. 2020;9(1).
110. Hartmann BGR, Heinrich P, Kollenda MC, Skrobranek B, Tropschug M, Weid W.

- Molecular Mechanism of Action of the Antibiotic Rifampicin. *Angew Chemie Int Ed*. 1985;24:1009–14.
111. Bala S, Khanna R, Dadhwal M, Prabakaran SR, Shivaji S, Cullum J, et al. Reclassification of *Amycolatopsis mediterranei* DSM 46095 as *Amycolatopsis rifamycinica* sp. nov. *Int J Syst Evol Microbiol*. 2004;54(4):1145–9.
 112. National Center for Biotechnology Information (2024). PubChem Compound Summary for CID 135398735, Rifampin. Retrieved April 25, 2024 from <https://pubchem.ncbi.nlm.nih.gov/compound/Rifampin>.
 113. Hardie KR, Fenn SJ. JMM profile: Rifampicin: a broad-spectrum antibiotic. *J Med Microbiol*. 2022;71(8):1–5.
 114. Rothstein DM. Rifamycins, alone and in combination. *Cold Spring Harb Perspect Med*. 2016;6(7):1–20.
 115. Abulfathi AA, Decloedt EH, Svensson EM, Diacon AH, Donald P, Reuter H. Clinical Pharmacokinetics and Pharmacodynamics of Rifampicin in Human Tuberculosis. *Clin Pharmacokinet* [Internet]. 2019;58(9):1103–29. Available from: <https://doi.org/10.1007/s40262-019-00764-2>
 116. Maymone MBC, Venkatesh S, Laughter M, Abdat R, Hugh J, Dacso MM, et al. Leprosy: Treatment and management of complications. *J Am Acad Dermatol* [Internet]. 2020;83(1):17–30. Available from: <https://doi.org/10.1016/j.jaad.2019.10.138>
 117. Cabellos C, Guillem L, Pelegrin I, Tubau F, Ardanuy C, Gudiol F, et al. Penicillin- and Cephalosporin-Resistant Pneumococcal Meningitis: Treatment in the Real World and in Guidelines. *Antimicrob Agents Chemother*. 2022;66(12).
 118. Peloquin C. The Role of Therapeutic Drug Monitoring in Mycobacterial Infections. *Microbiol Spectr*. 2017;5(1):549–63.
 119. Saktiawati AMI, Sturkenboom MGG, Stienstra Y, Subronto YW, Sumardi, Kosterink JGW, et al. Impact of food on the pharmacokinetics of first-line anti-TB drugs in treatment-naïve TB patients: A randomized cross-over trial. *J Antimicrob Chemother*. 2016;71(3):703–10.
 120. Loos U, Musch E, Jensen JC, Schwabe HK, Eichelbaum M. Influence of the enzyme induction by rifampicin on its presystemic metabolism. *Pharmacol Ther* [Internet]. 1987 Jan [cited 2022 Sep 5];33(1):201–4. Available from: <https://linkinghub.elsevier.com/retrieve/pii/0163725887900520>
 121. Sturkenboom MGG, Märtsen AG, Svensson EM, Sloan DJ, Dooley KE, van den Elsen SHJ, et al. Population Pharmacokinetics and Bayesian Dose Adjustment to Advance TDM of Anti-TB Drugs. *Clin Pharmacokinet* [Internet]. 2021 Jun 1 [cited 2022 Aug 11];60(6):685–710. Available from: <https://pubmed.ncbi.nlm.nih.gov/33674941/>
 122. Justesen US, Andersen ÅB, Klitgaard NA, Brøsen K, Gerstoft J, Pedersen C. Pharmacokinetic Interaction between Rifampin and the Combination of Indinavir and Low-Dose Ritonavir in HIV-Infected Patients. *Clin Infect Dis*. 2004;38(3):426–9.

123. Acocella G. Clinical Pharmacokinetics of Rifampicin. *Clin Pharmacokinet.* 1978;3:108–27.
124. Jayaram R, Gaonkar S, Kaur P, Suresh BL, Mahesh BN, Jayashree R, et al. Pharmacokinetics-Pharmacodynamics of Rifampin in an Aerosol Infection Model of Tuberculosis. *Antimicrob Agents Chemother* [Internet]. 2003 Jul 1 [cited 2022 Sep 19];47(7):2118. Available from: /pmc/articles/PMC161844/
125. Gumbo T, Louie A, Deziel MR, Liu W, Parsons LM, Salfinger M, et al. Concentration-Dependent Mycobacterium tuberculosis Killing and Prevention of Resistance by Rifampin. *Antimicrob Agents Chemother* [Internet]. 2007 Nov [cited 2022 Sep 19];51(11):3781. Available from: /pmc/articles/PMC2151424/
126. Schimmel J, Epperson LC, Aldy K, Wax P, Brent J, Buchanan J, et al. Remdesivir Discontinuation Decisions Based on Thresholds of Aminotransferase in an Observational Registry. *Drugs* [Internet]. 2024;84(2):209–17. Available from: <https://doi.org/10.1007/s40265-023-01981-7>
127. FDA Approved Labeling. Veklury (remdesivir). Highlights of prescribing information. Revised: 06/2022. 2020; Available from: www.fda.gov/medwatch.
128. Al Bujuq N. Methods of Synthesis of Remdesivir, Favipiravir, Hydroxychloroquine, and Chloroquine: Four Small Molecules Repurposed for Clinical Trials during the Covid-19 Pandemic. *Synthesis (Stuttg).* 2020;52(24):3735–50.
129. Hamdy MMA, Abdel Moneim MM, Kamal MF. Accelerated stability study of the ester prodrug remdesivir: Recently FDA-approved Covid-19 antiviral using reversed-phase-HPLC with fluorimetric and diode array detection. *Biomed Chromatogr.* 2021;35(12):1–11.
130. Bakheit AH, Darwish H, Darwish IA, Al-Ghusn AI. Remdesivir. *Profiles Drug Subst Excipients Relat Methodol.* 2023;48:71–108.
131. Konkolova E, Dejmek M, Hřebabecký H, Šála M, Böserle J, Nencka R, et al. Remdesivir triphosphate can efficiently inhibit the RNA-dependent RNA polymerase from various flaviviruses. *Antiviral Res.* 2020;182(May):10–3.
132. EMA. Summary on compassionate use Remdesivir Gilead International Nonproprietary Name: remdesivir. *Eur Med Agency* [Internet]. 2020;31(April):41. Available from: https://www.ema.europa.eu/en/documents/other/summary-compassionate-use-remdesivir-gilead_en.pdf
133. Aleissa MM, Silverman EA, Paredes Acosta LM, Nutt CT, Richterman A, Marty FM. New perspectives on antimicrobial agents: Remdesivir treatment for COVID-19. *Antimicrob Agents Chemother.* 2021;65(1).
134. Cross RW, Woolsey C, Chu VC, Babusis D, Bannister R, Vermillion MS, et al. Oral administration of obeldesivir protects nonhuman primates against Sudan ebolavirus. *Science* (80-). 2024;383(6688).
135. Lo MK, Feldmann F, Gary JM, Jordan R, Bannister R, Cronin J, et al. Remdesivir (GS-5734) protects African green monkeys from Nipah virus challenge. *Sci Transl Med.* 2019;11(494):1–6.

136. Sörgel F, Malin JJ, Hagmann H, Kinzig M, Bilal M, Eichenauer DA, et al. Pharmacokinetics of remdesivir in a COVID-19 patient with end-stage renal disease on intermittent haemodialysis. *J Antimicrob Chemother.* 2021;76(3):825–7.
137. Humeniuk R, Mathias A, Cao H, Osinusi A, Shen G, Chng E, et al. Safety, Tolerability, and Pharmacokinetics of Remdesivir, An Antiviral for Treatment of COVID-19, in Healthy Subjects. *Clin Transl Sci.* 2020;13(5):896–906.
138. Luke DR, Tomaszewski K, Damle B, Schlamm HT. Review of the basic and clinical pharmacology of sulfobutylether- β - cyclodextrin (SBECD). *J Pharm Sci.* 2010;99(8):3291–301.
139. Szente L, Puskás I, Sohajda T, Varga E, Vass P, Nagy ZK, et al. Sulfobutylether-beta-cyclodextrin-enabled antiviral remdesivir: Characterization of electrospun- and lyophilized formulations. *Carbohydr Polym.* 2021;264(March).
140. Ackley TW, McManus D, Topal JE, Cicali B, Shah S. Erratum: A valid warning or clinical lore: An evaluation of safety outcomes of remdesivir in patients with impaired renal function from a multicenter matched cohort (*Antimicrobial Agents and Chemotherapy* (2021) 65:2 (e02290-20) DOI: 10.1128/AAC.02290-20). *Antimicrob Agents Chemother.* 2021;65(7).
141. Gevers S, Welink J, van Nieuwkoop C. Remdesivir in COVID-19 patients with impaired renal function. *J Am Soc Nephrol.* 2021;32(2):518–9.
142. Zhang X, Yang Y, Grimstein M, Liu G, Kitabi E, Fan J, et al. Anti-SARS-CoV-2 Repurposing Drug Database: Clinical Pharmacology Considerations. *CPT Pharmacometrics Syst Pharmacol.* 2021;10(9):973–82.
143. Choy KT, Wong AYL, Kaewpreedee P, Sia SF, Chen D, Hui KPY, et al. Remdesivir, lopinavir, emetine, and homoharringtonine inhibit SARS-CoV-2 replication in vitro. *Antiviral Res* [Internet]. 2020;178(March):104786. Available from: <https://doi.org/10.1016/j.antiviral.2020.104786>
144. Wang M, Cao R, Zhang L, Yang X, Liu J, Xu M, et al. Remdesivir and chloroquine effectively inhibit the recently emerged novel coronavirus (2019-nCoV) in vitro. *Cell Res.* 2020;30(3):269–71.
145. Sato T, Yamawaki K. Cefiderocol: Discovery, Chemistry, and in Vivo Profiles of a Novel Siderophore Cephalosporin. *Clin Infect Dis.* 2019;69(S7):538–43.
146. European Medicines Agency. EMEA/H/C/004829: summary of product characteristics of Fectroja. 2020.
147. Neilands JB. Siderophores: Structure and function of microbial iron transport compounds. *J Biol Chem* [Internet]. 1995;270(45):26723–6. Available from: <http://dx.doi.org/10.1074/jbc.270.45.26723>
148. Dobias J, Dénervaud-Tendon V, Poirel L, Nordmann P. Activity of the novel siderophore cephalosporin cefiderocol against multidrug-resistant Gram-negative pathogens. *Eur J Clin Microbiol Infect Dis.* 2017;36(12):2319–27.

149. Saisho Y, Katsube T, White S, Fukase H, Shimada J. Pharmacokinetics, Safety, and Tolerability of Cefiderocol, a Novel Siderophore Cephalosporin for Gram-Negative Bacteria, in Healthy Subjects [Internet]. 2018 [cited 2021 Mar 23]. Available from: <http://aac.asm.org/>
150. Kawaguchi N, Katsube T, Echols R, Wajima T. Population pharmacokinetic analysis of cefiderocol, a parenteral siderophore cephalosporin, in healthy subjects, subjects with various degrees of renal function, and patients with complicated urinary tract infection or acute uncomplicated pyelonephritis. *Antimicrob Agents Chemother*. 2018;62(2).
151. Katsube T, Saisho Y, Shimada J, Furuie H. Intrapulmonary pharmacokinetics of cefiderocol, a novel siderophore cephalosporin, in healthy adult subjects. *J Antimicrob Chemother*. 2019;74(7):1971–4.
152. Saisho Y, Katsube T, White S, Fukase H. Pharmacokinetics, Safety, and Tolerability of Cefiderocol, a Novel Siderophore Cephalosporin for Gram-Negative Bacteria, in Healthy Subjects. *Antimicrob Agents Chemother*. 2018;62(3):1–12.
153. Kidd JM, Abdelraouf K, Nicolau DP. Development of neutropenic murine models of iron overload and depletion to study the efficacy of siderophore-antibiotic conjugates. *Antimicrob Agents Chemother*. 2020;64(1).
154. Takayuki Katsube, Toshihiro Wajima, Toru Ishibashi, Juan Camilo Arjona Ferreira RE. Pharmacokinetic/Pharmacodynamic Modeling and Simulation of Cefiderocol, a Parenteral Siderophore Cephalosporin, for Dose Adjustment Based on Renal Function Takayuki. *Antimicrob Agents Chemother*. 2017;61(1):1–12.
155. Shuhei Matsumoto CMS, Jennifer Hoover RN, Roger Echols SR, Masakatsu Tsuji YY. Efficacy of Cefiderocol against Carbapenem-Resistant Gram-Negative Bacilli in Immunocompetent-Rat Respiratory Tract Infection Models Recreating Human Plasma Pharmacokinetics. *Antimicrob Agents Chemother*. 2017;61(9):1–8.
156. Aoki T, Yoshizawa H, Yamawaki K, Yokoo K, Sato J, Hisakawa S, et al. Cefiderocol (S-649266), A new siderophore cephalosporin exhibiting potent activities against *Pseudomonas aeruginosa* and other gram-negative pathogens including multi-drug resistant bacteria: Structure activity relationship. *Eur J Med Chem* [Internet]. 2018;155:847–68. Available from: <https://doi.org/10.1016/j.ejmech.2018.06.014>
157. Portsmouth S, van Veenhuizen D, Echols R, Machida M, Ferreira JCA, Ariyasu M, et al. Cefiderocol versus imipenem-cilastatin for the treatment of complicated urinary tract infections caused by Gram-negative uropathogens: a phase 2, randomised, double-blind, non-inferiority trial. *Lancet Infect Dis* [Internet]. 2018;18(12):1319–28. Available from: [http://dx.doi.org/10.1016/S1473-3099\(18\)30554-1](http://dx.doi.org/10.1016/S1473-3099(18)30554-1)
158. Wunderink RG, Matsunaga Y, Ariyasu M, Clevenbergh P, Echols R, Kaye KS, et al. Cefiderocol versus high-dose, extended-infusion meropenem for the treatment of Gram-negative nosocomial pneumonia (APEKS-NP): a randomised, double-blind, phase 3, non-inferiority trial. *Lancet Infect Dis* [Internet]. 2021;21(2):213–25. Available from: [http://dx.doi.org/10.1016/S1473-3099\(20\)30731-3](http://dx.doi.org/10.1016/S1473-3099(20)30731-3)
159. Gainey AB, Burch AK, Brownstein MJ, Brown DE, Fackler J, Horne B, et al. Combining bacteriophages with cefiderocol and meropenem/vaborbactam to treat a pan-drug resistant

- Achromobacter species infection in a pediatric cystic fibrosis patient. *Pediatr Pulmonol*. 2020;55(11):2990–4.
160. Cordero J, Lopez J, Lora J, Martinez J, Mercado L. Development of Neurotoxicity Syndrome Associated With the Use of Cefepime. *Heal Sci J* [Internet]. 2022 [cited 2022 May 21];16(S6):921. Available from: <http://www.hsj.gr/>
161. Beaucaire G. Clinical activity of cefepime in severe infections. *Clin Microbiol Infect* [Internet]. 1999 [cited 2023 Jan 3];5(SUPPL. 1):S6–14. Available from: <https://onlinelibrary.wiley.com/doi/full/10.1111/j.1469-0691.1999.tb00718.x>
162. Bilal M, Zoller M, Fuhr U, Jaehde U, Ullah S, Liebchen U, et al. Cefepime Population Pharmacokinetics, Antibacterial Target Attainment, and Estimated Probability of Neurotoxicity in Critically Ill Patients. *Antimicrob Agents Chemother*. 2023;67(7):1–13.
163. Turnidge JD. The pharmacodynamics of beta-lactams. *Clin Infect Dis* [Internet]. 1998 [cited 2022 May 23];27(1):10–22. Available from: <https://pubmed.ncbi.nlm.nih.gov/9675443/>
164. Nicasio AM, Ariano RE, Zelenitsky SA, Kim A, Crandon JL, Kuti JL, et al. Population pharmacokinetics of high-dose, prolonged-infusion cefepime in adult critically ill patients with ventilator-associated pneumonia. *Antimicrob Agents Chemother*. 2009;53(4):1476–81.
165. Roos JF, Bulitta J, Lipman J, Kirkpatrick CMJ. Pharmacokinetic-pharmacodynamic rationale for cefepime dosing regimens in intensive care units. *J Antimicrob Chemother* [Internet]. 2006;58:987–93. Available from: <https://academic.oup.com/jac/article/58/5/987/739570>
166. Al-Shaer MH, Neely MN, Liu J, Cherabuddi K, Venugopalan V, Rhodes NJ, et al. Population Pharmacokinetics and Target Attainment of Cefepime in Critically Ill Patients and Guidance for Initial Dosing. 2020 [cited 2022 Dec 12]; Available from: <https://journals.asm.org/journal/aac>
167. Craig WA. Pharmacokinetic/pharmacodynamic parameters: rationale for antibacterial dosing of mice and men. *Clin Infect Dis* [Internet]. 1998 [cited 2022 Jun 21];26(1):1–12. Available from: <https://pubmed.ncbi.nlm.nih.gov/9455502/>
168. Aitken SL, Altshuler J, Guervil DJ, Hirsch EB, Ostrosky-Zeichner LL, Ericsson CD, et al. Cefepime free minimum concentration to minimum inhibitory concentration (fC_{min}/MIC) ratio predicts clinical failure in patients with Gram-negative bacterial pneumonia. *Int J Antimicrob Agents* [Internet]. 2015;45(5):541–4. Available from: <http://dx.doi.org/10.1016/j.ijantimicag.2014.12.018>
169. Payne LE, Gagnon DJ, Riker RR, Seder DB, Glisic EK, Morris JG, et al. Cefepime-induced neurotoxicity: A systematic review. *Crit Care* [Internet]. 2017 Nov 14 [cited 2023 Jan 5];21(1):1–8. Available from: <https://ccforum.biomedcentral.com/articles/10.1186/s13054-017-1856-1>
170. Lamoth F, Buclin T, Pascual A, Vora S, Bolay S, Decosterd LA, et al. High cefepime plasma concentrations and neurological toxicity in febrile neutropenic patients with mild impairment of renal function. *Antimicrob Agents Chemother*. 2010;54(10):4360–7.

171. Boschung-Pasquier L, Atkinson A, Kastner LK, Banholzer S, Haschke M, Buetti N, et al. Cefepime neurotoxicity: thresholds and risk factors. A retrospective cohort study. *Clin Microbiol Infect* [Internet]. 2020 Mar 1 [cited 2022 May 24];26(3):333–9. Available from: <https://pubmed.ncbi.nlm.nih.gov/31284030/>
172. Huwyler T, Lenggenhager L, Abbas M, Ing Lorenzini K, Hughes S, Huttner B, et al. Cefepime plasma concentrations and clinical toxicity: a retrospective cohort study. *Clin Microbiol Infect*. 2017 Jul;23(7):454–9.
173. Verhave JC, Fesler P, Ribstein J, Du Cailar G, Mimran A. Estimation of renal function in subjects with normal serum creatinine levels: influence of age and body mass index. *Am J Kidney Dis* [Internet]. 2005 Aug [cited 2022 Jun 22];46(2):233–41. Available from: <https://pubmed.ncbi.nlm.nih.gov/16112041/>
174. Sekaggya-Wiltshire C, Chirehwa M, Musaazi J, Von Braun A, Buzibye A, Muller D, et al. Low antituberculosis drug concentrations in HIV-tuberculosis-coinfected adults with low body weight: Is it time to update dosing guidelines? *Antimicrob Agents Chemother*. 2019;63(6).
175. Chirehwa MT, Rustomjee R, Mthiyane T, Onyebujoh P, Smith P, McIlleron H, et al. Model-based evaluation of higher doses of rifampin using a semimechanistic model incorporating autoinduction and saturation of hepatic extraction. *Antimicrob Agents Chemother* [Internet]. 2016 Jan 1 [cited 2022 Sep 11];60(1):487–94. Available from: <https://journals.asm.org/doi/10.1128/AAC.01830-15>
176. Medellín-Garibay SE, Milán-Segovia RDC, Magaña-Aquino M, Portales-Pérez DP, Romano-Moreno S. Pharmacokinetics of rifampicin in Mexican patients with tuberculosis and healthy volunteers. *J Pharm Pharmacol*. 2014;66(10):1421–8.
177. Janmahasatian S, Duffull SB, Ash S, Ward LC, Byrne NM, Green B. Quantification of lean bodyweight. *Clin Pharmacokinet* [Internet]. 2005 [cited 2022 Aug 4];44(10):1051–65. Available from: <https://pubmed.ncbi.nlm.nih.gov/16176118/>
178. Horita Y, Alsultan A, Kwara A, Antwi S, Enimil A, Orsin A, et al. Evaluation of the adequacy of WHO revised dosages of the first-line antituberculosis drugs in children with tuberculosis using population pharmacokinetic modeling and simulations. *Antimicrob Agents Chemother*. 2018 Sep 1;62(9).
179. Nishimura T, Kohno H, Nagai H, Maruoka D, Koike Y, Kobayashi M, et al. The Population Pharmacokinetics of Rifampicin in Japanese Pulmonary Tuberculosis Patients. *Drug Res (Stuttg)* [Internet]. 2020 May 1 [cited 2022 Sep 19];70(5):199–205. Available from: <https://pubmed.ncbi.nlm.nih.gov/32193878/>
180. Mukonzo JK, Kengo A, Kutesa B, Nanzigu S, Pohanka A, McHugh TD, et al. Role of pharmacogenetics in rifampicin pharmacokinetics and the potential effect on TB–rifampicin sensitivity among Ugandan patients. *Trans R Soc Trop Med Hyg* [Internet]. 2020 Feb 7 [cited 2022 Sep 19];114(2):107–14. Available from: <https://academic.oup.com/trstmh/article/114/2/107/5649022>
181. Kim ES, Kwon BS, Park JS, Chung JY, Seo SH, Park KU, et al. Relationship among genetic polymorphism of SLCO1B1, rifampicin exposure and clinical outcomes in patients with

- active pulmonary tuberculosis. *Br J Clin Pharmacol* [Internet]. 2021 Sep 1 [cited 2022 Sep 19];87(9):3492–500. Available from: <https://pubmed.ncbi.nlm.nih.gov/33538008/>
182. Goutelle S, Bourguignon L, Maire PH, Van Guilder M, Conte JE, Jelliffe RW. Population modeling and Monte Carlo simulation study of the pharmacokinetics and antituberculosis pharmacodynamics of rifampin in lungs. *Antimicrob Agents Chemother* [Internet]. 2009 Jul [cited 2022 Sep 19];53(7):2974–81. Available from: <https://journals.asm.org/doi/10.1128/AAC.01520-08>
183. Jeremiah K, Denti P, Chigutsa E, Faurholt-Jepsen D, PrayGod G, Range N, et al. Nutritional supplementation increases rifampin exposure among tuberculosis patients coinfectd with HIV. *Antimicrob Agents Chemother* [Internet]. 2014 [cited 2022 Sep 11];58(6):3468–74. Available from: <https://pubmed.ncbi.nlm.nih.gov/24709267/>
184. Svensson RJ, Aarnoutse RE, Diacon AH, Dawson R, Gillespie SH, Boeree MJ, et al. A Population Pharmacokinetic Model Incorporating Saturable Pharmacokinetics and Autoinduction for High Rifampicin Doses. *Clin Pharmacol Ther* [Internet]. 2018 Apr 1 [cited 2022 Aug 4];103(4):674. Available from: </pmc/articles/PMC5888114/>
185. Becker C, Dressman JB, Junginger HE, Kopp S, Midha KK, Shah VP, et al. Biowaiver monographs for immediate release solid oral dosage forms: Rifampicin. *J Pharm Sci*. 2009 Jul 1;98(7):2252–67.
186. Gao Y, Davies Forsman L, Ren W, Zheng X, Bao Z, Hu Y, et al. Drug exposure of first-line anti-tuberculosis drugs in China: A prospective pharmacological cohort study. *Br J Clin Pharmacol* [Internet]. 2021 Mar 1 [cited 2022 Sep 19];87(3):1347–58. Available from: <https://pubmed.ncbi.nlm.nih.gov/33464624/>
187. Sinha J, Duffull SB, Al-Sallami HS. A Review of the Methods and Associated Mathematical Models Used in the Measurement of Fat-Free Mass. *Clin Pharmacokinet* [Internet]. 2018 Jul 1 [cited 2022 Sep 24];57(7):781–95. Available from: <https://link.springer.com/article/10.1007/s40262-017-0622-5>
188. Lamb YN. Remdesivir: First Approval. *Drugs* [Internet]. 2020;80(13):1355–63. Available from: <https://doi.org/10.1007/s40265-020-01378-w>
189. European Medicines Agency. Veklury (remdesivir) [Internet]. 2022. Available from: <https://www.ema.europa.eu/en/medicines/human/EPAR/vazkepa>
190. Godwin PO, Polsonetti B, Caron MF, Oppelt TF. Remdesivir for the Treatment of COVID-19: A Narrative Review. *Infect Dis Ther* [Internet]. 2024;13(1):1–19. Available from: <https://doi.org/10.1007/s40121-023-00900-3>
191. de Wit E, Feldmann F, Cronin J, Jordan R, Okumura A, Thomas T, et al. Prophylactic and therapeutic remdesivir (GS-5734) treatment in the rhesus macaque model of MERS-CoV infection. *Proc Natl Acad Sci U S A*. 2020;117(12):6771–6.
192. Schulz A, Huynh N, Heger M, Bakir M. Adverse effects of remdesivir for the treatment of acute COVID-19 in the pediatric population: a retrospective observational study. *Mol Cell Pediatr* [Internet]. 2024;11(1). Available from: <https://doi.org/10.1186/s40348-024-00175-9>

193. Humeniuk R, Mathias A, Kirby BJ, Lutz JD, Cao H, Osinusi A, et al. Pharmacokinetic, Pharmacodynamic, and Drug-Interaction Profile of Remdesivir, a SARS-CoV-2 Replication Inhibitor. *Clin Pharmacokinet* 2021 605. 2021 Mar;60(5):569–83.
194. Veklury (remdesivir): summary of product characteristics. 2020;(June):1–56. Available from: https://www.ema.europa.eu/en/documents/product-information/perjeta-epar-product-information_en.pdf
195. Sukeishi A, Itohara K, Yonezawa A, Sato Y, Matsumura K, Katada Y, et al. Population pharmacokinetic modeling of GS-441524, the active metabolite of remdesivir, in Japanese COVID-19 patients with renal dysfunction. *CPT Pharmacometrics Syst Pharmacol*. 2022;11(1):94–103.
196. Tempestilli M, Caputi P, Avataneo V, Notari S, Forini O, Scorzolini L, et al. Pharmacokinetics of remdesivir and GS-441524 in two critically ill patients who recovered from COVID-19. *J Antimicrob Chemother*. 2020;75(10):2977–80.
197. Hu W juan, Chang L, Yang Y, Wang X, Xie Y chao, Shen J shan, et al. Pharmacokinetics and tissue distribution of remdesivir and its metabolites nucleotide monophosphate, nucleotide triphosphate, and nucleoside in mice. *Acta Pharmacol Sin* [Internet]. 2021;42(7):1195–200. Available from: <http://dx.doi.org/10.1038/s41401-020-00537-9>
198. Yan VC, Muller FL. Advantages of the Parent Nucleoside GS-441524 over Remdesivir for Covid-19 Treatment. *ACS Med Chem Lett*. 2020;11(7):1361–6.
199. Kawaguchi N, Katsube T, Echols R, Wajima T. Population pharmacokinetic analysis of cefiderocol, a parenteral siderophore cephalosporin, in healthy subjects, subjects with various degrees of renal function, and patients with complicated urinary tract infection or acute uncomplicated pyelonephritis. *Antimicrob Agents Chemother*. 2018 Feb 1;62(2).
200. Katsube T, Echols R, Arjona Ferreira JC, Krenz HK, Berg JK, Galloway C. Cefiderocol, a Siderophore Cephalosporin for Gram-Negative Bacterial Infections: Pharmacokinetics and Safety in Subjects With Renal Impairment. *J Clin Pharmacol*. 2017;57(5):584–91.
201. Katsube T, Miyazaki S, Narukawa Y, Hernandez-Illas M, Wajima T. Drug-drug interaction of cefiderocol, a siderophore cephalosporin, via human drug transporters. *Eur J Clin Pharmacol*. 2018 Jul 1;74(7):931–8.
202. Zhanel GG, Golden AR, Zelenitsky S, Wiebe K, Lawrence CK, Adam HJ, et al. Cefiderocol: A Siderophore Cephalosporin with Activity Against Carbapenem-Resistant and Multidrug-Resistant Gram-Negative Bacilli. Vol. 79, *Drugs*. Springer International Publishing; 2019. p. 271–89.
203. Katsube T, Echols R, Wajima T. Pharmacokinetic and Pharmacodynamic Profiles of Cefiderocol, a Novel Siderophore Cephalosporin. *Clin Infect Dis*. 2019 Nov 13;69:S552–8.
204. Katsube T, Echols R, Camilo J, Ferreira A, Krenz HK, Berg JK, et al. Cefiderocol , a Siderophore Cephalosporin for Gram-Negative Bacterial Infections : Pharmacokinetics and Safety in Subjects With Renal Impairment. 2017;(September 2016).
205. Kim PW, Wu Y, Cooper C, Rochester G, Valappil T, Wang Y, et al. Meta-Analysis of a

- Possible Signal of Increased Mortality Associated with Cefepime Use. *Clin Infect Dis*. 2010;51(4):381–9.
206. Pais GM, Chang · Jack, Barreto EF, Stitt G, Downes KJ, Mohammad ·, et al. Clinical Pharmacokinetics and Pharmacodynamics of Cefepime. *Clin Pharmacokinet* [Internet]. 2022 [cited 2023 Feb 28];61:929–53. Available from: <https://doi.org/10.1007/s40262-022-01137-y>
 207. Fugate JE, Kalimullah EA, Hocker SE, Clark SL, Wijdicks EFM, Rabinstein AA. Cefepime neurotoxicity in the intensive care unit: a cause of severe, underappreciated encephalopathy. *Crit Care* [Internet]. 2013 Nov 7 [cited 2022 May 31];17(6). Available from: <https://pubmed.ncbi.nlm.nih.gov/24200036/>
 208. Sensi P. History of the development of rifampin. *Rev Infect Dis* [Internet]. 1983 [cited 2022 Aug 11];5 Suppl 3:S402–6. Available from: <https://pubmed.ncbi.nlm.nih.gov/6635432/>
 209. World Health Organization. World Health Organization (2010) Treatment of tuberculosis: guidelines.
 210. Rockwood N, Meintjes G, Chirehwa M, Wiesner L, McIlleron H, Wilkinson RJ, et al. HIV-1 Coinfection Does Not Reduce Exposure to Rifampin, Isoniazid, and Pyrazinamide in South African Tuberculosis Outpatients. *Antimicrob Agents Chemother* [Internet]. 2016 Oct 1 [cited 2022 Sep 19];60(10):6050–9. Available from: <https://pubmed.ncbi.nlm.nih.gov/27480859/>

Information on the assistance received and resources used

General

Introduction to pharmacometric modeling, statistical software and software packages (including coding), i.e. NONMEM®, R, Piraña, Pearl-speaks-NONMEM, Monolix, assisted by: Dr. Sami Ullah and Dr. Max Taubert.

Chapter 3: Clinical Pharmacokinetics and Pharmacodynamics of Cefiderocol

Dr. Lobna El Tabei, Dr. Sören Büsker, Christian Krauss, Prof. Dr. Uwe Fuhr and Dr. Max Taubert assisted in outlining the literature review. Dr. Lobna El Tabei, Dr. Sören Büsker, Christian Krauss assisted in literature search. All authors screened articles and abstracts for inclusion, discussed results and conclusions, and wrote the manuscript. Prof. Dr. Uwe Fuhr and Dr. Max Taubert supervised the review process.

Chapter 4: Cefepime Population Pharmacokinetics, Antibacterial Target Attainment, and Estimated Probability of Neurotoxicity in Critically Ill Patients

This study was conducted at the Department of Anesthesiology, University Hospital, Ludwig-Maximilians-Universität (LMU) München, Munich, Germany.

Dr. Michael Zoller and Dr. Johannes Zander provided the data for pharmacometrics analysis. Dr. Baharak Babouee Flury provided the logistic regression model of cefepime-induced neurotoxicity. Prof. Dr. Uwe Fuhr, Dr. Sami Ullah and Dr. Max Taubert assisted in pharmacometric analysis. All co-authors contributed to writing the manuscript.

Chapter 5: Assessment of body mass-related covariates for rifampicin pharmacokinetics in healthy Caucasian volunteers

The study was conducted in the department I of pharmacology, Center for Pharmacology, Faculty of Medicine and University Hospital Cologne, University of Cologne, Cologne, Germany.

Dr. Dario Zaremba organized the study from the University of Cologne. Dr. Bertil Wachall organized the study from InfectoPharm. Dr. Manfred Wargenau conducted the study from MARCO GmbH. Dr. Bernhard Scheidel carried out the analysis of the samples. Dr. Martin H. J. Wiesen, Dr. Christina Trueck, Dr. Malaz Gazzaz and Prof. Dr. Uwe Fuhr conducted the study. Dr. Sami Ullah made the initial data set and prepared initial model. Prof. Dr. Uwe Fuhr and Dr. Max Taubert supervised the pharmacometrics analysis. Prof. Dr. Uwe Fuhr and Dr. Max Taubert reviewed the

manuscript. Dr. Chunli Chen and Dr. S Sören Büsker, Dr. Charalambos Dokos Prof. Dr. Ulrich Jaehde review the manuscript. All co-authors contributed to writing the manuscript.

Chapter 6: A population pharmacokinetic model of remdesivir and its major metabolites based on published mean values from healthy subjects

Ahmed Abouellil developed the population pharmacokinetic model and performed simulations Prof. Dr. Uwe Fuhr and Dr. Max Taubert assisted and supervised the model development and communicated with trial authors. Ahmed Abouellil wrote the initial draft of the manuscript. All authors contributed in and agreed upon the final version of the manuscript.



Clinical Pharmacokinetics and Pharmacodynamics of Cefiderocol

Muhammad Bilal^{1,2} · Lobna El Tabei¹ · Sören Büsker¹ · Christian Krauss¹ · Uwe Fuhr¹ · Max Taubert¹ 

Accepted: 26 July 2021 / Published online: 22 August 2021
© The Author(s) 2021

Abstract

Cefiderocol is a new broad-spectrum cephalosporin antibiotic with promising activity against various Gram-negative bacteria including carbapenem-resistant strains. A chlorocatechol group in the C-3 side chain provides cefiderocol with a siderophore activity, improving its stability against β -lactamases and facilitating the transportation of cefiderocol across outer bacterial membranes. Cefiderocol shows linear pharmacokinetics over a broad range of clinically relevant doses, with unchanged renal excretion constituting the main route of elimination. Geometric means (coefficient of variation) of the volume of distribution and clearance in individuals with normal kidney function were 15.8 (15%) L and 4.70 (27%) L/h, respectively. In patients with end-stage renal disease, clearance was 1.10 (24%) L/h. Time above the minimum inhibitory concentration is the main predictor of efficacy. There is no evidence for clinically relevant interactions of cefiderocol with other drugs mediated by metabolizing enzymes or drug transporters. Simulations based on population pharmacokinetic modeling suggest that dosing regimens should be adjusted based on kidney function to optimize therapeutic exposure to cefiderocol. Clinical efficacy trials indicated that cefiderocol is non-inferior to imipenem/cilastatin in the treatment of complicated urinary tract infections and acute uncomplicated pyelonephritis, and to meropenem in the treatment of nosocomial pneumonia. In the one study currently available, cefiderocol performed similarly to the best available therapy in the treatment of severe carbapenem-resistant Gram-negative infections regarding clinical and microbiological efficacy. In summary, cefiderocol shows favorable pharmacokinetic/pharmacodynamic properties and an acceptable safety profile, suggesting that cefiderocol might be a viable option to treat infections with bacteria resistant to other antibiotics.

Key Points

Cefiderocol is a siderophore cephalosporin providing promising activity against Gram-negative bacteria, resistant to other antibiotics.

The drug shows linear pharmacokinetics and a kidney function-dependent elimination, supporting respective dose adjustments.

Clinical efficacy trials indicate that cefiderocol might be valuable to treat infections with bacteria resistant to other antibiotics.

1 Introduction

Cefiderocol, formerly known as S-649266, is a novel catechol-substituted siderophore cephalosporin antibiotic developed by Shionogi & Co., Ltd, Japan. Siderophores are iron-chelating agents produced by bacterial species that facilitate the uptake of iron into the bacterial cell, which is needed for survival and growth. Similar to bacterial siderophores, cefiderocol binds to iron transport channels and thereby enters the periplasmic space of bacteria. This is called a “trojan horse” mechanism. Inside the cell, cefiderocol dissociates from the iron transport channel and exerts its antibacterial activity [1]. The cefiderocol molecule comprises functional groups that improve the stability against β -lactamases, facilitate the transport across the outer membrane of Gram-negative bacteria, and provide cefiderocol with its siderophore activity [2]. The strong activity of cefiderocol is a result of its stability against serine and metallo-type carbapenemases, and extended-spectrum β -lactamases [3]. Consequently, cefiderocol shows a solid in vitro activity against carbapenem-resistant (CR)

✉ Max Taubert
max.taubert@uk-koeln.de

¹ Department I of Pharmacology, Faculty of Medicine and University Hospital Cologne, Center for Pharmacology, University of Cologne, Gleueler Straße 24, 50931 Cologne, Germany

² Department of Clinical Pharmacy, Institute of Pharmacy, University of Bonn, Bonn, Germany

Gram-negative bacteria, including carbapenem-resistant *Enterobacteriales* and non-fermenters [4].

Cefiderocol has been approved in the USA in 2019 for the treatment of complicated urinary tract infections (cUTIs), including kidney infections caused by susceptible Gram-negative microorganisms with limited or no alternative treatment options, and for the treatment of hospital-acquired and ventilator-associated bacterial pneumonia [5]. In Europe, approval was granted in 2020 for the treatment of infections caused by aerobic Gram-negative bacteria in adults with limited treatment options [6]. Despite the approval of several new antibiotics to treat carbapenem-resistant Gram-negative infections, randomized clinical trials including the target pathogens of cefiderocol have been limited to carbapenem-resistant *Enterobacteriaceae* and carbapenem-resistant *Pseudomonas aeruginosa*. Randomized trials for the treatment of carbapenem-resistant infections including *Acinetobacter baumannii* have been limited to mostly colistin-based generic antibiotics. Recently, Bassetti et al. [4] compared cefiderocol to the best available therapy (BAT) in a heterogeneous patient population with infections caused by carbapenem-resistant Gram-negative bacteria in a randomized phase III study (CREDIBLE-CR). In this trial, cefiderocol was found to have similar clinical and microbiological efficacy compared to the BAT. The authors concluded that cefiderocol might be an option for the treatment of carbapenem-resistant infections in patients with limited treatment options. Furthermore, the broad-spectrum activity of cefiderocol coupled with the preserved efficacy irrespective of carbapenem resistance makes cefiderocol a good candidate for investigations in serious infections involving multiple infection sites. Thus, the target populations for cefiderocol treatment will be particularly patients who are immunocompromised, have relevant co-morbidities, and are critically ill. Recently, an extensive review of the drug has been provided by Abdul-Mutakabbir et al. [7].

The present review provides a comprehensive summary of the clinical pharmacokinetics (PK) and pharmacodynamics of cefiderocol. Studies evaluated include in vivo animal studies as well as recent phase II and III trials. The discussion refers primarily to studies carried out between 2017 and 2021. The literature for this review was obtained through a comprehensive search of PubMed, PubChem, and Google Scholar, including the terms “cefiderocol,” “cefiderocol pharmacokinetics,” “cefiderocol pharmacodynamics,” and “cefiderocol clinical trials” from 2010 until May 2021. PubMed was queried using the terms “cefiderocol chemical structure” and “cefiderocol antimicrobial activity” without restricting the date of publication to a certain range. The US Food and Drug Administration and European Medicines Agency briefing documents for cefiderocol were also included in this review.

2 Chemical and Antimicrobial Overview

Cefiderocol is a novel antimicrobial compound developed by Shionogi & Co, Ltd., Japan [2]. The basis of this molecule is a cephalosporine nucleus coupled with an amino thiazolyl acetic acid derivative as a C-7 side chain. Quaternization with a tertiary amine as a C-3 side chain resulted in a precursor molecule, and the removal of all protective groups resulted in a novel cephalosporine derivative [2]. C-3 and C-7 side chain substituents were specifically chosen to achieve a potent antibacterial activity against multi-drug-resistant (MDR) Gram-negative bacteria. Important chemical characteristics of the cefiderocol molecule are shown in Fig. 1, and a comprehensive description of the chemical properties of cefiderocol has been provided by Aoki et al. [2]. Cefiderocol belongs to the group of siderophore cephalosporines. The name “siderophore” derives from the Greek term for “iron carrier”, describing the capability of siderophore molecules to carry iron into cells via siderophore transport systems [8]. Certain microorganisms, such as bacteria and fungi, release siderophore molecules into their environment to ensure a sufficient iron supply to the cell [9]. Siderophores combined with chemical moieties with antibacterial activity are called sideromycins. Although the vast majority of sideromycins is synthetic, a small number of natural sideromycins has been discovered including albomycin and salmycin [10]. Sideromycins make use of the siderophore transport systems to enrich inside bacterial cells, resulting in a pronounced antibacterial activity even at low extracellular concentrations [11].

In comparison to antibiotics such as meropenem or ceftazidime-avibactam, cefiderocol has been shown to provide a superior in vitro activity against a selection of Gram-negative bacteria compared with cephalosporines, fluoroquinolones, monobactams, and carbapenems. This includes MDR strains of *A. baumannii*, *Enterobacteriaceae*, and *P. aeruginosa* [1, 12]. For example, cefiderocol showed a higher in vitro potency against these three strains compared with meropenem [13], and an increased stability to *Klebsiella pneumoniae* carbapenemases (KPC) compared with meropenem and cefepime [14]. The Clinical and Laboratory Standards Institute recently reported cefiderocol breakpoints of 4 (susceptible), 8 (intermediate), and 16 mg/L (resistant) for *P. aeruginosa*, *A. baumannii*, *Stenophomonas maltophilia*, and *Enterobacteriaceae* including *K. pneumoniae* and *Escherichia coli*. In the SIDERO-WT-2015 trial conducted by Karlowsky et al., 8954 clinical isolates of Gram-negative bacteria from various clinical laboratories in North America and Europe were collected and assessed according to the Clinical and Laboratory Standards Institute guidelines [15]. For *Enterobacteriaceae*, *Klebsiella* spp., and *E. coli*, the MIC₉₀ was 0.5 mg/L for samples collected in North America

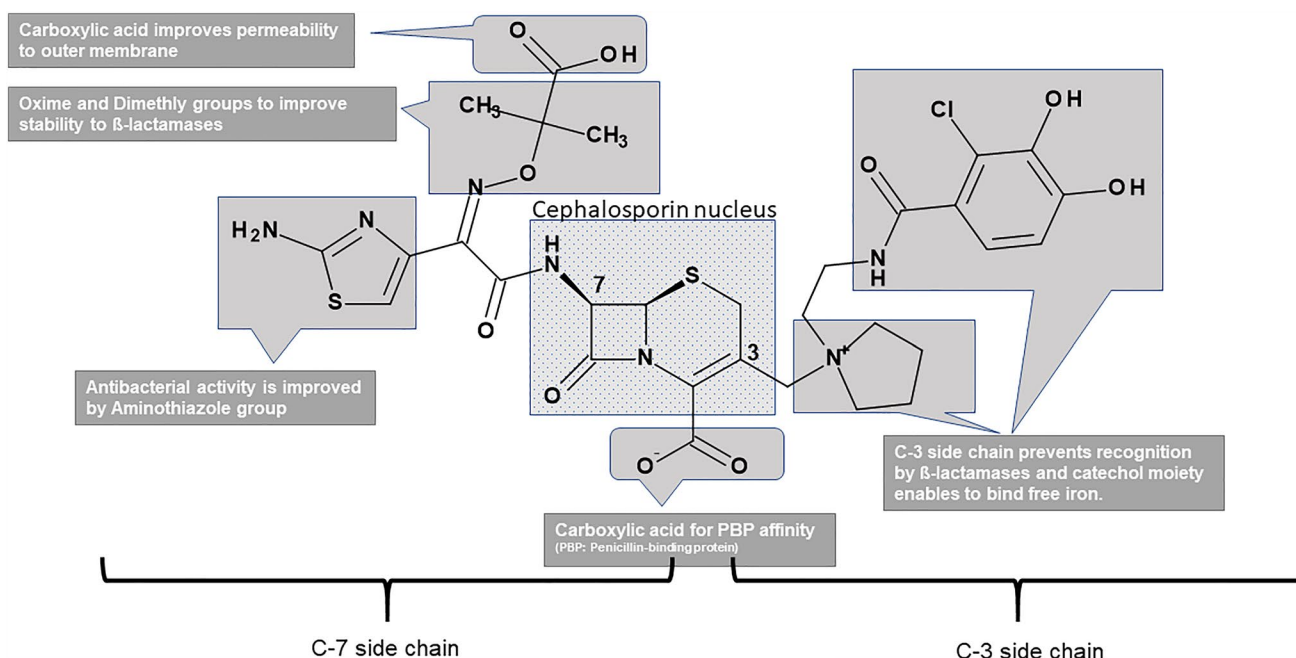


Fig. 1 Illustration of important functional groups in the cefiderocol molecule [1]. The cephalosporin nucleus is complemented by five functional groups in the C-3 and C-7 side chains, resulting in an

improved outer membrane permeability, antibacterial activity, beta-lactamase stability, and the capability to bind free iron. Based on [1]

and 1 mg/L for samples collected in Europe. The MIC_{90} for *Acinetobacter* spp. was 2 mg/L in both regions, while the MIC_{90} for *S. maltophilia* was 0.5 mg/L and 0.25 mg/L for North America and Europe, respectively. In the case of *P. aeruginosa*, the MIC_{90} was 0.5 mg/L in both regions. For *Bacteroides* spp., *Clostridium difficile*, and *Prevotella* spp., the MIC_{90} of cefiderocol was > 32 mg/L [3]. Overall, currently available data show that cefiderocol provides a strong activity against a selection of clinically relevant MDR Gram-negative bacteria in vitro.

3 PK

3.1 PK in Healthy Volunteers

Cefiderocol has demonstrated linear PK in a randomized, double-blind, single ascending dose (SAD) and multiple (MAD) ascending dose phase I study in healthy Japanese and Caucasian volunteers [17]. A total of 54 volunteers received cefiderocol (30 in the SAD, 24 in the MAD part), while 16 volunteers received placebo (ten in the SAD, six in the MAD part). The SAD part covered doses of 100–2000 mg, while the MAD part comprised two groups receiving 1000 mg and a third group receiving 2000 mg every 8 h (q8h) for 10 days. The infusion duration was 60 min. Based on observed plasma concentration profiles, steady state was achieved within 24 h. Both data from

the SAD and the MAD part indicated dose-proportional increases in maximum plasma concentrations (C_{max}) and areas under the concentration–time curve (AUC) with increasing dose, with no statistically significant dose dependency of half-life and clearance. Maximum plasma concentration (geometric mean) of cefiderocol ranged from 7.76 mg/L at 100 mg to 156 mg/L at 2000 mg in the SAD part, and from 72.2 at 1000 mg to 153 mg/L at 2000 mg on day 10 of the MAD part, respectively. The AUC from time zero to the last quantifiable concentration (AUC_{0-last}) was 389 mg•h/L in SAD and 337 mg•h/L in MAD for a 2000-mg dose, respectively, as shown in Table 1. Maximum plasma concentration, AUC_{0-last} , and the AUC from time zero to infinity (AUC_{0-inf}) indicated a limited inter-individual variability for plasma exposure in all dose groups. By administering single intravenous doses of 1000 mg of radio-labeled cefiderocol to healthy volunteers, Miyazaki et al. explored the fate of cefiderocol in the human body using radiolabeled cefiderocol. This included partitioning into red blood cells, urinary excretion, and the formation of metabolites [18]. Cefiderocol was found to only marginally partition into red blood cells, with a blood-to-plasma ratio range from 0.53 to 0.56. Unchanged excretion in urine constituted the main route of elimination, with 90.6% of the administered dose being recovered in urine on average. Metabolism contributed less than 10% to overall elimination. Metabolites were mainly excreted via urine, while fecal excretion was negligible. In

an additional study in 15 healthy volunteers, Katsube et al. [19] evaluated the penetration of cefiderocol into epithelial lining fluid and alveolar macrophages, concluding that cefiderocol penetrated lung tissues with exposure ratios (based on AUC) with a range from 0.0927 to 0.116 for epithelial lining fluid and a range from 0.00496 to 0.104 for alveolar macrophages. Data on the penetration of cefiderocol into cerebrospinal fluid are currently missing [20]. Finally, limited data on protein binding of cefiderocol are available. The protein binding ratio in mice was found to be 38% [21], while in vitro plasma protein binding (primarily to albumin) of cefiderocol in humans was 57.8% [22]. In summary, pharmacokinetic studies in healthy volunteers indicate linear PK over a range of doses and time, with unchanged urinary excretion constituting the main route of elimination. Renal function is the main predictor of the PK of cefiderocol and should be considered for dosing considerations.

3.2 PK in Subjects with Impaired Kidney Function

Katsube et al. [23] evaluated the PK and the safety of cefiderocol in subjects with various levels of kidney dysfunction. Thirty-eight subjects were recruited and 37 completed the study. Eight control subjects with normal renal function were identified based on an evaluation of Cockcroft-Gault creatinine clearance ($CGCL_{CR}$), which was defined to be ≥ 90 mL/min in subjects with normal renal function. The Modification of Diet in Renal Disease (MDRD) formula was used to estimate the glomerular filtration rate (eGFR), which served as a criterion to distinguish between mild (eGFR 60 to < 90 mL/min/1.73 m²), moderate (eGFR 30 to < 60 mL/min/1.73 m²), and severe (eGFR < 30 mL/min/1.73 m²) kidney impairment, and end-stage renal disease (ESRD) with and without hemodialysis. The PK of cefiderocol following a single intravenous infusion of 1000 mg was compared between subjects with normal and impaired renal function based on a non-compartmental analysis. As expected based on the predominating renal excretion of cefiderocol, the AUC_{0-last} differed clearly between different renal function

Table 1 Summary pharmacokinetic parameters of cefiderocol in plasma following an intravenous infusion [17, 18, 22]

Pharmacokinetic parameters	Phase I PK, safety, and tolerability study				^[14C] CF-study ^a	Phase I study in renally impaired subjects		
	Single IV infusion		Multiple IV infusion day 1			Normal ^b	Severe ^c	ESRD (w/o HD)
	1000 mg	2000 mg	1000 mg	2000 mg		1000 mg	1000 mg	1000 mg
	(n = 6)	(n = 6)	(n = 8)	(n = 8)		(n = 6)	(n = 8)	(n = 6)
C _{max} (mg/L)	74.4 (4.6)	156 (7.90)	68.1 (11.5)	141 (22.7)	72.9 (12.4)	81.0 (27.4)	80.1 (19.8)	93.0 (27.8)
t _{max} (h)	1.00 (1.00–1.00)	1.00 (1.00–1.00)	1.00 (1.00–1.00)	1.00 (1.00–1.20)	0.97 (0.50–1.00)	1.00 (1.0–1.0)	1.00 (1.00–1.10)	1.00 (1.00–1.00)
AUC _{0–last} (mg•h/L)	167 (6.90)	389 (9.00)	171 (10.6)	337(15.6)	171 (8.40)	212 (26.7)	540 (23.6)	872 (23.9)
AUC _{0–inf} (mg•h/L)	168 (7.00)	390 (9.00)	172 (10.6)	338 (15.5)	172 (8.40)	213 (26.5)	543 (23.6)	880 (24.2)
t _{1/2,z} (h)	2.26 (5.80)	2.74 (10.2)	2.19 (4.30)	2.40 (13.2)	2.30 (9.50)	2.80 (16.5)	6.90 (30.6)	9.60 (33.4)
CL (L/h)	5.95 (7.00)	5.13 (9.00)	5.93 (11.0)	5.91 (15.5)	4.78 (7.6)	4.70 (26.5)	1.80 (23.6)	1.10 (24.2)
V _z (L)	–	–	–	–	15.8 (15.1)	–	–	–
V _{ss} (L)	–	–	–	–	–	13.5 (30.2)	16.4 (23.4)	14.2 (22.5)
CL _R (L/h)	–	–	–	–	–	3.2 (28.0)	–	–
fe (%)	–	–	–	–	–	68.6 (17.3)	–	–
fu (8 h)	–	–	–	–	–	0.44 (9.8)	0.44 (10.1)	0.370 (27.0)

The geometric mean (coefficient of variation) for all parameters except t_{max} for which the median (range) is shown

AUC_{0-inf} area under the plasma concentration–time curve from zero to infinity, AUC_{0-last} area under the plasma concentration–time curve from zero to the time of the last quantifiable concentration, CL total clearance, CL_{cr} creatinine clearance, CL_R renal clearance of the drug, C_{max} maximum plasma concentration, $eGFR$ estimated glomerular filtration rate, $ESRD$ (w/o HD) an end-stage renal disease without hemodialysis, fe fraction of dose excreted unchanged into urine, fu fraction of total drug that is unbound in plasma, IV intravenous, n number of subjects, PK pharmacokinetics, $t_{1/2,z}$ terminal elimination half-life, T_{max} time to C_{max} , V_z apparent volume of distribution during the terminal elimination phase, V_{ss} volume of distribution at the steady-state phase

^aPK of [¹⁴C] cefiderocol in healthy subjects

^bNormal CL_{cr} , 90 mL/min

^cSevere impairment, $eGFR < 30$ mL/[min•1.73 m²]. Based on [17, 18, 22]

groups. In subjects with normal vs severely impaired renal function and subjects with ESRD without hemodialysis, an AUC_{0-last} (geometric mean) of 212, 540, and 873 mg•h/L was attained, respectively (Table 1). Patients with mildly impaired kidney function showed only a slightly higher exposure (AUC_{0-last} of 218 mg•h/L). Furthermore, the half-life of cefiderocol increased clearly with deteriorating kidney function, with a geometric mean range from 2.8 h in normal kidney function to 9.6 h in ESRD without dialysis. In patients with ESRD undergoing hemodialysis, approximately 60% of cefiderocol were removed during dialysis [23]. Differences in PK between subjects with normal and impaired kidney function were mainly attributed to differences in clearance. In contrast, C_{max} and volumes of distribution were similar among different kidney function groups. Furthermore, Katsube et al. reported that hemodialysis did not relevantly affect protein binding. In a small study in five critically ill patients, König et al. observed that cefiderocol doses could be adjusted based on the presence of acute kidney injury and continuous renal replacement therapy, concluding that therapeutic drug monitoring might be viable [24]. In summary, dosing regimens should be adjusted based on kidney function to provide an appropriate exposure to cefiderocol [6].

3.3 Pharmacokinetic Drug–Drug Interactions

Based on data from in vitro experiments and phase I trials, no clinically relevant potential for drug–drug interactions is expected for cefiderocol [6]. Initial in vitro experiments indicated a potential inhibition of organic anion transporters 1 and 3, organic cation transporters 1 and 2, multidrug and toxin extrusion protein 2K, and organic anion transporting polypeptide 1B3, but a clinical trial in healthy volunteers concomitantly receiving cefiderocol with probe substrates indicated that cefiderocol had either no or no clinically relevant impact on the PK of the probe substrates [36]. The AUC_{0-inf} and C_{max} ratios ranged from 0.92 to 1.28 (Table 1 of the Electronic Supplementary Material [ESM]) [25]. Overall, the risk of cefiderocol being either a perpetrator or victim of drug–drug interactions appears to be low.

3.4 Population Pharmacokinetic Models

Katsube et al. described the population PK of cefiderocol based on phase I data in healthy volunteers [17] and patients with impaired kidney function [23], including patients receiving intermittent hemodialysis [26]. This modeling work focused on the evaluation of covariates affecting the PK of cefiderocol, and a subsequent evaluation of dosing regimens using simulations. A linear three-compartment model was found to describe the PK of cefiderocol sufficiently well (Table 2). The authors identified MDRD as an

important predictor of cefiderocol clearance, while volumes of distribution were found to be related to body weight. Arguing that $CGCL_{CR}$ might be a better predictor in patients with an augmented clearance, the authors alternatively used the $CGCL_{CR}$ equation to identify patients with a creatinine clearance of at least 120 mL/min. Consequently, the authors presented a selection of final models comprising MDRD or $CGCL_{CR}$ combined with body weight. In contrast to kidney function, body weight was found to have a limited and possibly clinically irrelevant impact on the PK of cefiderocol. For example, the central volume of distribution was estimated to be 83% in patients with a body weight of 50 kg compared to 70 kg, and 115% for a body weight of 90 kg compared to 70 kg. The clearance via hemodialysis was estimated to be 7.37 L/h, with a limited inter-individual variability of 12.7%, which exceeded the typical clearance of 5.59 L/h in healthy volunteers. Overall, the inter-individual variability of pharmacokinetic parameters was limited both in healthy volunteers and patients with impaired kidney function. For example, the inter-individual variability of clearance range was from only 12% in healthy volunteers to 17% in subjects with impaired kidney function based on a model including MDRD. Based on simulations, Katsube et al. presented dosing regimens that were found to be suitable to reach a probability of target attainment (PTA) of > 90% given an fT > MIC target of 75% and an MIC of up to 4 mg/L in a simulated patient population. Starting from a prolonged 3-h infusion of 2000 mg of cefiderocol administered q8h in patients with an MDRD $GFR > 90$ mL/min/1.73 m², a shorter dosing interval was assumed in patients with augmented clearance and a decreased dose and/or an increased dosing interval was assumed in patients with impaired kidney function. In patients with augmented clearance, i.e., with a $CGCL_{CR} > 120$ mL/min, the dosing interval was reduced to 6 hours. In patients with a moderately or severely impaired kidney function, lower doses of 1500 and 1000 mg q8h, respectively, were chosen. In patients with ESRD with and without intermittent hemodialysis, a dose of 750 mg every 12 h was used. In the case of intermittent hemodialysis, the authors furthermore simulated the administration of a supplemental dose of 750 mg as a prolonged infusion after completion of the hemodialysis. Finally, the authors concluded that the evaluated dosing regimen is expected to provide a therapeutic drug exposure across different levels of renal function.

More recently, Kawaguchi et al. published an extensive population pharmacokinetic evaluation of cefiderocol based on 3427 plasma concentrations from 516 patients and healthy volunteers [27]. The evaluated data stemmed from the phase III trial CREDIBLE-CR, which included patients with pneumonia, blood-stream infection (BSI)/sepsis and cUTI [4], the phase III trial APEKS-NP, which included patients with pneumonia [28], as well as the phase II trial APEKS-cUTI, which included patients with cUTI and

Table 2 Population pharmacokinetic parameters [22, 26, 27]

Parameter	Final model* with CrCL ^a (<i>n</i> = 3427)		Final model** with CrCL ^a (<i>n</i> = 2571)		Final model*** with CrCL ^a (<i>n</i> = 1624)	
	Estimate	%RSE	Estimate	%RSE	Estimate	%RSE
CL (L/h)	4.04	1.80	4.23	1.50	4.83	2.90
V1 (L)	7.78	5.20	7.93	3.10	7.58	2.70
Q2 (L/h)	6.19	5.70	5.75	5.30	5.45	4.50
V2 (L)	5.77	3.20	5.41	3.30	5.54	2.50
Q3 (L/h)	0.127	14.1	0.109	17.2	0.0969	17.0
V3 (L)	0.798	6.40	0.734	7.30	0.681	8.30
Effect of CrCL on CL (CrCL cut-off value of 150 mL/min)	0.682	4.00	0.653	3.90	–	–
Effect of body weight on V1	0.580	12.2	0.798	12.2	–	–
Effect of pneumonia on CL	0.981	4.10	–	–	–	–
Effect of BSI/sepsis on CL	1.08	10.4	–	–	–	–
Effect of infection with cUTI in CREDIBLE-CR study on CL	0.872	6.40	–	–	–	–
Effect of infection with cUTI/AUP in APEKS-cUTI study on CL	1.27	3.10	–	–	–	–
Effect of albumin level on V1	0.617	10.9	–	–	–	–
Effect of infection on V1	1.39	6.70	–	–	–	–
IIV for CL (CV%)	37.5	10.4	31.8	15.8	11.9	18.7
IIV for V1 (CV%)	56.9	19.8	45.8	28.2	19.3	19.7
IIV for V2 (CV%)	33.6	35.0	38.2	35.5	14.2	42.6
Proportional residual error (CV%)	20.5	5.10	15.1	12.8	12.0	14.1

This table show point estimates and %RSE of parameters reported for different population pharmacokinetic models

AUP acute uncomplicated pyelonephritis, BSI blood-stream infection, CL clearance from central compartment, CrCL creatinine clearance, cUTI complicated urinary tract infection, CV coefficient of variation, IIV inter-individual variability, *n* number of included samples, Q2 first inter-compartmental clearance, Q3 second inter-compartmental clearance, RSE relative standard error, V1 central volume of distribution, V2 second peripheral volume of distribution, V3 third peripheral volume of distribution

Based on *[27], **[22], ***[26]

^aCreatinine clearance calculated by the Cockcroft-Gault equation

acute uncomplicated pyelonephritis (AUP) [29], and from the abovementioned phase I trials in healthy volunteers [17] and subjects with impaired kidney function [23]. A total of 1861 plasma concentrations were available from healthy volunteers and 1566 from patients. Based on a linear three-compartment model (Table 2), Kawaguchi et al. found that the clearance of cefiderocol was strongly related to CGCL_{CR}. Differences in the PK of cefiderocol between different sites of infection (BSI/sepsis, pneumonia, or cUTI/AUP) and compared to subjects without infection were deemed clinically irrelevant despite statistical significance. This comprised a 27% higher clearance in patients with cUTI/AUP compared with subjects without infection and a 39% higher central volume of distribution in infected patients compared with subjects without infection. Additionally, a negative correlation between albumin levels and the central volume of distribution was observed. Using the established model, Kawaguchi et al. concluded that the *ft* > MIC based on

MICs of pathogens isolated from 60 patients of the CREDIBLE-CR study and 97 patients of the APEKS-NP study was 100% in 97% of the patients. Based on simulations with the kidney function-specific dosing regimens described by Katsube et al. [26], the authors concluded that a PTA of > 95% was attained for an MIC up to 4 mg/L irrespective of the site of infection and renal function when assuming an *ft* > MIC target of 75%. Given an *ft* > MIC target of 100%, the PTA was > 90% for MICs up to 4 mg/L in all but one patient group. The only exception was the group of patients with normal renal function and BSI/sepsis, who achieved a PTA of 86%. The respective results are shown in Table 2 of the ESM. Consequently, the authors concluded that the evaluated dosing regimens provide adequate plasma exposure to cefiderocol in patients with pneumonia, BSI/sepsis, and cUTI. Kidney function was confirmed as the main predictor of cefiderocol PK, while differences between subjects

without infection and different patient groups were deemed clinically irrelevant.

4 Pharmacodynamics

Cefiderocol shows a time-dependent killing activity, with $fT > MIC$ being the main predictor of efficacy [21, 30]. Nakamura et al. studied the pharmacodynamics of cefiderocol using neutropenic murine thigh and lung infection models, in which infections were caused by multiple Gram-negative bacteria [21]. A dose fractionation study showed that $fT > MIC$ was superior to predict efficacy compared to the maximum free drug concentration or the AUC divided by the MIC in describing the in vivo efficacy of cefiderocol. Moreover, the authors determined the $fT > MIC$ required for efficacy against multiple carbapenem-susceptible and carbapenem-resistant bacterial strains with cefiderocol MICs between 0.125 and 16 mg/L (Table 3). Matsumoto et al. investigated the efficacy of cefiderocol against carbapenem-resistant isolates of *K. pneumoniae* ($n = 2$), *P. aeruginosa* ($n = 2$), and *A. baumannii* ($n = 2$) in an immunocompetent-rat respiratory tract infection model (MIC range from 0.125 to 8 mg/L) [30]. Humanized exposures of 2000 mg of cefiderocol q8h administered over 3 h led to enhanced efficacy compared with infusions over 1 h, expressed by \log_{10} -reductions in the number of colony-forming units (CFU) per lung of 3.0–4.4 for the prolonged infusion time and 0.7–3.7 for the shorter infusion time. The authors extrapolated that 3-h infusions would achieve 100% $fT > MIC$ for MICs up to 4 mg/L, whereas 1-h infusions would achieve 75% $fT > MIC$. In a neutropenic murine thigh model, Monogue et al. studied the efficacy of cefiderocol against 95 Gram-negative isolates of *Enterobacteriaceae* ($n = 39$), *P. aeruginosa* ($n = 21$), and *A. baumannii* ($n = 35$) with MICs between 0.12 and > 256 mg/L to identify a potential MIC breakpoint [31]. They used humanized dosing regimens of 2000 mg of cefiderocol

given q8h as 3-h infusions. In isolates with MICs ≤ 4 mg/L ($n = 67$), bacterial stasis or a ten-fold reduction in CFU was achieved for 77%, 85%, and 88% of *Enterobacteriaceae*, *P. aeruginosa*, and *A. baumannii*, respectively. For 28 tested strains with MICs ≥ 8 mg/L, similar efficacy was observed in only two isolates. Based on humanized pharmacokinetic data, the authors predicted an $fT > MIC$ of 96.2% in isolates with MICs ≤ 4 mg/L. Using a subset of 15 isolates, the authors compared the efficacies of cefiderocol, ceftazidime, and meropenem in the same model, concluding that cefiderocol provided efficacy against all ceftazidime-resistant or meropenem-resistant isolates with a mean bacterial reduction of 1.5 \log_{10} CFU after 24 h. Humanized exposures of cefiderocol showed sustained killing activity without the development of adaptive resistance over 72 h against a group of different Gram-negative bacteria ($n = 11$) with an MIC range from 0.5 to 8 mg/L in a neutropenic murine thigh model performed by Stainton et al. [32]. In a murine urinary tract infection model, cefiderocol led to a > 3 - \log_{10} reduction in CFU against carbapenem-resistant *K. pneumoniae*-expressing KPC-2 and *P. aeruginosa*-expressing IMP-1 [33]. Cefiderocol was furthermore tested against eight *P. aeruginosa* isolates that showed a tendency to develop resistance to other non-catechol siderophore antibiotics in preclinical trials in another neutropenic murine thigh model [34]. Humanized exposures of cefiderocol produced a > 1 - \log_{10} reduction in CFU in all eight isolates (≥ 2 - \log reduction in seven of the eight tested isolates), irrespective of their resistance to other non-catechol siderophore antibiotics, ceftazidime, or levofloxacin. In vitro experiments indicate that the antibacterial activity of cefiderocol is enhanced under iron-limited conditions [35]. Kidd et al. [36] investigated whether iron-overloaded conditions in the host affect the efficacy of cefiderocol using a murine thigh infection model. The authors observed no significant difference in efficacy against Gram-negative bacteria comparing iron-overloaded and normal hosts. In a recently published analysis based on the clinical

Table 3 Cefiderocol $fT > MIC$ required for efficacy against multiple bacterial strains in neutropenic murine thigh and lung infection models (MICs: 0.125–16 mg/L) [6, 21]

Model	Organism (number of tested strains)	$fT > MIC$ (mean \pm SD)	
		Static	1 - \log_{10} reduction
Thigh infection	<i>Enterobacteriaceae</i> ^a (10)	62.5 \pm 27.4	73.3 \pm 23.3
	<i>Pseudomonas aeruginosa</i> (3)	63.0 \pm 15.5	72.2 \pm 21.4
	Carbapenem-resistant strains (7)	NA	85.2 \pm 12.1
	Carbapenem-susceptible strains (6)	NA	61.3 \pm 25.0
Lung infection	<i>Enterobacteriaceae</i> ^a (9)	54.7 \pm 24.1	64.4 \pm 22.5
	<i>Pseudomonas aeruginosa</i> (3)	57.4 \pm 10.2	70.3 \pm 9.0
	<i>Acinetobacter baumannii</i> (3)	82.0 \pm 4.6	88.1 \pm 3.4
	<i>Stenotrophomonas maltophilia</i> (4)	45.6 \pm 18.9	53.9 \pm 18.1

$fT > MIC$ fraction of time during the dosing interval where the free plasma drug concentration exceeds the minimum inhibitory concentration, NA not available, SD standard deviation

^a*Enterobacteriaceae* included strains of *Escherichia coli* and *Klebsiella pneumoniae*. Based on [6, 21]

trials CREDIBLE-CR and APEKS-NP, Kawaguchi et al. [27] tried to relate human pharmacokinetic data to clinical efficacy measures such as clinical outcome, microbiological outcome, and vital status. The authors were unable to identify a clear pharmacokinetic/pharmacodynamic relationship for any of the efficacy measures because the $fT > MIC$ was 100% in 97% of patients ($MICs: \leq 0.03$ to 64 mg/L). This finding indicates that the dosing regimen of 2000 mg q8h, adjusted based on renal function, is likely to provide sufficient exposure for patients with pneumonia, BSI/sepsis, or cUTI. Overall, an $fT > MIC$ of at least 90% appears to be a suitable pharmacokinetic/pharmacodynamic target in clinical practice as it provided a $\geq 1 - \log_{10}$ reduction in CFU in vitro and in animal models. An $fT > MIC$ of 50%, which is a typical target for other β -lactam antibiotics [37], might be insufficient in this case (Table 3).

5 Clinical Efficacy Trials

The clinical efficacy of ceftiderocol has been studied in one phase II trial for the treatment of cUTI and AUP (APEKS-cUTI) and two phase III trials (CREDIBLE-CR and APEKS-NP). APEKS-cUTI, a multinational, multicenter, double-blind, non-inferiority trial, evaluated the efficacy of ceftiderocol compared to imipenem/cilastatin in patients diagnosed with cUTI or AUP caused by carbapenem-susceptible Gram-negative bacteria [29]. Patients ≥ 18 years of age were randomized 2:1 to receive ceftiderocol (2000 mg q8h) or imipenem/cilastatin (1000/1000 mg q8h). The treatment duration was 7–14 days and doses were adjusted based on renal function and body weight. The primary endpoint was defined as the composite of clinical response and microbiological eradication at the test of cure assessment, 7 days after the end of treatment. The primary efficacy analysis was performed in the microbiological intention-to-treat (mITT) population, which consisted of treated patients who had a Gram-negative uropathogen at baseline with $> 10^5$ CFU/mL in urine. The primary efficacy endpoint was achieved by 73% (183/252) in the ceftiderocol group and 55% (65/119) in the imipenem/cilastatin group (adjusted treatment difference 18.6%, 95% confidence interval 8.2–28.9). Ceftiderocol showed non-inferiority to imipenem/cilastatin for the primary endpoint at a – 15% non-inferiority margin.

CREDIBLE-CR investigated the efficacy of ceftiderocol vs BAT for the treatment of severe carbapenem-resistant Gram-negative infections [4]. This multinational, multicenter, open-label trial was exploratory in nature and did not comprise predefined hypothesis testing. Furthermore, it was not limited to a single infection site if infections were caused by carbapenem-resistant bacteria. Forty-five percent of patients had hospital-acquired pneumonia (HAP), ventilator-acquired pneumonia (VAP), or healthcare-associated

pneumonia (HCAP), 31% had BSI and/or sepsis (secondary to any source of infection), and 24% had cUTI. Patients were randomized 2:1 to receive ceftiderocol (2000 mg administered q8h) or BAT. Best available therapy was determined by the investigator and could include a maximum of three antibiotic agents in combination, whereas in the ceftiderocol group only one additional Gram-negative antibiotic was allowed (for cUTI, only monotherapy was permitted). In the carbapenem-resistant mITT population, 29% of patients treated with BAT received monotherapy, whereas 83% of patients in the ceftiderocol group received monotherapy. Most of the treatment regimens in the BAT group included colistin (66%), while only one patient in the ceftiderocol group received colistin. Treatment duration was 7–14 days (could be extended up to 21 days) in HAP/VAP/HCAP or BSI/sepsis and ≥ 5 days for cUTIs. The carbapenem-resistant mITT population consisted of treated patients with a confirmed carbapenem-resistant Gram-negative pathogen. *Acinetobacter baumannii* was the most common pathogen isolated in both treatment groups, followed by *K. pneumoniae* and *P. aeruginosa*. The primary efficacy endpoints for patients in the carbapenem-resistant mITT population were clinical cure at the test of cure assessment for patients with HAP/VAP/HCAP and BSI/sepsis and microbiological eradication for patients with cUTI (Table 4). All-cause mortality was a secondary endpoint (Table 5). In absolute numbers, there was a higher all-cause mortality in the ceftiderocol group compared with the BAT group at all study timepoints. In the safety population, 6.4% (95% confidence interval – 8.6 to 19) more deaths were observed at day 28, 15% (– 0.2 to 29) more deaths were observed at the end of the study, and 13% (– 2.5 to 27) more deaths were observed at day 49 in the ceftiderocol group compared with the BAT group. At the end of the study, 34% (34/101) of the patients in the ceftiderocol group and 18% (9/49) in the BAT group died in the safety population. In particular, infections with *Acinetobacter* spp. were related to higher all-cause mortality at end of the study in the ceftiderocol group (50%) compared with the BAT group (18%). Whether these observations reflect a true difference between the two groups needs further investigation. A comparison of post-hoc estimates of ceftiderocol C_{max} and AUC_{0-8h} values at steady state showed no significant relationship between ceftiderocol exposure and survival in the CREDIBLE-CR trial [38].

APEKS-NP, a multinational, multicenter, double-blind, non-inferiority trial, compared ceftiderocol and meropenem in the treatment of nosocomial pneumonia caused by Gram-negative bacteria [28]. Patients with nosocomial pneumonia were randomized 1:1 to receive 2000 mg of ceftiderocol or 2000 mg of meropenem q8h, for a treatment duration of 7–14 days. To cover MRSA as well as Gram-positive bacteria in the ceftiderocol arm, patients in both treatment groups received 600 mg of linezolid every 12 h for at least 5 days.

Table 4 Clinical efficacy results from cefiderocol phase II and III clinical trials in the mITT populations [4, 28, 29]

Trial	Description	n	Clinical outcome at TOC ^a		Difference (95% CI)	Microbiological eradication at TOC		Difference (95% CI)
			Cefiderocol	Comparator		Cefiderocol	Comparator	
APEKS-cUTI	Cefiderocol vs imipenem/cilastatin for the treatment of cUTI or AUP	452	90% (226/252)	87% (104/119)	2.39% (− 4.66 to 9.44)	73% (184/252)	56% (67/119)	17.25% (6.92–27.58)
CREDIBLE-CR	Cefiderocol vs best available therapy for the treatment of NP ^b , BSI/sepsis, and cUTI	152	Overall					
			53% (42/80)	50% (19/38)		31% (25/80)	24% (9/38)	
			NP ^b					
			50% (20/40)	53% (10/19)		23% (9/40)	21% (4/19)	
			BSI/sepsis					
APEKS-NP	Cefiderocol vs meropenem for the treatment of NP	300	43% (10/23)	43% (6/14)		30% (7/23)	29% (4/14)	
			cUTI					
			71% (12/17)	60% (3/5)		53% (9/17)	20% (1/5)	
APEKS-NP	Cefiderocol vs meropenem for the treatment of NP	300	65% (94/145)	67% (98/147)	− 1.8% (− 12.7 to 9.0)	41% (59/145)	42% (61/147)	− 0.8% (− 12.1 to 10.5)

BSI blood-stream infection, CI confidence interval, cUTI complicated urinary tract infection, HAP hospital-acquired pneumonia, HCAP healthcare-associated pneumonia, mITT microbiological intention-to-treat, n number of randomized patients, NP nosocomial pneumonia, TOC test of cure, VAP ventilator-acquired pneumonia

^aDefined as clinical response in APEKS-cUTI and clinical cure in CREDIBLE-CR/APEKS-NP

^bIncluded HAP/VAP/HCAP. APEKS-cUTI and APEKS-NP were randomized, double-blind, non-inferiority trials. CREDIBLE-CR was a randomized, open-label, descriptive trial. Based on [4, 28, 29]

Table 5 All-cause mortality in cefiderocol phase III clinical trials [4, 28]

Trial	Day 14		Day 28		End of study	
	Cefiderocol	Comparator	Cefiderocol	Comparator	Cefiderocol	Comparator
CREDIBLE-CR ^a	Overall					
	19% (19/101)	12% (6/49)	25% (25/101)	18% (9/49)	34% (34/101)	18% (9/49)
	HAP/VAP/HCAP					
	24% (11/45)	14% (3/22)	31% (14/45)	18% (4/22)	42% (19/45)	18% (4/22)
	BSI/sepsis					
APEKS-NP ^b	17% (5/30)	6% (1/17)	23% (7/30)	18% (3/17)	37% (11/30)	18% (3/17)
	cUTI					
	12% (3/26)	20% (2/10)	15% (4/26)	20% (2/10)	15% (4/26)	20% (2/10)
APEKS-NP ^b	12% (18/145)	12% (17/146)	21% (30/143)	21% (30/146)	27% (38/142)	23% (34/146)

Numbers in brackets represent deceased/total patients in the respective group. Based on [4, 28]

BSI blood-stream infection, cUTI complicated urinary tract infection, HAP hospital-acquired pneumonia, HCAP healthcare-associated pneumonia, mITT microbiological intention-to-treat, VAP ventilator-acquired pneumonia

^aReference safety population, comparator best available therapy

^bReference mITT population, comparator meropenem

All-cause mortality at day 14 was defined as the primary efficacy endpoint for the mITT population, which consisted of treated patients diagnosed with nosocomial pneumonia not only caused by Gram-positive pathogens. At day 14,

all-cause mortality was 12.4% for cefiderocol and 11.6% for meropenem, with a treatment difference of 0.8% (95% confidence interval − 6.6 to 8.2). Cefiderocol showed non-inferiority to meropenem for the primary efficacy endpoint

at a – 12.5% non-inferiority margin. Clinical cure and microbiological eradication rates in the mITT population were secondary endpoints (Table 4). Patients included in the APEKS-NP study were comparable to those in the CREDIBLE-CR study diagnosed with HAP/VAP/HCAP, regarding sex distribution, age, creatinine clearance, APACHE score, and the need for ventilation (59.7% in APEKS-NP and 74.6% in CREDIBLE-CR). Notably, *A. baumannii* caused 55.2% of infections in the CREDIBLE-CR HAP/VAP/HCAP subgroup, while only 15.8% of patients in the APEKS-NP study were infected by *A. baumannii*. The proportion of patients with treatment failure before randomization was 64.2% in the CREDIBLE-CR subgroup and 32.6% in the APEKS-NP study [39].

Overall, cefiderocol showed non-inferiority to imipenem/cilastatin in the treatment of cUTI/AUP (APEKS-cUTI) and meropenem in the treatment of nosocomial pneumonia (APEKS-NP). Cefiderocol performed similarly to BAT in the treatment of severe carbapenem-resistant Gram-negative infections regarding clinical and microbiological efficacy (CREDIBLE-CR), but there was a numerically higher all-cause mortality in the cefiderocol group.

6 Safety and Tolerability

Safety data are available for subjects with renal impairment, patients with cUTI/AUP (APEKS-cUTI), patients with BSI/sepsis or pneumonia (CREDIBLE-CR), and patients with nosocomial pneumonia (APEKS-NP) [4, 17, 23, 28, 29]. In the CREDIBLE-CR study, the cure rate of cefiderocol and BAT were similar, but an increased mortality rate was reported in the cefiderocol group. Fourteen (of $n = 49$ [29%]) subjects in the BAT group and 36 (of $n = 101$ [36%]) subjects in the cefiderocol group died after the end of the study. Five deaths were considered due to the BAT and two deaths were attributed to cefiderocol by the investigators [4]. The APEKS-NP study found that in terms of mortality, cefiderocol was non-inferior to meropenem. In the APEKS-NP study, 34 ($n = 150$ [23%]) deaths were observed in the meropenem group while 39 ($n = 148$ [26%]) deaths were observed in the cefiderocol group [28]. One death ($n = 300$ [$< 1\%$]) occurred due to cardiac arrest in the cefiderocol group of the APEKS-cUTI study, but it was considered unrelated to cefiderocol by the investigator because of the past complicated medical history of the subject [29]. In the CREDIBLE-CR study, 13 ($n = 101$ [13%]) subjects discontinued in the cefiderocol group, with three discontinuations being considered to result from adverse events (AEs) to cefiderocol. While in the BAT group, five ($n = 49$ [10%]) subjects discontinued, in which two were considered due to drug-related AEs [4]. In the APEKS-NP study, 14 ($n = 148$ [9%]) subjects in the cefiderocol group and 16 ($n = 150$ [10%]) subjects in the meropenem group discontinued the study [29].

One healthy volunteer withdrew from a phase I trial because of a raised body temperature [17], and one subject from the group with moderate renal impairment (eGFR 30 to < 60 mL/min) withdrew prematurely from the phase I study in renal impaired subjects because of an AE of urticaria [23]. Nearly half of the subjects in both the groups of the CREDIBLE-CR study had severe AEs [4]. In the APEKS-NP study, the most common AEs were urinary tract infection and hypokalemia with diarrhea, also reported in the CREDIBLE-CR study [4], and constipation. In the cefiderocol and meropenem groups, 3% of patients developed a *C. difficile* infection [28]. The safety profile observed in patients with and without renal impairment in phase II clinical trials (APEKS-cUTI) is consistent in terms of AEs, with the majority of AEs being mild to moderate. No deaths or serious AEs were reported and the drug was well tolerated [23]. Adverse events that occurred in both groups (cefiderocol and imipenem-cilastatin) were gastrointestinal disorders, including abdominal pain, nausea, vomiting, constipation, and diarrhea. The most common serious AE was *C. difficile* colitis in one patient in the cefiderocol group vs two patients in the imipenem-cilastatin group [29]. Please refer to Table 6 for an overview of AEs reported in phase I–III trials. Data on the relationship between cefiderocol plasma concentrations and the risk of adverse effects are currently not available for typical patient groups.

7 Special Populations

Available data on the PK, pharmacodynamics, efficacy, and safety of cefiderocol in special patient populations are scarce. This particularly concerns pediatric patients, pregnant and breastfeeding women, geriatric patients, and patients with hepatic impairments.

The safety, tolerability, and PK of single and multiple doses of cefiderocol in pediatric patients with confirmed or suspected Gram-negative bacterial infections are currently under evaluation in a non-randomized clinical trial (NCT04335539). Results from this trial are not available yet. Katsube et al. [40] recently proposed dosing regimens for pediatric patients with an age range of < 3 months to 18 years by combining a population pharmacokinetic model in adults with allometric scaling and a maturation factor that describes kidney maturation. Based on simulations, dosing regimens that provided AUCs comparable to adults were identified. Katsube et al. [40] suggested to consider chronological age, gestational age, and body weight to choose a proper dose and infusion duration. Of note, this evaluation is not based on data obtained from pediatric patients, and it is currently only published as an abstract. Single case reports in pediatric patients are available, such as the successful combined use of cefiderocol, meropenem/vaborbactam, and bacteriophages to treat a 10-year-old female patient with

Table 6 Adverse events reported for cefiderocol [4, 17, 23, 28, 29]

Type of adverse event	Phase I (HS)		Phase I (RIS) (n = 38)	Phase II APEKS-cUTI		Phase III APEKS-NP		Phase III CREDIBLE-CR	
	Cefiderocol (n = 32)	Placebo (n = 10)		Cefiderocol (n = 300)	Imipenem-cilastatin (n = 148)	Cefiderocol (n = 148)	Meropenem (n = 150)	Cefiderocol (n = 101)	Best available therapy (n = 49)
Deaths	–	–	–	–	–	39	35	34	09
Withdrawal	01	–	01	05	03	14	16	13	05
Skin and subcutaneous disorders ^a	14	–	05	12	08	–	–	–	–
Gastrointestinal disorders ^b	06	–	03	38	22	20	19	32	13
Upper respiratory tract infections/cough	02	–	01	07	01	–	–	–	–
Metabolism and nutrition disorder ^c	–	–	02	05	04	16	23	–	–
Infections and infestations ^d	–	–	01	02	07	04	04	29	11
Nervous system disorders ^e	02	–	02	11	17	–	–	–	–
Cardiac failure/hypertension	–	–	–	15	11	–	–	–	–
Renal and urinary disorders ^f	–	–	01	04	05	23	16	–	–
Laboratory investigations ^g	23	06	–	–	–	–	–	30	07
Other ^h	–	–	07	–	–	–	–	27	13

HS healthy subjects, n number of randomized subjects, RIS renally impaired subjects

^aSkin and subcutaneous disorders = rash, dermatitis, urticaria, pain on the infusion site, infusion-site erythema

^bGastrointestinal disorders = constipation, diarrhea, vomiting, nausea

^cMetabolism and nutrition disorder = gout, hypoglycemia, hypokalemia

^dInfections and infestations = *Clostridium difficile* infection, vaginal infection

^eNervous system disorders = headache, dizziness, insomnia, paresthesia, nausea

^fRenal and urinary disorders = polyuria, renal cyst, renal tract infections

^gLaboratory investigations = elevated aminotransferase, increase in blood creatine phosphokinase, increase in white blood cell count, blood lactate dehydrogenase level, blood urea level increased

^hOther = injury, poisoning, and procedural complications, arteriovenous fistula-site complication, postoperative wound complication, septic shock, vascular disorders, pyrexia, musculoskeletal and connective tissue disorder. Based on [4, 17, 23, 28, 29]

cystic fibrosis infected with pandrug-resistant *Achromobacter xylosoxidans* [41]. Because of the lack of relevant data, the Food and Drug Administration and European Medicines Agency labels of cefiderocol provide no recommendation on its use in pediatric patients.

Cefiderocol might be a viable treatment option in patients with cystic fibrosis, who often suffer from infections with MDR bacteria. However, only limited data are currently available for this special patient group. A study in patients with cystic fibrosis suffering from infections with MDR *A. xylosoxidans* before or after lung transplantation reported a good tolerability and clinical efficacy of cefiderocol [16]. Consequently, cefiderocol was considered a useful option in

treating *A. xylosoxidans* bacteremia in combination with other antibiotics by the authors. However, the authors also reported a high baseline resistance to cefiderocol and a high risk of relapse, defined as the isolation of *A. xylosoxidans* 6 months after completion of the antibiotic therapy. For example, in vitro resistance to cefiderocol at baseline was observed in three out of eight cases and microbiologic relapse occurred in 11 out of 12 cases. Consequently, further investigations on the use of cefiderocol in patients with cystic fibrosis are needed.

Data on the use of cefiderocol during pregnancy in humans are currently not available. Studies in rats and mice provided no signs of embryo-fetal toxicity or fetal malformations at a mean plasma exposure of 90% (rats) and 130% (mice) of the

average exposure attained in patients receiving cefiderocol doses of 2000 mg q8h [5]. Studies with radio-labeled cefiderocol administered to pregnant rats indicated that cefiderocol crosses the placenta, but the amount of cefiderocol found in rat fetuses was limited ($< 0.5\%$ of the administered dose) [5]. Similarly, human data on the excretion of cefiderocol into milk are currently not available. After the administration of radio-labeled cefiderocol to rats, peak cefiderocol concentrations in rat milk were approximately 6% of peak plasma concentrations in lactating rats [5]. Therefore, the Food and Drug Administration and European Medicines Agency labels suggest to carefully weigh the risks and benefits associated with breastfeeding, the exposure to cefiderocol, and the impact of the bacterial infection on the breastfeeding woman and the child [5, 6].

No dedicated evaluation of the PK, pharmacodynamics, efficacy, and safety of cefiderocol in geriatric patients is currently available. In the APEKS-cUTI trial, 158/67 out of 300 patients who received cefiderocol were aged 65/75 years or older. In this trial, no difference in efficacy and safety was observed across age ranges [42]. Furthermore, the potential effect of hepatic impairment on the treatment with cefiderocol has not been systematically evaluated in clinical trials yet. However, it appears unlikely that hepatic impairment relevantly affects cefiderocol treatments as the liver plays a negligible role in the PK of cefiderocol [5, 43].

8 Conclusions

The predominantly renal excretion, the limited inter-individual pharmacokinetic variability, the low potential for drug–drug interactions, and the limited differences between a selection of evaluated patient groups and healthy volunteers are desirable pharmacokinetic properties that suggest that cefiderocol exposure might be well predictable in a clinical setting. However, data in several relevant patient groups, such as critically ill patients, are currently lacking. The short half-life demands a frequent administration of q8h, with even shorter dosing intervals in the case of augmented clearance. Available evaluations suggest that doses and dosing intervals should be adjusted in patients with impaired kidney function. A significant removal of cefiderocol from the body is expected during hemodialysis, which might be alleviated by administering an additional dose after completion of the hemodialysis. Clinical efficacy trials indicate that cefiderocol is non-inferior to imipenem/cilastatin in the treatment of cUTI/AUP and to meropenem in the treatment of nosocomial pneumonia, while cefiderocol performed similarly to the BAT in the treatment of severe carbapenem-resistant Gram-negative infections regarding clinical and microbiological efficacy. A numerically higher all-cause mortality was observed in the cefiderocol group, which is not yet fully understood. Overall, cefiderocol shows

favorable pharmacokinetic/pharmacodynamic properties and an acceptable safety profile, suggesting that cefiderocol might be a viable option to treat infections with bacteria resistant to other antibiotics in the future. Additional data from patient groups of interest are expected to further clarify the role of cefiderocol in specific clinical scenarios.

Supplementary Information The online version contains supplementary material available at <https://doi.org/10.1007/s40262-021-01063-5>.

Declarations

Funding Open Access funding enabled and organized by Projekt DEAL. This work was based on internal funding of the Department I of Pharmacology, University of Cologne, Cologne, Germany.

Conflicts of Interest/Competing Interests Muhammad Bilal, Lobna El Tabei, Sören Büsker, Christian Krauss, and Uwe Fuhr declare no conflict of interest. Max Taubert is an employee of Novartis AG.

Ethics Approval Not applicable.

Consent to Participate Not applicable.

Consent for Publication Not applicable.

Availability of Data and Material Not applicable.

Code Availability Not applicable.

Authors' Contributions All authors screened articles and abstracts for inclusion, discussed results and conclusions, and wrote the manuscript. MT and UF supervised the review process.

Open Access This article is licensed under a Creative Commons Attribution-NonCommercial 4.0 International License, which permits any non-commercial use, sharing, adaptation, distribution and reproduction in any medium or format, as long as you give appropriate credit to the original author(s) and the source, provide a link to the Creative Commons licence, and indicate if changes were made. The images or other third party material in this article are included in the article's Creative Commons licence, unless indicated otherwise in a credit line to the material. If material is not included in the article's Creative Commons licence and your intended use is not permitted by statutory regulation or exceeds the permitted use, you will need to obtain permission directly from the copyright holder. To view a copy of this licence, visit <http://creativecommons.org/licenses/by-nc/4.0/>.

References




1. Sato T, Yamawaki K. Cefiderocol: discovery, chemistry, and in vivo profiles of a novel siderophore cephalosporin. *Clin Infect Dis*. 2019;69:S538–43.
2. Aoki T, Yoshizawa H, Yamawaki K, Yokoo K, Sato J, Hisakawa S, et al. Cefiderocol (S-649266), a new siderophore cephalosporin exhibiting potent activities against *Pseudomonas aeruginosa* and other gram-negative pathogens including multi-drug resistant bacteria: structure activity relationship. *Eur J Med Chem*. 2018;155:847–68.

3. El-Lababidi RM, Rizk JG. Cefiderocol: a siderophore cephalosporin. *Ann Pharmacother*. 2020;54:1215–31.
4. Bassetti M, Echols R, Matsunaga Y, Ariyasu M, Doi Y, Ferrer R, et al. Efficacy and safety of cefiderocol or best available therapy for the treatment of serious infections caused by carbapenem-resistant Gram-negative bacteria (CREDIBLE-CR): a randomised, open-label, multicentre, pathogen-focused, descriptive, phase 3 trial. *Lancet Infect Dis*. 2021;21:226–40.
5. Shionogi & Co. Ltd. Structured product label of Fetroja. 2020. https://www.accessdata.fda.gov/drugsatfda_docs/label/2020/209445s0021bl.pdf. Accessed 31 Jul 2021
6. European Medicines Agency. EMEA/H/C/004829: summary of product characteristics of Fetroja. 2020. <https://www.ema.europa.eu/en/medicines/human/EPAR/fetroja>. Accessed 31 Jul 2021
7. Abdul-Mutakabbir JC, Alosaimy S, Morrisette T, Kebriaei R, Rybak MJ. Cefiderocol: a novel siderophore cephalosporin against multidrug-resistant Gram-negative pathogens. *Pharmacotherapy*. 2020;40:1228–47.
8. Neilands JB. Siderophores: structure and function of microbial iron transport compounds. *J Biol Chem*. 1995;270:26723–6.
9. Hider RC, Kong X. Chemistry and biology of siderophores. *Nat Prod Rep*. 2010;27:637–57.
10. Braun V, Pramanik A, Gwinner T, Köberle M, Bohn E. Sideromycins: tools and antibiotics. *Biometals*. 2009;22:3–13.
11. Wenciewicz TA, Miller MJ. Sideromycins as pathogen-targeted antibiotics. *Top Med Chem*. 2017;26:151–83. https://doi.org/10.1007/7355_2017_19
12. Dobias J, Dénervaud-Tendon V, Poirel L, Nordmann P. Activity of the novel siderophore cephalosporin cefiderocol against multidrug-resistant Gram-negative pathogens. *Eur J Clin Microbiol Infect Dis*. 2017;36:2319–27.
13. Hackel M, Tsuji M, Echols R, Sahm D. In vitro antibacterial activity of cefiderocol (S-649266) against Gram-negative clinical strains collected in North America and Europe (SIDERO-WT-2014 study). Poster Present IDWeek. 2016; pp. 26–30. www.ihma.com/app/uploads/1828.pdf
14. Kohira N, West J, Ito A, Ito-Horiyama T, Nakamura R, Sato T, et al. In vitro antimicrobial activity of a siderophore cephalosporin, S-649266, against enterobacteriaceae clinical isolates, including carbapenem-resistant strains. *Antimicrob Agents Chemother*. 2016;60:729–34.
15. Karlowsky JA, Hackel MA, Tsuji M, Yamano Y, Echols R, Sahm DF. In vitro activity of cefiderocol, a siderophore cephalosporin, against Gram-negative bacilli isolated by clinical laboratories in North America and Europe in 2015–2016: SIDERO-WT-2015. *Int J Antimicrob Agents*. 2019;53:456–66.
16. Warner NC, Bartelt LA, Lachiewicz AM, Tompkins KM, Miller MB, Alby K, et al. Cefiderocol for the treatment of adult and pediatric patients with cystic fibrosis and *Achromobacter xylosoxidans* infections. *Clin Infect Dis*. 2020;ciaa1847. <https://doi.org/10.1093/cid/ciaa1847>
17. Saisho Y, Katsube T, White S, Fukase H, Shimada J. Pharmacokinetics, safety, and tolerability of cefiderocol, a novel siderophore cephalosporin for Gram-negative bacteria, in healthy subjects. *Antimicrob Agents Chemother*. 2018;62:e02163–e2217.
18. Miyazaki S, Katsube T, Shen H, Tomek C, Narukawa Y. Metabolism, excretion, and pharmacokinetics of [14C]-cefiderocol (S-649266), a siderophore cephalosporin, in healthy subjects following intravenous administration. *J Clin Pharmacol*. 2019;59:958–67.
19. Katsube T, Saisho Y, Shimada J, Furuie H. Intrapulmonary pharmacokinetics of cefiderocol, a novel siderophore cephalosporin, in healthy adult subjects. *J Antimicrob Chemother*. 2019;74:1971–4.
20. Lee YR, Yeo S. Cefiderocol, a new siderophore cephalosporin for the treatment of complicated urinary tract infections caused by multidrug-resistant pathogens: preclinical and clinical pharmacokinetics, pharmacodynamics, efficacy and safety. *Clin Drug Investig*. 2020;40:901–13.
21. Nakamura R, Ito-Horiyama T, Takemura M, Toba S, Matsumoto S, Ikehara T, et al. In vivo pharmacodynamic study of cefiderocol, a novel parenteral siderophore cephalosporin, in murine thigh and lung infection models. *Antimicrob Agents Chemother*. 2019;63:1–9.
22. Kawaguchi N, Katsube T, Echols R, Wajima T. Population pharmacokinetic analysis of cefiderocol, a parenteral siderophore cephalosporin, in healthy subjects, subjects with various degrees of renal function, and patients with complicated urinary tract infection or acute uncomplicated pyelonephritis. *Antimicrob Agents Chemother*. 2018;62:e01391–e1417.
23. Katsube T, Echols R, Ferreira JCA, Krenz HK, Berg JK, Gallo-way C. Cefiderocol, a siderophore cephalosporin for Gram-negative bacterial infections: pharmacokinetics and safety in subjects with renal impairment. *J Clin Pharmacol*. 2017;57:584–91.
24. König C, Both A, Rohde H, Kluge S, Frey OR, Röhr AC, et al. Cefiderocol in critically ill patients with multi-drug resistant pathogens: real-life data on pharmacokinetics and microbiological surveillance. *Antibiotics*. 2021;10:649.
25. Katsube T, Miyazaki S, Narukawa Y, Hernandez-Illas M, Wajima T. Drug–drug interaction of cefiderocol, a siderophore cephalosporin, via human drug transporters. *Eur J Clin Pharmacol*. 2018;74:931–8.
26. Katsube T, Wajima T, Ishibashi T, Ferreira JCA, Echols R. Pharmacokinetic/pharmacodynamic modeling and simulation of cefiderocol, a parenteral siderophore cephalosporin, for dose adjustment based on renal function. *Antimicrob Agents Chemother*. 2017;61:e01381–e1416.
27. Kawaguchi N, Katsube T, Echols R, Wajima T. Population pharmacokinetic and pharmacokinetic/pharmacodynamic analyses of cefiderocol, a parenteral siderophore cephalosporin, in patients with pneumonia, bloodstream infection/sepsis, or complicated urinary tract infection. *Antimicrob Agents Chemother*. 2021;65:e01437–e1520.
28. Wunderink RG, Matsunaga Y, Ariyasu M, Clevenbergh P, Echols R, Kaye KS, et al. Cefiderocol versus high-dose, extended-infusion meropenem for the treatment of Gram-negative nosocomial pneumonia (APEKS-NP): a randomised, double-blind, phase 3, non-inferiority trial. *Lancet Infect Dis*. 2021;21:213–25.
29. Portsmouth S, van Veenhuizen D, Echols R, Machida M, Ferreira JCA, Ariyasu M, et al. Cefiderocol versus imipenem-cilastatin for the treatment of complicated urinary tract infections caused by Gram-negative uropathogens: a phase 2, randomised, double-blind, non-inferiority trial. *Lancet Infect Dis*. 2018;18:1319–28.
30. Matsumoto S, Singley CM, Hoover J, Nakamura R, Echols R, Rittenhouse S, et al. Efficacy of cefiderocol against carbapenem-resistant gram-negative bacilli in immunocompetent-rat respiratory tract infection models recreating human plasma pharmacokinetics. *Antimicrob Agents Chemother*. 2017;61:e00700–e717.
31. Monogue ML, Tsuji M, Yamano Y, Echols R, Nicolau DP. Efficacy of humanized exposures of cefiderocol (S-649266) against a diverse population of Gram-negative bacteria in a murine thigh infection model. *Antimicrob Agents Chemother*. 2017;61:e01022–e1117.
32. Stainton SM, Monogue ML, Tsuji M, Yamano Y, Echols R, Nicolau DP. Efficacy of humanized cefiderocol exposures over 72 hours against a diverse group of Gram-negative isolates in the neutropenic murine thigh infection model. *Antimicrob Agents Chemother*. 2019;63:e01040–e1118.
33. Matsumoto S, Kanazawa S, Nakamura R, Tsuji M, Sato T, Yamano Y. In vivo efficacy of cefiderocol against carbapenem-resistant

- Gram-negative bacilli in murine urinary tract infection models. *Open Forum Infect Dis.* 2017;4:S472.
34. Ghazi IM, Monogue ML, Tsuji M, Nicolau DP. Humanized exposures of cefiderocol, a siderophore cephalosporin, display sustained in vivo activity against siderophore-resistant *Pseudomonas aeruginosa*. *Pharmacology.* 2018;101:278–84.
 35. Ito A, Nishikawa T, Matsumoto S, Yoshizawa H, Sato T, Nakamura R, et al. Siderophore cephalosporin cefiderocol utilizes ferric iron transporter systems for antibacterial activity against *Pseudomonas aeruginosa*. *Antimicrob Agents Chemother.* 2016;60:7396–401.
 36. Kidd JM, Abdelraouf K, Nicolau DP. Development of neutropenic murine models of iron overload and depletion to study the efficacy of siderophore-antibiotic conjugates. *Antimicrob Agents Chemother.* 2020;64:e01961–e2019.
 37. Roberts JA, Paul SK, Akova M, Bassetti M, De Waele JJ, Dimopoulos G, et al. DALI: defining antibiotic levels in intensive care unit patients: are current β -lactam antibiotic doses sufficient for critically ill patients? *Clin Infect Dis.* 2014;58:1072–83.
 38. Federal Drug Administration. FDA briefing document for the AMDAC. 2019. <https://www.fda.gov/media/131703/download>. Accessed 31 Jul 2021
 39. Shionogi Inc. Cefiderocol advisory committee briefing document. 2019. <https://www.fda.gov/media/131705/download>. Accessed 31 Jul 2021
 40. Katsube T, Echols R, Wajima T. 739. Prediction of cefiderocol pharmacokinetics and probability of target attainment in pediatric subjects for proposing dose regimens. *Open Forum Infect Dis.* 2019;6:S330–1.
 41. Gainey AB, Burch AK, Brownstein MJ, Brown DE, Fackler J, Horne B, et al. Combining bacteriophages with cefiderocol and meropenem/vaborbactam to treat a pan-drug resistant *Achromobacter* species infection in a pediatric cystic fibrosis patient. *Pediatr Pulmonol.* 2020;55:2990–4.
 42. Center for Drug Evaluation and Research (Food and Drug Administration). Approval package for Fetroja. 2020. https://www.accessdata.fda.gov/drugsatfda_docs/nda/2020/209445Orig1s002.pdf. Accessed 31 Jul 2021
 43. Parsels KA, Mastro KA, Steele JM, Thomas SJ, Kufel WD. Cefiderocol: a novel siderophore cephalosporin for multidrug-resistant Gram-negative bacterial infections. *J Antimicrob Chemother.* 2021;76:1379–91.



Cefepime Population Pharmacokinetics, Antibacterial Target Attainment, and Estimated Probability of Neurotoxicity in Critically Ill Patients

 Muhammad Bilal,^{a,b} Michael Zoller,^c Uwe Fuhr,^a Ulrich Jaehde,^b Sami Ullah,^a  Uwe Liebchen,^c Sören Büsker,^a Johannes Zander,^d  Baharak Babouee Flury,^e Max Taubert^a

^aUniversity of Cologne, Faculty of Medicine and University Hospital Cologne, Center for Pharmacology, Department I of Pharmacology, Cologne, Germany

^bDepartment of Clinical Pharmacy, Institute of Pharmacy, University of Bonn, Bonn, Germany

^cDepartment of Anaesthesiology, Hospital of the Ludwig Maximilians University of Munich, Munich, Germany

^dLaboratory of Dr. Brunner, Constance, Germany

^eDivision of Infectious Diseases and Hospital Epidemiology, Kantonsspital St. Gallen, St. Gallen, Switzerland

ABSTRACT Cefepime has been reported to cause concentration-related neurotoxicity, especially in critically ill patients with renal failure. This evaluation aimed to identify a dosing regimen providing a sufficient probability of target attainment (PTA) and the lowest justifiable risk of neurotoxicity in critically ill patients. A population pharmacokinetic model was developed based on plasma concentrations over four consecutive days obtained from 14 intensive care unit (ICU) patients. The patients received a median dose of 2,000 mg cefepime by 30-min intravenous infusions with dosing intervals of every 8 h (q8h) to q24h. A time that the free drug concentration exceeds the MIC over the dosing interval ($fT_{>MIC}$) of 65% and an $fT_{>2 \times MIC}$ of 100% were defined as treatment targets. Monte Carlo simulations were carried out to identify a dosing regimen for a PTA of 90% and a probability of neurotoxicity not exceeding 20%. A two-compartment model with linear elimination best described the data. Estimated creatinine clearance was significantly related to the clearance of cefepime in nondialysis patients. Interoccasion variability on clearance improved the model, reflecting dynamic clearance changes. The evaluations suggested combining thrice-daily administration as an appropriate choice. In patients with normal renal function (creatinine clearance, 120 mL/min), for the pharmacodynamics target of 100% $fT_{>2 \times MIC}$ and a PTA of 90%, a dose of 1,333 mg q8h was found to be related to a probability of neurotoxicity of $\leq 20\%$ and to cover MICs up to 2 mg/L. Continuous infusion appears to be superior to other dosing regimens by providing higher efficacy and a low risk of neurotoxicity. The model makes it possible to improve the predicted balance between cefepime efficacy and neurotoxicity in critically ill patients. (This study has been registered at ClinicalTrials.gov under registration no. NCT01793012).

KEYWORDS cefepime, population pharmacokinetics, probability of target attainment, neurotoxicity

Cefepime is a fourth-generation cephalosporin antibiotic covering both Gram-positive and Gram-negative bacteria (1). It was first approved in Europe in 1993 and in 1996 by the U.S. Food and Drug Administration (FDA) for the treatment of moderate to severe pneumonia, complicated and uncomplicated urinary tract infections, uncomplicated skin and skin structure infections, intra-abdominal infections, and, later, febrile neutropenia (2, 3). Through its property as a zwitterion, cefepime has an enhanced ability to penetrate the outer cell membrane porins of Gram-negative bacteria more rapidly than third-generation cephalosporins (4). In addition, it is relatively stable to chromosomally encoded AmpC beta-lactamase, representing the treatment of choice in AmpC producers that do not harbor

Copyright © 2023 American Society for Microbiology. All Rights Reserved.

Address correspondence to Muhammad Bilal, muhammad.bilal@uk-koeln.de.

The authors declare no conflict of interest.

Received 8 March 2023

Returned for modification 27 April 2023

Accepted 1 June 2023

Published 27 June 2023

extended-spectrum beta-lactamase enzymes (5). Cefepime has activity comparable to that of ceftazidime against *Pseudomonas aeruginosa* (4). This broad-spectrum activity of cefepime and its relative beta-lactamase stability make this drug suitable as an empirical treatment for patients in intensive care units (ICUs) (6). The recommended standard dose of cefepime according to EUCAST (European Committee on Antimicrobial Susceptibility Testing) is 1 g every 8 h (q8h) or 2 g q12h (7). The manufacturer's recommended dose of cefepime for adults with mild to moderate infections and normal kidney function is 0.5 g to 1 g q12h and for those with moderate to severe infections is 1 g to 2 g q12h (8). This dosing regimen has been effective against the vast majority of streptococci, members of the *Enterobacterales*, and *Staphylococcus aureus* (9). For patients with febrile neutropenia, the recommended dose is 2 g q8h, all with a 30-min infusion (8). Cefepime doses of 2 g q8h in patients with normal renal function are required to achieve adequate exposure and increase antibacterial effect against susceptible *P. aeruginosa* infections (10). To account for the mainly renal elimination of cefepime, in patients with an estimated creatinine clearance below 60 mL/min, dose adjustment is required. The manufacturer's dosing recommendations for the maintenance dose for adults weighing more than 40 kg with renal impairment for severe infection are as follows: 2 g q24h, 1 g every day, and 0.5 g every day for creatinine clearance estimated by the Cockcroft-Gault equation (eCL_{CR}) of 30 to 60 mL/min, 11 to 29 mL/min, and ≤ 10 mL/min, respectively (8).

Pathophysiological changes in severely ill patients may cause high pharmacokinetic variability, which may result in under- and overexposure to the drug. It is important to understand that the interindividual variability (IIV) of pharmacokinetic (PK) parameters, specifically clearance and volume of distribution, determines the probability of target attainment (PTA) for optimal bacterial cell killing by β -lactams after the administration of a fixed dose (9).

Cefepime is administered parenterally. It exhibits linear pharmacokinetic behavior and low plasma protein binding, which ranges from 16% to 19%, and is widely distributed in body tissues and fluids. It is mainly eliminated by the kidneys through glomerular filtration, with more than 80% of the drug being unchanged in subjects with normal kidney function. The elimination half-life is about 2 to 2.5 h (11). The percentage of time that the free drug concentration exceeds the MIC over the dosing interval ($fT_{>MIC}$) is the PK/pharmacodynamic (PD) index that best describes its efficacy (12). In line with other beta-lactam antibiotics, the efficacy of cefepime is optimal when the free-drug concentration exceeds the MIC for at least 50% of the dosing interval (13). For Gram-negative bacteria, an $fT_{>MIC}$ of 60 to 70% is generally required to achieve sufficient killing (14). Nicasio et al. reported a PD target of $>50\%$ $fT_{>MIC}$ for cefepime in patients with ventilator-associated pneumonia (13), while Roos et al. used a 65% $fT_{>MIC}$ as a target (9). Treatment of severe infections may require the administration of doses that keep free serum concentrations at least 1- to 2-fold higher than the MIC throughout the dosing interval. Accordingly, Aitken et al. used a PD target of 100% $fT_{>2 \times MIC}$ or 100% $fC_{min>2 \times MIC}$ (free minimum concentration to MIC) ratio of ≥ 2.1 in patients with Gram-negative bacterial pneumonia (15). Al-Shaer et al. suggested PD targets of 100% $fT_{>MIC}$ and 100% $fT_{>4 \times MIC}$ (16).

A comprehensive review and meta-analysis published in 2006 revealed that the use of cefepime in febrile neutropenic patients was associated with higher mortality (17). The same study team expanded their meta-analysis in 2007 to include all cefepime-treated patients, and they still discovered higher mortality rates than in individuals receiving other broad-spectrum β -lactam antibiotics (18). It has been reported that 15% of all ICU patients will experience one symptom of cefepime neurotoxicity or another (19), but recognition of these symptoms is difficult, as they reflect common conditions in critically ill patients. Symptoms of neurotoxicity include confusion, encephalopathy, abnormal electroencephalography (EEG), nonconvulsive status epilepticus, and severe toxicity leading to coma (20). In general, the neurotoxic symptoms, including encephalopathy, are reversible after discontinuation of cefepime and/or after hemodialysis. The mechanism of the neurotoxic effect is not yet known, but it has been related to the inhibition of γ -aminobutyric acid A (GABA-A) receptors (21). Researchers have been attempting to link the neurotoxicity to plasma cefepime exposure, but the available data are limited by the availability of trough-only

TABLE 1 Cefepime-induced neurotoxicity based on plasma trough concentrations reported in various studies

Trough concn (mg/L)	Probability of neurotoxicity (%)	Reference
≥12	25	22
≥16	50	22
≥38	100	22
>20	24	24
>40	39	24
≥22	50	23

concentrations, retrospective study designs, total or calculated unbound concentrations, difficulties in defining the events, and lack of control for covariates affecting these events, which are frequent in intensive care units (16).

To assess the risk for neurotoxicity in this study, the logistic regression model reported by Boschung-Pasquier et al. was used (22). According to the model, at cefepime plasma trough concentrations less than 7.7 mg/L, no patients showed signs of potential neurotoxicity. The risk of neurotoxicity was 25% when plasma trough concentrations were ≥12 mg/L. In patients with trough concentrations of ≥16 mg/L, this risk increased to 50% when plasma trough concentrations were ≥16 mg/L. At plasma trough concentrations of ≥38.1 mg/L, all patients experienced neurotoxicity. On the other hand, Lamoth et al. reported a 50% probability of neurotoxicity at a trough concentration of ≥22 mg/L (23), while Huwylar et al. recommended avoiding a trough concentration of >20 mg/L in patients receiving intermittent dosing and a steady-state concentration of >35 mg/L in patients receiving a continuous infusion (CI) (24) (Table 1).

The aims of this study were (i) to quantify PK variability and explore predictors of cefepime clearance and (ii) to identify a dosing regimen of cefepime in critically ill patients providing a sufficient PTA and an acceptably low risk of neurotoxicity.

RESULTS

Fourteen medical-surgical ICU patients were included in the study. Four of the patients were on continuous venovenous hemodialysis (CVVHD), and all but one patient had sepsis. Sepsis was defined according to the European Society of Intensive Care Medicine/Society of Critical Care Medicine Consensus Conference Committee (25). The median numbers of available blood samples per patient were 11.5, 6, 6.5, and 6 on days 1 to 4 of sampling, respectively. A total of 344 plasma concentrations were used for the development of the model. Four very high plasma concentrations ranging between 447.17 and 848.36 mg/L were considered implausible and removed from the evaluation. The patients' characteristics are shown in Table 2. The median age and body weight of the patients were 62 (range, 22 to 94) years and 70 (45 to 120) kg, respectively.

TABLE 2 Summary of demographic and clinical characteristics of the patients

Characteristic ^a	Median (range) or no. of patients
eCL _{CR} (mL/min)	60.8 (16.7–217)
mCL _{CR} (mL/min)	56 (0–219)
Body wt (kg)	70 (45–120)
Age (yrs)	62 (22–94)
Sex (male/female)	6/8
Body ht (m)	1.68 (1.5–1.83)
BMI (kg/m ²)	25 (20–37)
Serum albumin concn (mg/dL)	2.5 (1.8–3.6)
Serum creatinine concn (mg/dL)	0.8 (0.3–4.4)
Serum urea concn (mg/dL)	53 (12–196)
Lung transplantation (yes/no)	4/10
Liver transplantation (yes/no)	1/13
Dialysis (yes/no)	4/10
Sepsis (yes/no)	13/1

^aeCL_{CR}, Cockcroft-Gault creatinine clearance; mCL_{CR}, measured creatinine clearance based on 24-h urinary excretion of creatinine and corresponding plasma concentration of creatinine in patients without hemodialysis; BMI, body mass index.

TABLE 3 Parameter estimates of cefepime obtained from the final model^a

Parameter	NONMEM			Bootstrap analysis		
	Estimate	RSE (%)	Shr (%)	Median	RSE (%)	95% CI
CL _D (L/h)	2.74	13		2.71	9.26	2.29–3.19
CL _{ND} (L/h)	2.94	10		2.96	12.3	2.36–3.78
V ₁ (L)	8.88	38		9.06	17.9	5.70–12.2
Q (L/h)	27.4	54		24.7	22.4	16.8–41.7
V ₂ (L)	18.7	22		18.0	12.4	14.2–23.5
eCL _{CR} effect on CL _{ND}	0.896	17		0.829	13.5	0.637–1.04
IIV CL _D (CV %)	22.7	15	51	20.6	37.0	12.5–27.9
IIV CL _{ND} (CV %)	31.3	20	21	28.8	51.4	9.80–40.8
IIV V ₁ (CV %)	47.3	25	14	44.2	42.3	26.7–65.0
IIV V ₂ (CV %)	19.3	26	34	19.8	51.8	5.8–29.7
IOV CL _{ND} (CV %)	22.4	23	8	22.3	47.6	14.1–35.5
Proportional residual error (SD)	0.278	11		0.276	14.4	0.217–0.324

^aRSE, relative standard error; CI, confidence interval; CL_D, elimination clearance in dialysis patients; CL_{ND}, elimination in nondialysis patients; V₁, central volume of distribution; Q, intercompartmental clearance; V₂, peripheral volume of distribution; eCL_{CR}, creatinine clearance estimated by the Cockcroft-Gault equation; IIV, interindividual variability; IOV, interoccasional variability; CV, coefficient of variation; shr, shrinkage; SD, standard deviation.

Population pharmacokinetic model. A two-compartment model with linear elimination best described cefepime concentrations. The base model was parametrized in terms of elimination clearance for nondialysis patients (CL_{ND}), clearance of CVHD patients (CL_D), central volume of distribution (V₁), the peripheral volume of distribution (V₂), and intercompartmental clearance (Q). IIV was found to be significant on clearance and volume of distribution. Interoccasional variability (IOV) estimated on clearance of both dialysis and nondialysis patients was significant and decreased objective value function (OVF) by 45 points. IOV was tested on the volume of distribution and decreased OVF (by 16.9 points) but was not properly identifiable. Parameter estimates of the final model and 95% confidence interval for the parameter estimates are given in Table 3.

Observations were uniformly distributed along the line of identity; no systematic over- or underprediction was evident from plots of residuals (Fig. 1). Relative standard errors of all parameters in the final model were less than 30% except for V₁ and Q, which suggests that

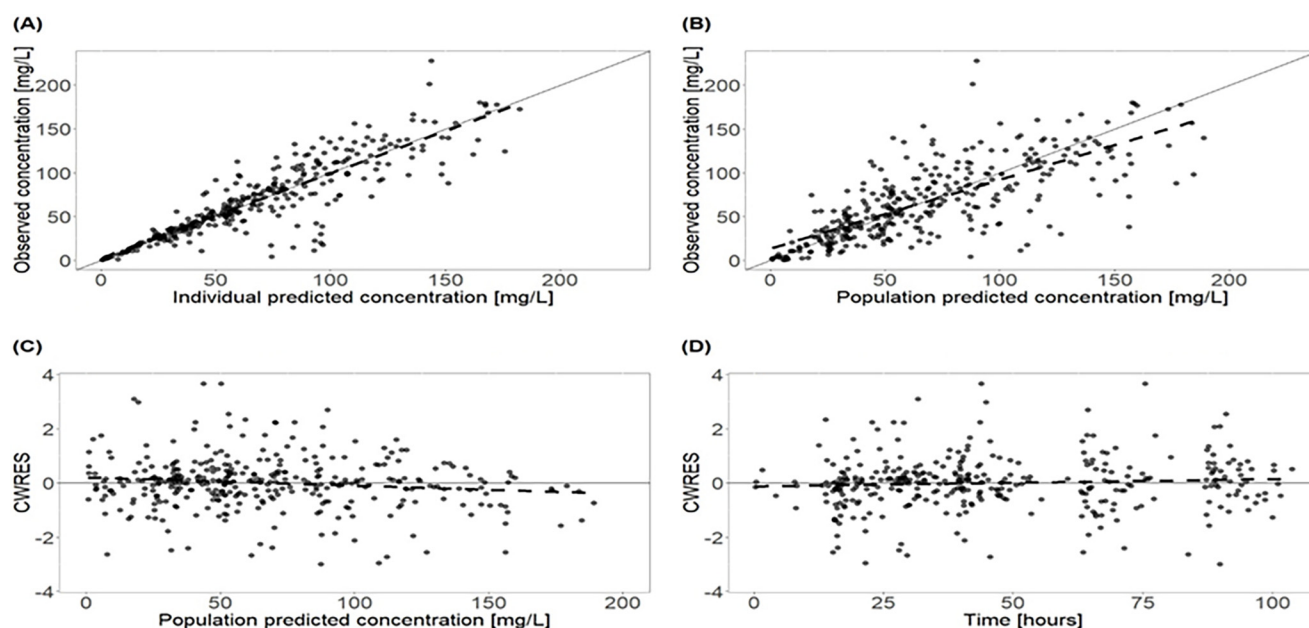


FIG 1 Goodness-of-fits plots for the final covariate cefepime population pharmacokinetic model. (A) Plot of observed concentrations versus individual predictions. (B) Plot of observed concentrations versus population predictions. (C) Plot of conditional weighted residuals (CWRES) versus population predictions. (D) Plot of CWRES versus time after the first dose. The dashed line represents the best linear fit. Black dots represent observed concentrations. The solid line represents the line of identity or unity. The total number of ICU patients is 14, including four patients with continuous venovenous hemodialysis. The patients received a median daily dose of 2,000 mg cefepime by 30-min intravenous infusions.

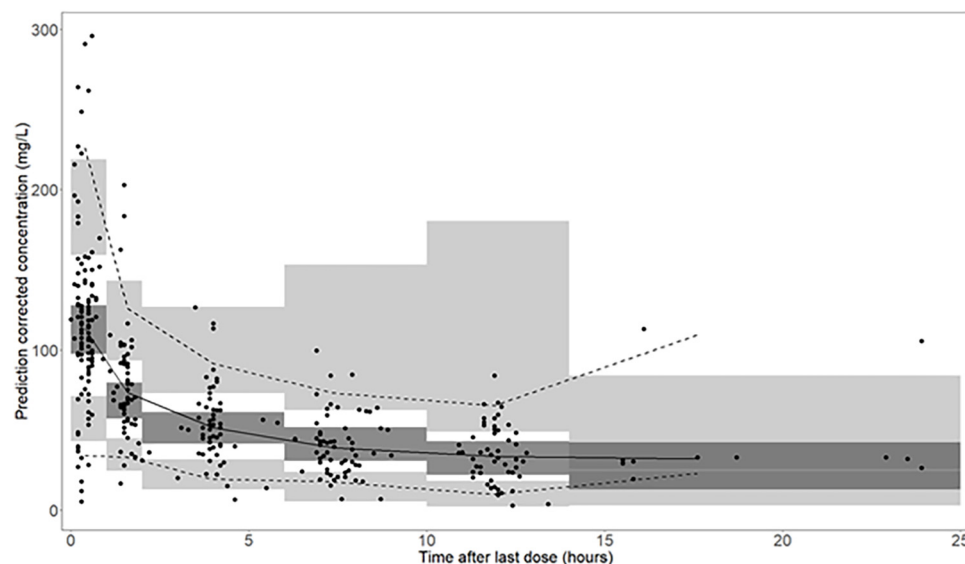


FIG 2 Prediction-corrected visual predictive check ($n = 1,000$). Solid dots represent observed concentrations. The black solid line represents the median, and the lower and upper dashed lines are the 5th and 95th percentiles of observed concentrations. Shaded areas are the respective model-predicted 95% confidence intervals. Dark-shaded areas represent the median prediction interval, and light-shaded areas show the 2.5th and 97.5th percentiles of the simulated data.

parameters were estimated with sufficient precision (Table 3). Figure 2 shows prediction-corrected visual predictive checks (pcVPC), confirming that the developed model was able to capture the central trend and variability in the data except for the last few observations.

In the covariate analysis, eCL_{CR} was found to significantly decrease OVf by 14 points. Serum creatinine was also found to be a significant covariate on clearance but to a lesser extent than eCL_{CR} , decreasing OVf by 7 points. Other covariates, such as measured creatinine clearance (mCL_{CR}), weight, sex, and age, tested on PK parameters did not significantly improve the model.

Monte Carlo simulations. Monte Carlo simulations were used to assess the combined effect of cefepime dose, dosing interval, and CL_{CR} on both PTA and the risk of neurotoxicity. While the published relationship between cefepime exposure and neurotoxicity was based on trough concentrations, we additionally used the (higher) average concentrations in the logistic regression equation provided by Boschung-Pasquier et al. (22) to increase the safety margin for patients.

Figure 3A and B show neurotoxicity estimates based on trough concentrations with the pharmacodynamics target of 65% $T_{>MIC}$ and 100% $T_{>2 \times MIC}$, respectively. For a PD target of 65% $T_{>MIC}$ and a PTA target of 90%, doses of 500 mg q8h and 2,000 mg q8h predicted around 20% neurotoxicity for patients with eCL_{CR} of 60 mL/min and 150 mL/min, respectively, covering MICs of up to 8 mg/L (Fig. 3A). Increasing the PD target to 100% $T_{>2 \times MIC}$, doses of 400 mg q8h and 2,250 mg q8h predicted $\leq 20\%$ neurotoxicity for patients with eCL_{CR} of 60 mL/min and 150 mL/min, respectively, covering MICs of 2 mg/L (Fig. 3B). With CI, daily doses of 500 mg and 1,250 mg predicted $< 10\%$ risk of neurotoxicity in patients with eCL_{CR} of 60 mL/min and 150 mL/min, respectively, for PD targets of 65% $T_{>MIC}$, covering MICs of up to 4 mg/L. For a similar risk of neurotoxicity, doses and renal function increasing the PD target to 100% $T_{>2 \times MIC}$ reduced MIC coverage to 2 mg/L with CI. Prolonging dosing intervals while maintaining daily doses was predicted to result in a decrease in efficacy (i.e., requiring higher daily doses to cover the same MICs) but even more so in a decrease in the risk of neurotoxicity, while overall any improvement was only marginal when balancing efficacy and neurotoxicity.

When the risk of neurotoxicity was estimated based on average plasma concentrations, this risk would depend only on daily dose and not on dosing intervals; accordingly, a prolonged dosing interval would deteriorate the efficacy-versus-neurotoxicity risk relationship in this evaluation (Fig. 4A and B).

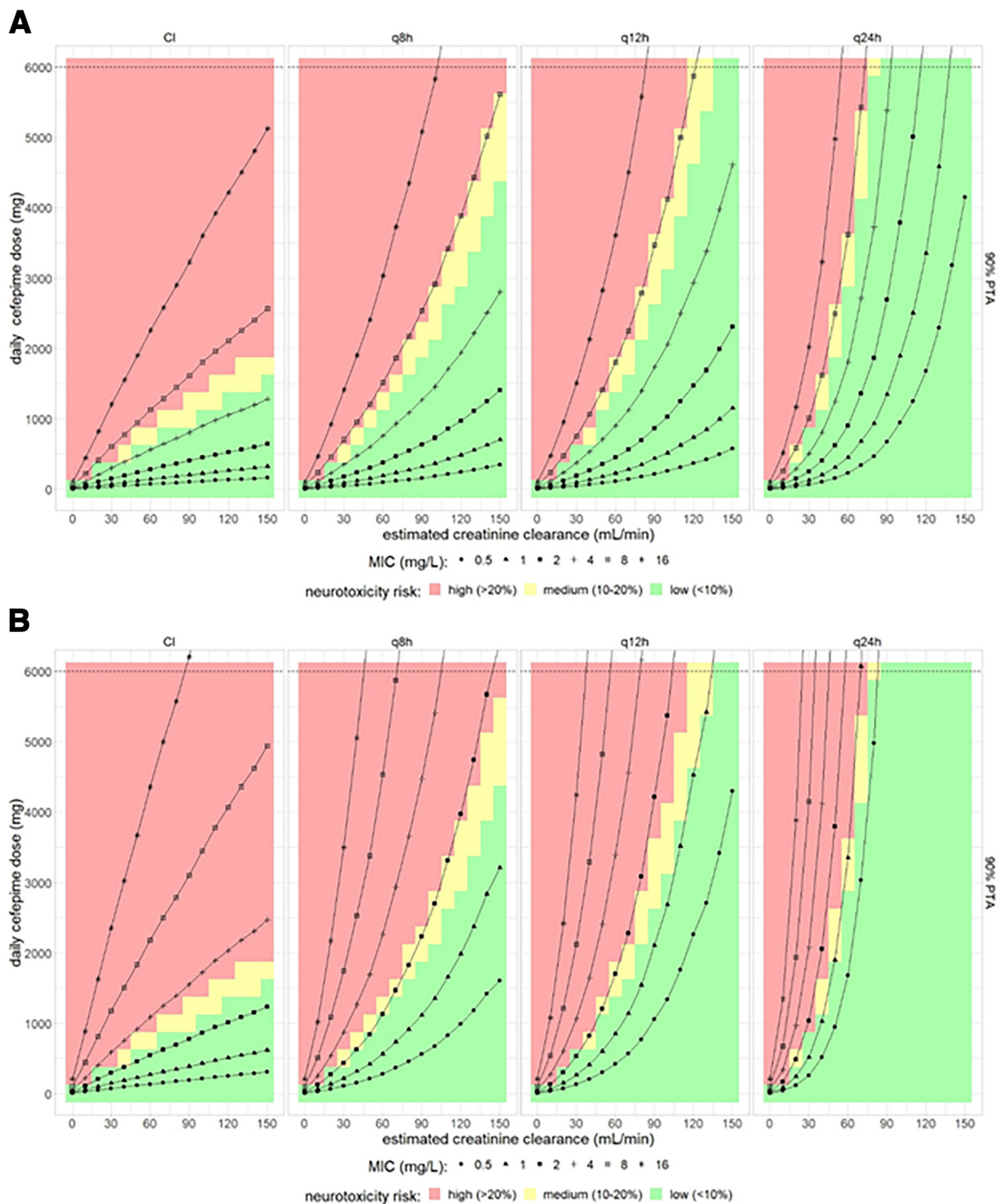


FIG 3 Combined effect of cefepime dose, dosing interval, and estimated creatinine clearance on both PTA and on the probability of neurotoxicity for an efficacy target of (A) 65% $T_{>MIC}$ and (B) 100% $T_{>2 \times MIC}$ based on plasma trough cefepime concentrations. The color gradient in the background indicates the estimated risk of neurotoxicity. The black lines represent 90% PTA for assumed MICs ranging from 0.5 to 16 mg/L.

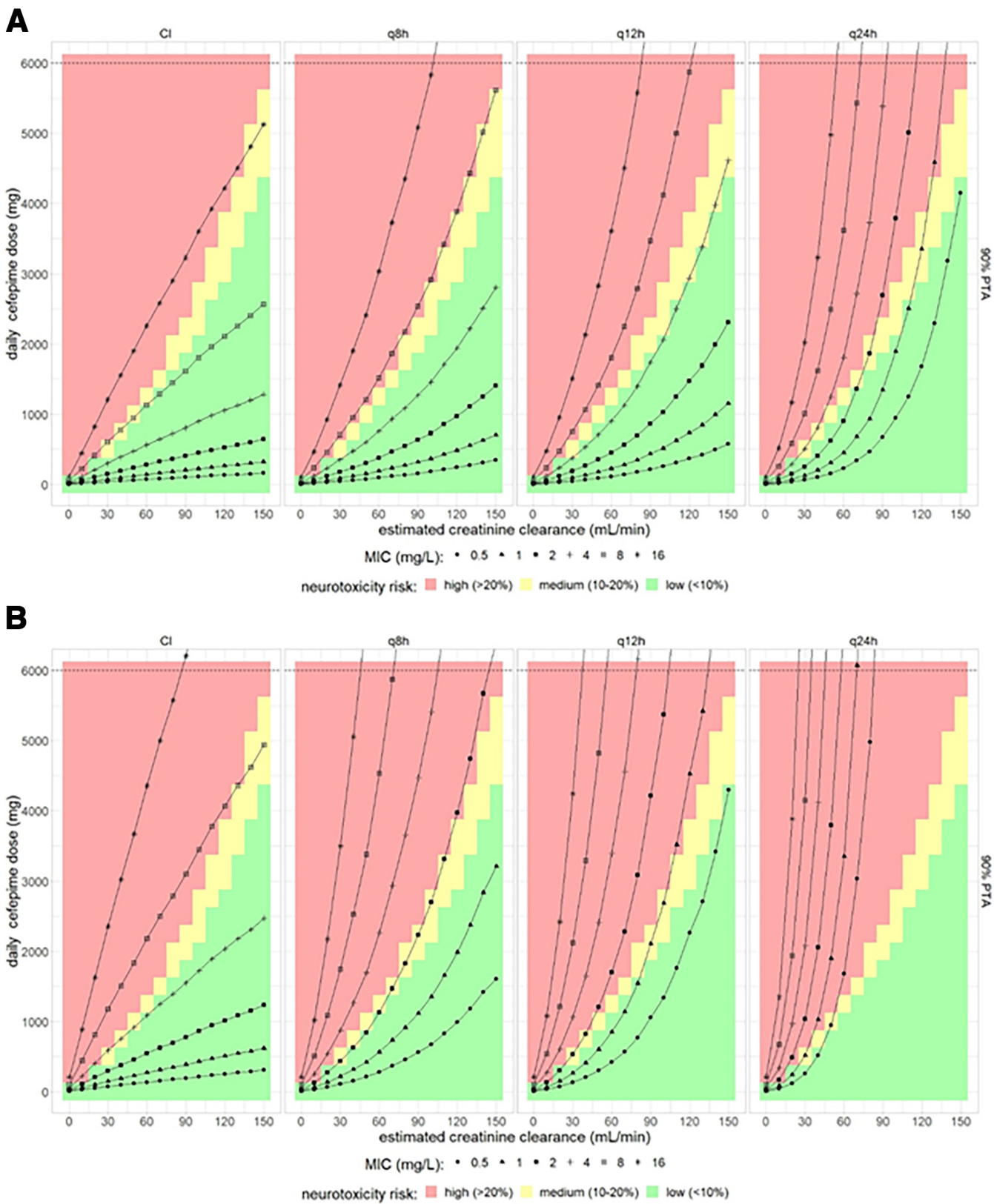


FIG 4 Combined effect of cefepime dose, dosing interval, and estimated creatinine clearance on both PTA and on the probability of neurotoxicity for an efficacy target of (A) 65% $T_{>MIC}$ and (B) 100% $T_{>2 \times MIC}$ based on plasma average cefepime concentrations. The color gradient in the background indicates the estimated risk of neurotoxicity. The black lines represent 90% PTA for assumed MICs ranging from 0.5 to 16 mg/L.

TABLE 4 Suitable predicted cefepime doses administered q8h with an acceptable risk for neurotoxicity (i.e., 20% or lower, based on average concentration) for selected creatinine clearance values^a

CL _{CR} (mL/min)	Dose (mg) required for 90% PTA
30	440
60	1,100
90	2,300
120	4,000
150	6,500

^aThe MIC target is up to 2 mg/L, and the PK/PD target used is 100% $T_{>2 \times \text{MIC}}$.

For the pharmacodynamics targets of 100% $T_{>2 \times \text{MIC}}$ and PTA target of 90%, doses of 200 mg q8h and 1,000 mg q8h for a patient with a creatinine clearance of 60 mL/min and 150 mL/min, respectively, was predicted to be related to a probability of neurotoxicity of less than 10% (based on average cefepime concentrations) and providing coverage for MICs up to 1 mg/L. For the same PD target, a daily dose of 1,000 mg and 1,500 mg for CI predicted low neurotoxicity risk for eCL_{CR} values of 60 mL/min and 90 mL/min, respectively, and provided coverage for MICs up to 4 mg/L (Fig. 4B). Doses to achieve 100% $T_{>2 \times \text{MIC}}$ and to cover MICs above 4 mg/L would in all cases be related to a high risk of neurotoxicity. Dosing intervals of q12h and q24h would require higher doses to achieve the pharmacodynamics target and thus would again deteriorate the balance of efficacy versus neurotoxicity risk as assessed based on average cefepime concentrations (Fig. 4B). In summary, it is essential to take renal function into account to select the appropriate daily cefepime dose, and a q8h dosing should be preferred over reduced dosing frequencies, as it provides higher pharmacodynamics target attainment, while a possible benefit regarding neurotoxicity risk because of lower trough values is negligible (Fig. 3A and 4A). Table 4 shows typically suitable doses with an acceptable risk of neurotoxicity for a MIC of 2 mg/L depending on the desired PTA.

While we did not carry out Monte Carlo simulations for CVHD patients because of the very limited data available, clearance point estimates for patients with CVHD (CL_D, 2.74 L/h) and without CVHD (CL_{ND}, 2.94 L/h) in our model were very similar; thus, the doses predicted for patients with normal kidney function might also be suitable for CVHD patients in ICUs; however, therapeutic drug monitoring (TDM) in these patients would be desirable to ensure appropriate exposure.

DISCUSSION

A population pharmacokinetic model of cefepime was developed to describe its pharmacokinetics in critically ill patients. Our model enabled stochastic simulations for proposing a dosing regimen balancing antibacterial effects and the risk of neurotoxicity for various degrees of renal impairment.

Balancing efficacy versus risk of neurotoxicity, continuous infusion provided the most favorable results, followed by the shortest dosing interval tested for intermittent infusions, i.e., 8 h. To reach the pharmacodynamics target of 100% $T_{>2 \times \text{MIC}}$ in 90% of patients with an eCL_{CR} of 120 mL/min, a q8h dose of 1,333 mg was related to a $\leq 20\%$ neurotoxicity risk and covered bacteria with MICs up to 2 mg/L.

A two-compartment model with eCL_{CR} as a covariate on clearance best described the cefepime data, which is in line with previous studies (13, 26, 27). In published evaluations, some authors also suggested a three-compartment model (9); however, the data in our study did not support adding a third compartment. Several studies have described cefepime pharmacokinetics in hospitalized patients (26–29). The typical value of clearance in our study for CL_{ND} was 2.96 L/h (mean eCL_{CR}, 87.1 mL/min). This is close to the clearance value previously reported in the literature: Cheng et al. reported a clearance of 2.43 L/h (mean eCL_{CR}, 75.6 mL/min) for five critically ill patients who required extracorporeal membrane oxygenation (ECMO) (27). However, the typical values of clearance reported by other studies (5.99 and 6.33 L/h) were notably higher (26, 29). The difference observed in the studies of Rhodes et al. (29) and Kois et al. (26) may be explained by the fact that in both studies, the mean eCL_{CR} of the cohort was higher, i.e., 126 and 149 mL/min, respectively, than the value of

87.1 mL/min in our study. This also is in agreement with the high dosing regimens suggested for cefepime in both studies.

Renal dysfunction is the major risk factor for cefepime overexposure and thus for cefepime-related toxicity. Among those who experienced neurotoxicity in intensive care units, 80% had renal dysfunction (30), suggesting that a proper dose adjustment may avoid this adverse event. Unfortunately, the assessment of renal function in ICU patients is a challenge (31). Despite the major limitations discussed below, estimated creatinine clearance (eCL_{CR}) is one of the most widely used markers of renal function. In this study, creatinine clearance estimated by the Cockcroft-Gault equation (eCL_{CR}) was found to be significantly related to cefepime clearance. In the present study, eCL_{CR} was better than serum creatinine concentration to predict cefepime clearance. Measured creatinine clearance did not improve the model in terms of OVF and goodness of fit. This finding is in line with the conclusions reported by Jonckheere et al. (32). Although determining measured creatinine clearance is considered the method of choice for renal function measurement in critically ill patients (33), it is poorly related to the clearance of drugs such as cefepime (32) and meropenem (34). This might be due to the error-prone nature of urine collection. As eCL_{CR} was a predictor of cefepime clearance, the patients with low eCL_{CR} are expected to reach high plasma averages and trough concentrations if cefepime doses are not reduced accordingly. However, the eCL_{CR} equation was created based on non-critically ill patients and the creatinine measurements were at a steady state (35). In addition, eCL_{CR} is not considered reliable for estimating renal function in obese individuals and is not recommended in subjects older than 65 years (36). These limitations of eCL_{CR} must be considered when the model is applied to patients with highly dynamic renal function.

An important outcome of the model development was that an ILV (coefficient of variation [CV]) of 89% was much higher than IOV on clearance, which reached 21.4% in the base model. This is in line with the high ILV reported by Roos et al. (9) for cefepime in ICU patients and supports the individualized-dose concept for the drug, which can be achieved by taking estimated creatinine clearance as a covariate into account and/or by taking blood samples during treatment and using an intervention approach based on a target concentration, as suggested for aminoglycosides (37). On the other hand, accounting for IOV on clearance of nondialysis patients significantly improved the model in terms of OVF and goodness of fit. IOV describes the changes in cefepime clearance over time which might be due to pathophysiological conditions, concomitant medication, excessive fluid resuscitation, changes in renal function, and other disease treatment-related interventions. Changes in cefepime pharmacokinetics between occasions are difficult to predict; to take them into account, dense TDM would probably be indispensable. More than 90% of patients in our data had sepsis. Cefepime clearance in sepsis patients can be quite variable, making appropriate dosing difficult (2). To reduce the risk of neurotoxicity or suboptimal efficacy in these patients, both plasma concentrations and renal function should be carefully monitored. In this model, variability in kidney function is reflected by estimating IOV on clearance, which can describe unexplained variation of clearance over time, and by covariate modeling, i.e., by incorporating eCL_{CR} as a covariate on clearance of nondialysis patients in the model.

A recently published study involving patients with hospital-acquired/ventilator-associated pneumonia with $>50\%$ $T_{>MIC}$ as a treatment target and trough concentration of <20 mg/L as a safety target recommended a dosing regimen of 2,000 mg via infusion every 12 h administered over 4 h in patients with normal renal function (CL_{CR} , 90 to 120 mL/min) for a MIC target of 4 mg/L (38) (Table 5). However, no information on the risk of neurotoxicity was provided. In our study, with a PD target of 65% $T_{>MIC}$, doses of 500 mg q8h and 1,000 mg q8h with 30 min infusion for eCL_{CR} values of 60 mL/min and 90 mL/min, respectively, appear to be optimal for MICs up to 4 mg/L and 1 mg/L, respectively, with $<10\%$ neurotoxicity (Fig. 4A and B). The dosing of 1,000 mg q8h is identical to the EUCAST recommendation for cefepime standard dosing (7), while in a study with patients infected with *Pseudomonas aeruginosa*, a higher dosage of 2,000 mg q8h was required to provide attainment of similar targets (10), but neurotoxicity was not addressed. Taking a trough concentration of ≥ 20 mg/L as the toxicity target and 100% $T_{>MIC}$ (with a MIC of 8 mg/L) as the efficacy target, Cheng et al. reported that for patients

TABLE 5 Published cefepime dosing recommendations based on trough concentrations and renal function^a

eCL _{CR} (mL/min)	Dose regimen	Patient population	Trough concn (mg/L)	Time of infusion	MIC (mg/L)	PKPD target (% T _{>MIC})	Probability of efficacy and neurotoxicity (%) ^a	Reference
90–130	2,000 mg q12h	Hospital-acquired-pneumonia patients	<20	4 h	4	>50	NA	38
30	1,000 mg q12h	ICU patients	≥20	30 min	8	100	E, 84–92; N, 8–44	27
65	1,000 mg q12h	ICU patients	≥20	30 min	8	100	E, 46–53; N, 1–8	27
120	1,000 mg q8h	ICU patients	≥20	30 min	8	100	E, 40–44; N, 1–6	27

^aE, efficacy; N, neurotoxicity; NA, not available.

with a CL_{CR} of 30 mL/min and 65 mL/min, 1,000 mg q12h will achieve 84 to 92% and 46 to 53% probability of efficacy and 8 to 44% and 1 to 8% probability of toxicity, respectively (Table 5). For patients with a CL_{CR} of 120 mL/min, the authors suggest that 1,000 mg q8h will achieve a 40 to 44% probability of efficacy and 1 to 6% probability of toxicity (27). With a PD target of 100% T_{>2×MIC} and neurotoxicity target of <10%, for eCL_{CR} of 60 mL/min and of 120 mL/min, our study found doses of 366 mg q8h and 1,333 mg q8h, respectively, for a PTA of 90% for MICs up to 2 mg/L (Table 4). In this evaluation, we determined optimized dosing regimens irrespective of the vial sizes currently available on the market. Therefore, combinations and divisions of vials of 500 or 1,000 mg might be required to provide doses close to the optimal doses we identified. Several clinical trials have reported high efficacy for continuous infusion (39, 40). Simulations for continuous infusion predicted high efficacy with lower daily doses than those used with q8h, q12h, and q24h administration (Fig. 3 and 4). The predicted neurotoxicity risk was <10%. Continuous infusion also has a pharmacoeconomic advantage over intermittent dosing by achieving the same effect with a lower daily dose of medication (41).

To date, mainly trough concentrations have been used for the evaluation of cefepime-induced neurotoxicity. We added respective simulations using the same equation based on average concentrations, because the basis for using trough concentrations only was that no other information was available in these studies. However, we expect that the exposure during the rest of the dosing interval is not meaningless, and therefore, we tried to increase the safety margin for patients by using average concentrations. The risk of neurotoxicity but also efficacy were found to be decreased for daily doses with prolonged dosing intervals, i.e., q12h and q24h, when trough concentrations were used, while predicted efficacy was decreased by prolonging dosing intervals; however, when average plasma concentrations were used, the risk for neurotoxicity remained unchanged. Thus, irrespective of the concentrations used to predict neurotoxicity, the shorter dosing interval of 8 h provides the best results in balancing the relationship between efficacy and risk of neurotoxicity.

Beyond modeling, clinical data confirm that patients with estimated glomerular filtration rates (eGFR) of 30 mL/min/1.73 m² or less have the highest proportion of suspected neurotoxicity (22). TDM in these patients seems to be another useful tool to account for the slower elimination of cefepime. Suttels et al. suggested TDM of cefepime in non-critically ill patients to monitor and prevent adverse events (42). In another study of patients who had CL_{CR} less than 30 mL/min and who were on renal replacement therapy, TDM or an alternative antimicrobial agent was suggested (27). When neurological symptoms appear or worsen, the possibility of a cefepime overdose must be considered, particularly in elderly patients (30). Renal function should also be carefully monitored when cefepime is combined with potentially nephrotoxic antibiotics (such as aminoglycosides) or potent diuretics (43).

This study had several limitations. The small sample size provided limited statistical power for the analysis. Individual PD data in our patients for exploration of a direct link between cefepime concentrations and neurotoxicity were not available. Another issue is heterogeneity in the patient population studied, with some of them being on dialysis. Moreover, little information on the relationship between exposure of cefepime and neurotoxicity was available in the literature.

Conclusion. In conclusion, the model makes it possible to balance the predicted efficacy and neurotoxicity risk of cefepime in critically ill patients, with emphasis on renal function as the main covariate for exposure. Overall, a daily administration frequency of q8h was found to have advantages over q12h and q24h. For the pharmacodynamics

target of 100% $T_{>2 \times \text{MIC}}$ and PTA target of 90%, a dose of 1,333 mg q8h was related to a medium to low neurotoxicity risk and coverage of bacteria with MICs up to 2 mg/L in patients with an eCL_{CR} of 120 mL/min. For MIC targets above 2 mg/L, higher doses are required, leading to a high risk of neurotoxicity. Continuous infusion improves the balance between efficacy and neurotoxicity risk and provides higher efficacy with lower daily doses than q8h, q12h, and q24h administration.

Further evaluations are needed, including studies with larger groups and studies that include experimental pharmacodynamics assessment, to further explore optimal dosing of cefepime in critically ill patients.

MATERIALS AND METHODS

Study design. This monocentric, prospective observational study was conducted at the Department of Anesthesiology, University Hospital, Ludwig-Maximilians-Universität (LMU) München, Munich, Germany. The study protocol (ClinicalTrials.gov; NCT01793012) was approved by the Ethics Committee of the Medical Faculty of the LMU (registration number 428-12) and conducted following the principles of the Declaration of Helsinki. Written informed consent from patients or their legal representatives was obtained. Patients over the age of 18 who were treated with cefepime and had an ICU stay were included. Following local guidelines, patients received a median dose of 2 g with dosing intervals of q8h, q12h, or q24h as 30-min intravenous infusions. Blood samples were taken on four consecutive days. If feasible/appropriate, the samples were collected prior to and 0.25, 0.5, 1.5, 4, 7.25 or 8, and 12 or 16 h after administration of a cefepime dose and immediately before (trough concentration) the next administration. Demographic information and laboratory data (including serum creatinine) were also collected along with patient-specific clinical information. Creatinine clearance was calculated using the Cockcroft-Gault equation based on daily serum creatinine results (35).

Blood samples were immediately centrifuged and stored at -80°C . Total plasma concentrations of cefepime were determined using a validated liquid chromatography-mass spectrometry method (44). Cefepime- D_3 , $^{13}\text{C}_1$ was used as an internal standard. Validation showed good analytical performance, with a CV for intra- and interassay ($n = 5$) imprecision of $\leq 8.6\%$, and the relative error for inaccuracy was between -8% and -1% .

Population pharmacokinetic analysis. A population pharmacokinetic model was developed by nonlinear mixed-effects modeling using NONMEM 7.4.3 software (45). Estimation was based on first-order conditional estimation with interaction (FOCE+I). One-, two-, and three-compartment models for plasma concentrations were explored. IIV and IOV were evaluated on clearance and central volume of distribution assuming log-normal distributions of the parameters. IOV was modeled over clearance, assuming that each administration was a separate occasion. For patients on CVVHD, a separate clearance was estimated.

The goodness of fit (GOF) was evaluated by visual assessment of predicted versus observed concentrations and scatterplots of the residuals. For the evaluation of uncertainty around PK parameter estimates, a nonparametric bootstrap ($n = 1,000$) was performed, and a 95% confidence interval for the parameters was obtained (37). To assess the predictive performance of the final model, pcVPC were performed, comparing observed data with model-based simulated data to assess the adequacy of the predictive ability of the model.

For covariate modeling, covariates were first screened based on physiological plausibility, and later, covariates were plotted against individual empirical Bayes estimates to explore relationships. mCL_{CR} and eCL_{CR} (not weight adjusted) were evaluated, as they are markers of renal function. Demographic characteristics such as total body weight, age, and sex were tested along with serum creatinine, since they are part of typical renal function and the eCL_{CR} equation. Body weight as a covariate on clearance and volume of distribution was also tested by simple allometric scaling with coefficients fixed at 0.75 and 1, respectively. The evaluation was guided by changes in OVF, with a change of 3.84 being considered statistically significant (P value less than 0.05, assuming that the OVF follows a chi-squared distribution with one degree of freedom). Continuous covariates were evaluated on cefepime clearance by the power relationship as shown in equation 1, while categorical covariates were evaluated by the linear equation shown in equation 2.

$$\text{CL} \left(\frac{L}{h} \right) = \text{CL}_{\text{TV}} \times \left(\frac{\text{covariate}}{\text{median}} \right)^{\theta} \quad (1)$$

$$\text{CL} \left(\frac{L}{h} \right) = \text{CL}_{\text{TV}} \times [1 + (\theta \times \text{covariate})] \quad (2)$$

where L is liter, h is hour, and CL_{TV} is typical value of clearance, θ is theta.

Monte Carlo simulations. Monte Carlo simulations for patients not on CVVHD were performed using 10,000 virtual subjects using the mrgsolv package, version 1.0.6, in R (46). Cefepime doses were simulated up to 6,000 mg with dosing intervals of q8h, q12h, and q24h and CI for 7 days. Plasma protein binding of 20% was assumed. Creatinine clearance was simulated ranging from 0 to 150 mL/min. Pharmacodynamics targets of 65% $T_{>\text{MIC}}$ and 100% $T_{>2 \times \text{MIC}}$ with a PTA of 90% described in the steady state were selected. To assess the risk for neurotoxicity, a logistic regression model developed by Boschung-Pasquier et al. (equation 3) was used, where cefepime was administered three times a day (2 g every 8 h), with dosing adjusted for patients with an eGFR of 50 mL/min/1.73 m^2 (22).

$$P(C_{\text{trough}}) = \frac{1}{1 + \exp[4.78 - (0.258 \times C_{\text{trough}})]} \quad (3)$$

In this study, the risk of neurotoxicity was evaluated based on the trough and average concentrations. Neurotoxicity of <10% was considered low (optimal), a value between 10 and 20% was considered medium (the maximum acceptable range), and beyond 20% was deemed a high risk of neurotoxicity.

Data availability. The data that support the findings of this study are available from the corresponding author upon request.

ACKNOWLEDGMENT

The Higher Education Commission of Pakistan provided financial support in the form of a Ph.D. scholarship for Muhammad Bilal through the German Academic Exchange Service (DAAD). The study's design, data collection and analysis, and the choice to submit the work for publication were all independent of the sponsor. We acknowledge support for the article processing charge from the DFG (German Research Foundation, 491454339).

REFERENCES

- Cordero J, Lopez J, Lora J, Martinez J, Mercado L, Vega R, Oliva M, Leudo D. 2022. Development of neurotoxicity syndrome associated with the use of cefepime. *Health Sci J* 16:921.
- Pais GM, Chang J, Barreto EF, Stitt G, Downes KJ, Mohammad AH, Lesnicki E, Panchal V, Bruzzone M, Argyle Bumanglag V, Burke SN, Marc Scheetz H, Scheetz MH. 2022. Clinical pharmacokinetics and pharmacodynamics of cefepime. *Clin Pharmacokinet* 61:929–953. <https://doi.org/10.1007/s40262-022-01137-y>.
- Kim PW, Wu Y, Cooper C, Rochester G, Valappil T, Wang Y, Kornegay C, Nambiar S. 2010. Meta-analysis of a possible signal of increased mortality associated with cefepime use. *Clin Infect Dis* 51:381–389. <https://doi.org/10.1086/655131>.
- Cunha BA, Gill MV. 1995. Cefepime. *Med Clin North Am* 79:721–732. [https://doi.org/10.1016/S0025-7125\(16\)30035-9](https://doi.org/10.1016/S0025-7125(16)30035-9).
- Donà V, Scheidegger M, Pires J, Furrer H, Atkinson A, Flury BB. 2019. Gradual in vitro evolution of cefepime resistance in an ST131 *Escherichia coli* strain expressing a plasmid-encoded CMY-2 β -lactamase. *Front Microbiol* 10:1–8. <https://doi.org/10.3389/fmicb.2019.01311>.
- Beaucaire G. 1999. Clinical activity of cefepime in severe infections. *Clin Microbiol Infect* 5:S6–S14. <https://doi.org/10.1111/j.1469-0691.1999.tb00718.x>.
- European Committee on Antimicrobial Susceptibility Testing. 2023. Breakpoint tables for interpretation of MICs and zone diameters, version 13.0.
- Bristol-Myers Squibb Company. 2003. Product information: Maxipime®, cefepime hydrochloride for injection. Bristol-Myers Squibb Company, Princeton, NJ.
- Roos JF, Bullitta J, Lipman J, Kirkpatrick CMJ. 2006. Pharmacokinetic-pharmacodynamic rationale for cefepime dosing regimens in intensive care units. *J Antimicrob Chemother* 58:987–993. <https://doi.org/10.1093/jac/dki349>.
- Crandon JL, Bulik CC, Kuti JL, Nicolau DP. 2010. Clinical pharmacodynamics of cefepime in patients infected with *Pseudomonas aeruginosa*. *Antimicrob Agents Chemother* 54:1111–1116. <https://doi.org/10.1128/AAC.01183-09>.
- Okamoto MP, Nakahiro RK, Chin A, Bedikian A. 1993. Cefepime clinical pharmacokinetics. *Clin Pharmacokinet* 25:88–102. <https://doi.org/10.2165/00003088-199325020-00002>.
- Turnidge JD. 1998. The pharmacodynamics of beta-lactams. *Clin Infect Dis* 27: 10–22. <https://doi.org/10.1086/514622>.
- Nicasio AM, Ariano RE, Zelenitsky SA, Kim A, Crandon JL, Kuti JL, Nicolau DP. 2009. Population pharmacokinetics of high-dose, prolonged-infusion cefepime in adult critically ill patients with ventilator-associated pneumonia. *Antimicrob Agents Chemother* 53:1476–1481. <https://doi.org/10.1128/AAC.01141-08>.
- Craig WA. 1998. Pharmacokinetic/pharmacodynamic parameters: rationale for antibacterial dosing of mice and men. *Clin Infect Dis* 26:1–12. <https://doi.org/10.1086/516284>.
- Aitken SL, Altshuler J, Guervil DJ, Hirsch EB, Ostrosky-Zeichner LL, Ericsson CD, Tam VH. 2015. Cefepime free minimum concentration to minimum inhibitory concentration (fCmin/MIC) ratio predicts clinical failure in patients with Gram-negative bacterial pneumonia. *Int J Antimicrob Agents* 45:541–544. <https://doi.org/10.1016/j.ijantimicag.2014.12.018>.
- Al-Shaer MH, Neely MN, Liu J, Cherabuddi K, Venugopalan V, Rhodes NJ, Klinker K, Scheetz MH, Peloquin CA. 2020. Population pharmacokinetics and target attainment of cefepime in critically ill patients and guidance for initial dosing. *Antimicrob Agents Chemother* 64:e00745–20. <https://doi.org/10.1128/AAC.00745-20>.
- Paul M, Yahav D, Fraser A, Leibovici L. 2006. Empirical antibiotic monotherapy for febrile neutropenia: systematic review and meta-analysis of randomized controlled trials. *J Antimicrob Chemother* 57:176–189. <https://doi.org/10.1093/jac/dki448>.
- Yahav D, Paul M, Fraser A, Sarid N, Leibovici L. 2007. Efficacy and safety of cefepime: a systematic review and meta-analysis. *Lancet Infect Dis* 7:338–348. [https://doi.org/10.1016/S1473-3099\(07\)70109-3](https://doi.org/10.1016/S1473-3099(07)70109-3).
- Fugate JE, Kalimullah EA, Hocker SE, Clark SL, Wijdicks EFM, Rabinstein AA. 2013. Cefepime neurotoxicity in the intensive care unit: a cause of severe, underappreciated encephalopathy. *Crit Care* 17:R264. <https://doi.org/10.1186/cc13094>.
- Alpay H, Altun Ö, Biyikli K. 2004. Cefepime-induced non-convulsive status epilepticus in a peritoneal dialysis patient. *Pediatr Nephrol* 19:445–447. <https://doi.org/10.1007/s00467-003-1333-8>.
- Durand-Maugard C, Lemaire-Hurtel A-S, Gras-Champel V, Hary L, Maizel J, Prud'homme-Bernardy A, Andréjak C, Andréjak M. 2012. Blood and CSF monitoring of cefepime-induced neurotoxicity: nine case reports. *J Antimicrob Chemother* 67:1297–1299. <https://doi.org/10.1093/jac/dks012>.
- Boschung-Pasquier L, Atkinson A, Kastner LK, Banholzer S, Haschke M, Buetti N, Furrer DI, Hauser C, Jent P, Que YA, Furrer H, Babouee Flury B. 2020. Cefepime neurotoxicity: thresholds and risk factors. A retrospective cohort study. *Clin Microbiol Infect* 26:333–339. <https://doi.org/10.1016/j.cmi.2019.06.028>.
- Lamoth F, Buclin T, Pascual A, Vora S, Bolay S, Decosterd LA, Calandra T, Marchetti O. 2010. High cefepime plasma concentrations and neurological toxicity in febrile neutropenic patients with mild impairment of renal function. *Antimicrob Agents Chemother* 54:4360–4367. <https://doi.org/10.1128/AAC.01595-08>.
- Huwyler T, Lenggenhager L, Abbas M, Ing Lorenzini K, Hughes S, Huttner B, Karmime A, Uçak I, von Dach E, Lescuyer P, Harbarth S, Huttner A. 2017. Cefepime plasma concentrations and clinical toxicity: a retrospective cohort study. *Clin Microbiol Infect* 23:454–459. <https://doi.org/10.1016/j.cmi.2017.01.005>.
- Dellinger RP, Levy M, Rhodes A, Annane D, Gerlach H, Opal SM, Sevransky JE, Sprung CL, Douglas IS, Jaeschke R, Osborn TM, Nunnally ME, Townsend SR, Reinhart K, Kleinpell RM, Angus DC, Deutschman CS, Machado FR, Rubenfeld GD, Webb SA, Beale RJ, Vincent JL, Moreno R, Aitken L, Al Rahma H, Bernard GR, Biban P, Bion JF, Calandra T, Carrillo JA, Clemmer TP, Divatia JV, Du B, Fujishima S, Gando S, Bruch CG, Guyatt G, Hazelzet JA, Hirasawa H, Hollenberg SM, Jacobi J, Jenkins I, Jimenez E, Jones AE, Kacmarek RM, Kern W, Koh SO, Kotani J, Machado F, Marini J, The Surviving Sepsis Campaign Guidelines Committee including The Pediatric Subgroup, et al. 2013. Surviving Sepsis Campaign: international guidelines for management of severe sepsis and septic shock, 2012. *Intensive Care Med* 39:165–228. <https://doi.org/10.1007/s00134-012-2769-8>.
- Kois AK, Gluck JA, Nicolau DP, Kuti JL. 2022. Pharmacokinetics and time above the MIC exposure of cefepime in critically ill patients receiving extracorporeal membrane oxygenation (ECMO). *Int J Antimicrob Agents* 60:106603. <https://doi.org/10.1016/j.ijantimicag.2022.106603>.
- Cheng V, Abdul-Aziz MH, Burrows F, Buscher H, Corley A, Diehl A, Jakob SM, Levkovich BJ, Pellegrino V, Que YA, Reynolds C, Rudham S, Wallis SC, Welch SA, Zacharias D, Roberts JA, Shekar K, Fraser JF. 2021. Population pharmacokinetics of cefepime in critically ill patients receiving extracorporeal membrane oxygenation (an ASAP ECMO study). *Int J Antimicrob Agents* 58:106466. <https://doi.org/10.1016/j.ijantimicag.2021.106466>.

28. Delattre IK, Musuamba FT, Jacqmin P, Taccone FS, Laterre PF, Verbeeck RK, Jacobs F, Wallemacq P. 2012. Population pharmacokinetics of four β -lactams in critically ill septic patients comedicated with amikacin. *Clin Biochem* 45:780–786. <https://doi.org/10.1016/j.clinbiochem.2012.03.030>.
29. Rhodes NJ, Grove ME, Kiel PJ, O'Donnell JN, Whited LK, Rose DT, Jones DR, Scheetz MH. 2017. Population pharmacokinetics of cefepime in febrile neutropenia: implications for dose-dependent susceptibility and contemporary dosing regimens. *Int J Antimicrob Agents* 50:482–486. <https://doi.org/10.1016/j.ijantimicag.2017.04.008>.
30. Payne LE, Gagnon DJ, Riker RR, Seder DB, Glisic EK, Morris JG, Fraser GL. 2017. Cefepime-induced neurotoxicity: a systematic review. *Crit Care* 21:276. <https://doi.org/10.1186/s13054-017-1856-1>.
31. Koyner JL. 2012. Assessment and diagnosis of renal dysfunction in the ICU. *Chest* 141:1584–1594. <https://doi.org/10.1378/chest.11-1513>.
32. Jonckheere S, De Neve N, De Beenhouwer H, Berth M, Vermeulen A, Van Bocxlaer J, Colin P. 2016. A model-based analysis of the predictive performance of different renal function markers for cefepime clearance in the ICU. *J Antimicrob Chemother* 71:2538–2546. <https://doi.org/10.1093/jac/dkw171>.
33. Ruiz S, Minville V, Asehnoune K, Virtos M, Georges B, Fourcade O, Conil J-M. 2015. Screening of patients with augmented renal clearance in ICU: taking into account the CKD-EPI equation, the age, and the cause of admission. *Ann Intensive Care* 5:49. <https://doi.org/10.1186/s13613-015-0090-8>.
34. Ehmann L, Zoller M, Minichmayr IK, Scharf C, Huisinga W, Zander J, Kloft C. 2019. Development of a dosing algorithm for meropenem in critically ill patients based on a population pharmacokinetic/pharmacodynamic analysis. *Int J Antimicrob Agents* 54:309–317. <https://doi.org/10.1016/j.ijantimicag.2019.06.016>.
35. Cockcroft DW, Gault MH. 1976. Prediction of creatinine clearance from serum creatinine. *Nephron* 16:31–41. <https://doi.org/10.1159/000180580>.
36. Verhave JC, Fesler P, Ribstein J, Du Cailar G, Mimran A. 2005. Estimation of renal function in subjects with normal serum creatinine levels: influence of age and body mass index. *Am J Kidney Dis* 46:233–241. <https://doi.org/10.1053/j.ajkd.2005.05.011>.
37. Matthews I, Kirkpatrick C, Holford N. 2004. Quantitative justification for target concentration intervention – parameter variability and predictive performance using population pharmacokinetic models for aminoglycosides. *Br J Clin Pharmacol* 58:8–19. <https://doi.org/10.1111/j.1365-2125.2004.02114.x>.
38. Seo H, Kim YK, Park S, Kim H, Lee D-H. 2023. Population pharmacokinetics and Monte Carlo simulation of cefepime in critically ill patients with hospital-acquired/ventilator-associated pneumonia. *Infect Chemother* 55:29–41. <https://doi.org/10.3947/ic.2022.0087>.
39. Tessier PR, Nicolau DP, Onyeji CO, Nightingale CH. 1999. Pharmacodynamics of intermittent- and continuous-infusion cefepime alone and in combination with once-daily tobramycin against *Pseudomonas aeruginosa* in an in vitro infection model. *Chemotherapy* 45:284–295. <https://doi.org/10.1159/000007198>.
40. Vondracek TG. 1995. Beta-lactam antibiotics: is continuous infusion the preferred method of administration? *Ann Pharmacother* 3:1.
41. Grant EM, Kuti JL, Nicolau DP, Nightingale C, Quintiliani R. 2002. Clinical efficacy and pharmacoeconomics of a continuous-infusion piperacillin-tazobactam program in a large community teaching hospital. *Pharmacotherapy* 22:471–483. <https://doi.org/10.1592/phco.22.7.471.33665>.
42. Suttels V, Andre P, Thoma Y, Veuve F, Decosterd L, Guery B, Buclin T. 2022. Therapeutic drug monitoring of cefepime in a non-critically ill population: retrospective assessment and potential role for model-based dosing. *JAC Antimicrob Resist* 4:dla043. <https://doi.org/10.1093/jacamr/dla043>.
43. Hurkacz M, Dobrek L, Wiela-Hojeriska A. 2021. Antibiotics and the nervous system—which face of antibiotic therapy is real, Dr. Jekyll (neurotoxicity) or Mr. Hyde (neuroprotection)? *Molecules* 26:7456. <https://doi.org/10.3390/molecules26247456>.
44. Zander J, Maier B, Suhr A, Zoller M, Frey L, Teupser D, Vogeser M. 2015. Quantification of piperacillin, tazobactam, cefepime, meropenem, ciprofloxacin and linezolid in serum using an isotope dilution UHPLC-MS/MS method with semi-automated sample preparation. *Clin Chem Lab Med* 53:781–791.
45. Beal SL, Sheiner LB, Boeckmann AJ, Bauer RJ (ed). 2018. N7 users guides <https://nonmem.iconplc.com/nonmem743/guides>.
46. Baron KT. 2022. Models, mrgsolve: simulate from ODE-based. R version 4.2.1.

Control stream

NONMEM® control stream of cefepime population pharmacokinetic model

```
$PROBLEM          Pop PK model of cefepime
$INPUT            ID TIME DAY OCC EVID DV AMT RATE CG BF_CRCL FLAG
                  AGE SEX HEIGHT WEIGHT DIALYSIS CR
$DATA             cef.csv IGNORE=@ IGNORE=(FLAG.GT.0)
$SUBROUTINE       ADVAN6 TOL=6
```

; Model Compartment s-----

```
$MODEL            COMP(CENT)
                  COMP(PEREIP)
```

; Model Compartment -----

\$PK

CRCL = (CG/60.8)**THETA(8)

```
IF(AMT.GT.0)THEN
TDOSE = TIME
ENDIF
TALD = TIME - TDOSE
```

; Intra-occasional variability -----

```
IF(OCC.EQ.1)THEN
IOV_CL = ETA(5)
```

```
ENDIF
IF(OCC.EQ.2)THEN
IOV_CL = ETA(6)
```

```
ENDIF
IF(OCC.EQ.3)THEN
IOV_CL = ETA(7)
ENDIF
```

```
IF(OCC.EQ.4)THEN
IOV_CL = ETA(8)
ENDIF
```

```
IF(OCC.EQ.5)THEN
IOV_CL = ETA(9)
ENDIF
```

```
IF(OCC.EQ.6)THEN
```

Control stream

```
IOV_CL = ETA(10)
ENDIF
```

```
IF(OCC.EQ.7)THEN
IOV_CL = ETA(11)
ENDIF
```

```
IF(OCC.EQ.8)THEN
IOV_CL = ETA(12)
ENDIF
```

```
IF (DIALYSIS.EQ.1) THEN
CL = THETA(1)*EXP(ETA(1)+IOV_CL)
ENDIF
```

```
IF(DIALYSIS.EQ.0) THEN
CL = THETA(2)*EXP(ETA(2)+IOV_CL)*CRCL
ENDIF
```

; Model Compartment -----

```
V1 = THETA(3) *EXP(ETA(3))
Q = THETA(4)
V2 = THETA(5) *EXP(ETA(4))
S1 = V1
```

; Ordinary differential equations-----

```
$DES
CONC1=A(1)/V1
CONC2=A(2)/V2

DADT(1) = CONC2*Q-CONC1*(Q+CL)
DADT(2) = (CONC1-CONC2)*Q
```

; Residual unexplained variability parameters -----

```
$ERROR
IPRED = A(1)/V1
W = SQRT(THETA(6)**2*IPRED**2+ THETA(7)**2)
Y = IPRED + W*EPS(1)
IRES = DV-IPRED
IWRES = IRES/W
```

; Initial estimates -----

```
$THETA
```

Control stream

(0,2.72431) ; CLDIA
(0,2.93462) ; CL_NONDIA
(0,8.87084) ; V1
(0,27.3031) ; Q
(0,18.639) ; V2
0.277448 ; Prop
0 FIX; ADD
(0,0.894216) ; CG

\$OMEGA 0.0500276 ; IIV_DIA

0.0938004 ; IIV_NONDIA
0.201737 ; IIV_V1
0.0366146 ; IIV_V2
\$OMEGA BLOCK(1)
0.0487528 ; IOV_CL
\$OMEGA BLOCK(1) SAME
\$OMEGA BLOCK(1) SAME
\$OMEGA BLOCK(1) SAME
\$OMEGA BLOCK(1) SAME
\$OMEGA BLOCK(1) SAME
\$OMEGA BLOCK(1) SAME
\$OMEGA BLOCK(1) SAME

\$SIGMA 1 FIX; Prop

; Estimation and table output-----

\$ESTIMATION METHOD=1 INTER MAXEVAL=9999 NOABORT SIG=3
PRINT=1 POSTHOC

; Xpose

\$COVARIANCE

\$TABLE ID TIME TALD DV EVID IPRED IWRES CWRES CG CRCL
ONEHEADER NOPRINT FILE=sdtab1

\$TABLE CL V1 V2 Q ONEHEADER NOPRINT FIRSTONLY FILE=patab1



Assessment of body mass-related covariates for rifampicin pharmacokinetics in healthy Caucasian volunteers

Muhammad Bilal^{1,2} · Sami Ullah¹ · Ulrich Jaehde² · Christina Trueck¹ · Dario Zaremba¹ · Bertil Wachall³ · Manfred Wargenau⁴ · Bernhard Scheidel⁵ · Martin H. J. Wiesen⁶ · Malaz Gazzaz⁷ · Chunli Chen^{1,8} · Sören Büsker¹ · Uwe Fuhr¹ · Max Taubert¹ · Charalambos Dokos¹

Received: 19 January 2024 / Accepted: 29 April 2024
© The Author(s) 2024

Abstract

Purpose Currently, body weight-based dosing of rifampicin is recommended. But lately, fat-free mass (FFM) was reported to be superior to body weight (BW). The present evaluation aimed to assess the influence of body mass-related covariates on rifampicin's pharmacokinetics (PK) parameters in more detail using non-linear mixed effects modeling (NLMEM).

Methods Twenty-four healthy Caucasian volunteers were enrolled in a bioequivalence study, each receiving a test and a reference tablet of 600 mg of rifampicin separated by a wash-out period of at least 9 days. Monolix version 2023R1 was used for NLMEM. Monte Carlo simulations (MCS) were performed to visualize the relationship of body size descriptors to the exposure to rifampicin.

Results A one-compartment model with nonlinear (Michaelis–Menten) elimination and zero-order absorption kinetics with a lag time best described the data. The covariate model including fat-free mass (FFM) on volume of distribution (V/F) and on maximum elimination rate (Vmax/F) lowered the objective function value (OFV) by 56.4. The second-best covariate model of sex on V/F and Vmax/F and BW on V/F reduced the OFV by 51.2. The decrease in unexplained inter-individual variability on Vmax/F in both covariate models was similar. For a given dose, MCS showed lower exposure to rifampicin with higher FFM and accordingly in males compared to females with the same BW and body height.

Conclusion Our results indicate that beyond BW, body composition as reflected by FFM could also be relevant for optimized dosing of rifampicin. This assumption needs to be studied further in patients treated with rifampicin.

Keywords Rifampicin · Population pharmacokinetics · Fat-free mass · Body weight · Covariate modeling

✉ Muhammad Bilal
muhammad.bilal@uk-koeln.de

¹ Department I of Pharmacology, Center for Pharmacology, Faculty of Medicine and University Hospital Cologne, University of Cologne, Cologne, Germany

² Department of Clinical Pharmacy, Institute of Pharmacy, University of Bonn, Bonn, Germany

³ InfectoPharm Arzneimittel Und Consilium GmbH, 64646 Heppenheim, Germany

⁴ M.A.R.C.O. GmbH & Co. KG, Dusseldorf, Germany

⁵ ACC GmbH Analytical Clinical Concepts, Leidersbach, Germany

⁶ Pharmacology at the Laboratory Diagnostics Centre, Faculty of Medicine, University Hospital Cologne, University of Cologne, Therapeutic Drug Monitoring, Cologne, Germany

⁷ Pharmaceutical Practices Department, College of Pharmacy, Umm Al-Qura University, Makkah, Saudi Arabia

⁸ Heilongjiang Key Laboratory for Animal Disease Control and Pharmaceutical Development, College of Veterinary Medicine, Northeast Agricultural University, 600 Changjiang Road, Xiangfang District, Harbin 150030, People's Republic of China

Introduction

Tuberculosis (TB) is still the leading cause of death in infectious diseases [1]. According to the World Health Organization (WHO), around 1.6 million people died of an estimated 10.6 million cases from TB in 2021, reflecting an increase of 4.5% from 2020 [2]. In addition, the COVID-19 pandemic has further compromised TB control programs [3].

Rifampicin remains a key anti-TB drug since its introduction in 1968. Rifampicin inhibits DNA-dependent RNA polymerase in *Mycobacterium tuberculosis* and suppresses RNA synthesis by binding to the β -subunit of the enzyme, leading to cell death. Moreover, it treats leprosy and is effective against Gram-positive cocci, including methicillin-resistant staphylococci [4–6].

Rifampicin is readily absorbed from an empty stomach and attains maximum plasma concentrations of approximately 10 mg/L within 2 h following a single dose of 600 mg [7]. Oral absorption of rifampicin is slower when administered with food [8]. The drug is highly lipophilic, and approximately 86 to 89% is bound to plasma proteins [9, 10]. Rifampicin is quickly distributed throughout the bodily fluids, with around 5% of plasma concentrations reaching cerebrospinal fluid [1]. Plasma elimination half-life is approximately 3 to 4 h but decreases to 1 to 2 h after multiple administrations due to massive auto-induction [11]. Both rifampicin and its major metabolite, desacetyl rifampicin, are primarily excreted in bile and removed in feces. Up to 30% of the administered dose is renally excreted, and only about 7% of a dose is excreted unchanged in urine [12, 13]. A greater than proportional increase in exposure in plasma is seen when the dose of rifampicin is increased (non-linear pharmacokinetics) [14]. A reduction in the exposure of concomitantly consumed medicines is frequently seen as a result of rifampicin's extensive induction of various phase I and II metabolic enzymes and drug transporter proteins [1]. Significant induction occurs within several doses after initiating rifampicin therapy, reaches full extent in about 1 week, and disappears within about 2 weeks after discontinuation [15].

The antibacterial effect of rifampicin in patients was formerly thought to be related to C_{\max} /minimum inhibitory concentration (MIC), but recent preclinical investigations have shown that the area under time concentration–time curve (AUC)/MIC is better correlated with the reduction of bacterial counts [16].

It is standard practice to adjust rifampicin doses to total body weight (BW) with 10 mg/kg as the target dose [17]. Lately, fat-free body mass (FFM) was reported to be a better predictor than BW in explaining inter-individual variability of rifampicin exposure, in particular with higher doses where greater variability is expected [18, 19].

Among other possible reasons, increased hepatic metabolism related to higher body size in males was discussed to explain the higher rifampicin clearance [20]. While potential sex differences are more relevant for patients with chronic dosing, assessing such differences in healthy volunteers with a single dose and in the absence of metabolic auto-induction might help understand the background of such an effect. In the present evaluation, population (Pop) PK modeling of rifampicin was applied to data from healthy Caucasian subjects to further assess the variability of PK parameters of rifampicin and to identify the optimal body mass-related predictors of PK parameters.

Methods

Subjects and method

The data were obtained from a phase I/IV randomized, cross-over, open-label bioequivalence study (EUDRACT-No: 2017–004418-24). The study was approved by the Ethics Committee of the Medical Faculty of the University of Cologne (18–006) and carried out in complete agreement with the pertinent version of the Declaration of Helsinki and all other relevant regulations. All volunteers provided written informed consent before participation in the study.

Study design

The study was carried out with twenty-five healthy Caucasian volunteers, with one drop-out before the first drug administration. All other volunteers completed the study, and pharmacokinetic and safety data were available in 24 individuals (11 men/13 women). Volunteers had to be between 18 and 85 years old and have a body mass index (BMI) between 18.5 and 30 kg/m². The subjects were deemed fit for the study after extensive standard pre-study screening (medical history, physical examination, vital signs, laboratory tests, electrocardiography, etc.). Main exclusion criteria included hypersensitivity to rifampicin or any of the excipients of the preparations, any relevant clinical abnormality, smoking, chronic or acute medication, extensive ethanol consumption (> 28 g per day for males, > 14 g per day for female subjects), special dietary requirements, and history of substance addiction. Subjects had to abstain from alcohol, methylxanthine-containing beverages, orange juice, apple juice, and grapefruit products, and from extreme physical activities starting 72 h before drug administration. Pregnant and lactating women were also excluded. Participants were randomly allocated to one of the two sequences of the study, each receiving a single dose of either the test or the reference tablet of 600 mg rifampicin first and the alternate treatment after a wash-out period of at least 9 days. Test preparation

was a novel rifampicin 600 mg tablet manufactured by Infec-toPharm Arzneimittel und Consilium GmbH, Heppenheim, Germany, while reference preparation was a single oral dose of 600 mg tablet (EREMFAT®) manufactured by RIEMSER Pharma GmbH, Frankfurt am Main, Germany.

Blood sampling

Blood samples were taken using an indwelling intravenous cannula inserted into a forearm vein. For each PK sample, up to 5 ml of blood was collected in sodium heparinized tubes at predose and 0.16, 0.33, 0.5, 0.75, 1, 1.25, 1.5, 1.75, 2, 2.25, 2.5, 3, 3.5, 4, 6, 9, 12, 16, and 24 h after drug administration. Within 30 min after withdrawal, blood samples were centrifuged at 4 °C at 1992 g for 10 min. After that, the plasma samples were stored at ≤ -70 °C until measurement.

Bioanalysis

The quantification of rifampicin was carried out by using a validated liquid chromatography-tandem mass spectrometry (LC–MS/MS) method [21–23]. This process was performed by Analytical Clinical Concepts GmbH, Leidersbach, Germany, and adhered to both EMA and FDA guidelines on bioanalysis. A Shimadzu liquid chromatography system (LC-20AD Pump, Duisburg, Germany) was used for separation. The Analyst® Software version 1.6.2 (AB Sciex, Concord, Canada) was used for data acquisition, peak integration, and quantification of analytes. Rifampicin was obtained from Sigma-Aldrich Chemie GmbH, Taufkirchen, Germany, and rifampicin (rifampicin- d_8) internal standard (IS) was obtained from Alsachim, Strasbourg, France. 200 μ L of plasma was mixed with 500 μ L of methanol, 20 μ L of ascorbic acid (0.5 mg/L), and 20 μ L of the internal standard (rifampicin- d_8 ; 100 μ g/mL). After shaking the mixture at a speed of 3000 min^{-1} , it was centrifuged at 10,500 g for 10 min (4 °C). 50 μ L of the supernatant mixed with 400 μ L mobile phase was transferred to a reaction vial and stored for 10 min at ≤ 20 °C. The sample was centrifuged for 10 min (4 °C) at 10,500 g, and the supernatant was transferred to an autosampler vial (HTC PAL, CTC Analytics AG, Zwingen, Switzerland). In the LC–MS/MS system, 10 μ L was injected. Analytes were separated using a Kinetex® C₁₈ chromatographic column (50 \times 4.6 mm internal diameter, Phenomenex, Aschaffenburg, Germany) with

a pre-column (4 \times 3 mm internal diameter, Phenomenex, Aschaffenburg, Germany) and detected using an AB Sciex 2000 (Concord, Canada) mass spectrometer equipped with electrospray ionization source (TurbolonSpray®). The chromatographic separation was achieved by isocratic elution at a flow rate of 0.65 mL/min. The mobile phase consisted of 600 mL ammonium formate (2 mM), 1400 mL methanol, and 2 mL formic acid. The ion spray voltage was 4000 V, and the temperature was set to 400 °C. Ions $[M+H]^+$ were detected in multiple reaction monitoring modes using the transitions of m/z 823.4 \rightarrow 791.4 for rifampicin and 831.4 \rightarrow 799.3 for IS, respectively. The column temperature was 25 °C. The linear calibration curve for rifampicin ranged between 100 and 50,000 ng/mL ($r > 0.9976$). The lower limit of quantification (LLOQ) was 100 ng/mL. Stability investigations during method validation showed that rifampicin was stable in plasma at room temperature for at least 6 h and during three thaw/freeze cycles (between ≤ -70 °C and room temperature). For the entire calibration range, accuracy given as a relative deviation of the mean from the nominal value was between -1.0 and 10.7% . The precision expressed in CV was $\leq 8.1\%$ for intra-day and inter-day measurements.

Population PK analysis

Monolix software version 2023R1 (Lixoft®, Antony, France) was used for non-linear mixed effect modeling [24]. The data were fitted using one and two-compartment models with linear and non-linear (Michaelis–Menten) elimination (see Fig. 1). Various absorption models were evaluated, including zero and first order, with and without lag time, and/or with transit compartments. In all models tested, elimination was assumed to take place from the central plasma compartment. The data below the limit of quantification (BQL) was defined as interval-censored at the limit of quantification, 0.1 mg/L [25]. The stochastic approximation expectation–maximization algorithm in Monolix includes simulations of the left-censored data in a right-truncated Gaussian distribution [26]. This is similar to the M4 method implemented in NONMEM to handle BQL data points [27]. Corrected Bayesian Information Criterion (BICc) was used to select non-nested models, and models with the lowest values of BICc were considered superior [28]. Inter-individual variability (IIV) was tested empirically on all PK parameters and was assumed to be log-normally

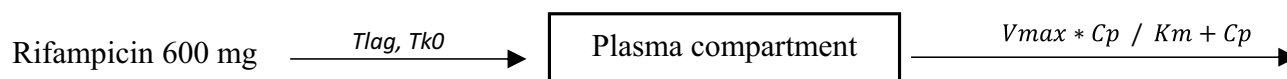


Fig. 1 Proposed structural model. Tlag, lag time; Tk0; zero-order process; V_{\max} , maximum elimination rate; K_m , Michaelis–Menten constant; C_p , plasma concentration

distributed. The two periods were assumed to be two separate occasions, and inter-occasion variability (IOV) was tested empirically on all PK parameters. The correlation between random effects was also investigated, and a strong correlation, i.e., lowering the BICc value by more than 2 points in the non-nested models, was added to the model. To describe the residual variability, constant, proportional, and combined error models were assessed.

Covariate analysis

In a prior non-compartmental analysis of this study, it was confirmed that both rifampicin preparations were bioequivalent (data not shown), which allowed us to pool the data for the present analysis. Using the base population pharmacokinetic model, the potential effect of the identity of the rifampicin preparation on rifampicin PK parameters was evaluated as a covariate, along with age, sex, BW, BH (body height), body surface area (BSA), BMI, and FFM. Continuous covariates were modeled using power models normalized by weighted means, i.e., the average of the individual covariate values weighted by the number of observations per individual. Continuous covariates were modeled as shown in Eq. 1, where PK_i is a PK parameter in the i th subject, PK_{pop} is the population parameter estimation, β is the estimated coefficient of the covariate effect, COV_i is the value of the covariate for subject i , and sex as a categorical covariate was modeled using a linear model where females were taken as reference. Subject characteristics used for covariate model development are given in Table 1. BSA was derived using the Mosteller formula [29], and FFM was calculated from

BW and BMI for both males and females, as shown in Eqs. 2 and 3, respectively [30]. Notably, the ranges of FFM for females and males in our study population do not overlap (Table 1). Physiological plausibility and statistical significance, i.e., a reduction in objective value function (OFV) with a decrease of 3.84 ($P < 0.05$) for forward inclusion and an increase in the OFV of 10.8 ($P < 0.01$) for backward elimination [31], usual diagnostic plots (GOF plots), and visual predicted check (VPC), were the basis of selection of the final covariate model. VPC was plotted by simulating 1000 virtual subjects to compare observed data with model-based simulated data to assess the adequate predictive ability of the models. A nonparametric bootstrap analysis (1000 samples) was performed in R using the `bootmlx` function from `Rsmx` (R speaks Monolix, version 2023.1.1) package.

$$PK_i = PK_{pop} * \left(\frac{COV_i}{COV_{i(\text{weighted mean})}} \right)^\beta \quad (1)$$

$$FFM(\text{male}) = \frac{9.27 * 10^3 * BW}{6.68 * 10^3 + 216 * BMI} \quad (2)$$

$$FFM(\text{female}) = \frac{9.27 * 10^3 * BW}{8.78 * 10^3 + 244 * BMI} \quad (3)$$

Monte Carlo simulations

Monte Carlo simulations (MCS) were performed for the base model and FFM covariate model only to explore the effect of FFM on exposure to rifampicin. Using the `mrgsolve` package version 1.0.6 in R, 10,000 virtual subjects were simulated for a single oral dose of 600 mg rifampicin [32].

Results

Population pharmacokinetic model

A total of 912 concentrations (median 8.19 (range 0.1 to 31.2) mg/L) obtained from 24 subjects were used for model building, of which 99 observations (10.8%) were BQL. The subject's median age and body weight were 39.5 years and 68 kg, respectively (Table 1). The PK data of rifampicin in our study was best described by a one-compartment model and zero-order absorption with lag time and nonlinear (Michaelis–Menten) elimination (Fig. 1). A comparison of different base models is given in Table 2. Random effects were applied to describe IIV on the volume of distribution (V/F), maximum elimination rate (V_{max}/F), and IOV on lag time (Tlag), zero-order absorption rate (Tk0), V/F, and V_{max}/F including a correlation between IOV of Tlag and

Table 1 Subject characteristics used for covariate model development

Demographics	Median (range)
Sex (male/female)	11/13
Female	
Body weight (kg)	63.8 (48.5–73.1)
Body height (m)	1.65 (1.55–1.76)
FFM (kg)	39.2 (33.7–44.8)
BMI (kg/m ²)	23.09 (18.7–26.7)
Age (years)	37.0 (21.0–58.0)
BSA (m ²)	1.66 (1.47–1.85)
Male	
Body weight (kg)	82.9 (57.8–91.0)
Body height (m)	1.81 (1.63–1.89)
FFM (kg)	63 (47.09–68.9)
BMI (kg/m ²)	24.7 (20.1–29.7)
Age (years)	43.0 (22.0–64.0)
BSA (m ²)	2.05 (1.62–2.18)

BMI body mass index, FFM fat-free mass, kg kilogram, m meter, m² meter square, BSA body surface area

Table 2 Comparisons of different base models with zero- and first-order absorption with or without delay and transit compartments, one or two or three distribution compartments, and linear and non-linear elimination

Nr:	Delay	Absorption	Distribution	Elimination	BICc	Δ BICc	OFV	Δ OFV
1	Lag time	Zero-order	One cmt	MM	3046	Final base model	2972	Final base model
2	Lag time	First-order	One cmt	MM	3159	113	3083	111
3	Lag time	Zero-order	One cmt	Linear	3180	134	3113	141
4	Lag time	First-order	One cmt	Linear	3270	224	3208	236
5	Transit cmt	First-order	One cmt	MM	3688	642	3622	650
6	Transit cmt	First-order	One cmt	Linear	3761	715	3702	730
7	No delay	Zero-order	One cmt	MM	4636	1590	4591	1619
8	No delay	Zero-order	One cmt	Linear	4696	1650	4655	1683
9	No delay	First-order	One cmt	Linear	4757	1711	4713	1741
10	No delay	First-order	One cmt	MM	4765	1719	4714	1742

BICc Corrected Bayesian Information criteria, *OFV* objective function value, *cmt* compartment, *MM* Michaelis–Menten, Δ *BICc* change in BICc value, Δ *OFV* change in OFV

Table 3 Parameter estimates of base and covariate models and bootstrap medians with respective 95% confidence intervals of the sex + body weight and FFM covariate models

	Base model	Sex + BW covariate model		FFM covariate model	
OFV	2972.77	2921.53		2916.33	
Parameter	Estimates (RSE %)	Estimates (RSE %)	Bootstrap median (95% CI)	Estimates (RSE %)	Bootstrap median (95% CI)
Fixed effects					
Tlag (h)	0.340 (5.52)	0.340 (5.49)	0.338 (0.300–0.382)	0.340 (5.53)	0.337 (0.301–0.382)
Tk0 (h)	0.460 (9.17)	0.470 (9.02)	0.466 (0.382–0.561)	0.470 (8.99)	0.463 (0.386–0.561)
V/F (L)	36.2 (5.28)	33.2 (3.11)	33.1 (31.0–36.4)	36.2 (2.21)	36.1 (34.5–38.2)
Vmax/F (mg/h)	191 (7.28)	157 (6.70)	154 (134–175)	190 (4.39)	188 (167–209)
K_m (mg/L)	20.4 (5.45)	20.2 (4.70)	19.7 (16.6–22.5)	20.1 (2.44)	19.8 (17.3–22.9)
Covariate effect					
β sex on V/F _{sex+BW}	-	0.190 (24.6)	0.190 (0.079–0.280)		
β BW on V/F _{sex+BW}		1.00 (Fixed)	1.00		
β sex on Vmax/F _{sex+BW}		0.420 (20.3)	0.417 (0.252–0.417)		
β FFM on V/F _{FFM}	-	-	-	1.00 (fixed)	1.00
FFM on Vmax/F _{FFM}		-	-	0.750 (fixed)	0.750
Random effects and correlation					
IIV V/F (CV %)	24.4 (17.4)	-	-	-	-
IIV Vmax/F (CV %)	39.0 (15.7)	19.7 (16.7)	20.2 (13.9–25.6)	18.5 (16.9)	19.6 (13.9–23.9)
IOV Tlag (CV %)	39.1 (10.5)	38.8 (10.5)	44.5 (28.0–63.7)	39.0 (10.6)	44.8 (27.3–63.3)
IOV Tk0 (CV %)	66.9 (11.3)	65.7 (11.1)	80.7 (58.7–106.2)	65.5 (11.2)	79.4 (56.8–105)
IOV V (CV %)	13.5 (15.9)	15.4 (10.9)	15.9 (9.52–23.6)	14.9 (10.9)	15.3 (9.63–22.8)
IOV Vmax (CV %)	9.38 (16.4)	9.32 (16.4)	9.52 (6.93–12.4)	9.39 (16.4)	9.63 (7.14–12.2)
Corr. IOV Tlag & IOV Tk0	0.390 (33.7)	0.420 (31.0)	0.439 (0.051–0.659)	0.410 (31.6)	0.425 (0.079–0.670)
Error model parameters					
Additive residual error (mg/L)	0.061 (0.060 (7.85)	0.060 (0.049–0.070)	0.060 (7.69)	0.060 (0.048–0.069)
Proportional residual error (%)	11.0 (3	11.0 (3.33)	10.8 (9.70–12.0)	11.0 (3.31)	10.8 (9.80–11.9)

OFV Objective function value, *BW* body weight, *RSE* relative standard error, *CV* coefficient of variation, *Tk0* zero-order absorption, *Tlag* lag time, *V/F* volume of distribution, *Vmax/F* maximum elimination rate, K_m Michaelis–Menten constant, *bio* bioavailability, *FFM* fat-free mass, *Sex_{V/F}* effect of sex on the volume of distribution, *BW_{V/F}* effect of body weight on volume of distribution, *FFM_{V/F}* effect of fat-free mass on volume of distribution, *IIV* inter-individual variability, *IOV* inter-occasion variability, *Corr* correlation, *CI* confidence interval, β estimated coefficient of the covariate effect

Table 4 Summary of covariate models with change in objective function value

Nr.	Covariate model	Δ OFV
1	BW on V/F & Vmax/F	- 37.
2	Sex on V/F & Vmax/F	- 38.
3	BH on V/F & Vmax/F	- 42.
4	Sex on Vmax/F and BSA on V/F	- 47.0
5	BSA on V/F & Vmax/F	- 48.
6	Sex on V/F & Vmax/F and BW on V/F	- 51.
7	FFM on V/F & Vmax/F	- 56.

Δ OFV change in objective function value, *BH* body height, *BW* body weight, *FFM* fat-free mass, *V/F* volume of distribution, *Vmax/F* maximum elimination rate

Tk0. Point estimates of the base model are given in Table 3. A combined additive and proportional error model best explained the residual unexplained variability. The model code and individual fits of all subjects of the base model are shown in Supplementary material.

Covariate modeling

Covariates tested on PK parameters were significant on V/F and Vmax/F (Table 4). The best covariate model included FFM only, followed by the sex + BW model. The covariate model with FFM on both V/F and Vmax/F decreased the objective function value (OFV) by 56.4 points compared

with the base model. Adding sex as a separate covariate in addition to FFM did not improve the model further. An alternative covariate model including sex on both V/F as well as Vmax/F and BW on V/F lowered the OFV by 51.2 points. The residual IIV on Vmax/F in the base model was 39.0 (CV (coefficient of variation) %), which was lowered to 18.5 and 19.7 for FFM and sex + BW covariate models, respectively. Estimating power parameters empirically did not result in a statistically significant improvement in the covariate models. Replacing BW by BSA in this model lowered the OFV by 3.24 points from the sex + BW model however failed to meet the backward deletion criteria. Body height only was also significant on V/F and Vmax/F but to a lower extent than the covariate models mentioned above, i.e., lowering OFV by 42.9 points. When tested on Tlag and V/F, BMI was significant and lowered OFV by 4.02 and 5.11, respectively. However, it did not meet the backward elimination criteria. Including the covariates explained most of the variability of V/F, making IIV on V/F non-significant. The point estimates of the sex + BW and the FFM covariate models are shown in Table 3. The identity of the preparation (test or reference) had no significant effect on any of the parameters.

Model evaluation

The individual and population prediction plots for sex + BW and FFM covariate models are shown in Figs. 2 and 3, respectively. Observations were uniformly distributed along the identity line for individual and population

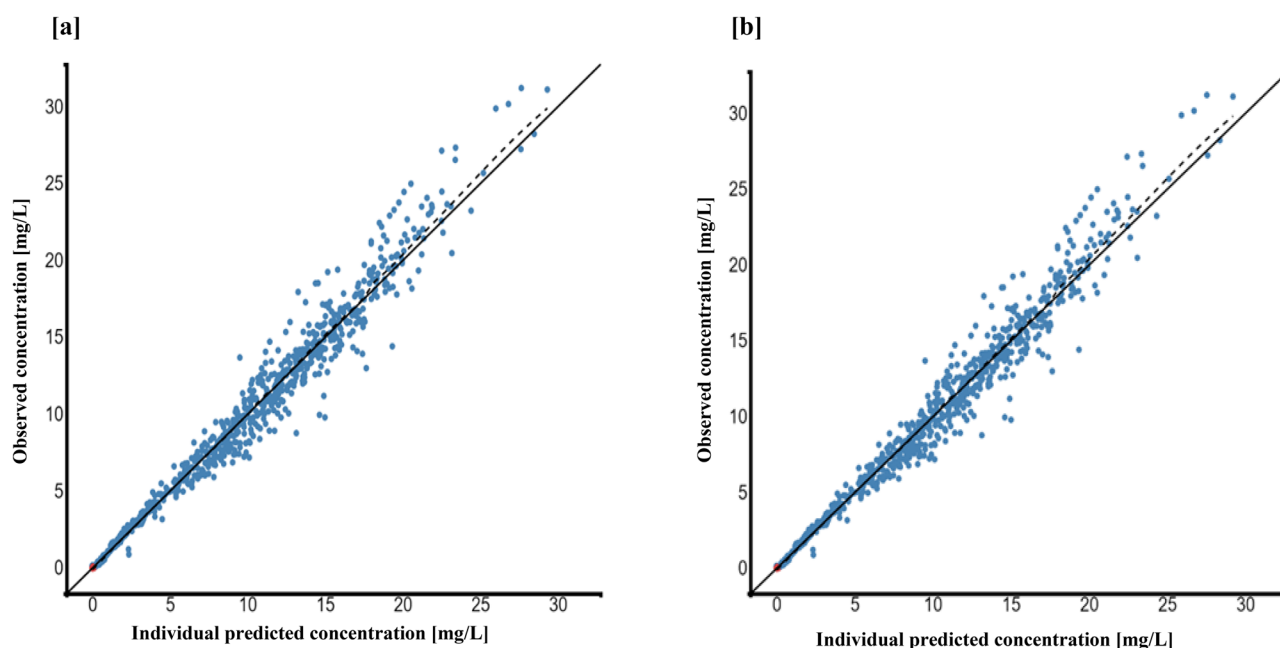


Fig. 2 Individual predictions vs observations of **a** sex + BW and **b** FFM covariate models. Solid blue dots represent observed concentration, and solid red dots represent data below the limit of quantification (BQL). The black line is the line of unity, and the dotted line represents the spline

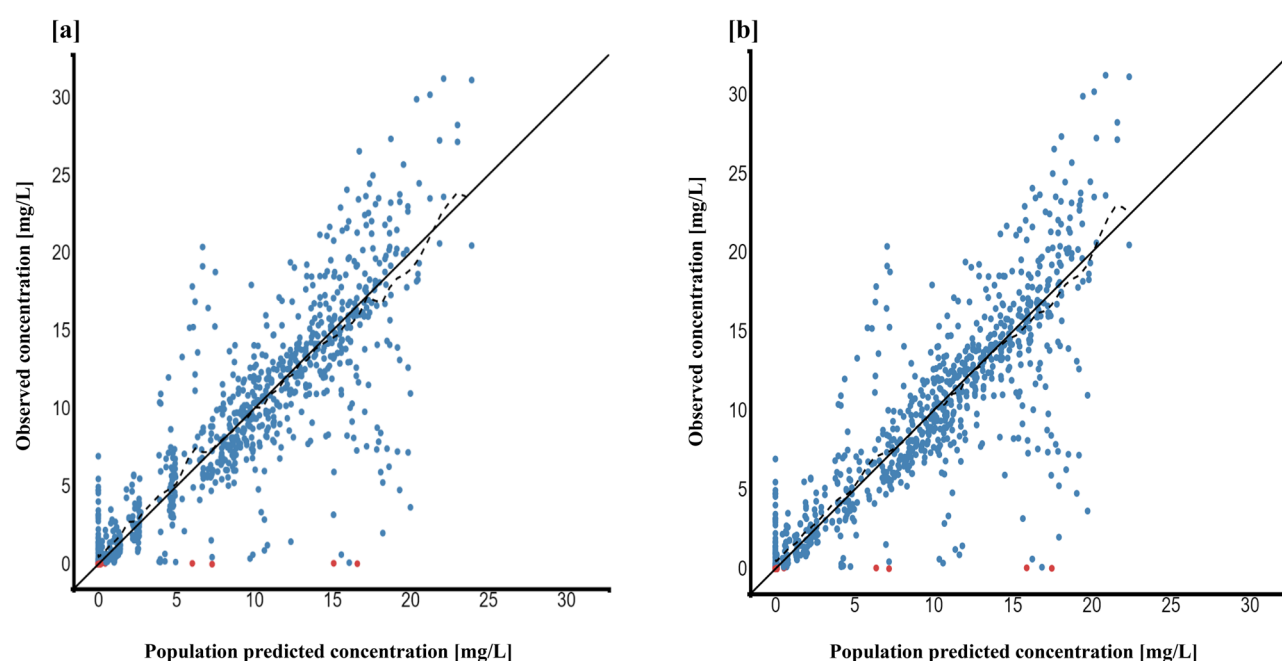


Fig. 3 Population predictions vs observations of **a** sex + BW and **b** FFM covariate models. Solid blue dots represent observed concentration, and solid red dots represent BQL data. The black line is the line of unity, and the dotted line represents the spline

predictions of both covariate models except for early high concentrations, i.e., above or ~ 25 mg/L in population prediction plots. No systematic over- or under-prediction was evident from plots of residuals (see Figs. 4 and 5). Figure 6 shows the prediction corrected (pc) VPC for both sex + BW and FFM covariate models. The figures show that both the models captured the central trend and variability in the data. A semi-logarithmic pc-VPC is provided in supplementary Fig. 2. All parameter point estimates were within the 95% CI and close to the bootstrap median (Table 3).

Monte Carlo simulations

Figure 7 illustrates the relationship of FFM to exposure to rifampicin. AUC and FFM ranging from 30 to 60 kg in female individuals and from 50 to 80 kg in male individuals were simulated for the FFM covariate model and the base model without covariates for an oral dose of 600 mg. MCS showed lower overall exposure to rifampicin with higher FFM. For each FFM value used for simulations, biometric characteristics for a male and a female individual with respective typical body height in our population are shown to illustrate the meaning of FFM. Furthermore, the error bars show a significant reduction in variability comparing the model with FFM to the base model, indicating that the covariates explained a relevant extent of random variability.

Discussion

We developed a population PK model of rifampicin based on a rich blood sampling schedule in healthy subjects. We found that either FFM or a combination (second-best) of body weight and sex explained some of the pharmacokinetic variability better than body weight alone did.

Published PK models of rifampicin vary in terms of absorption, presence of non-linearity, and auto-induction components, all typical characteristics of rifampicin. Most studies reported a one-compartment model with various approaches to describe absorption, including first-order absorption, sequential zero, and first-order absorption with lag time [20, 33–36], or incorporating transit compartments [37–42]. Most studies reported first-order elimination [20, 36, 37, 42–45], while a few investigations reported saturable elimination for rifampicin [19, 39, 41]. A two-compartment model [46, 47] and a three-compartment model have also been reported in the literature for rifampicin [48]. In the present study, one distribution compartment with zero-order absorption and lag time linked with Michaelis–Menten elimination best fits the data.

The identity of the rifampicin preparation in this study did not influence the pharmacokinetic parameters, including those describing drug absorption. A study conducted by Männistö nicely demonstrated that the bioavailability of oral preparations of rifampicin may differ considerably, with liquid preparations achieving much higher bioavailability

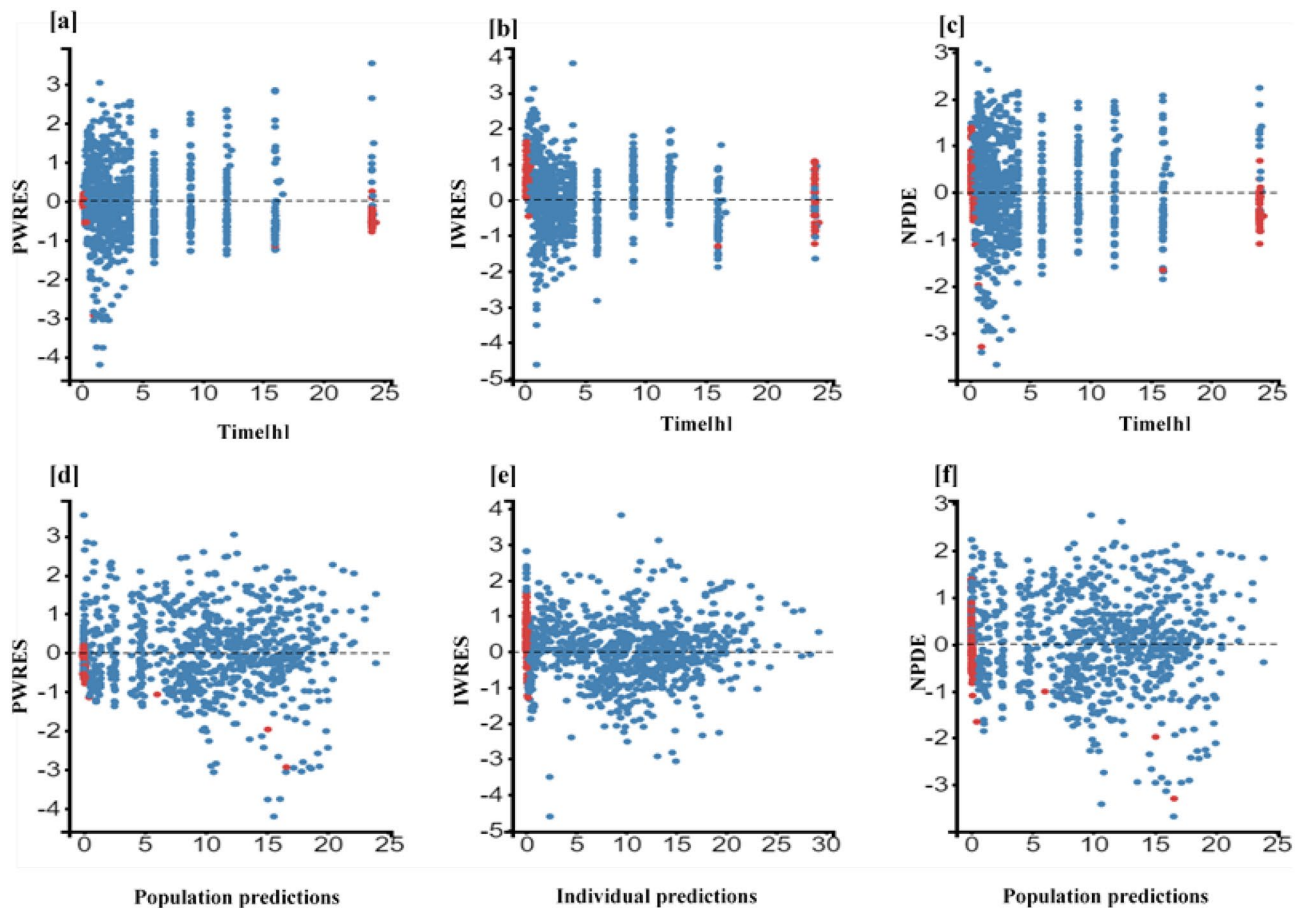


Fig. 4 Scatter plots of the residuals of sex + weight covariate model. The dotted line is the mean of the residuals. Solid red dots represent simulated observations below the limit of quantification data. **a** PWRES versus time, **b** IWRES versus time, **c** NPDE versus time,

d PWRES versus population prediction, **e** IWRES versus individual prediction, and **f** NPDE versus population prediction. PWRES, population-weighted residuals; IWRES, individual weighted residuals; NPDE, normalized prediction distribution errors

[49]. It is difficult to predict the bioavailability of immediate release solid oral rifampicin preparation by in vitro dissolution studies, which is mainly attributable to the poor solubility at neutral pH, making rifampicin a BCS (Biopharmaceutics Classification System) class 2 drug [50]. In addition, a more than linear increase of exposure with the dose may contribute to the poor predictability of the bioavailability of rifampicin preparations.

Since the early 1970s, it has been known that rifampicin exposure increases more than linearly with dose [51], with saturable hepatic extraction/saturable biliary excretion being the reported reasons [7, 19, 51]. Several studies have also reported saturable (Michaelis–Menten) elimination of rifampicin [16, 35], which is confirmed by our results. We could not include auto-induction in our model, which is to be expected as only a single dose of rifampicin was administered. In other reports, rifampicin is also reported to follow first-order elimination. However, in the respective population's PK models, rifampicin is administered along

with other anti-TB drugs and/or other medication for comorbidities, and sampling densities may not have been suitable to derive more complex PK models [35, 37, 52].

A typical form of dose individualization is drug dosing based on total body weight. The use of weight-band dosing of rifampicin is well established. BW has been reported to be a significant covariate on clearance and volume of distribution of rifampicin. A decrease of 8% in unexplained IIV using BW as a covariate on volume of distribution had been reported [53], while Schipani et al. reported a reduction of 15.5% in a joint covariate model of weight and age on clearance [45]. However, Susanto et al. reported that weight-band dosing of rifampicin could not reduce between-subject variability in AUC_{0-24} for high doses in adult TB patients. The authors concluded that weight-band dosing of rifampicin does not provide any benefit over flat dosing [54]. Despite body weight-adjusted dosing, previous studies indicated that in comparison to females, males are more likely to have lower plasma rifampicin concentrations [55]. When tested as a covariate, male gender increased

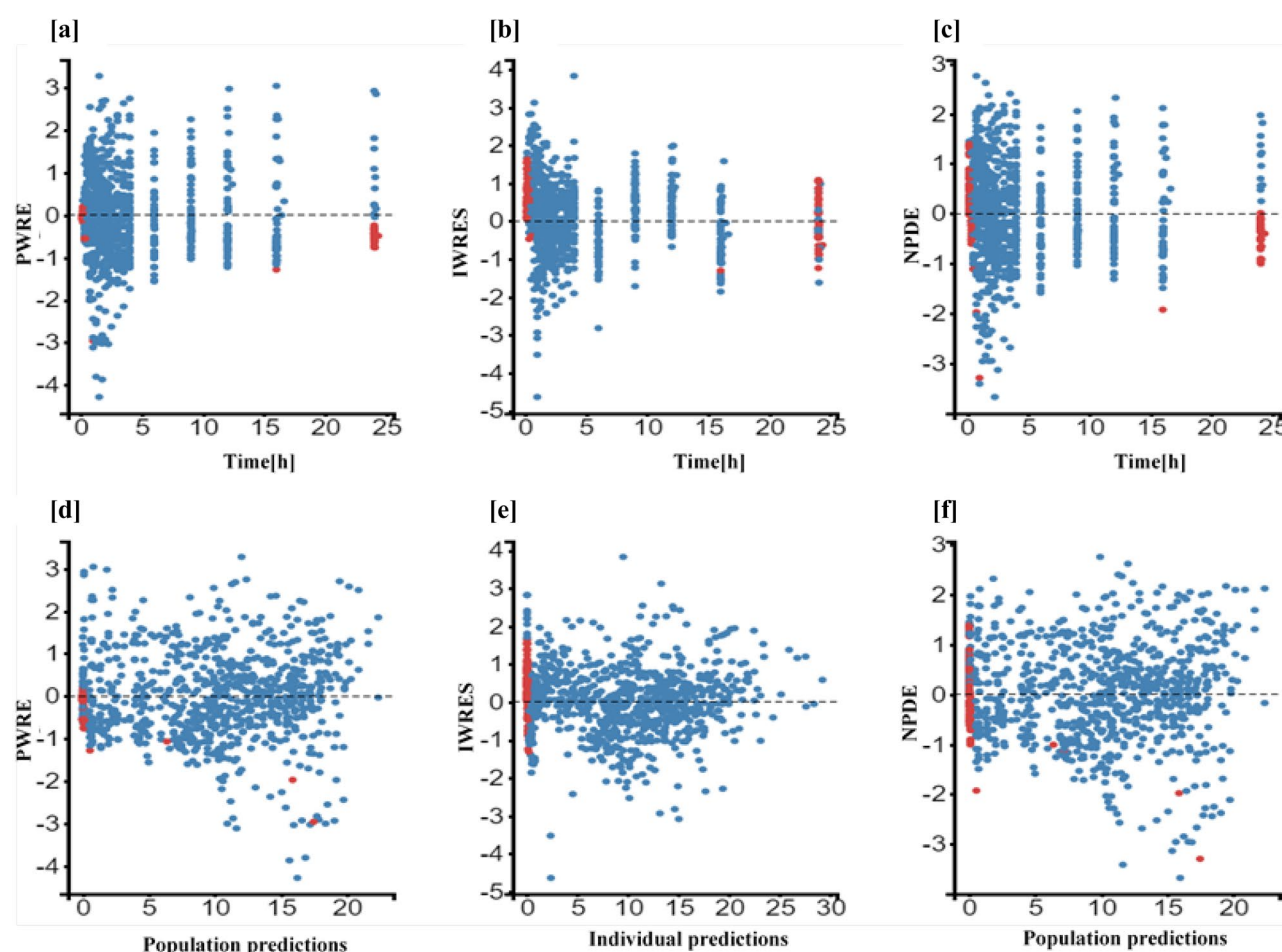


Fig. 5 Scatter plots of the residuals of the FFM covariate model. The dotted line is the mean of the residuals. Solid red dots represent simulated observations below the limit of quantification data. **a** PWRES versus time, **b** IWRES versus time, **c** NPDE versus time, **d** PWRES

versus population prediction, **e** IWRES versus individual prediction, and **f** NPDE versus population prediction. PWRES, population-weighted residuals; IWRES, individual weighted residuals; NPDE, normalized prediction distribution errors

the value of clearance and volume of distribution by 40% and 29%, respectively, in Mexican patients with TB [20]. Medellín-Garibay et al. reported a high volume of distribution and clearance in male individuals compared to females [36]. In one of our models, sex together with body weight were significant covariates and jointly decreased residual IIV on V_{\max}/F by 19.3 (CV%) (Table 3), while the FFM-based model (in terms of OFV) suggests that the relationship to sex may be the result of different body composition between men and women (see below). Still, despite being related to V_{\max}/F , none of the significant covariates in our models are causally linked to this parameter and therefore must be regarded as empirical surrogate parameters. Overall, the majority of available data supports that body weight as a descriptor of body size improves the prediction of rifampicin exposure. However, it may not be the most suitable or only useful respective descriptor, as body composition also depending on sex is not taken into account when dosing rifampicin based on body weight.

Indeed, FFM as another body size descriptor in the pharmacokinetic literature performed better than BW + sex or BSA + sex in our evaluation. FFM was derived in 1945 by Rathbun and Pace [56]. Jeremiah et al. reported that FFM is a better size predictor of both clearance and volume of distribution of rifampicin when compared to BW in TB patients coinfecting with HIV [39]. A semi-mechanistic model of FFM developed by Janmahasatian et al. [30] by incorporating sex, body weight, and BH was used for FFM covariate modeling (Eqs. 2 and 3). FFM was the most significant covariate of all the covariates tested (Table 4) and decreased residual IIV on V_{\max}/F by 20.5(CV%) (Table 3). The simulation results in our study, based on the FFM model, illustrate (Fig. 7) the degree to which exposure depends on FFM. According to the differences in FFM, the exposure of rifampicin was higher in females than males and decreased in both sexes with an increase in FFM. Measuring FFM requires experimental procedures that are complex and/or costly, precluding their

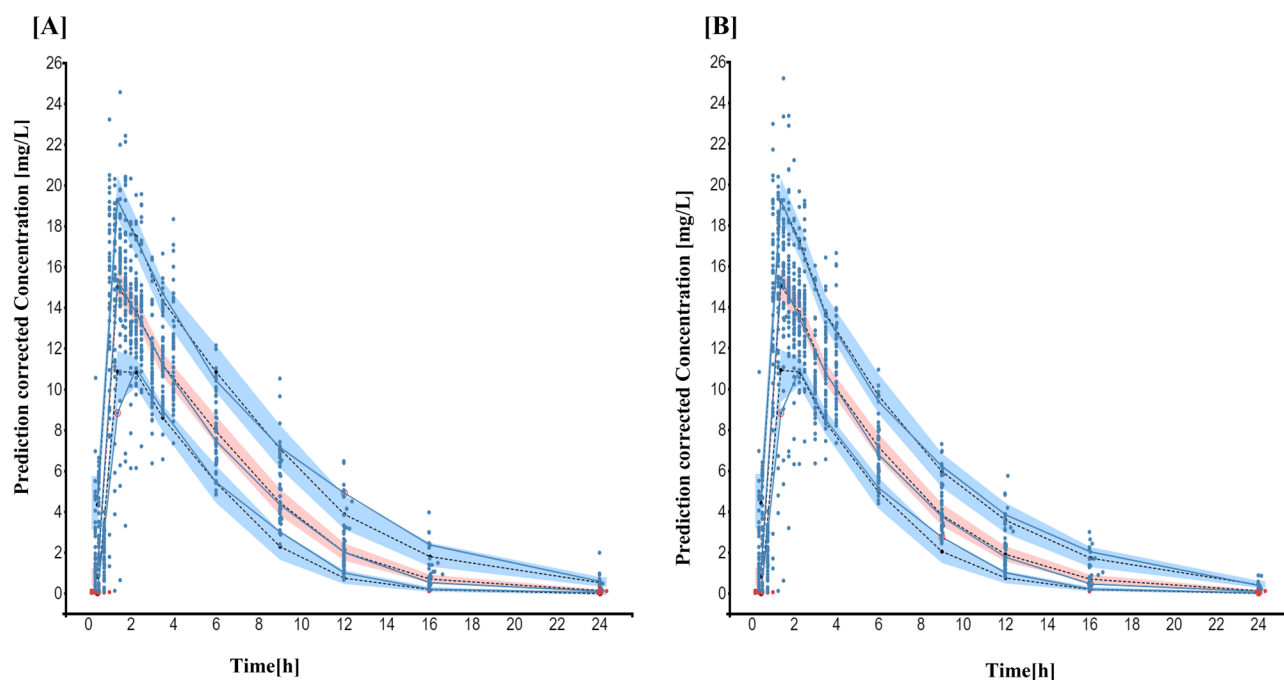


Fig. 6 Prediction corrected visual predictive check ($n=1000$) of **A** sex + BW and **B** FFM covariate model. Solid blue dots represent observed concentrations. Solid red dots represent BQL data. Solid blue lines represent observed concentrations' median and 10th and

90th percentiles. Shaded areas are the model-predicted 90% confidence intervals of 10th, 50th, and 90th percentiles (lower blue area, red area, upper blue area, respectively). Black dotted lines represent medians of the respective confidence intervals of simulated data

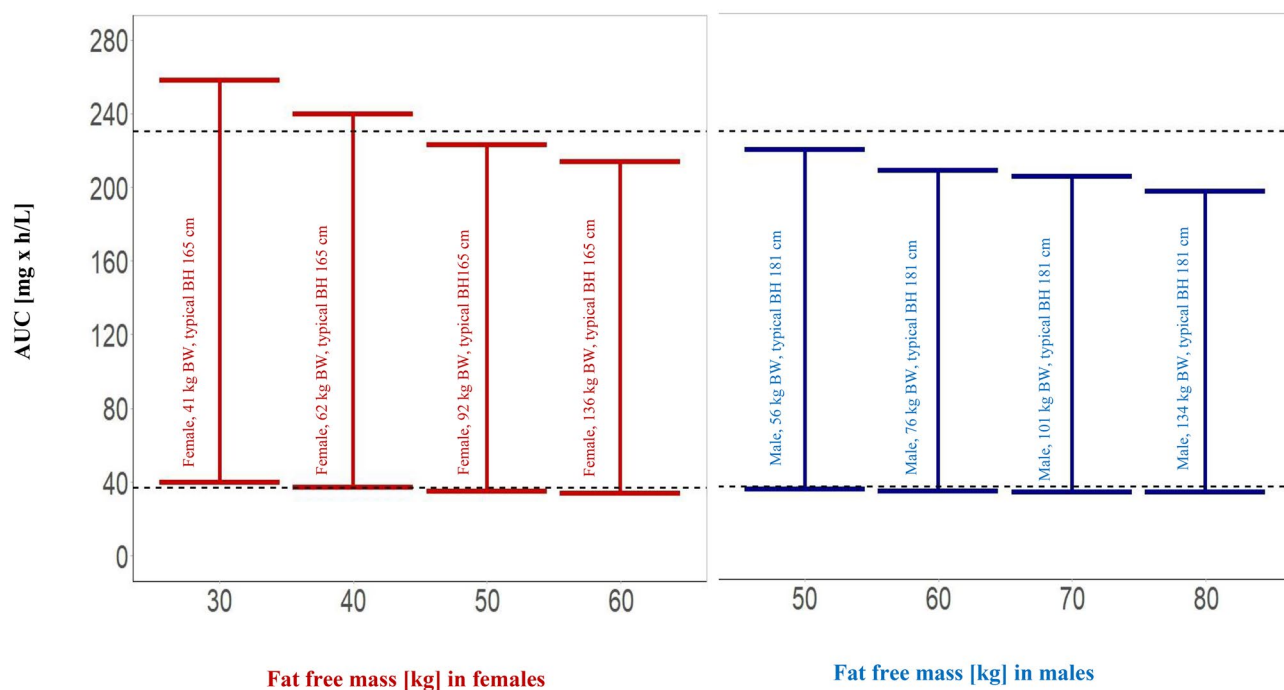


Fig. 7 Effect of weight on simulated exposure of rifampicin for a 600 mg oral dose with FFM as a covariate and without covariate effect. Bars represent 5th and 95th percentiles, and dotted black lines represent 5th and 95th percentiles without taking a body size-related covariate into account. AUC, area under the concentration–time

curve. Body weight (BW) is given with each FFM value for a male individual with a typical body height (BH) in the study population of 185 cm and a female individual with a typical body height of 165 cm to illustrate the meaning of FFM

application in standard clinical practice. The methods used to experimentally assess FFM vary depending on principles such as whole-body counting, bioimpedance, densitometry, dual-energy X-ray absorptiometry, medical imaging, and hydrometry. They differ in their methods and fundamental biological presumptions that are often not applicable to some populations, such as children, the elderly, and those with specific disease states [57]. As a result, models that forecast FFM from quantifiable factors, including body weight and height, are employed in both population pharmacokinetic modeling and clinical practice. It is unclear which of the various procedures to forecast FFM are the most reliable [57]. This uncertainty is a caveat for the use of FFM for individualized dosing, and using covariates that are available without further assumptions such as body weight together with sex has the advantage of easy implementation.

The U.S. Food and Drug Administration recommends BSA scaling for using animal model species data to establish safe starting doses for the first in human clinical studies [58]. Most established BSA formulae are based on variables including body weight and height [59]. In 1987, Mosteller [29] introduced a simplified method of the BSA equation initially proposed by Gehan and George [60] without taking sex differences into account. Sex differences in the pharmacokinetics of drugs have been reported in the literature. FDA identified statistically significant sex differences in about 28% of data sets from bioequivalence trials and suggested that drug exposure difference could exceed 50% [61]. Similarly to FFM, BSA is also a derived parameter based on an individual's BW and body height. When considered with sex, BSA did not offer a significant advantage over BW and sex only (Table 4). BMI is currently the typical worldwide measure for classifying obesity. In this study and the study conducted by Gao et al., BMI was not a significant covariate on PK parameters of rifampicin [52]. BMI increases with total body weight but cannot distinguish adipose tissue from muscle mass, and its usefulness as a dosage scalar is restricted because patients with a large muscle mass would get the same dose as patients with a large fat mass. Additionally, BMI is not sex-specific, is not derived using data from women, and has not been tested for its ability to predict morbidity in women [56].

This study has a few limitations. It was primarily designed for assessing the bioequivalence of two rifampicin preparations and not for covariate analysis. Furthermore, it was designed as a single-dose study and not a multiple-dose study; thus, auto-induction of rifampicin metabolism could not be considered. On the other hand, identification of a sex effect with single doses avoids a potential bias caused by possible sex differences in autoinduction and thus may help assess individual components in rifampicin pharmacokinetics explaining sex differences. This study only included healthy volunteers from a Caucasian population. Further analysis would be required in

TB patients and other populations, and it should include the achievement of pharmacokinetic/pharmacodynamics targets to assess the clinical relevance differences in rifampicin exposure based on body composition.

Based on PK principles, it stands to reason that FFM is the primary biological covariate directly affecting PK in our evaluation, while sex exerts its effect as a covariate indirectly via affecting FFM. The current approach to derive FFM has the disadvantage that it is estimated from sex, body weight, and height only (Eqs. 2 and 3) and thus takes individual body composition to some degree into account while it does not consider fat vs. muscle mass within the male and female groups. Estimated FFM was the best covariate to explain inter-individual variability in PK of rifampicin in healthy volunteers indicating that body composition could also be considered for optimized dosing of rifampicin. The assumption that FFM is preferable to BW confirms previous findings in the African population [39] but needs to be studied further in Caucasian and Asian patients treated with rifampicin.

Supplementary Information The online version contains supplementary material available at <https://doi.org/10.1007/s00228-024-03697-3>.

Author contribution Sami Ullah: Mada data set and prepared initial model. Ulrich Jaehde: supervision. Christina Trueck: conducting the study. Dario Zarembo: organized the study from the University of Cologne. Bertil Wachall: organized the study from InfectoPharm. Manfred Wargenau: conducted the study from MARCO GmbH. Bernhard Scheidel: carried out the analysis of the samples. Martin H. J. Wiesen: conducting the study. Malaz Gazzaz: conducting the study. Chunli Chen: review the manuscript. Sören Büsker: reviewed the manuscript. Uwe Fuhr: supervision and review of the manuscript. Max Taubert: supervision and reviewed the manuscript and provided technical support in modeling. Charalambos Dokos: review the manuscript.

Funding Open Access funding enabled and organized by Projekt DEAL. The Higher Education Commission of Pakistan provided financial support through a PhD scholarship for Muhammad Bilal and Sami Ullah through the German Academic Exchange Service (DAAD). A grant from the Government of Saudi Arabia supported Malaz Gazzaz. Chunli Chen was supported by the 2022 ESI International High Impact Research Article Cooperation Program (No. 212–54900112), the National Natural Science Foundation of Heilongjiang Province (No. YQ2022C017), and the International Postdoctoral Exchange Fellowship Program from the Office of China Postdoctoral Council (No. 2020106 and PC2020013). The clinical study was the work for hire funded by InfectoPharm Arzneimittel und Consilium GmbH, 64646 Heppenheim, Germany.

Declarations

Competing interests The authors declare no competing interests.

Open Access This article is licensed under a Creative Commons Attribution 4.0 International License, which permits use, sharing, adaptation, distribution and reproduction in any medium or format, as long as you give appropriate credit to the original author(s) and the source, provide a link to the Creative Commons licence, and indicate if changes were made. The images or other third party material in this article are included in the article's Creative Commons licence, unless indicated otherwise in a credit line to the material. If material is not included in the article's Creative Commons licence and your intended use is not

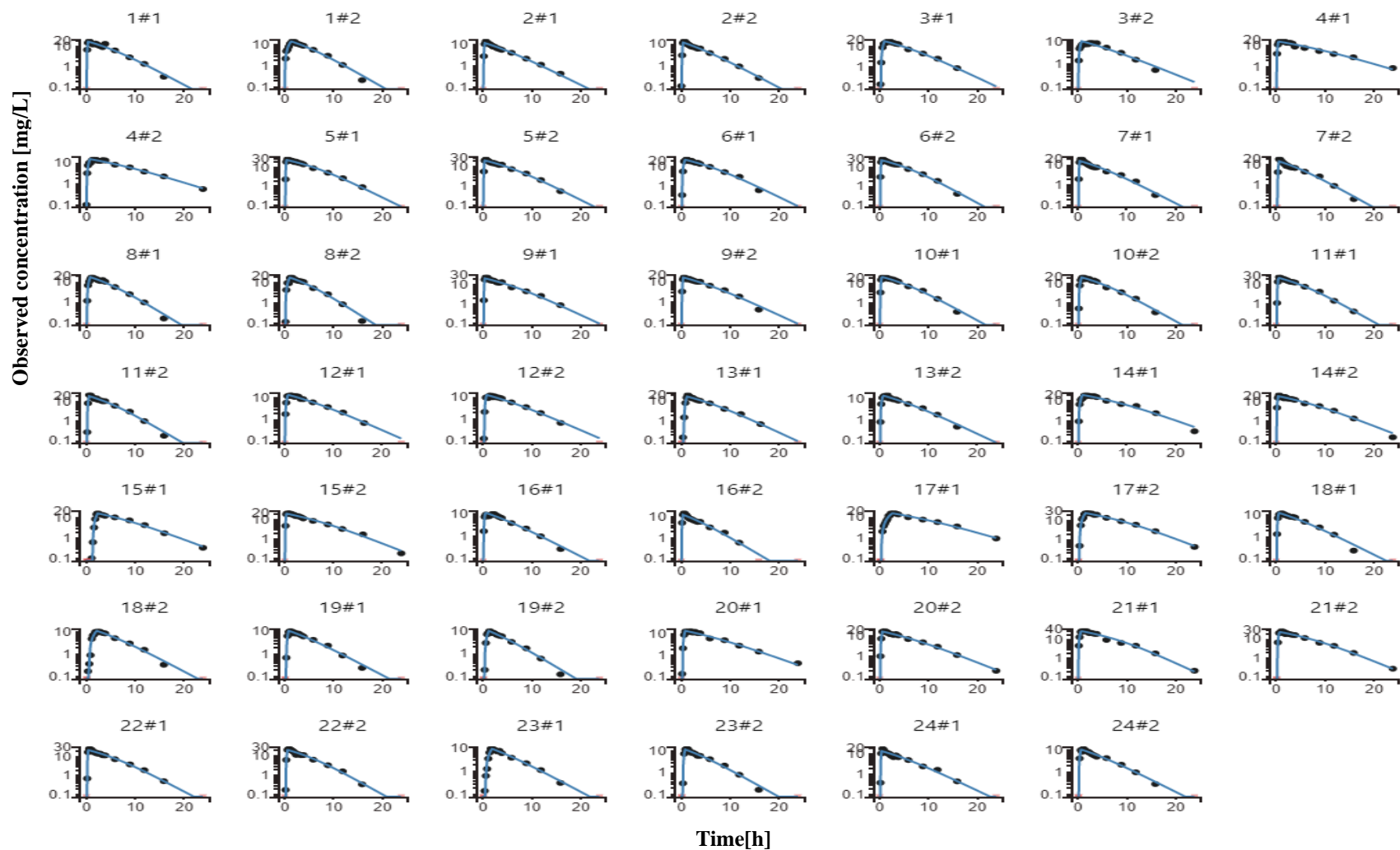
permitted by statutory regulation or exceeds the permitted use, you will need to obtain permission directly from the copyright holder. To view a copy of this licence, visit <http://creativecommons.org/licenses/by/4.0/>.

References

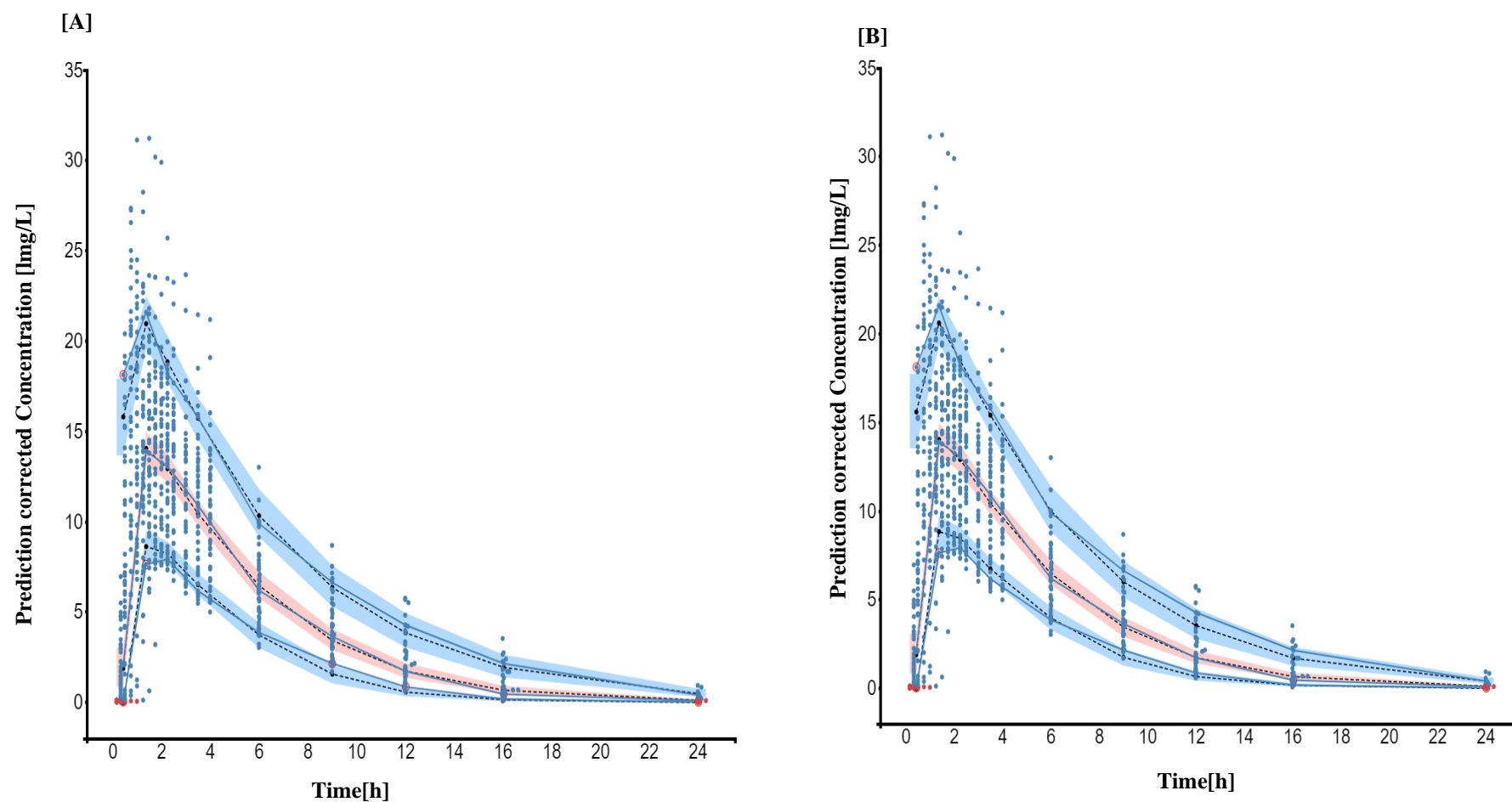
1. Sturkenboom MGG, Märtson AG, Svensson EM et al (2021) Population pharmacokinetics and Bayesian dose adjustment to advance TDM of anti-TB drugs. *Clin Pharmacokinet* 60:685–710. <https://doi.org/10.1007/S40262-021-00997-0>
2. World Health organization (2022) Global tuberculosis report. <https://iris.who.int/bitstream/handle/10665/363752/9789240061729-eng.pdf>
3. Migliori GB, Thong PM, Akkerman O et al (2020) Worldwide effects of coronavirus disease pandemic on tuberculosis services, January–April 2020. *Emerg Infect Dis* 26:2709–2712. <https://doi.org/10.3201/EID2611.203163>
4. Wright G (1937) Treatment of staphylococcal infections. *Br Med J* 2:994–995. <https://doi.org/10.1136/bmj.2.4010.994-b>
5. Sensi P (1983) History of the development of rifampin. *Rev Infect Dis* 5(Suppl 3):S402–S406. https://doi.org/10.1093/CLINIDS/5.SUPPLEMENT_3.S402
6. Mosaei H, Zenkin N (2020) Inhibition of RNA polymerase by rifampicin and rifamycin-like molecules. *EcoSal Plus*. <https://doi.org/10.1128/ecosalplus.esp-0017-2019>
7. Acocella G (1978) Clinical pharmacokinetics of rifampicin. *Clin Pharmacokinet* 3:108–127. <https://doi.org/10.2165/00003088-197803020-00002>
8. Polasa K, Krishnaswamy K (1983) Effect of food on bioavailability of rifampicin. *J Clin Pharmacol* 23:433–437
9. Boman G (1974) Ringberger VA (1974) Binding of rifampicin by human plasma proteins. *Eur J Clin Pharmacol* 75(7):369–373. <https://doi.org/10.1007/BF00558209>
10. Sousa M, Pozniak A, Boffito M (2008) Pharmacokinetics and pharmacodynamics of drug interactions involving rifampicin, rifabutin and antimalarial drugs. *J Antimicrob Chemother* 62:872–878. <https://doi.org/10.1093/jac/dkn330>
11. Curci G, Bergamini N, Veneri FD et al (1972) Half-life of rifampicin after repeated administration of different doses in humans. *Chemotherapy* 17:373–381. <https://doi.org/10.1159/000220873>
12. Rana F (2013) Rifampicin-an overview. *Int J Res Pharm Chem* 3:83–87
13. Howard P, Twycross R, Grove G et al (2015) Rifampin (INN Rifampicin). *J Pain Symptom Manage* 50:891–895. <https://doi.org/10.1016/j.jpainsymman.2015.09.004>
14. Ruslami R, Nijland HMJ, Alisjahbana B et al (2007) Pharmacokinetics and tolerability of a higher rifampin dose versus the standard dose in pulmonary tuberculosis patients. *Antimicrob Agents Chemother* 51:2546–2551. <https://doi.org/10.1128/AAC.01550-06>
15. Niemi M, Backman JT, Fromm MF et al (2003) Pharmacokinetic interactions with rifampicin: clinical relevance. *Clin Pharmacokinet* 42:819–850. <https://doi.org/10.2165/00003088-200342090-00003>
16. Jayaram R, Gaonkar S, Kaur P et al (2003) Pharmacokinetics-pharmacodynamics of rifampin in an aerosol infection model of tuberculosis. *Antimicrob Agents Chemother* 47:2118. <https://doi.org/10.1128/AAC.47.7.2118-2124.2003>
17. World Health Organization (2010) Treatment of tuberculosis: guidelines. https://iris.who.int/bitstream/handle/10665/44165/9789241547833_eng.pdf
18. Rockwood N, Meintjes G, Chirehwa M et al (2016) HIV-1 coinfection does not reduce exposure to rifampin, isoniazid, and pyrazinamide in South African tuberculosis outpatients. *Antimicrob Agents Chemother* 60:6050–6059. <https://doi.org/10.1128/AAC.00480-16>
19. Chirehwa MT, Rustomjee R, Mthiyane T et al (2016) Model-based evaluation of higher doses of rifampin using a semimechanistic model incorporating autoinduction and saturation of hepatic extraction. *Antimicrob Agents Chemother* 60:487–494. <https://doi.org/10.1128/AAC.01830-15>
20. Milán Segovia RC, Domínguez Ramírez AM, Jung Cook H et al (2013) Population pharmacokinetics of rifampicin in Mexican patients with tuberculosis. *J Clin Pharm Ther* 38:56–61. <https://doi.org/10.1111/JCPT.12016>
21. Kumar R, Police A (2015) Simultaneous quantitation of rifampicin and piperine in rat plasma by a selective and sensitive liquid chromatography–tandem mass spectrometric method and its pharmacokinetic application
22. Srivastava A, Waterhouse D, Ardrey A, Ward SA (2012) Quantification of rifampicin in human plasma and cerebrospinal fluid by a highly sensitive and rapid liquid chromatographic–tandem mass spectrometric method. *J Pharm Biomed Anal* 70:523. <https://doi.org/10.1016/J.JPBA.2012.05.028>
23. Patil JS, Suresh S, Sureshbabu A, Rajesh M (2011) Development and validation of liquid chromatography-mass spectrometry method for the estimation of rifampicin in plasma. *Indian J Pharm Sci* 73:558. <https://doi.org/10.4103/0250-474X.99014>
24. Monolix - Lixoft (2022) <https://lixoft.com/products/monolix/>
25. Couffignal C, Pajot O, Laouénan C et al (2014). Population pharmacokinetics of imipenem in critically ill patients with suspected ventilator-associated pneumonia and evaluation of dosage regimens. <https://doi.org/10.1111/bcp.12435>
26. Samson A, Lavielle M, Mentré F (2006) Extension of the SAEM algorithm to left-censored data in nonlinear mixed-effects model: application to HIV dynamics model. *Comput Stat Data Anal* 51:1562–1574. <https://doi.org/10.1016/J.CSDA.2006.05.007>
27. Bergstrand A, Karlsson MO (2009) Handling data below the limit of quantification in mixed effect models. *AAPS J* 11:371. <https://doi.org/10.1208/S12248-009-9112-5>
28. Kass RE, Raftery AE (1995) Bayes factors. *J Am Stat Assoc* 90:773–795. <https://doi.org/10.1080/01621459.1995.10476572>
29. Mosteller RD (1987) The New England Journal of Medicine Downloaded from nejm.org at DUKE MEDICAL CENTER LIBRARY on November 25, 2012. For personal use only. No other uses without permission. From the NEJM Archive. Copyright © 2010 Massachusetts Medical Society. All rights re. *N Engl J Med* 2012
30. Janmahasatian S, Duffull SB, Ash S et al (2005) Quantification of lean bodyweight. *Clin Pharmacokinet* 44:1051–1065. <https://doi.org/10.2165/00003088-200544100-00004>
31. de Velde F, de Winter BCM, Neely MN et al (2020) Population pharmacokinetics of imipenem in critically ill patients: a parametric and nonparametric model converge on CKD-EPI estimated glomerular filtration rate as an impactful covariate. *Clin Pharmacokinet* 59:885–898. <https://doi.org/10.1007/s40262-020-00859-1>
32. Baron KT (2022) Models, mrgsolve: simulate from ODE-based
33. Nishimura T, Kohno H, Nagai H et al (2020) The population pharmacokinetics of rifampicin in Japanese pulmonary tuberculosis patients. *Drug Res (Stuttg)* 70:199–205. <https://doi.org/10.1055/A-1122-8129>
34. Horita Y, Alsultan A, Kwara A et al (2018) Evaluation of the adequacy of WHO revised dosages of the first-line antituberculosis drugs in children with tuberculosis using population pharmacokinetic modeling and simulations. *Antimicrob Agents Chemother*. <https://doi.org/10.1128/AAC.00008-18>
35. Sekaggya-Wiltshire C, Chirehwa M, Musaazi J et al (2019) Low antituberculosis drug concentrations in HIV-tuberculosis-coinfected adults with low body weight: is it time to update dosing guidelines? *Antimicrob Agents Chemother*. <https://doi.org/10.1128/AAC.02174-18>

36. Medellín-Garibay SE, Milán-Segovia RDC, Magaña-Aquino M et al (2014) Pharmacokinetics of rifampicin in Mexican patients with tuberculosis and healthy volunteers. *J Pharm Pharmacol* 66:1421–1428. <https://doi.org/10.1111/jphp.12275>
37. Naidoo A, Chirehwa M, Ramsuran V et al (2019) Effects of genetic variability on rifampicin and isoniazid pharmacokinetics in South African patients with recurrent tuberculosis. *Pharmacogenomics* 20:224–240. <https://doi.org/10.2217/PGS-2018-0166>
38. Wilkins JJ, Savic RM, Karlsson MO et al (2008) Population pharmacokinetics of rifampin in pulmonary tuberculosis patients, including a semimechanistic model to describe variable absorption. *Antimicrob Agents Chemother* 52:2138–2148. <https://doi.org/10.1128/AAC.00461-07>
39. Jeremiah K, Denti P, Chigutsa E et al (2014) Nutritional supplementation increases rifampin exposure among tuberculosis patients coinfecting with HIV. *Antimicrob Agents Chemother* 58:3468–3474. <https://doi.org/10.1128/AAC.02307-13>
40. Denti P, Martinson N, Cohn S et al (2016) Population pharmacokinetics of rifampin in pregnant women with tuberculosis and HIV coinfection in Soweto, South Africa. *Antimicrob Agents Chemother* 60:1234–1241. <https://doi.org/10.1128/AAC.02051-15>
41. Svensson RJ, Aarnoutse RE, Diacon AH et al (2018) A population pharmacokinetic model incorporating saturable pharmacokinetics and autoinduction for high rifampicin doses. *Clin Pharmacol Ther* 103:674. <https://doi.org/10.1002/CPT.778>
42. Seng KY, Hee KH, Soon GH et al (2015) Population pharmacokinetics of rifampicin and 25-deacetyl-rifampicin in healthy Asian adults. *J Antimicrob Chemother* 70:3298–3306. <https://doi.org/10.1093/JAC/DKV268>
43. Pcloquin CA, Namdar R, Singleton MD, Nix DE (1999) Pharmacokinetics of rifampin under fasting conditions, with food, and with antacids. *Chest* 115:12–18. <https://doi.org/10.1378/chest.115.1.12>
44. Denti P, Jeremiah K, Chigutsa E et al (2015) Pharmacokinetics of isoniazid, pyrazinamide, and ethambutol in newly diagnosed pulmonary TB patients in Tanzania. *PLoS One*. <https://doi.org/10.1371/JOURNAL.PONE.0141002>
45. Schipani A, Pertinez H, Mlota R et al (2016) A simultaneous population pharmacokinetic analysis of rifampicin in Malawian adults and children. *Br J Clin Pharmacol* 81:679–687. <https://doi.org/10.1111/BCP.12848>
46. Mukonzo JK, Kengo A, Kutesa B et al (2020) Role of pharmacogenetics in rifampicin pharmacokinetics and the potential effect on TB–rifampicin sensitivity among Ugandan patients. *Trans R Soc Trop Med Hyg* 114:107–114. <https://doi.org/10.1093/TRSTMH/TRZ108>
47. Kim ES, Kwon BS, Park JS et al (2021) Relationship among genetic polymorphism of SLCO1B1, rifampicin exposure and clinical outcomes in patients with active pulmonary tuberculosis. *Br J Clin Pharmacol* 87:3492–3500. <https://doi.org/10.1111/BCP.14758>
48. Goutelle S, Bourguignon L, Maire PH et al (2009) Population modeling and Monte Carlo simulation study of the pharmacokinetics and antituberculosis pharmacodynamics of rifampin in lungs. *Antimicrob Agents Chemother* 53:2974–2981. <https://doi.org/10.1128/AAC.01520-08/ASSET/199547C9-91B5-4A56-899B-A734826D6345/ASSETS/GRAPHIC/ZAC0070982520005.JPEG>
49. Männistö P (1977) Absorption of rifampin from various preparations and pharmaceutical forms. *Clin Pharmacol Ther* 21:370–374. <https://doi.org/10.1002/cpt1977213370>
50. Becker C, Dressman JB, Junginger HE et al (2009) Biowaiver monographs for immediate release solid oral dosage forms: Rifampicin. *J Pharm Sci* 98:2252–2267. <https://doi.org/10.1002/JPS.21624>
51. Acocella G, Pagani V, Marchetti M et al (1971) Kinetic studies on rifampicin. I. Serum concentration analysis in subjects treated with different oral doses over a period of two weeks. *Chemotherapy* 16:356–370. <https://doi.org/10.1159/000220750>
52. Gao Y, Davies Forsman L, Ren W et al (2021) Drug exposure of first-line anti-tuberculosis drugs in China: a prospective pharmacological cohort study. *Br J Clin Pharmacol* 87:1347–1358. <https://doi.org/10.1111/BCP.14522>
53. Muda MR, Harun SN, Syed Sulaiman SA, Sheikh Ghadzi SM (2022) Population pharmacokinetics analyses of rifampicin in adult and children populations: a systematic review. *Br J Clin Pharmacol* 88:3132–3152. <https://doi.org/10.1111/BCP.15298>
54. Abulfathi AA, Decloedt EH, Svensson EM et al (2019) Significant correlations: Clinical pharmacokinetics and pharmacodynamics of rifampicin in human tuberculosis. *Clin Pharmacokinet* 58:1103–1129. <https://doi.org/10.1007/s40262-019-00764-2>
55. Susanto BO, Svensson RJ, Svensson EM et al (2020) Rifampicin can be given as flat-dosing instead of weight-band dosing. *Clin Infect Dis* 71:3055–3060. <https://doi.org/10.1093/CID/CIZ1202>
56. Rathbun EN, Pace N (1945) Studies on body composition: the determination of total body fat by mean of the body specific gravity, part I. *J Biol Chem* 158:667–676
57. Sinha J, Duffull SB, Al-Sallami HS (2018) A review of the methods and associated mathematical models used in the measurement of fat-free mass. *Clin Pharmacokinet* 57:781–795. <https://doi.org/10.1007/s40262-017-0622-5/FIGURES/7>
58. Blanchard OL, Smoliga JM (2015) Translating dosages from animal models to human clinical trials-revisiting body surface area scaling. *FASEB J* 29:1629–1634. <https://doi.org/10.1096/fj.14-269043>
59. Redlarski G, Palkowski A, Krawczuk M (2016) Body surface area formulae: an alarming ambiguity. *Sci Rep* 6:1–8. <https://doi.org/10.1038/srep27966>
60. Gehan EA, George SL (1970) Estimation of human body surface area from height and weight. *Cancer Chemother Rep* 54:225–235
61. Schwartz JB (2003) The influence of sex on pharmacokinetics. *Clin Pharmacokinet* 42:107–121

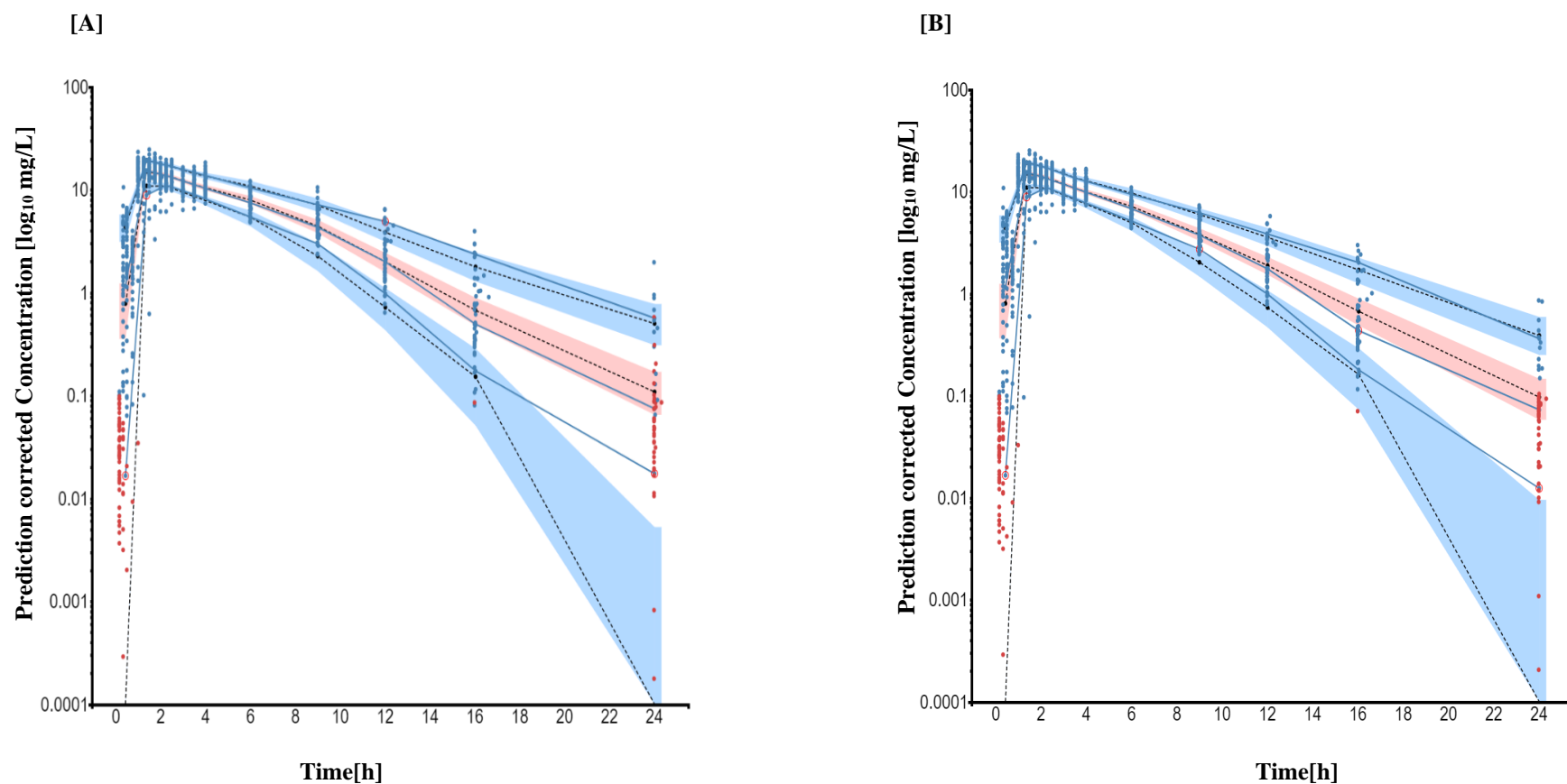
Publisher's Note Springer Nature remains neutral with regard to jurisdictional claims in published maps and institutional affiliations.



Supplementary Fig 1. Individual fits of all the subjects of the base model. #1 and #2 designate test and reference preparations, respectively, and solid dark dots represent observed concentration. Blue lines represent the prediction.



Supplementary Fig 2. Prediction corrected visual predictive check ($n = 1000$) of [A] sex + BW and [B] FFM covariate model. Solid blue dots represent observed concentrations. Solid red dots represent BQL data. Solid blue lines represent median, 10th, and 90th percentiles of observed concentrations. Shaded areas are the model-predicted 90% confidence intervals of 10th, 50th, and 90th percentiles (lower blue area, red area, upper blue area, respectively). Black dotted lines represent medians of the respective confidence intervals of simulated data



Supplementary Fig 3. Prediction corrected visual predictive check ($n = 1000$) of [A] sex + BW and [B] FFM covariate model. Solid blue dots represent observed concentrations. Solid red dots represent BQL data. Solid blue lines represent median, 10th, and 90th percentiles of observed concentrations. Shaded areas are the model-predicted 90% confidence intervals of 10th, 50th, and 90th percentiles (lower blue area, red area, upper blue area, respectively). Black dotted lines represent medians of the respective confidence intervals of simulated data

Monolix control stream of rifampicin population pharmacokinetic model

[INDIVIDUAL]

```
input = {Km_pop, V_pop, Vm_pop, Tlag_pop, Tk0_pop, omega_V, omega_Vm, gamma_Tlag,
gamma_Tk0, gamma_V, gamma_Vm, corr2_Tlag_Tk0}
```

DEFINITION:

```
Km = {distribution=logNormal, typical=Km_pop, no-variability}
V = {distribution=logNormal, typical=V_pop, varlevel={id, id*occ}, sd={omega_V, gamma_V}}
Vm = {distribution=logNormal, typical=Vm_pop, varlevel={id, id*occ}, sd={omega_Vm,
gamma_Vm}}
Tlag = {distribution=logNormal, typical=Tlag_pop, varlevel=id*occ, sd=gamma_Tlag}
Tk0 = {distribution=logNormal, typical=Tk0_pop, varlevel=id*occ, sd=gamma_Tk0}
correlation = {level=id*occ, r(Tlag, Tk0)=corr2_Tlag_Tk0}
```

[LONGITUDINAL]

```
input = {a, b}
;;; Included file 'oral0_1cpt_TlagTk0VVmKm.txt'
```

DESCRIPTION:

The administration is extravascular with a zero-order process (duration Tk0) with a lag time (Tlag). The PK model has one compartment (volume V) and a Michaelis-Menten elimination (Vm, Km).

```
input = {Tlag, Tk0, V, Vm, Km}
```

EQUATION:

```
odeType = stiff
```

PK:

```
; PK model definition
Cc = pkmodel(Tlag, Tk0, V, Vm, Km)
```

OUTPUT:

```
output = {Cc}
```

;;;

DEFINITION:

```
DV = {distribution=normal, prediction=Cc, errorModel=combined1(a, b)}
```



A population pharmacokinetic model of remdesivir and its major metabolites based on published mean values from healthy subjects

Ahmed Abouellil^{1,2} · Muhammad Bilal^{1,3} · Max Taubert¹ · Uwe Fuhr¹

Received: 19 May 2022 / Accepted: 8 September 2022 / Published online: 20 September 2022
© The Author(s) 2022

Abstract

Remdesivir is a direct-acting anti-viral agent. It was originally evaluated against filoviruses. However, during the COVID-19 pandemic, it was investigated due to its anti-viral activities against (SARS-CoV-2) virus. Therefore remdesivir received conditional approval for treatment of patients with severe coronavirus disease. Yet, its pharmacokinetic properties are inadequately understood. This report describes the population pharmacokinetics of remdesivir and its two plasma-detectable metabolites (GS-704277 and GS-441524) in healthy volunteers. The data was extracted from published phase I single escalating and multiple i.v remdesivir dose studies conducted by the manufacturer. The model was developed by standard methods using non-linear mixed effect modeling. Also, a series of simulations were carried out to test suggested clinical doses. The model describes the distribution of remdesivir and each of its metabolites by respective two compartments with sequential metabolism between moieties, and elimination from central compartments. As individual data were not available, only inter-cohort variability could be assessed. The estimated point estimates for central (and peripheral) volumes of distribution for remdesivir, GS-704277, and GS-441524 were 4.89 L (46.5 L), 96.4 L (8.64 L), and 26.2 L (66.2 L), respectively. The estimated elimination clearances of remdesivir, GS704277, and GS-441524 reached 18.1 L/h, 36.9 L/h, and 4.74 L/h, respectively. The developed model described the data well. Simulations of clinically approved doses showed that GS-441524 concentrations in plasma exceeded the reported EC₅₀ values during the complete duration of treatment. Nonetheless, further studies are needed to explore the pharmacokinetics of remdesivir and its relationship to clinical efficacy, and the present model may serve as a useful starting point for additional evaluations.

Keywords Anti-virals · Population pharmacokinetics · COVID-19 · Remdesivir · Pharmacometrics · GS-441524 · GS-704277

Introduction

Current management of patients with severe COVID-19 mainly focuses on immune response modulation and symptomatic therapy. In critically ill patients, management would also include supplemental oxygen and

mechanical ventilation, along with the suppression of inadequate immune response. Healthcare providers also attempt to control secondary infections and thrombosis by either prophylaxis or treatment (Sieswerda et al. 2021; Godino et al. 2021). So far, only two anti-viral small-molecule medications have been authorized for the treatment of COVID-19 in 2020/2021, which includes the use of remdesivir under certain conditions (CDC 2021; EMA 2021; Diaz et al. 2021), and molnupiravir which has just been authorized in Great Britain for the use in patients with mild to moderate COVID-19 with risk factors for developing severe illness (UK-MHRA 2021). And recently, the FDA has expanded the use of remdesivir to certain non-hospitalized adults and pediatric patients for the treatment of mild-to-moderate COVID-19 disease (FDA 2022).

✉ Ahmed Abouellil
s4ahabou@uni-bonn.de; a.abouellil@gmail.com

¹ Faculty of Medicine, Center for Pharmacology, Department I of Pharmacology, University Hospital Cologne, University of Cologne, Gleueler Straße 24, 50931 Cologne, Germany

² Immunosenescence Cluster of Excellence, University Hospital Bonn, Bonn, Germany

³ Department of Clinical Pharmacy, Institute of Pharmacy, University of Bonn, Bonn, Germany

Remdesivir was originally evaluated as a broad-spectrum filovirus inhibitor that can protect against the development of Ebola virus disease (de Wit et al. 2020). During the COVID-19 pandemic, remdesivir showed anti-SARS-CoV-2 activities in vitro and in animal models. These activities were attributed to its triphosphate nucleoside analog, which acts as an inhibitor of the viral RNA-dependent RNA polymerase. However, evidence that supports its efficacy is still under investigation (Wang et al. 2020; de Wit et al. 2020; Alsayed et al. 2021). Remdesivir is also being investigated as a part of drug cocktails that might be used to treat hospitalized COVID-19 patients (Kalil et al. 2021; Vitiello and Ferrara 2021).

Remdesivir needs to go through an extensive metabolic process to be active, and from those metabolism products, only GS-704277 and GS-441524 can be quantified in plasma (Figure S1) (Humeniuk et al. 2021a).

To date, publicly available information on the pharmacokinetics of remdesivir and its metabolites is limited. A non-compartmental description of data in healthy volunteers has been published and serves as the basis for the present evaluation (Humeniuk et al. 2020). Several bottom-up approaches using physiologically based pharmacokinetic models have recently been reported (Deb and Reeves 2021; Fan et al. 2021; Humeniuk et al. 2021b; Gallo 2021), of which the most recent one was generated by scientists of the U.S. Food and Drug Administration (FDA) (Fan et al. 2021). Such models are very useful but in part are based on assumptions that remain to be verified, and occasionally use “optimization” of some of their predefined parameters, with no other reason than that simulations should match the observed data. As an empirical compartmental approach, the manufacturers of remdesivir developed a population pharmacokinetic model of which only parts are publicly available (LHartman et al. 2020). Unfortunately, the information provided there is not sufficient to retrace and assess the performance of the model in detail. Finally, a population pharmacokinetic model has been reported for the GS-441524 metabolite only in Japanese patients with renal impairment (Sukeishi et al. 2021). Overall, the available information reflects only a first step to support more precise dosing strategies for remdesivir. Such information is needed to integrate intrinsic and extrinsic factors for a better understanding of the pharmacokinetics and dynamics of remdesivir. The main objective of the present report was therefore to develop an independent compartmental population pharmacokinetic model that can fit the observed data obtained from literature and empirically describe the pharmacokinetic parameters of remdesivir, GS-704277, and GS-441524. This model may be further used in determining suitable dosing

strategies in patients, with a perspective to be expanded for patients with chronic conditions.

Methods

Arithmetic-concentration data were obtained from published randomized, blinded, placebo-controlled, phase I program that evaluated the safety and pharmacokinetics of single and multiple ascending intravenous doses of remdesivir (Humeniuk et al. 2020). Data points were extracted using GetData Graph Digitizer software (get-data-graph-digitizer.com) and R.

In this trial, remdesivir was administrated as a single 2-h intravenous infusion at doses of 3 mg, 10 mg, 30 mg, 75 mg, 150 mg, and 225 mg. Or as a once-daily 1-h intravenous infusion for 7 and 14 days. This program was carried out in healthy male and non-pregnant, non-lactating female volunteers with an age range of 18 to 55 years and a body mass index of 18 to 30 kg/m². No detailed information regarding individual parameters for each cohort was given, and the study was conducted by the manufacturing company, Gilead Sciences, Inc., USA (Humeniuk et al. 2020).

Population pharmacokinetic (PK) parameters were estimated by standard methods using non-linear mixed effect modeling software (Monolix 2019R2 - Antony, France).

The model was developed by testing different distribution patterns and different compartment numbers for remdesivir, GS-774277, and GS-441524, in addition to different elimination and metabolic models that describe the conversion of remdesivir to GS-704277, and GS-704277 to GS-441524. For this purpose, metabolism was assumed to occur solely in the central compartment or in the central and peripheral compartments simultaneously.

Estimated PK parameters included total body clearance (CL), the volume of distribution for central and peripheral compartments (Vd_c and Vd_p), inter-compartmental clearance (Q), and formation clearance of metabolites (CL_m). Terminal elimination half-life using regression ($t_{1/2cc}$) was also calculated using GraphPad Prism 8 (GraphPad Softwares, 2019, CA, USA). Microsoft Excel (Microsoft, 2021, Redmond, USA) and RStudio (PBC, 2021, Boston, USA) were used for dataset construction, analysis, and graph generation.

The published concentration–time profile of remdesivir showed a sharp increase in plasma concentration immediately following the end of the 2-h intravenous infusion. This could be explained by intravenous line saline washing following the 2-h infusion (Rita Humeniuk, personal communication). To incorporate this sudden increase of remdesivir concentrations into the model, 4% of the total administered dose was subtracted from the continuous infusion dose and given instantaneously at the end of the infusion. The choice of this method and

Table 1 Ordinary differential equations that best describe the pharmacokinetic model for remdesivir and its two metabolites GS-774277 and GS-441524

$$C_c \text{ RDV} = A_{(\text{RDV Central compartment})} / Vd_c \text{ RDV}$$

$$C_p \text{ RDV} = A_{(\text{RDV Peripheral compartment})} / Vd_p \text{ RDV}$$

$$C_c \text{ GS-774277} = A_{(\text{GS-774277 Central compartment})} / Vd_c \text{ GS-774277}$$

$$C_p \text{ GS-774277} = A_{(\text{GS-774277 Peripheral compartment})} / Vd_p \text{ GS-774277}$$

$$C_c \text{ GS-441524} = A_{(\text{GS-441524 Central compartment})} / Vd_c \text{ GS-441524}$$

$$C_p \text{ GS-441524} = A_{(\text{GS-441524 Peripheral compartment})} / Vd_p \text{ GS-441524}$$

$$\frac{DA}{DT}(\text{RDV Central compartment}) = (\text{Input}) + (Q_{\text{RDV}} \times C_p \text{ RDV}) - (Q_{\text{RDV}} \times C_c \text{ RDV}) - (CL_{\text{RDV}} \times C_c \text{ RDV}) - (CLm_c \text{ GS-774277} \times C_c \text{ RDV})$$

$$\frac{DA}{DT}(\text{RDV Peripheral compartment}) = (Q_{\text{RDV}} \times C_c \text{ RDV}) - (Q_{\text{RDV}} \times C_p \text{ RDV}) - (CLm_p \text{ GS-774277} \times C_p \text{ RDV})$$

$$\frac{DA}{DT}(\text{GS-774277 Central compartment}) = (CLm_c \text{ GS-774277} \times C_c \text{ RDV}) + (Q_{\text{GS-774277}} \times C_p \text{ GS-774277}) - (Q_{\text{GS-774277}} \times C_c \text{ GS-774277}) -$$

$$CL_{\text{GS-774277}} \times C_c \text{ GS-774277}) - (CLm_c \text{ GS-441524} \times C_c \text{ GS-774277})$$

$$\frac{DA}{DT}(\text{GS-774277 Peripheral compartment}) = (Q_{\text{GS-774277}} \times C_c \text{ GS-774277}) + (CLm_p \text{ GS-774277} \times C_p \text{ RDV}) - (Q_{\text{GS-774277}} \times C_p \text{ GS-774277})$$

$$\frac{DA}{DT}(\text{GS-441524 Central compartment}) = (CLm_c \text{ GS-441524} \times C_c \text{ GS-774277}) + (Q_{\text{GS-441524}} \times C_p \text{ GS-441524}) - (CL_{\text{GS-441524}} \times C_c \text{ GS-441524}) - (Q_{\text{GS-441524}} \times C_c \text{ GS-441524})$$

$$\frac{DA}{DT}(\text{GS-441524 Peripheral compartment}) = (Q_{\text{GS-441524}} \times C_c \text{ GS-441524}) - (Q_{\text{GS-441524}} \times C_p \text{ GS-441524})$$

Ordinary differential equation pharmacokinetic behavior model was developed based on mean concentration data obtained from phase I clinical trials, where remdesivir was administered in different doses as single-dose 2-h intravenous infusion in healthy subjects. DA/DT represents the change rate of drug amount in the respective compartment. C_c concentration in the central compartment; C_p concentration in the peripheral compartment; A the amount of a substance at a time; CL total body clearance; Vd_c and Vd_p the volume of distribution for central and peripheral compartments, respectively; Q inter-compartmental clearance; CLm formation clearance of metabolites

the selected percentage were based on other published methodology (Anh et al. 2006).

The final model was chosen based on goodness-of-fit plots, visual predictive checks, metabolic plausibility,

parameter shrinkage, and the $-2 \times \log$ of likelihood (Figure S2).

The most suitable model was developed using ordinary differential equations (ODE) in non-linear mixed-effect modeling software (Table 1). The probable post

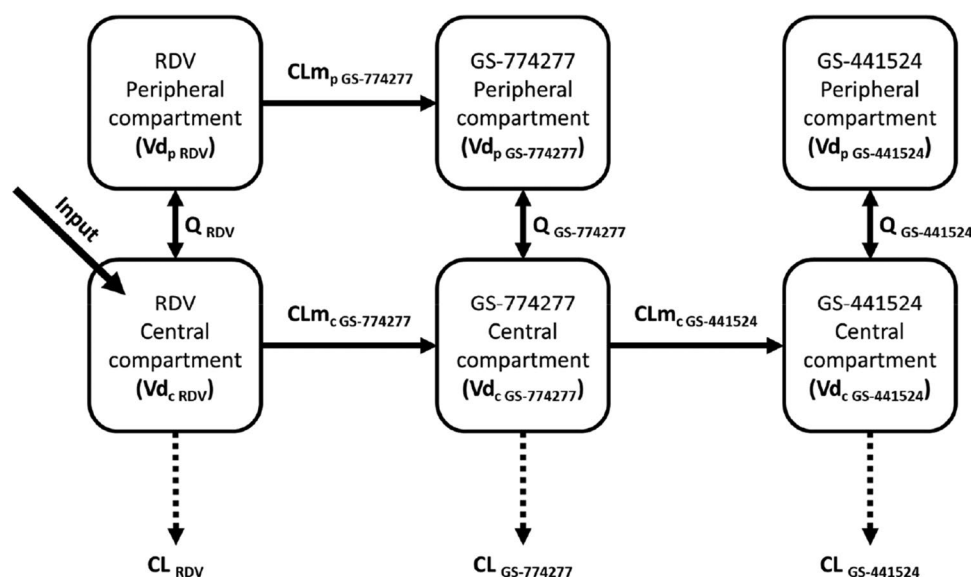
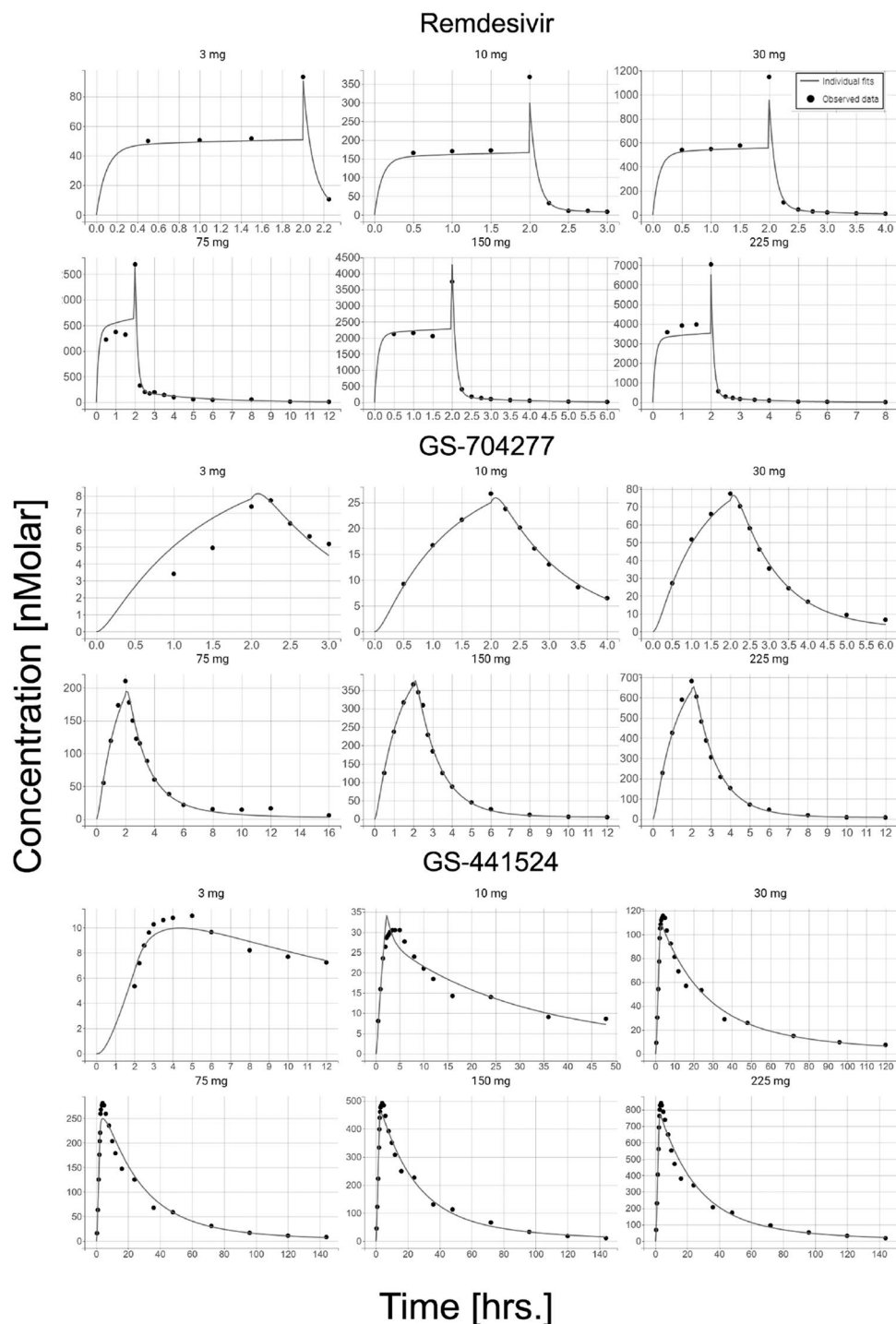


Fig. 1 Overview of the final population pharmacokinetic model for remdesivir (RDV) and its metabolites: GS-774277 and GS-441524 that was developed using non-linear mixed effect modeling software. The model described each moiety to have a 2-compartment distribution, with sequential metabolism occurring from the central compart-

ment, in addition to remdesivir peripheral metabolism to GS-774277. And elimination is modeled to occur in the central compartments. CL total body clearance (CL), Vd_c and Vd_p the volume of distribution for central and peripheral compartments, Q inter-compartmental clearance, CLm formation clearance of metabolites

Fig. 2 Observed mean concentrations (black dots) and model predictions (black line) of each given dose, following single 2-h intravenous infusion of either 3 mg, 10 mg, 30 mg, 75 mg, 150 mg, or 225 mg of remdesivir



hoc values of each dose's fixed parameters were calculated using empirical Bayes method in Monolix software.

As no individual values were available, the obtained variability of fixed parameters reflects inter-cohort variabilities rather than inter-individual variability. And they lump the variability due to differences between volunteers in the different cohorts and they were defined with a log-normal distribution as.

$$\log(\theta_i) = \log(\theta_{\text{population}}) + \eta_i$$

where θ_i is the estimated parameter for the mean concentration of the i th dose, $\theta_{\text{population}}$ is the mean across doses, and η_i is a random effect describing the deviation of the PK parameter for the i th dose level from the typical PK parameter estimated for all doses. Parameter η_i is assumed

Fig. 3 Goodness-of-fit plots describing remdesivir model-predicted plasma concentration value agreement with the observed values

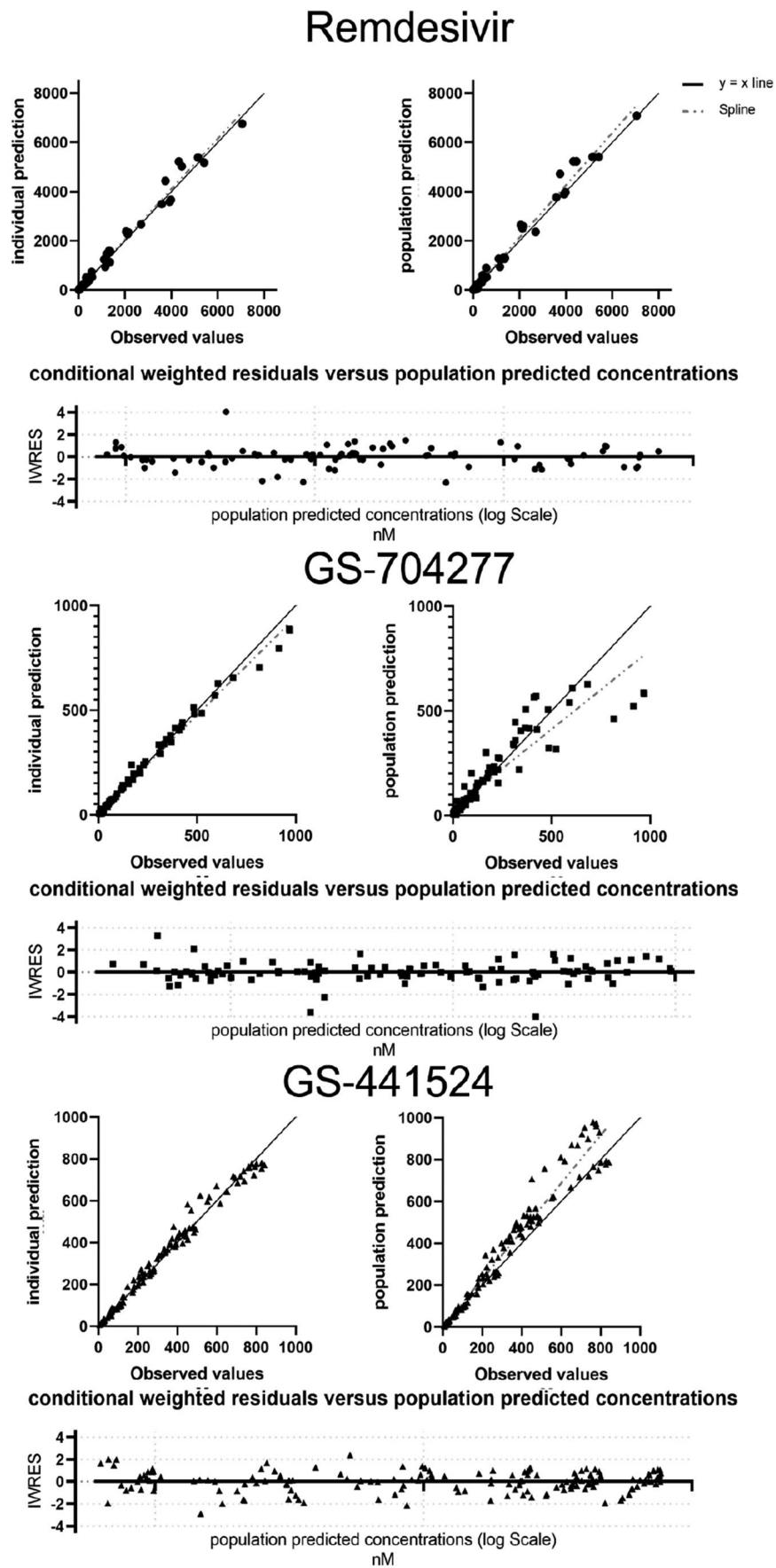


Table 2 Pharmacokinetic population parameter estimates of remdesivir, GS-441524, and GS-704277 following remdesivir single-dose administration (2-h infusion) in healthy subjects

PK parameters	Remdesivir	GS-704277	GS-441524
Central compartment volume of distribution (L)	4.89	96.4	26.2 (0.71)
Peripheral compartment volume of distribution (L)	46.5	8.64	66.2 (0.24)
Inter-compartmental clearance (L/h)	13.2	0.12	55
Total body clearance (L/h)	18.1 (0.39)	36.9 (0.31)	4.74
Central formation clearance (L/h)	-	16.9 (0.25)	50.5 (0.27)
Peripheral formation clearance (L/h)	-	18.9 (0.53)	-

Population parameter estimates of the fixed effects (SD of the random effects) for remdesivir and its metabolites (GS-704277 and GS-441524). The estimates were generated by Monolix software and using mean concentration data points obtained from Gileads' phase I clinical trials, where remdesivir was administered in doses of 3 mg, 10 mg, 30 mg, 75 mg, 150 mg, and 225 mg as single 2-h intravenous infusion in healthy subjects

to follow a normal distribution with a mean of zero and a variance of ω^2 .

Additive, proportional, and combined error models were tested:

$$\text{Additive : } C_{ij} = Y_{ij} + \alpha$$

$$\text{Proportional : } C_{ij} = Y_{ij} + (b) \times Y_{ij}$$

$$\text{Mixed : } C_{ij} = Y_{ij} + \sqrt{(\alpha)^2 + ((b) \times Y_{ij})^2}$$

Here, C_{ij} is the observed value for the mean concentration of the dose i at time point j . Y_{ij} is the predicted concentration value of the dose i at time point j estimated by the model. Parameters a and b are additive and proportional residual errors, respectively.

Simulations were run using R (R Core Team 2021), Simulx 2020R1, and Simulx R package bootstrapping and simulation function (Lixoft, Antony, France), with 256 simulated subjects. To simulate a real-life clinically relevant dosing regimen, the simulation also included a 200 mg, 30-min intravenous infusion of remdesivir on day 1, with subsequent 100 mg, 30-min intravenous infusions for the following 4 days. The choice of this regimen schedule was based on what is recommended by internal hospital physicians, the FDA (U.S. Food and Drug Administration) fact sheet for healthcare providers, and the EMA (European Medicines Agency) Summary of Product Characteristics (CHMP 2020; FDA 2020). The fraction of censored observations for remdesivir, GS-774277, and GS-441524 were calculated by determining the ratio of numbers of observations with values below the reported lower limit of quantification to the total number of observations at a time point.

Results

The best model describing PK data of all moieties included two compartments for remdesivir and each metabolite. The model suggested metabolism to occur mainly in the central compartment from one moiety to

the next one. Additional metabolism was assumed to take place from the peripheral remdesivir compartment to the peripheral GS-704277 compartment, and elimination was assumed to occur from the central compartments of remdesivir and both metabolites (Fig. 1).

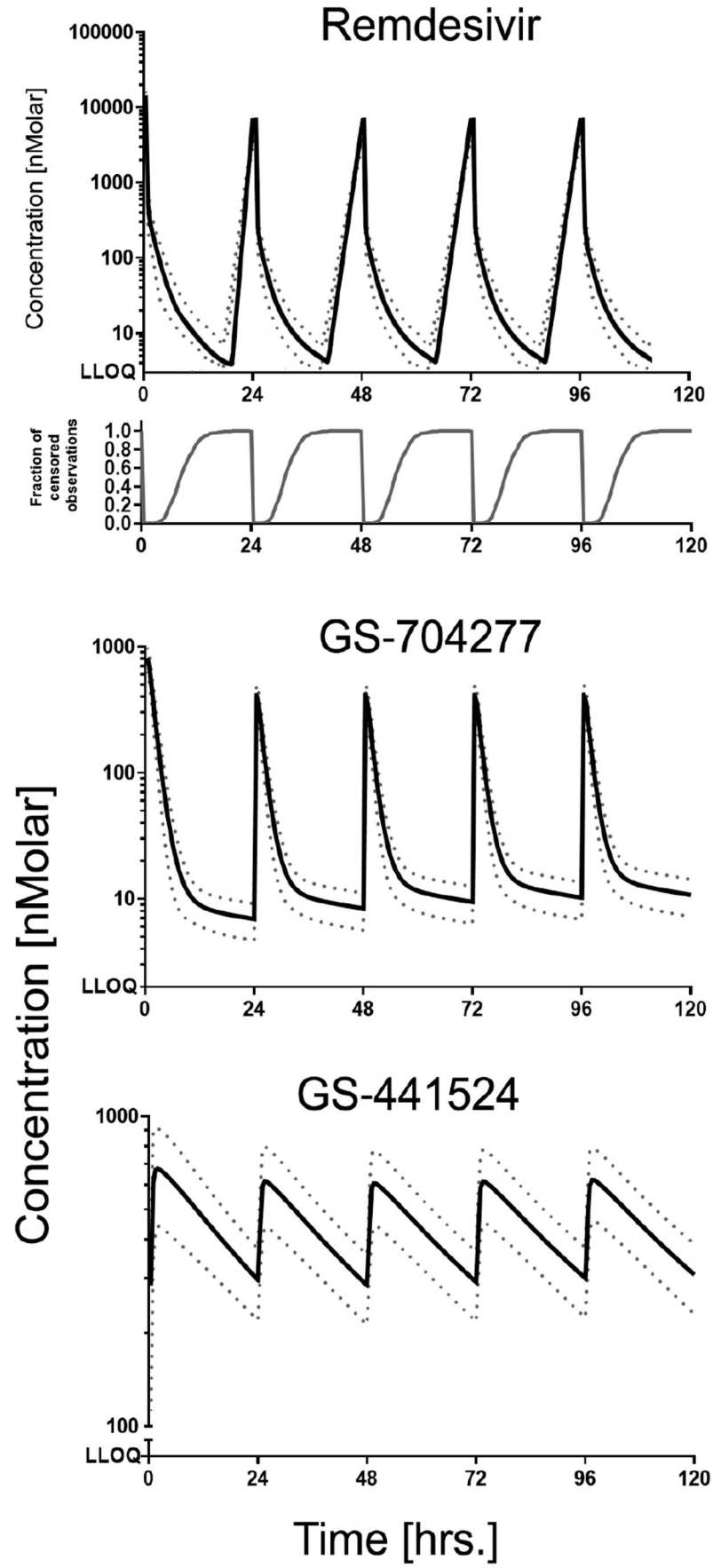
The final model predicted PK profiles for remdesivir, GS-704277, and GS-441524 at individual dose levels. The predicted concentration values were in good agreement with the observed concentrations at each time point (Figs. 2 and 3).

Population parameter estimates for the mean of the published plasma concentration-vs.-time profiles of remdesivir, GS-704277, and GS-441524 following remdesivir 2-h single-dose intravenous administration in healthy volunteers are described in detail in Table 2. Exposure values were similar to previously published remdesivir PK non-compartmental analysis (Table S1). The terminal elimination half-lives in the central compartment for remdesivir, GS-704277, and GS-441524 were 1 h, 1.1 h, and 20 h, respectively.

The final model had exponential inter-cohort variabilities for the following PK parameters: $Vd_{c \text{ GS-441524}}$, $Vd_{p \text{ GS-441524}}$, CL_{RDV} , $CLm_{p \text{ GS-774277}}$, $CLm_{c \text{ GS-774277}}$, $CL_{\text{GS-774277}}$, and $CLm_{c \text{ GS-441524}}$ (Table 2). Also, the error models which matched the data best were proportional for remdesivir, combined for GS-704277, and proportional for GS-441524.

We found by simulating remdesivir administration at the recommended dosage that the C_{\max} (between-dose SD) of remdesivir, GS-704277, and GS-441524 were 13.7 μM (2.39), 807 nM (173), and 726 nM (240), respectively, following the initial loading dose. GS-704277 t_{\max} was reached immediately after the end of the infusion, while GS-441524 reached its t_{\max} 1 h after the end of the infusion. The fraction of censored observations for remdesivir reached the value of 1 after 20 h following the initial 200-mg infusion, and 17 h for each sequential 100-mg infusion. In contrast, GS-774277 and GS-441524 did not reach the values of their reported LLOQ during the whole duration of therapy (Fig. 4).

Fig. 4 Simulated plasma concentration-vs.-time profiles of remdesivir, GS-704277, and GS-441524 following a simulated 30-min intravenous infusion of 200 mg of remdesivir on day 1, with 100 mg, 30-min intravenous infusion for the following 4 days. The bottom part of the remdesivir panel shows the fraction of censored observation numbers to the total observations at a given time. There were no censored observations for the metabolites. Dotted lines reflect standard deviation values



Subsequent C_{\max} value for GS-441524, following the administration of multiple 100-mg remdesivir doses, was 645.5 nM (17.57) and the half-life reached 29.36 h both estimated by simulation.

The simulation used the previously generated population parameters of fixed effects, the standard deviation of the random effects, and error model estimates (Figure S3).

Discussion

In this report, we were able to develop a compartmental non-linear mixed effect model that can describe the mean concentration vs. time course of remdesivir and its two detectable metabolites reasonably well, while also adapting for and describing inter-dose variability.

Both the developed model and the simulations gave similar values for the derived PK parameters (AUC, elimination half-life, C_{\max}) compared to other published non-compartmental analyses of remdesivir, GS-441524, and GS-704277 (Tables 2 and S2) (Humeniuk et al. 2020; Tempestilli et al. 2020). The model itself is empirical but physiologically and metabolically plausible. The model incorporates a sequential metabolism from remdesivir to GS-704277 followed by GS-704277 metabolism to GS-441524, which is in agreement with the known metabolic fate of remdesivir (Humeniuk et al. 2021a; Wen et al. 2021). As a peculiarity, the developed model incorporated a peripheral metabolism to GS-704277, and this does not contradict physiological considerations. A comparison of the parameters to those reported by Sukeishi et al. (2021) is difficult because their evaluation could not consider that a remdesivir dose is not metabolized completely to GS-441524, and therefore, any values reported indeed are values relative to the fraction metabolized (fm) to GS-441524. Assuming a fraction of about 0.5 (Humeniuk et al. 2021a, b), the basic clearance value reported of about 12 L/h (= CL/fm) corresponds to a true clearance of 6 L/h, which is close to our result of about 5 L/h and also not far from 5.71 L/h value, which was reported by Gilead (Hartman et al. 2020).

We found by the simulation of the clinically approved regimen that plasma concentrations of GS-441524 after 20 min from the beginning of the 200-mg infusion would reach the reported EC_{50} value (180 nM) in SARS-CoV primary human airway epithelial cells (Yan and Muller 2020). The concentration stayed above EC_{50} values throughout the whole simulated 6 days (Fig. 4). Here we assume that lung epithelial cell exposure is close to plasma exposure. However, PBPK modeling predicts that lung concentrations of GS-441524 are several-fold lower than plasma concentration and that GS-441524 plasma concentrations would not be useful to predict lung exposure of the active metabolite GS-443902 (Fan et al. 2021).

At the end, clinical data are required to assess any relationship between plasma pharmacokinetics of remdesivir and its metabolites and efficacy in patients.

A recent study showed that early administration of remdesivir among non-hospitalized patients with at least one risk factor for disease progression could in fact lower the risk of hospitalization or death compared to placebo groups (Gottlieb et al. 2021). However, this study did not associate efficacy with the level of exposure to remdesivir or its metabolite. And so far, the relevance of EC_{50} level interpretation for remdesivir or its metabolite levels is still unclear.

We attempted to apply our model to the data we reported for a patient with renal impairment (Sörgel et al. 2021) — but we failed. The concentrations in this patient were much higher than those observed by Humeniuk et al. (2020) already at the end of the infusion, which cannot be readily explained by a decreased elimination only. A reason for this could be that the model here is estimating the variability in mean concentrations across cohorts, which might be magnitudes lower than the variability at the level of individual patients.

Thus, further testing by independent datasets including data obtained from various patient populations is required to assess the external validity of this model. Also taking into account that this model was developed from data including only healthy volunteers with a focus on a Hispanic population, and no detailed information regarding age, BMI, or renal and hepatic function was available.

The model lacks variabilities on individual levels and does not consider reported standard errors in the clinical trials, which are considered to be some limitations associated with the model. Further investigations on drug efficacy, target tissues and/or intracellular concentrations, and protein binding are needed for a better understanding of the overall pharmacokinetics of remdesivir. Ideally, a comprehensive population model of remdesivir would also integrate pharmacodynamic data. The present model however may serve as a good starting point for such additional evaluations.

Supplementary Information The online version contains supplementary material available at <https://doi.org/10.1007/s00210-022-02292-6>.

Acknowledgements The authors would like to thank Dr. Rita Humeniuk for providing some general information that was helpful for the development of the model.

Author contribution A. A. developed the population pharmacokinetic model and performed simulations with the assistance of M. T. and M. B. . F. supervised the population pharmacokinetic analysis and communication with trial authors. A. A. wrote the initial draft of the manuscript. All authors contributed in and agreed upon the final version of the manuscript. The authors declare that all data were generated in-house and that no paper mill was used.

Funding Open Access funding enabled and organized by Projekt DEAL. This study was carried out as part of our routine work.

Data availability Further data are available from the corresponding author, A. A., upon reasonable request.

Declarations

Ethics approval Not applicable.

Consent to participate Not applicable.

Consent for publication Not applicable.

Conflict of interest The authors declare no competing interests.

Open Access This article is licensed under a Creative Commons Attribution 4.0 International License, which permits use, sharing, adaptation, distribution and reproduction in any medium or format, as long as you give appropriate credit to the original author(s) and the source, provide a link to the Creative Commons licence, and indicate if changes were made. The images or other third party material in this article are included in the article's Creative Commons licence, unless indicated otherwise in a credit line to the material. If material is not included in the article's Creative Commons licence and your intended use is not permitted by statutory regulation or exceeds the permitted use, you will need to obtain permission directly from the copyright holder. To view a copy of this licence, visit <http://creativecommons.org/licenses/by/4.0/>.

References

- Alsayed HAH, Sharif-Askari FS, Sharif-Askari NS et al (2021) Early administration of remdesivir to COVID-19 patients associates with higher recovery rate and lower need for ICU admission: a retrospective cohort study. *PLoS ONE* 16:e0258643. <https://doi.org/10.1371/JOURNAL.PONE.0258643>
- Anh AVQ, Norris RLG, Charles BG (2006) Modelling drug loss during intravenous infusion to premature neonates. *J Pharm Pract Res* 36:262–265. <https://doi.org/10.1002/j.2055-2335.2006.tb00626.x>
- CHMP (2020) Annex I Summary of product characteristics for Veklury, https://www.ema.europa.eu/en/documents/other/veklury-product-information-approved-chmp-25-june-2020-pending-endorsement-european-commission_en.pdf
- COVID-19 treatments: authorised | European Medicines Agency (2021) <https://www.ema.europa.eu/en/human-regulatory/overview/public-health-threats/coronavirus-disease-covid-19/treatments-vaccines/treatments-covid-19/covid-19-treatments-authorised>. Accessed 11 May 2021
- de Wit E, Feldmann F, Cronin J et al (2020) Prophylactic and therapeutic remdesivir (GS-5734) treatment in the rhesus macaque model of MERS-CoV infection. *Proc Natl Acad Sci U S A* 117:6771–6776. <https://doi.org/10.1073/pnas.1922083117>
- Deb S, Reeves AA (2021) Simulation of remdesivir pharmacokinetics and its drug interactions. *J Pharm Pharm Sci* 24:277–291. <https://doi.org/10.18433/JPPS32011>
- Diaz JV, Appiah J, Askie L, Baller A, Banerjee A, Barkley S, Bertagnolli S, Hemmingsen B, Mercedes Bonet JC (2021) Clinical management: living guidance COVID-19. World Heal Organ
- FDA (2022) FDA takes actions to expand use of treatment for outpatients with mild-to-moderate COVID-19 | FDA. <https://www.fda.gov/news-events/press-announcements/fda-takes-actions-expand-use-treatment-outpatients-mild-moderate-covid-19>. Accessed 24 Jan 2022
- Fact Sheet for Health Care Providers Emergency Use Authorization (EUA) of Veklury® (2020) (remdesivir). <https://www.fda.gov/media/143189/download>
- Fan J, Yang Y, Grimstein M et al (2021) Whole body PBPK modeling of remdesivir and its metabolites to aid in estimating active metabolite exposure in the lung and liver in patients with organ dysfunction. *Clin Pharmacol Ther*. <https://doi.org/10.1002/CPT.2445>
- Gallo JM (2021) Hybrid physiologically-based pharmacokinetic model for remdesivir: application to SARS-CoV-2. *Clin Transl Sci* 14:1082–1091. <https://doi.org/10.1111/CTS.12975>
- GetData Graph Digitizer - graph digitizing software. <http://www.getdata-graph-digitizer.com/>. Accessed 14 Nov 2021c
- Godino C, Scotti A, Maugeri N et al (2021) Antithrombotic therapy in patients with COVID-19? — Rationale and evidence. *Int J Cardiol* 324:261–266. <https://doi.org/10.1016/j.ijcard.2020.09.064>
- Gottlieb RL, Vaca CE, Paredes R et al (2021) Early remdesivir to prevent progression to severe COVID-19 in outpatients. *N Engl J Med*. https://doi.org/10.1056/NEJMOA2116846/SUPPL_FILE/NEJMOA2116846_DATA-SHARING.PDF
- Hartman N, Kim M, Kruhlak N, et al. (2020) Center for Drug Evaluation and Research application number: 214787Orig1s000 Clinical Pharmacology Review(s)
- Humeniuk R, Mathias A, Cao H et al (2020) Safety, tolerability, and pharmacokinetics of remdesivir, an antiviral for treatment of COVID-19, in healthy subjects. *Clin Transl Sci* 13:896–906. <https://doi.org/10.1111/cts.12840>
- Humeniuk R, Mathias A, Kirby BJ et al (2021b) Pharmacokinetic, pharmacodynamic, and drug-interaction profile of remdesivir, a SARS-CoV-2 replication inhibitor. *Clin Pharmacokinet* 60(5):569–583. <https://doi.org/10.1007/S40262-021-00984-5>
- Humeniuk R, Mathias A, Kirby BJ, et al. (2021a) Pharmacokinetic, pharmacodynamic, and drug-interaction profile of remdesivir, a SARS-CoV-2 replication inhibitor. *Clin Pharmacokinet*. 1–15
- Juan HuW, Chang L, Yang Y et al (2021) Pharmacokinetics and tissue distribution of remdesivir and its metabolites nucleotide monophosphate, nucleotide triphosphate, and nucleoside in mice. *Acta Pharmacol Sin* 42:1195–1200. <https://doi.org/10.1038/s41401-020-00537-9>
- Kalil AC, Mehta AK, Patterson TF et al (2021) Efficacy of interferon beta-1a plus remdesivir compared with remdesivir alone in hospitalised adults with COVID-19: a double-blind, randomised, placebo-controlled, phase 3 trial. *Lancet Respir Med*. [https://doi.org/10.1016/S2213-2600\(21\)00384-2](https://doi.org/10.1016/S2213-2600(21)00384-2)
- LHartman N, Kim M, Kruhlak N, Kruhlak N (2020) In silico analyses on the potential association of remdesivir with renal and hepatic events (NDA 21487). https://www.accessdata.fda.gov/drugsatfda_docs/nda/2020/214787Orig1s000ClinPharmR.pdf. Accessed 15 Dec 2021
- Monolix (2019R2) Antony, France. <https://monolix.lixoft.com/>. Accessed 14 Nov 2021
- R Core Team (2021) R: A language and environment for statistical computing. R Foundation for Statistical Computing, Vienna, Austria. <https://www.R-project.org/>
- Sieswerda E, de Boer MGJ, Bonten MMJ et al (2021) Recommendations for antibacterial therapy in adults with COVID-19 — an evidence based guideline. *Clin Microbiol Infect* 27:61–66
- Sörgel F, Malin JJ, Hagmann H et al (2021) Pharmacokinetics of remdesivir in a COVID-19 patient with end-stage renal

- disease on intermittent haemodialysis. *J Antimicrob Chemother* 76:825–827. <https://doi.org/10.1093/JAC/DKAA500>
- Sukeishi A, Itohara K, Yonezawa A et al (2021) Population pharmacokinetic modeling of GS-441524, the active metabolite of remdesivir, in Japanese COVID-19 patients with renal dysfunction. *CPT Pharmacometrics Syst Pharmacol*. <https://doi.org/10.1002/PSP4.12736>
- Tempestilli M, Caputi P, Avataneo V et al (2020) Pharmacokinetics of remdesivir and GS-441524 in two critically ill patients who recovered from COVID-19. *J Antimicrob Chemother* 75:2977–2980. <https://doi.org/10.1093/jac/dkaa239>
- Therapeutic options for COVID-19 patients | CDC (2021) <https://www.cdc.gov/coronavirus/2019-ncov/hcp/therapeutic-options.html>. Accessed 11 May 2021
- UK-MHRA (2021) First oral antiviral for COVID-19, Lagevrio (molnupiravir), approved by MHRA - GOV.UK. <https://www.gov.uk/government/news/first-oral-antiviral-for-covid-19-lagevrio-molnupiravir-approved-by-mhra>. Accessed 6 Nov 2021
- Vitiello A, Ferrara F (2021) Association and pharmacological synergism of the triple drug therapy baricitinib/remdesivir/rhACE2 for the management of COVID-19 infection. *Naunyn-Schmiedeberg's Arch Pharmacol* 2021:1–6. <https://doi.org/10.1007/S00210-021-02169-0>
- Wang M, Cao R, Zhang L et al (2020) Remdesivir and chloroquine effectively inhibit the recently emerged novel coronavirus (2019-nCoV) in vitro. *Cell Res* 30:269–271
- Wen-juan, Hu Lu, Chang Ying, Yang Xin, Wang Yuan-chao, Xie Jing-shan, Shen Bo, Tan Jia, Liu (2021) Pharmacokinetics and tissue distribution of remdesivir and its metabolites nucleotide monophosphate nucleotide triphosphate and nucleoside in mice. *Acta Pharmacol Sin* 42(7):1195–1200. <https://doi.org/10.1038/s41401-020-00537-9>
- Yan VC, Muller FL (2020) Advantages of the parent nucleoside GS-441524 over remdesivir for COVID-19 treatment. *ACS Med Chem Lett* 11:1361–1366

Publisher's note Springer Nature remains neutral with regard to jurisdictional claims in published maps and institutional affiliations.

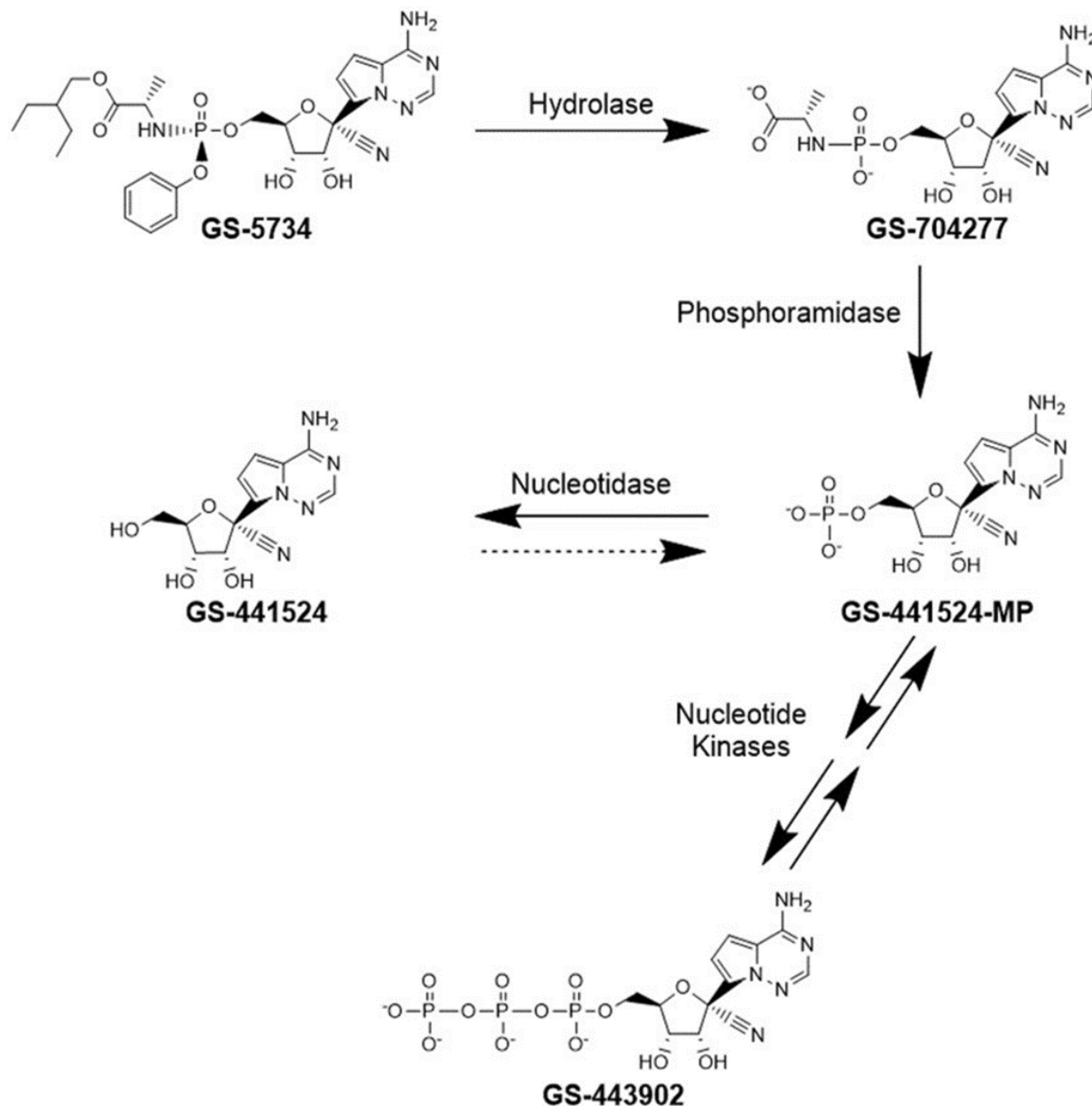
Supplementary Material:**Metabolic pathway of remdesivir (GS-5734)**

Figure S1, Remdesivir undergoes metabolism to form its active moiety, GS-443902. The metabolism process includes cleavage of remdesivir by carboxylesterases to form GS-704277 which can be measured in plasma. Subsequently, metabolism by phosphoramidase results in the formation of GS-441524-monophosphate (MP), which is further phosphorylated to the active nucleoside triphosphate, GS-443902. Dephosphorylation of GS-441524-MP results in the formation of the nucleoside analog, GS-441524 which is the 2nd plasma quantifiable metabolite (193).

Estimation of different distribution patterns of Remdesivir, GS-774277, and GS-441524 with different metabolic models

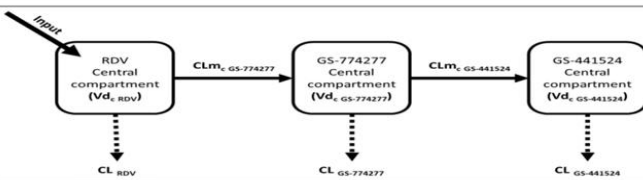
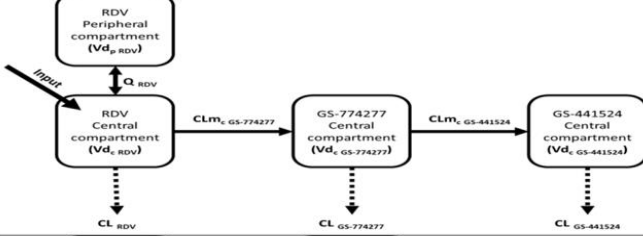
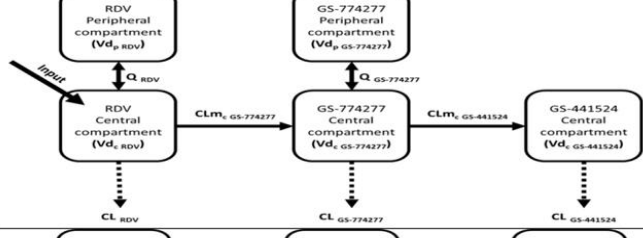
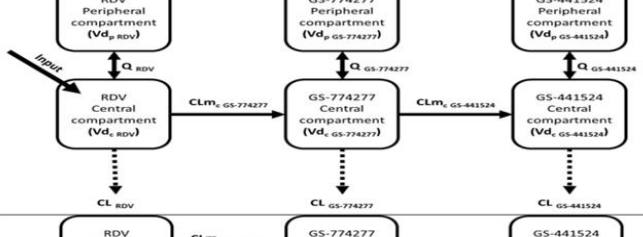
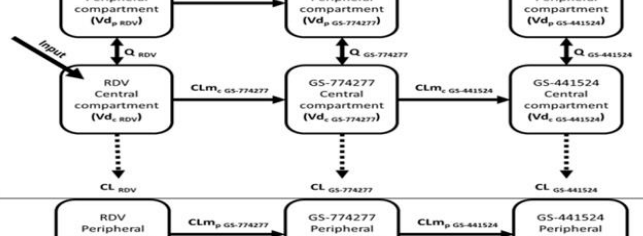
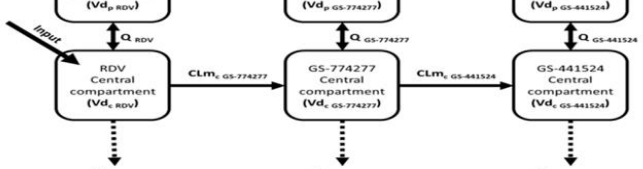
Model Design	-2 x log-likelihood	Δ of the selected model
	3353.04	1083.53
	2955.97	686.46
	2936.55	667.04
	2496.54	227.03
	2269.51	0
	2262.23	-7.28

Figure S2, -2 x Log of Likelihood estimation of different distribution patterns of Remdesivir, GS-774277, and GS-441524 with different metabolic models that control the conversion of Remdesivir to GS-704277, and GS-704277 to GS-441524 following the conversion of the models using Monolix

Distribution of Model Parameters

Distribution of Model parameters used for the simulation of remdesivir, GS-704277, and GS-441524 exposure following administration of the clinically used regimen

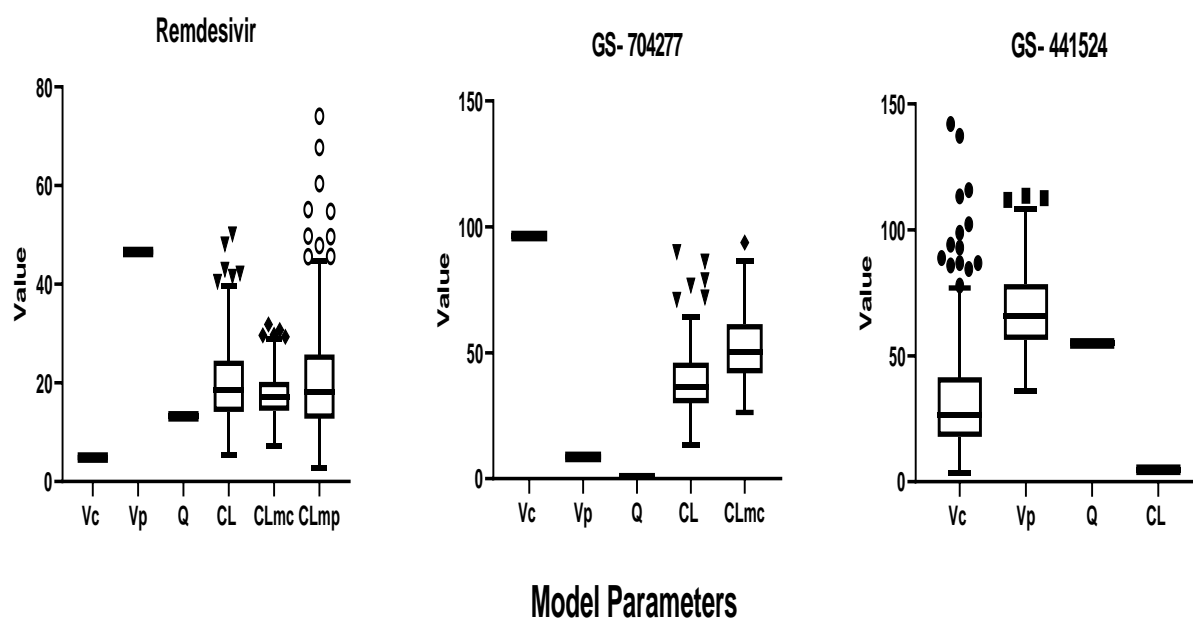


Figure S3 Fixed model parameters of remdesivir (RDV), GS-704277, and GS-441524 following a simulated 30-minute 200 mg intravenous infusion of remdesivir on day one, with 100 mg, 30 minutes intravenous infusion for the following 4 days. Total body clearance (CL); the volume of distribution for different compartments (Vdc, and Vdp), intercompartmental clearance (Q); formation clearance of metabolites (CLm). Dotted values resemble outliers according to Tukey's range test.

Simulation of plasma concentration-vs-time profiles

Simulation of plasma concentration-vs-time profiles for remdesivir, GS-704277, and GS-441524 following 2 hours of Intravenous infusion of either 3 mg, 10 mg, 30 mg, 75 mg, 150 mg, or 225 mg of remdesivir

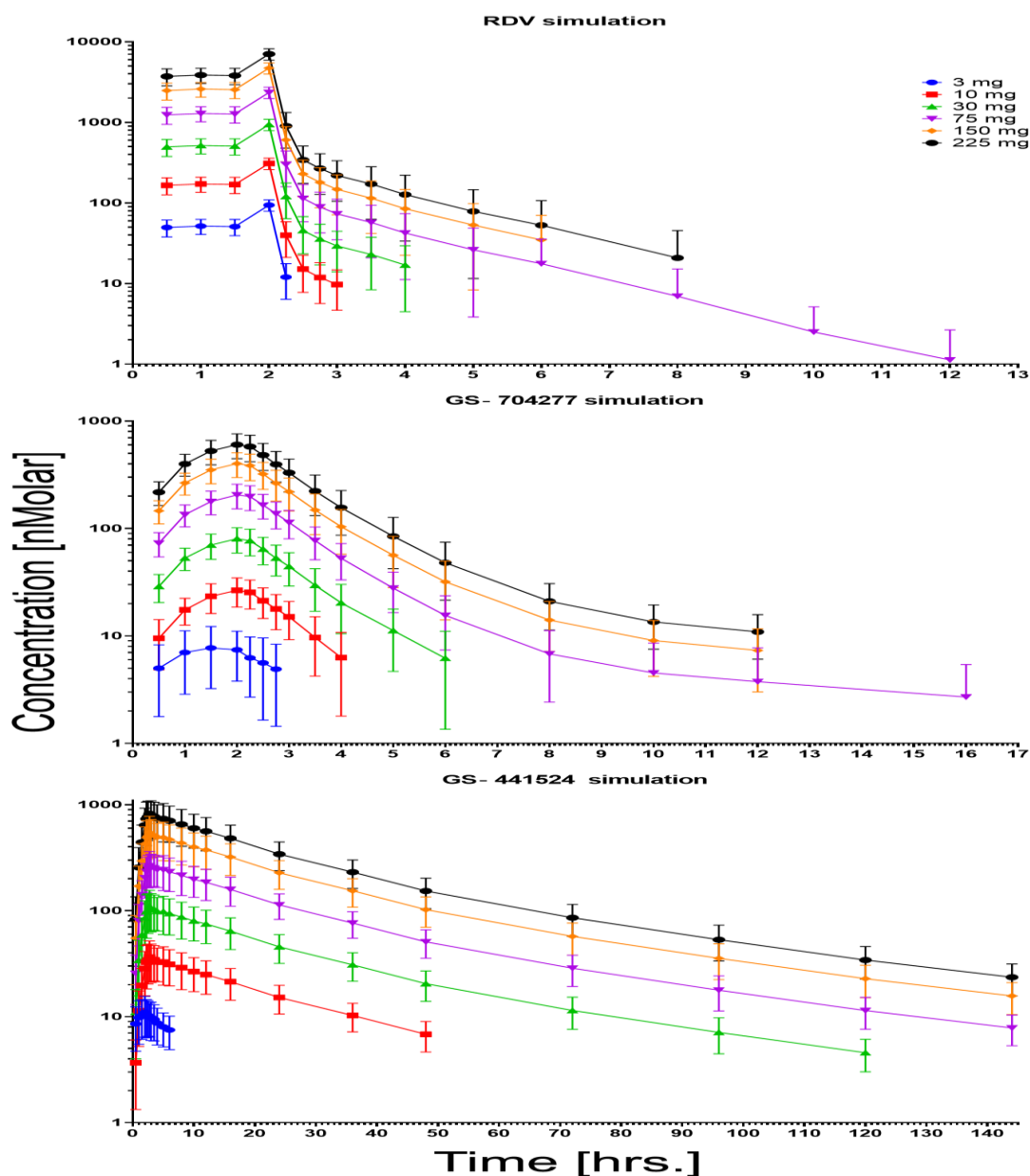


Figure S4 Doses of 3 mg, 10 mg, 30mg, 75mg, 150mg, and 225 mg of remdesivir were simulated as a single two hours infusion followed by a saline flush using previously obtained population parameter estimates. Simulation of remdesivir dosing was run as a 2 hours infusion using the bootstrapping function in Simulx package in R.

NONMEM® control stream of remdesivir population pharmacokinetic model

\$PROBLEM Pop PK of remdesivir
\$INPUT ID TIME DV EVID AMT RATE CMT ADDL II
\$DATA REMIwithmetaNONMEM2.csv IGNORE=@
\$SUBROUTINE ADVAN13 TOL=4

;Model Compartment -----

\$MODEL

COMP(CREMI)	;Cent cmt of Rem
COMP(PREMI)	;Peri cmt of Rem
COMP(CMETA77)	;Cent cmt of Met I
COMP(PMETA77)	;Peri cmt of Met I
COMP(CMETA24)	;Cent cmt of Met II
COMP(PMETA24)	; Peri cmt of Met II

; PK paramters-----

\$PK

VP	=	THETA(1)	;vol of distribution of cent cmt of Rem
VPP	=	THETA(2)	; vol of distribution of peri cmt of Rem
Vm1	=	THETA(3)	; vol of distribution of cent cmt of Met I
Vm2	=	THETA(4)	; vol of distribution of peri cmt of Met I
Vmm	=	THETA(5) * EXP(ETA(1))	; vol of distribution of cent cmt of Met II
Vmm2	=	THETA(6) * EXP(ETA(2))	; vol of distribution of peri cmt of Met II
Q1	=	THETA(7)	; Inter-compartmental clearance of remdesivir
CL	=	THETA(8) * EXP(ETA(3))	; CL from cent cmt of Rem
CLM1	=	THETA(9) * EXP(ETA(4))	; CL form cent cmt of Rem to cent cmt of Met I
CLM11	=	THETA(10)* EXP(ETA(5))	; CL from peri cmt of Rem to peri cmt of Met I
Qm	=	THETA(11)	; Inter-cmt CL of Met I
CLM2	=	THETA(12)* EXP(ETA(6))	; CL from central cmt of Met I to cent cmt of Met II
CLMM2	=	THETA(13)	; CL from cent cmt of Met II
Qmm	=	THETA(14)	; Inter-cmt CL between Met II
CLMM1	=	THETA(15)	; CL from cent cmt of Met I

;Ordinary differential equations-----

\$DES

CONC1	=	A(1)/ VP
CONC2	=	A(2)/ Vpp
CONC3	=	A(3)/ Vm1
CONC4	=	A(4)/ Vm2
CONC5	=	A(5)/ Vmm
CONC6	=	A(6)/ Vmm2

$DADT(1) = Q1*CONC2 - Q1*CONC1 - CL*CONC1 - CLM1*CONC1$
 $DADT(2) = Q1*CONC1 - Q1*CONC2 - CLM11*CONC2$
 $DADT(3) = CLM1*CONC1 - CLMM1*CONC3 - CLM2*CONC3 - Qm*CONC3 + Qm*CONC4$
 $DADT(4) = Qm*CONC3 - Qm*CONC4 + CLM11*CONC2$
 $DADT(5) = CLM2*CONC3 - CLMM2*CONC5 - Qmm*CONC5 + Qmm*CONC6$
 $DADT(6) = Qmm*CONC5 - Qmm*CONC6$

; Residual unexplained variability parameters-----

\$ERROR

IF (CMT.EQ.1) THEN
 $IPRED = A(1)/VP$
 $W = \sqrt{THETA(16)**2*IPRED**2 + THETA(17)**2}$
 END IF

IF (CMT.EQ.3) THEN
 $IPRED = A(3)/Vm1$
 $W = \sqrt{THETA(18)**2*IPRED**2 + THETA(19)**2}$
 END IF

IF (CMT.EQ.5) THEN
 $IPRED = A(5)/Vmm$
 $W = \sqrt{THETA(20)**2*IPRED**2 + THETA(21)**2}$
 END IF

$IRES = DV - IPRED$
 $IWRES = IRES/W$

$Y = IPRED + W*EPS(1)$

; Initial estimates -----

\$THETA

(0, 5.01027)	; VP
(0, 38.482)	; VPP
(0, 124.586)	; Vm1
(0, 5.74209)	; Vm2
(0, 13.3259)	; Vmm
(0, 23.1694)	; Vmm2
(0, 10.0834)	; Q1
(0, 17.9352)	; CL
(0, 13.4651)	; CLM1
(0, 16.0286)	; CLM11
(0, 0.0826804)	; Qm

```
(0, 12.1661) ; CLM2
(0, 1.73025) ; CLMM2
(0, 16.0068) ; Qmm
(0, 102.814) ; CLMM1
(0, 0.253164) ; Prop.RE (sd) REMI
0 FIX ; Add.RE (sd) REMI ;
(0, 0.0765656) ; Prop.RE (sd) META77
(0, 1.92091) ; Add.RE (sd) META77
(0, 0.0834543) ; Prop.RE (sd) META24
0 FIX ; Add.RE (sd) META24
```

\$OMEGA

```
0.000262039 ;IIV Vmm
000296852 ;IIV Vmm2
0.0781623 ;IIV CL
0.0679066 ;IIV CLM1
0.228309 ;IIV CLM11
0.064425 ;IIV Qm
```

\$SIGMA

```
1 FIX
```

```
; Estimation and table output-----
```

```
$ESTIMATION METHOD=1 INTER MAXEVAL=9999 NOABORT SIG=3
PRINT=1 MSFO=Cc2METa.msf
```

```
$TABLE ID TIME DV EVID CMT IPRED CWRES ONEHEADER
NOPRINT
FILE=sdCc2METa.tab
```

```
$TABLE VP VPP VM1 Vm1 Vm2 Vmm Vmm2 Q1 Qm Qmm CL CLM1
CLM11 CLM2 CLMM2 CMT ONEHEADER NOPRINT
FIRSTONLY FILE=Cc2METa1.tab
```

```
$TABLE NOPRINT ONEHEADER FILE=Cc2METapar.tab ID TIME EVID
CMT IPRED MDV ETA1 ETA2 ETA3 ETA4 ETA5 ETA6
```

```
$TABLE NOPRINT ONEHEADER FILE=Cc2METa.tab ID TIME IPRED
EVID CMT MDV
```

```
;-----
```